Advances in Civil Engineering

# Digital Twin Technology in the Architectural, Engineering and Construction (AEC) Industry

Lead Guest Editor: Zhen-Zhong Hu
Guest Editors: Jia-Rui Lin, Jiansong Zhang, and Qian Wang

# Digital Twin Technology in the Architectural, Engineering and Construction (AEC) Industry

Advances in Civil Engineering

# Digital Twin Technology in the Architectural, Engineering and Construction (AEC) Industry

Lead Guest Editor: Zhen-Zhong Hu
Guest Editors: Jia-Rui Lin, Jiansong Zhang, and Qian Wang

Copyright © 2021 Hindawi Limited. All rights reserved.

This is a special issue published in “Advances in Civil Engineering.” All articles are open access articles distributed under the Creative Commons Attribution License, which permits unrestricted use, distribution, and reproduction in any medium, provided the original work is properly cited.

# Chief Editor

Cumaraswamy Vipulanandan, USA

## Associate Editors

Chiara Bedon, Italy
Constantin Chalioris, Greece
Ghassan Chehab, Lebanon
Ottavia Corbi, Italy
Mohamed ElGawady, USA
Husnain Haider, Saudi Arabia
Jian Ji, China
Jiang Jin, China
Shazim A. Memon, Kazakhstan
Hossein Moayedi, Vietnam
Sanjay Nimbalkar, Australia
Giuseppe Oliveto, Italy
Alessandro Palmeri, United Kingdom
Arnaud Perrot, France
Hugo Rodrigues, Portugal
Victor Yepes, Spain
Xianbo Zhao, Australia

## Academic Editors

José A.F.O. Correia, Portugal
Glenda Abate, Italy
Khalid Abdel-Rahman, Germany
Ali Mardani Aghabaglou, Turkey
José Aguiar, Portugal
Afaq Ahmad, Pakistan
Muhammad Riaz Ahmad, Hong Kong
Hashim M.N. Al-Madani, Bahrain
Luigi Aldieri, Italy
Angelo Aloisio, Italy
Maria Cruz Alonso, Spain
Filipe Amarante dos Santos, Portugal
Serji N. Amirkhanian, USA
Eleftherios K. Anastasiou, Greece
Panagiotis Ch. Anastasopoulos, USA
Mohamed Moafak Arbili, Iraq
Farhad Aslani, Australia
Siva Avudaiappan, Chile
Ozgur BASKAN, Turkey
Adewumi Babafemi, Nigeria
Morteza Bagherpour, Turkey
Qingsheng Bai, Germany
Nicola Baldo, Italy
Daniele Baraldi, Italy
Eva Barreira, Portugal
Emilio Bastidas-Arteaga, France
Rita Bento, Portugal
Rafael Bergillos, Spain
Han-bing Bian, China
Xia Bian, China
Huseyin Bilgin, Albania
Giovanni Biondi, Italy
Hugo C. Biscaia, Portugal
Rahul Biswas, India
Edén Bojórquez, Mexico
Giosuè Boscato, Italy
Melina Bosco, Italy
Jorge Branco, Portugal
Bruno Briseghella, China
Brian M. Broderick, Ireland
Emanuele Brunesi, Italy
Quoc-Bao Bui, Vietnam
Tan-Trung Bui, France
Nicola Buratti, Italy
Gaochuang Cai, France
Gladis Camarini, Brazil
Alberto Campisano, Italy
Qi Cao, China
Qixin Cao, China
Iacopo Carnacina, Italy
Alessio Cascardi, Italy
Paolo Castaldo, Italy
Nicola Cavalagli, Italy
Liborio Cavaleri, Italy
Anush Chandrappa, United Kingdom
Wen-Shao Chang, United Kingdom
Muhammad Tariq Amin Chaudhary, Kuwait
Po-Han Chen, Taiwan
Qian Chen, China
Wei Tong Chen, Taiwan
Qixiu Cheng, Hong Kong
Zhanbo Cheng, United Kingdom
Nicholas Chileshe, Australia
Prinya Chindaprasirt, Thailand
Corrado Chisari, United Kingdom
Se Jin Choi, Republic of Korea
Heap-Yih Chong, Australia
S.H. Chu, USA
Ting-Xiang Chu, China

Zhaofei Chu, China
Wonseok Chung, Republic of Korea
Donato Ciampa, Italy
Gian Paolo Cimellaro, Italy
Francesco Colangelo, Italy
Romulus Costache, Romania
Liviu-Adrian Cotfas, Romania
Antonio Maria D'Altri, Italy
Bruno Dal Lago, Italy
Amos Darko, Hong Kong
Arka Jyoti Das, India
Dario De Domenico, Italy
Gianmarco De Felice, Italy
Stefano De Miranda, Italy
Maria T. De Risi, Italy
Tayfun Dede, Turkey
Sadik O. Degertekin, Turkey
Camelia Delcea, Romania
Cristoforo Demartino, China
Giuseppe Di Filippo, Italy
Luigi Di Sarno, Italy
Fabio Di Trapani, Italy
Aboelkasim Diab, Egypt
Thi My Dung Do, Vietnam
Giulio Dondi, Italy
Jiangfeng Dong, China
Chao Dou, China
Mario D'Aniello, Italy
Jingtao Du, China
Ahmed Elghazouli, United Kingdom
Francesco Fabbrocino, Italy
Flora Faleschini, Italy
Dingqiang Fan, Hong Kong
Xueping Fan, China
Qian Fang, China
Salar Farahmand-Tabar, Iran
Ilenia Farina, Italy
Roberto Fedele, Italy
Guang-Liang Feng, China
Luigi Fenu, Italy
Tiago Ferreira, Portugal
Marco Filippo Ferrotto, Italy
Antonio Formisano, Italy
Guoyang Fu, Australia
Stefano Galassi, Italy
Junfeng Gao, China
Meng Gao, China
Giovanni Garcea, Italy
Enrique García-Macías, Spain
Emilio García-Taengua, United Kingdom
DongDong Ge, USA
Khaled Ghaedi, Malaysia
Khaled Ghaedi, Malaysia
Gian Felice Giaccu, Italy
Agathoklis Giaralis, United Kingdom
Ravindran Gobinath, India
Rodrigo Gonçalves, Portugal
Peilin Gong, China
Belén González-Fonteboa, Spain
Salvatore Grasso, Italy
Fan Gu, USA
Erhan Güneyisi, Turkey
Esra Mete Güneyisi, Turkey
Pingye Guo, China
Ankit Gupta, India
Federico Gusella, Italy
Kemal Hacıefendioğlu, Turkey
Jianyong Han, China
Song Han, China
Asad Hanif, Macau
Hadi Hasanzadehshooiili, Canada
Mostafa Fahmi Hassanein, Egypt
Amir Ahmad Hedayat, Iran
Khandaker Hossain, Canada
Zahid Hossain, USA
Chao Hou, China
Biao Hu, China
Jiang Hu, China
Xiaodong Hu, China
Lei Huang, China
Cun Hui, China
Bon-Gang Hwang, Singapore
Jijo James, India
Abbas Fadhil Jasim, Iraq
Ahad Javanmardi, China
Krishnan Prabhakan Jaya, India
Dong-Sheng Jeng, Australia
Han-Yong Jeon, Republic of Korea
Pengjiao Jia, China
Shaohua Jiang, China

MOUSTAFA KASSEM, Malaysia
Mosbeh Kaloop, Egypt
Shankar Karuppannan, Ethiopia
John Kechagias, Greece
Mohammad Khajehzadeh, Iran
Afzal Husain Khan, Saudi Arabia
Mehran Khan, Hong Kong
Manoj Khandelwal, Australia
Jin Kook Kim, Republic of Korea
Woosuk Kim, Republic of Korea
Vaclav Koci, Czech Republic
Loke Kok Foong, Vietnam
Hailing Kong, China
Leonidas Alexandros Kouris, Greece
Kyriakos Kourousis, Ireland
Moacir Kripka, Brazil
Anupam Kumar, The Netherlands
Emma La Malfa Ribolla, Czech Republic
Ali Lakirouhani, Iran
Angus C. C. Lam, China
Thanh Quang Khai Lam, Vietnam
Luciano Lamberti, Italy
Andreas Lampropoulos, United Kingdom
Raffaele Landolfo, Italy
Massimo Latour, Italy
Bang Yeon Lee, Republic of Korea
Eul-Bum Lee, Republic of Korea
Zhen Lei, Canada
Leonardo Leonetti, Italy
Chun-Qing Li, Australia
Dongsheng Li, China
Gen Li, China
Jiale Li, China
Minghui Li, China
Qingchao Li, China
Shuang Yang Li, China
Sunwei Li, Hong Kong
Yajun Li, China
Shun Liang, China
Francesco Liguori, Italy
Jae-Han Lim, Republic of Korea
Jia-Rui Lin, China
Kun Lin, China
Shibin Lin, China
Tzu-Kang Lin, Taiwan
Yu-Cheng Lin, Taiwan
Hexu Liu, USA
Jian Lin Liu, China
Xiaoli Liu, China
Xuemei Liu, Australia
Zaobao Liu, China
Zhuang-Zhuang Liu, China
Diego Lopez-Garcia, Chile
Cristiano Loss, Canada
Lyan-Ywan Lu, Taiwan
Jin Luo, USA
Yanbin Luo, China
Jianjun Ma, China
Junwei Ma, China
Tian-Shou Ma, China
Zhongguo John Ma, USA
Maria Macchiaroli, Italy
Domenico Magisano, Italy
Reza Mahinroosta , Australia
Yann Malecot, France
Prabhat Kumar Mandal, India
John Mander, USA
Iman Mansouri, Iran
André Dias Martins, Portugal
Domagoj Matesan, Croatia
Jose Matos, Portugal
Vasant Matsagar, India
Claudio Mazzotti, Italy
Ahmed Mebarki, France
Gang Mei, China
Kasim Mermerdas, Turkey
Giovanni Minafò, Italy
Masoomeh Mirrashid, Iran
Abbas Mohajerani, Australia
Fadzli Mohamed Nazri, Malaysia
Fabrizio Mollaioli, Italy
Rosario Montuori, Italy
H. Naderpour, Iran
Hassan Nasir, Pakistan
Hossein Nassiraei, Iran
Satheeskumar Navaratnam, Australia
Ignacio J. Navarro, Spain
Ashish Kumar Nayak, India
Behzad Nematollahi, Australia

Chayut Ngamkhanong, Thailand
Trung Ngo, Australia
Tengfei Nian, China
Mehdi Nikoo, Canada
Youjun Ning, China
Olugbenga Timo Oladinrin, United Kingdom
Oladimeji Benedict Olalusi, South Africa
Timothy O. Olawumi, Hong Kong
Alejandro Orfila, Spain
Maurizio Orlando, Italy
Siti Aminah Osman, Malaysia
Walid Oueslati, Tunisia
SUVASH PAUL, Bangladesh
John-Paris Pantouvakis, Greece
Fabrizio Paolacci, Italy
Giuseppina Pappalardo, Italy
Fulvio Parisi, Italy
Dimitrios G. Pavlou, Norway
Daniele Pellegrini, Italy
Gatheeshgar Perampalam, United Kingdom
Daniele Perrone, Italy
Giuseppe Piccardo, Italy
Vagelis Plevris, Qatar
Andrea Pranno, Italy
Adolfo Preciado, Mexico
Chongchong Qi, China
Yu Qian, USA
Ying Qin, China
Giuseppe Quaranta, Italy
Krishanu ROY, New Zealand
Vlastimir Radonjanin, Serbia
Carlo Rainieri, Italy
Rahul V. Ralegaonkar, India
Raizal Saifulnaz Muhammad Rashid, Malaysia
Alessandro Rasulo, Italy
Chonghong Ren, China
Qing-Xin Ren, China
Dimitris Rizos, USA
Geoffrey W. Rodgers, New Zealand
Pier Paolo Rossi, Italy
Nicola Ruggieri, Italy
JUNLONG SHANG, Singapore
Nikhil Saboo, India
Anna Saetta, Italy
Juan Sagaseta, United Kingdom
Timo Saksala, Finland
Mostafa Salari, Canada
Ginevra Salerno, Italy
Evangelos J. Sapountzakis, Greece
Vassilis Sarhosis, United Kingdom
Navaratnarajah Sathiparan, Sri Lanka
Fabrizio Scozzese, Italy
Halil Sezen, USA
Payam Shafigh, Malaysia
M. Shahria Alam, Canada
Yi Shan, China
Hussein Sharaf, Iraq
Mostafa Sharifzadeh, Australia
Sanjay Kumar Shukla, Australia
Amir Si Larbi, France
Okan Sirin, Qatar
Piotr Smarzewski, Poland
Francesca Sollecito, Italy
Rui Song, China
Tian-Yi Song, Australia
Flavio Stochino, Italy
Mayank Sukhija, USA
Piti Sukontasukkul, Thailand
Jianping Sun, Singapore
Xiao Sun, China
T. Tafsirojjaman, Australia
Fujiao Tang, China
Patrick W.C. Tang, Australia
Zhi Cheng Tang, China
Weerachart Tangchirapat, Thailand
Xiaxin Tao, China
Piergiorgio Tataranni, Italy
Elisabete Teixeira, Portugal
Jorge Iván Tobón, Colombia
Jing-Zhong Tong, China
Francesco Trentadue, Italy
Antonello Troncone, Italy
Majbah Uddin, USA
Tariq Umar, United Kingdom
Muahmmad Usman, United Kingdom
Muhammad Usman, Pakistan
Mucteba Uysal, Turkey

Ilaria Venanzi, Italy
Castorina S. Vieira, Portugal
Valeria Vignali, Italy
Claudia Vitone, Italy
Liwei WEN, China
Chunfeng Wan, China
Hua-Ping Wan, China
Roman Wan-Wendner, Austria
Chaohui Wang, China
Hao Wang, USA
Shiming Wang, China
Wayne Yu Wang, United Kingdom
Wen-Da Wang, China
Xing Wang, China
Xiuling Wang, China
Zhenjun Wang, China
Xin-Jiang Wei, China
Tao Wen, China
Weiping Wen, China
Lei Weng, China
Chao Wu, United Kingdom
Jiangyu Wu, China
Wangjie Wu, China
Wenbing Wu, China
Zhixing Xiao, China
Gang Xu, China
Jian Xu, China
Panpan, China
Rongchao Xu, China
HE YONGLIANG, China
Michael Yam, Hong Kong
Hailu Yang, China
Xu-Xu Yang, China
Hui Yao, China
Xinyu Ye, China
Zhoujing Ye , China
Gürol Yildirim, Turkey
Dawei Yin, China
Doo-Yeol Yoo, Republic of Korea
Zhanping You, USA
Afshar A. Yousefi, Iran
Xinbao Yu, USA
Dongdong Yuan, China
Geun Y. Yun, Republic of Korea
Hyun-Do Yun, Republic of Korea
Cemal YİĞİT, Turkey
Paolo Zampieri, Italy
Giulio Zani, Italy
Mariano Angelo Zanini, Italy
Zhixiong Zeng, Hong Kong
Mustafa Zeybek, Turkey
Henglong Zhang, China
Jiupeng Zhang, China
Tingting Zhang, China
Zengping Zhang, China
Zetian Zhang, China
Zhigang Zhang, China
Zhipeng Zhao, Japan
Jun Zhao , China
Annan Zhou, Australia
Jia-wen Zhou, China
Hai-Tao Zhu, China
Peng Zhu, China
QuanJie Zhu, China
Wenjun Zhu, China
Marco Zucca, Italy
Haoran Zuo, Australia
Junqing Zuo, China
Robert Černý, Czech Republic
Süleyman İpek, Turkey

# Contents

**Intelligent Construction, Operation, and Maintenance of a Large Wastewater-Treatment Plant Based on BIM**
Jiu-Lin Li, Li-Min Chen, and Hao Xu
Research Article (11 pages), Article ID 6644937, Volume 2021 (2021)

**An Experiment-Based Simplified Method for the Model of Building Groups in CFD Simulation**
Hongling Guo, Ying Zhou, Yingxin Li, Zhihui Zhang, and Heng Li
Research Article (13 pages), Article ID 8811684, Volume 2021 (2021)

**Digital Twin in Computational Design and Robotic Construction of Wooden Architecture**
Ye Zhang, A. Meina, Xuhao Lin, Kun Zhang, and Zhen Xu
Research Article (14 pages), Article ID 8898997, Volume 2021 (2021)

**A New Framework to Address BIM Interoperability in the AEC Domain from Technical and Process Dimensions**
Ran Ren and Jiansong Zhang
Research Article (17 pages), Article ID 8824613, Volume 2021 (2021)

**Joint Investigation and 3D Visual Evaluation of Rock Mass Quality**
Haiping Yuan, Chenghao Chen, Yixian Wang, Hanbing Bian, and Yan Liu
Research Article (16 pages), Article ID 8858322, Volume 2020 (2020)

**A Novel HDF-Based Data Compression and Integration Approach to Support BIM-GIS Practical Applications**
Zeyu Pan, Jianyong Shi, and Liu Jiang
Research Article (22 pages), Article ID 8865107, Volume 2020 (2020)

**Prediction of Highway Tunnel Pavement Performance Based on Digital Twin and Multiple Time Series Stacking**
Gang Yu, Shuang Zhang, Min Hu, and Y. Ken Wang
Research Article (21 pages), Article ID 8824135, Volume 2020 (2020)

**Factors Influencing BIM Adoption for Construction Enterprises in China**
Ruixue Zhang, Yuyan Tang, Liang Wang, and Zeyu Wang
Research Article (15 pages), Article ID 8848965, Volume 2020 (2020)

**Special Issue "Digital Twin Technology in the AEC Industry"**
Jisong Zhang, Lihua Zhao, Guoqian Ren, Haijiang Li, and Xiaofei Li
Review Article (18 pages), Article ID 8842113, Volume 2020 (2020)

**Digital Twin Hospital Buildings: An Exemplary Case Study through Continuous Lifecycle Integration**
Yang Peng, Ming Zhang, Fangqiang Yu, Jinglin Xu, and Shang Gao
Research Article (13 pages), Article ID 8846667, Volume 2020 (2020)

**A Deep Learning-Based Approach to Enable Action Recognition for Construction Equipment**
Jinyue Zhang, Lijun Zi, Yuexian Hou, Mingen Wang, Wenting Jiang, and Da Deng
Research Article (14 pages), Article ID 8812928, Volume 2020 (2020)

Hindawi
Advances in Civil Engineering
Volume 2021, Article ID 6644937, 11 pages
https://doi.org/10.1155/2021/6644937

*Research Article*

# Intelligent Construction, Operation, and Maintenance of a Large Wastewater-Treatment Plant Based on BIM

**Jiu-Lin Li,[1,2] Li-Min Chen,[3] and Hao Xu[2]**

[1]*Tsinghua University, Beijing 100084, China*
[2]*Beijing Urban Construction Group Co.,Ltd., Beijing 100088, China*
[3]*National Speed Skating Oval Co.Ltd., Beijing 100101, China*

Correspondence should be addressed to Hao Xu; 804713698@qq.com

Received 11 November 2020; Accepted 27 April 2021; Published 10 May 2021

Academic Editor: Hui Yao

Copyright © 2021 Jiu-Lin Li et al. This is an open access article distributed under the Creative Commons Attribution License, which permits unrestricted use, distribution, and reproduction in any medium, provided the original work is properly cited.

Building information modeling (BIM) is a data-based tool for engineering, design, and building management, which is used to parameterize and model various types of information. This information may then be shared and introduced throughout the building life-cycle phases (planning, design, construction and operation, and maintenance (O&M)). Therefore, BIM allows engineers to correctly understand and efficiently respond to varying types of building information as well as serves as a foundation for cooperation between the design and construction teams. Hence, BIM plays an important role in increasing productivity, minimizing costs, and shortening construction times. In this article, we present a case example where BIM was used for intelligent construction of a large wastewater-treatment plant (WTP). The process involved intelligent design and simulation techniques, management and simulation of construction works, digital delivery solutions, BIM-based Internet of things O&M, and environmental monitoring. BIM was used to digitalize the construction, delivery, and O&M processes of the WTP. According to this case example, we also offer suggestions on how deep learning and intelligent control techniques can be used to enhance intelligent O&M in WTPs.

## 1. Introduction

As a traditional industry, the construction industry has an important contribution to the development of the world economy. According to the statistical data of Statista and Global Infrastructure Outlook, the scale of the world's construction industry has grown from USD 9.5 trillion in 2014 to USD 11.4 trillion in 2019, and in the next 20 years, global infrastructure investment will reach USD 94 trillion. However, the problems caused by the development of the construction industry have become increasingly prominent, such as high resource consumption, high pollution emissions, and low quality and efficiency (Q&E). The buildings and construction sector accounted for 36% of final energy use and 39% of energy and process-related carbon dioxide ($CO_2$) emissions in 2018, 11% of which resulted from manufacturing building materials and products such as steel, cement, and glass. As a raw material, building materials consume almost 60% of the raw materials in the lithosphere, and a large amount of energy consumption is also caused during their extraction, process, and production [1–5]. At the same time, the construction industry occupies 60% of the main agricultural land and 70% of the wood and the construction process consumes 12–16% of global water resources and produces about 45% to 65% of the global landfill waste components. More and more evidences show that the construction industry is one of the main factors causing the global environmental deterioration, which makes the green sustainable development of construction industry more widely recognized [6–10]. Information application is an important means for the construction industry to transform its development mode, improve Q&E, save energy, and reduce emissions. Informatization construction refers to the system method that integrates information technology, tool software, management system, and so on and provides technical support for the project construction team from the

whole construction process of planning, design, production, construction, and operation. Due to the transferability of information data in each phase, the application of information technology is only used in some links in the previous, which is a decentralized and fragmented application. With the development of BIM, Internet of things (IoT), mobile communication, and other technologies, information construction has gradually been equipped with the conditions throughout a building's life cycle. It is an important part of the development strategy of the construction industry. Building information modelling (BIM) is one of the crucial topics in the informatization of the construction industry, which is the basis for intelligent construction. This paper presents the influence of BIM benefits on the intelligent construction, operation, and maintenance of a large WTP. The manuscript is organized as follows. Section 2 illustrates the literature background and research review. Section 3 introduces the methodology. Section 4 shows how the case study for a large WTP is. Finally, Section 5 summarizes the conclusions and sets the goals for future developments.

This paper introduces the application of BIM technology in large urban infrastructure projects. By analysing a case example where BIM was used for intelligent construction of a large wastewater-treatment plant, the effects of BIM technology on the design, construction, and O&M processes of engineering were carefully studied, and thus, the intelligent construction technology system based on BIM technology is developed. This study could also be a reference for other intelligent construction and scientific management and control of large-scale public service facilities.

## 2. Background

As a traditional industry, the construction industry has been a major driver of economic growth. However, it is also a classic example of "resource intensive, polluting, inefficient, and low-quality" extensive development industry, which has hampered its rapid and sustainable development. The construction industry shall thus become much more efficient, competitive, and beneficent and will simultaneously create social, economic, and environmental benefits. BIM is a new approach introduced in construction projects to manage building design, construction, and O&M data in digital form throughout a building's life cycle and an approach that provides the exchange and interoperability of information among the stakeholders [11, 12]. BIM is utilized not just as a model but also as a suitable platform for coworking and information transferring between participants in all processes of the project and ensures that no information faults will occur when information is transferred from one stage to another. Its great advantages in deepening design, saving construction time, reducing cost, and improving Q&E have driven construction players to adopt it and increasingly implement it in all stages of construction [13–17]. It is a multidimensional model information integration technology which realizes the digital bearer and visual expression of physical characteristics and functional information of construction projects [18]. Hence, BIM provides the foundation for the virtual construction and refined management of engineering projects and at the same time provides technical guarantee for improving Q&E and industrial upgrading [19].

## 3. Methodology

*3.1. Intelligent Design and Simulation Technologies.* During the design, building information models were used to provide intuitive illustrations of the underground structures. The BIM models were then exported into Revit, Ecotect, Phoenics, CadnaA, and Pathfinder to perform specialized simulations of the key nodes to help optimize its design. The BIM model that was developed in the design phase was then introduced to the construction and O&M phases, thus creating a foundation for the use of BIM throughout in the WTP life cycle. The BioWin simulator was used to simulate and optimize the WTP processes and provide technical support for the O&M processes. First of all, we need to calculate and determine the size and operation parameters of each treatment structure by using the traditional design method according to the design of the water quality and water treatment process. Then, the design parameters are input into the BioWin application and transformed into the structures and parameters in the model. Based on this, the process flow is established on the model, and the process design is optimized through the comparison and selection of different design schemes. The use of BIM and BioWin in the design phase sets the stage for the creation of an intelligent WTP.

*3.2. Construction Management and Simulation Technologies.* By combining the BIM models with the 3D geographic information systems (3D-GISs) and IoT technology, we independently built a 3D IoT construction management platform to ensure the safety, progress, quality, and cost efficiency of the construction site, which effectively improved our ability to precisely manage this construction project using information technologies. In addition, a simulation analysis was performed on the construction process using the "interval casting method" to ensure that the construction would be smoothly implemented in WTP. Before construction, ANSYS software is used to simulate the whole process of construction so as to determine the sequence, spacing, and size of the interval casting method. During construction, permanent temperature and stress sensors were installed in the HWTP structure to collect stress and temperature data and to monitor structural changes in the concrete. Finally, the interval casting method was carried out orderly according to the data comprehensive of finite-element analysis and real-time monitoring.

*3.3. Digital Delivery and O&M Technologies.* We established a BIM delivery standard by developing an industry foundation classes (IFC) interface and defining a BIM O&M coding system, which effectively integrated the engineering data that were scattered across different life-cycle phases and specializations and established crosslinks among these data. The BIM delivery data were thus integrated to develop a

complete O&M model (Table 1), which will serve as O&M management information source in the future. In addition, a hierarchical O&M information system and a corresponding set of modeling methods were proposed for the research object based on its intrinsic features. This information system provided natural groupings for the subinformation models (e.g., GIS and BIM models) of the WTP, which varied in scale and scope. Local data augmentation, model scale conversions, and information fusion were performed to provide a low-level support for the construction of this hierarchical information system. In addition, a cloud infrastructure was used to enable integration and sharing of big data from the WTP O&M processes (Figure 1).

## 4. Case Study

*4.1. Case Study Description.* As a super-large city, Beijing is a severely water-scarce city. With the rapid development of society and economy, the contradiction between supply and demand of water resources has become prominent. In order to improve the level of sewage treatment and utilization of reclaimed water, Beijing has formulated the "Three-year Action Plan for Accelerating the Construction of Wastewater Treatment and Reclaimed Water Utilization Facilities in Beijing (2013–2015)," which promotes the construction of reclaimed water plant. Wastewater-treatment plants (WTPs) are typically constructed aboveground or underground. The former type is more common. Aboveground WTPs are cheaper to construct and operate than their underground counterparts, and operating and maintaining them are relatively straightforward. However, the construction of aboveground WTPs inevitably results in land waste, environmental pollution, and devaluation of its surrounding lands. By comparison, underground WTPs take up very little space, produce lesser noise, exert a lower environmental effect, help conserve land resources, and are more aesthetically pleasing (see Table 2). With the rapid urbanization of China and the growing environmental demands of its residents, underground WTPs have become the preferred choice for urban wastewater treatment in land-scarce areas whenever local economic conditions permit. This preference may be attributed to the sealed nature of underground WTPs and their ability to maintain harmony with their surrounding areas. The Huaifang Water Treatment Plant (HWTP) is currently the largest underground WTP in Asia. Most of its water treatment processes are performed underground, and a 15.62 $hm^2$ wetland park lies on its surface, making it a place for rest and relaxation of nearby residents. HWTP represents a future direction of WTP developments in China.

*4.2. Case Study Implementation*

*4.2.1. Intelligent BIM-Based Construction of HWTP*

*(1) Intelligent BIM-Based Design of HWTP.* The BIM models played an important role in the optimization of the HWTP design because they provided an intuitive display of the complex spatial relationships of its underground structures and enabled specialized simulations of its key nodes by exporting the models into simulation software. The design process was mainly performed using Autodesk Revit, aided by supplementary programs such as Civil3D and Navisworks. The BIM model was employed in the computational analyses and simulation programs to perform supplementary computations and simulation analyses for the survey design, comparison of design alternatives, design optimization, and construction collaboration phases. The performed simulations and analyses including site analysis, daylight visualization, visibility analysis, evacuation simulations, ventilation and deodorization simulations, noise simulations, interference checking, and sheet creation. These processes enhanced the level of precision and refinement of the HWTP design and created a basic model for its construction and O&M processes.

In a complex project such as HWTP, BIM is very important for such tasks as three-dimensional (3D) pipeline design. According to the interference-checking functionality of the BIM technique, Revit modeling was used to visualize the spatial relationships among the pipelines and perform interference checking. The design of the pipelines was then modified according to the interference-checking report to create a rational plan for the HWTP 3D spaces (Figure 2).

*(2) BioWin Simulation of Wastewater-Treatment Processes.* During the design phase of a WTP, the BioWin simulator can be used to perform steady-state simulations of a process flow solution so that appropriate modifications can be made according to the simulation results. This process allows the construction and operation costs to be reduced without any detriment to the output water quality. In HWTP, dynamic simulations can be performed according to the actual inflow water-quality levels and current state of its water treatment facilities. The results of these simulations can then be used to formulate technical solutions to optimize its operations and develop a rational basis for modifications to improve its efficiency.

In the present work, traditional methods were first used to determine the dimensions and operating parameters of the HWTP structures based on the designed inflow water-quality levels and preliminary HWTP process. The design parameters were then input into the BioWin simulator and converted into buildings and parameters using a BioWin model, which was then used to construct the process flows for the water treatment process. After the inflow water quality was determined, simulations were performed on several biological tank designs. Each design had a hydraulic retention time of 17.8 h and varying partitions for its anaerobic, anoxic, and aerobic zones (Figure 3). The effluent water qualities in each design were then compared, and the best design was selected for the biological tank.

*(3) IoT-Based Comprehensive Construction Management.* According to the BIM, cloud computing, and IoT technology, we integrated engineering-information modeling, building-performance analysis, detailed design, factory processing, high-precision measurements, structural monitoring, five-dimensional construction management, and O&M management in the BIM application and thus established a BIM- and IoT-based construction platform for

Table 1: Types of information in the O&M model of the HWTP.

| No. | Type | Size/ number | Format | Description |
|---|---|---|---|---|
| 1 | Building structure model | 1.4 GB | rvt | Includes the structural models of all buildings in the water and production zones |
| 2 | Mechanical and electrical equipment models | 1.6 GB | rvt, dwf | Include the main equipment in the water zones and some in the pipeline models |
| 3 | Drawings | 63 | dwg | Include the blueprints of the coarse screen, membrane screen, biological tank, and membrane bioreactor as well as the treatment process diagrams |
| 4 | Photographs | 41 | jpg | Photographs of some of the wastewater-treatment equipment in the water zones |
| 5 | Electronic files | 56 | doc, pdf | Process descriptions and equipment manuals |
| 6 | Equipment parameter files | 111 types | xls | Parameter tables of all equipment, including the coarse screen, membrane screen, biological tank, and membrane bioreactor |
| 7 | Monitoring data | — | Provided by OPC | Flow measurement and water-quality monitoring of the inlet and outlet (effluent), water-level monitoring in all water zones, and data from the membrane screen toxic-gas warning system |

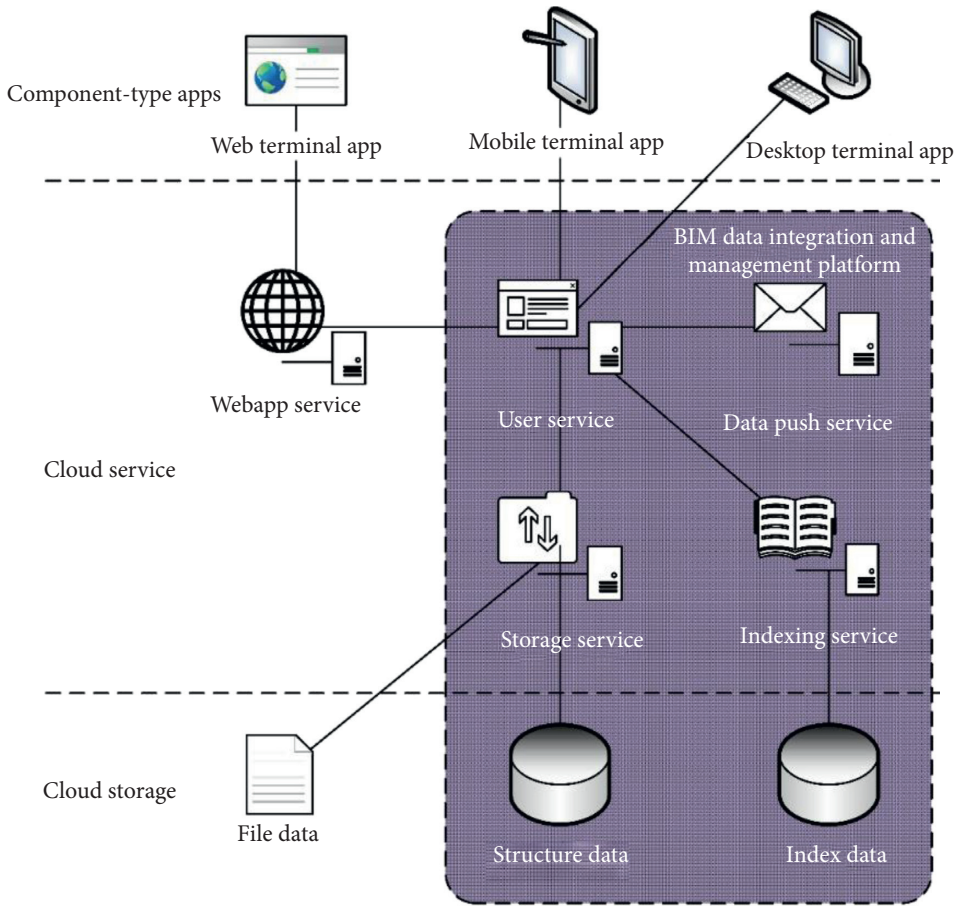


Figure 1: Cloud-based BIM O&M database.

"intelligent WTPs." Through the 3D-GIS, BIM, and IoT technologies, this platform can be used to manage on-site personnel, machinery, and materials.

This platform was implemented using website and mobile application (Figure 4) terminals, and it included video monitoring, personnel management, material management, and automated monitoring modules. This system effectively centralized much of the site-management data, allowed managers to operate from mobile offices, enabled real-time project management, and facilitated storage and querying of historical data. Further, the platform provided up-to-date and accurate data for the O&M processes. Therefore, this platform is a valuable addition to the project.

*(4) Implementation of the "Interval Casting Method" Based on Computational Simulations.* This study is the first one to

Table 2: Comparison between conventional aboveground and underground WTPs.

| Aspect | Conventional aboveground WTPs | Underground WTPs |
|---|---|---|
| Environmental and landscaping effects | The upper parts of the WTP structures can be used for "greenification" and landscaping, but they tend to be quite scattered. Furthermore, much of their equipment is exposed. Consequently, the environmental and landscaping effects of aboveground WTPs are mediocre at best. | Other than the processing rooms and their ancillary facilities that must be constructed at the surface, the only other features of an underground WTP that lie on the surface are the equipment hatch, escape hatch, ventilation ports, and odor discharge port. Therefore, large swathes of surface area are still available for greenification, which allows underground WTPs to have excellent environmental and landscaping effects. |
| Social benefits | Integrating aboveground WTPs into natural landscapes and using these sites for other purposes are difficult. As urbanization progresses in China, regional development has been restricted to some extent by wastewater-treatment facilities that were constructed in the past. | Underground WTPs have, to an extent, changed the perception of the general public on WTPs, and they are useful for increasing environmental awareness. Underground WTPs are viable as "in-city treatment plants." |
| Economic benefits | Aboveground WTPs are inefficient in terms of land use, and they exert a negative effect on the usability and market prices of their surrounding lands. | Underground WTPs are more flexible in terms of where they can be built, and they can be constructed near their serviced areas to reduce delivery and maintenance costs. Because the structures of underground WTPs are tightly clustered, they use less land and thus incur lower land-purchase costs. Furthermore, the land above and around an underground WTP still retains a high level of usability and value. |
| Construction costs | Low | High |
| Operational costs | Low | High |
| O&M | Inspection, repair, maintenance, and equipment hoisting in aboveground WTPs are relatively straightforward. | O&M conditions are far less ideal in underground WTPs, and high levels of ventilation and illumination are required. Using large machinery for equipment maintenance in underground WTPs is not possible. Hoisting large pieces of equipment requires hoisting holes, and the process depends on the layout of the underground space. Communication between aboveground and underground spaces can be difficult. |
| Working environment | Aboveground WTPs have an amenable working environment because they are usually on the surface or inside a processing room where ventilation and illumination issues can be trivially resolved. | Because the working environment is underground, artificial illumination and comprehensive mechanical air supply and exhaust systems are required to maintain these environments, which effectively increase the operational costs. |
| Noise and deodorization | Environmental requirements can be met by sealing parts of the WTP or by collecting odorous gases. However, any malfunction in the deodorization system will have a significant effect on the WTP surroundings. | Because the wastewater-treatment facilities are tightly clustered in an underground WTP, the exhaust ports for deodorization are also clustered. Sealing and collecting odorous gases from the treatment facilities are relatively straightforward, and odorous gases are unlikely to spread to the WTP surroundings in the event of a malfunction in the deodorization system. Because the vast majority of the WTP equipment is located underground, restricting noise emissions is relatively straightforward. |
| Fire control and safety | Most of the processing rooms only require outdoor and indoor fire-hydrant systems. Workers inside a processing room can easily escape. In addition, flooding is unlikely to occur. | Underground WTPs are required by law to have many fire compartments and a large number of fire escapes that directly lead to the surface. In addition to the fire-hydrant systems, automatic fire-extinguishing systems must be installed. Care must be taken to prevent flooding. |

use the interval casting method for the first time to construct a hydraulic structure. Although precedents existed that may have served as references for this project, the suitability of the interval casting method for hydraulic structures remained uncertain. Therefore, finite-element analysis and real-time monitoring were used to ensure the reliability of the interval casting method. According to computational simulations, permanent temperature and stress sensors were

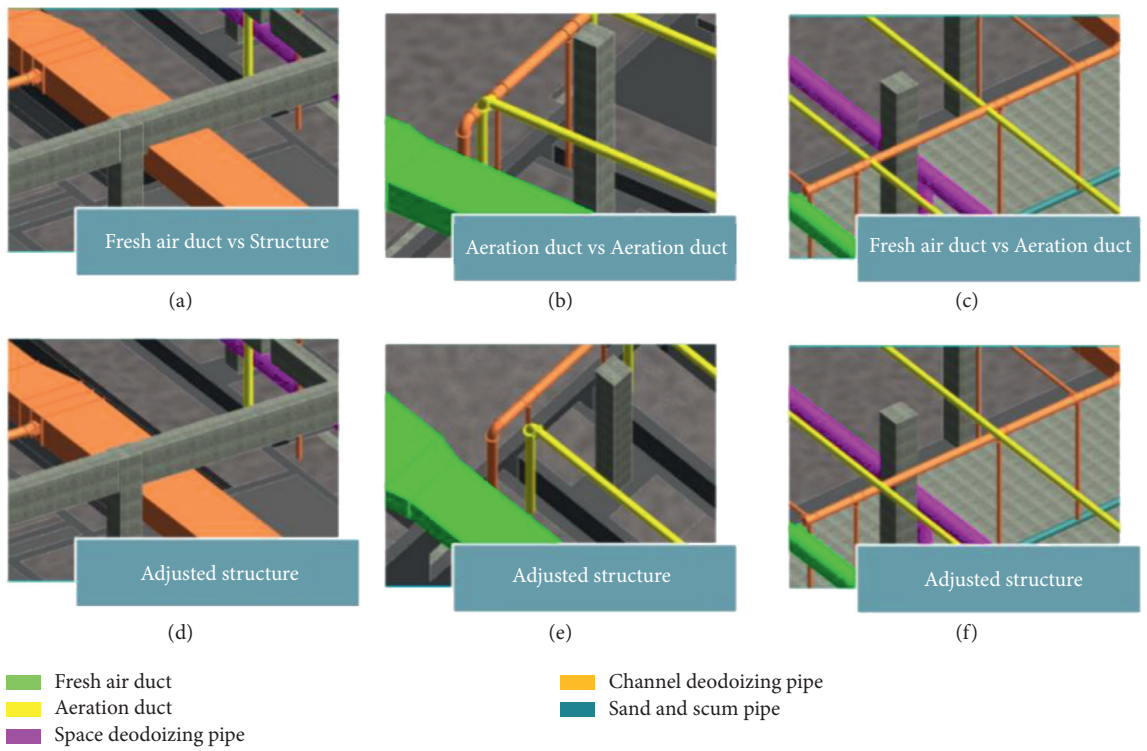


Figure 2: Interference checking and comparison with adjusted structure.

installed in the HWTP structure to collect stress and temperature data and to monitor structural changes in the concrete. Since the interval casting method was used in this project, we were able to create amenable conditions for the subsequent equipment-installation steps and reduce construction time by 35 days (compared with the delayed pour-strip method), thus allowing the single and combined testing processes to be carried out at an earlier date. This process allowed quicker detection and resolution of structural problems, which helped ensure that HWTP could be commissioned on schedule.

*4.2.2. BIM- and IoT-Based Technologies for O&M and Environmental Monitoring*

*(1) BIM- and IoT-Based Monitoring and Analysis of Water Quality and Quantity*. A dynamic digital model for WTP water quantity and quality was created to help control the water treatment processes of HWTP and thus facilitate intelligent O&M management. The intelligent O&M systems of HWTP allowed monitoring of water levels, flow rates, and water quality at its inputs and outputs and in all relevant areas. On this basis, an improved neural network-based algorithm was created to predict the input water quantity. Firstly, we construct the input data and output data; if the BP neural network model contains $n$ variables, we take the data of N consecutive time points in the time-series data ($x_{t\text{-}n+1}$, $x_{t\text{-}n+2}$, $\cdots$, $x_t$) as the input and $x_{t+1}$ as the output, where $x_t$ is the water inflow at $x_t$ time in the time series. The second is to initialize the BP neural network model. The third is model training. Finally, we predict the input water quantity based on the model. The predictions of this algorithm were used to construct a dynamic water-level control model (Figure 5), which helped control the water levels at HWTP under normal conditions and prevented flooding in emergency situations. In addition, the HWTP processes were simulated in BioWin, and the simulation results were then introduced to the BIM system where mathematical models were used to predict the performance of the water treatment process. Therefore, the BIM system could simultaneously analyse the simulated and observed water-quality data (Figure 6) and assist in the regulation of wastewater-treatment processes. Compared with the currently available methods, the proposed method enhanced the predictive and regulation capabilities of the HWTP water treatment processes and helped reduce operational risks. These advantages effectively solve many of the problems associated with the experience-based approach in controlling the wastewater-treatment processes, which is often slow, risky, and wasteful.

*(2) BIM- and IoT-Based Environmental Monitoring and Early Warning System*. According to the HWTP features, we developed a method for the integration of multiprotocol dynamic-monitoring systems using BIM, which incorporated the state-of-the-art multiprotocol real-time data-integration techniques. The integration of currently existing automation systems with the BIM system was a challenging process because it involved a multitude of data-transmission protocols, large amounts of data, and stringent demands for responsiveness. To overcome these issues, we developed a method for integrating BIM with the

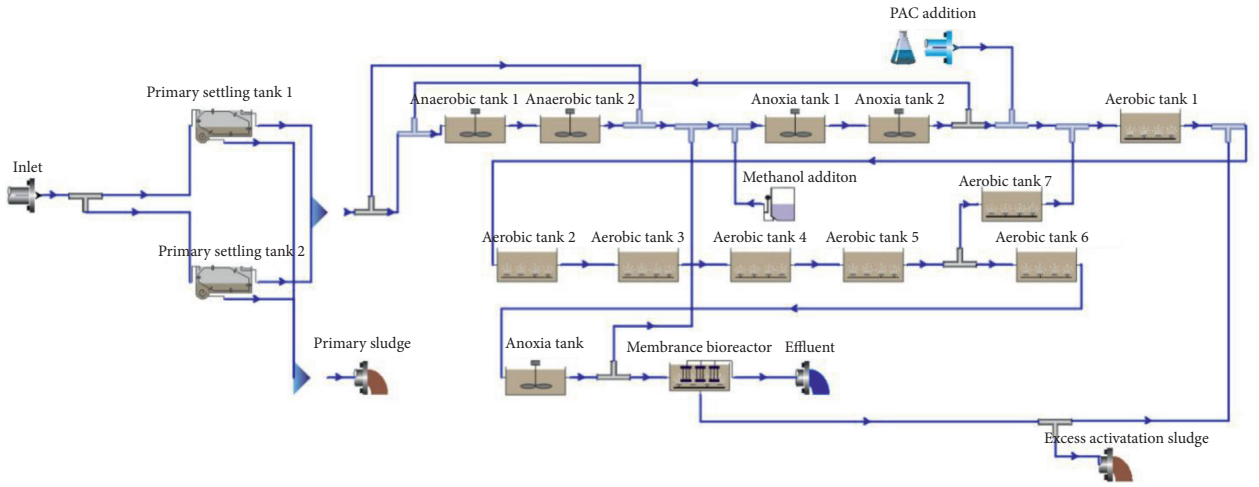


(a)

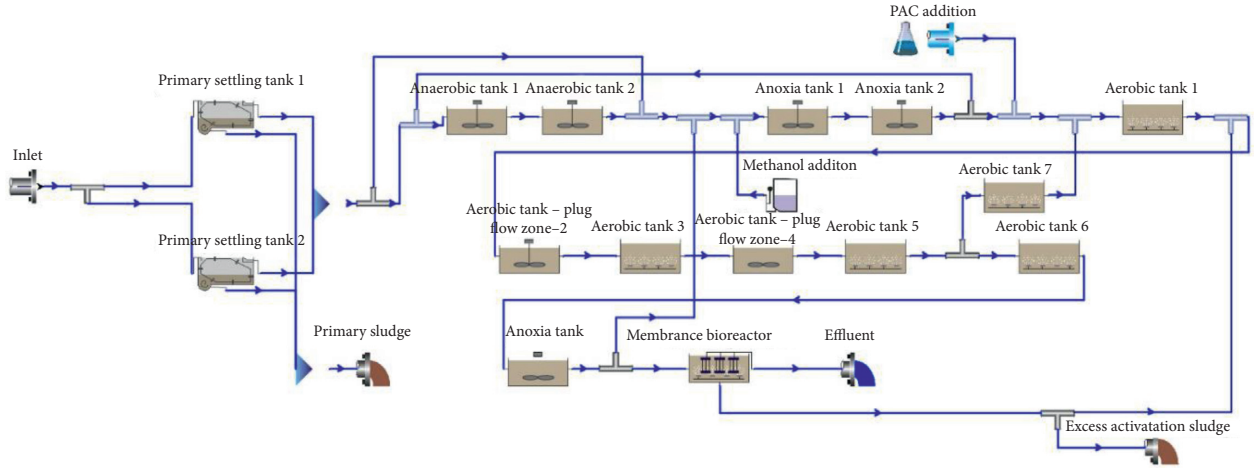


(b)

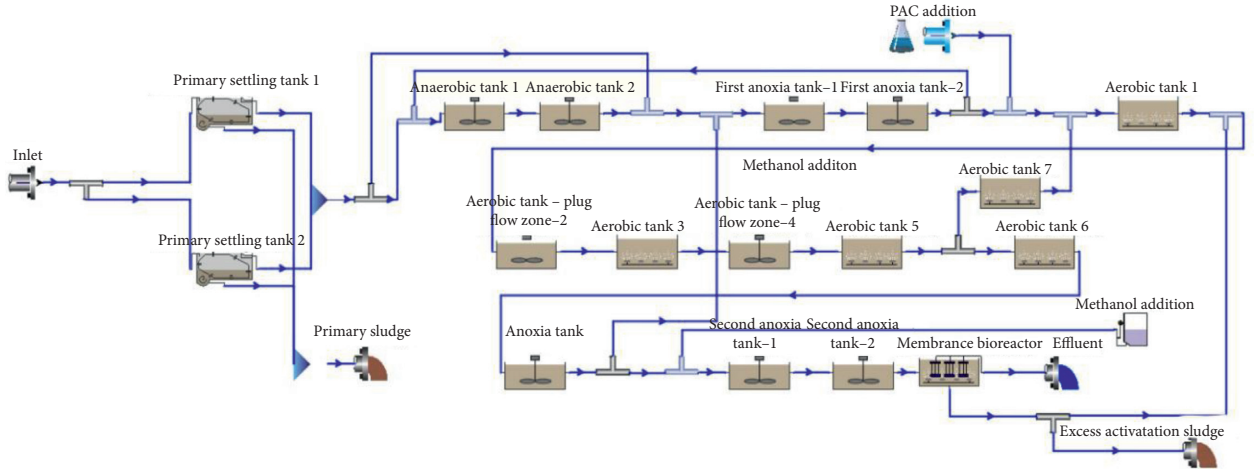


(c)

Figure 3: Simulated process flows: (a) Solution 1; (b) Solution 2; (c) Solution 3.

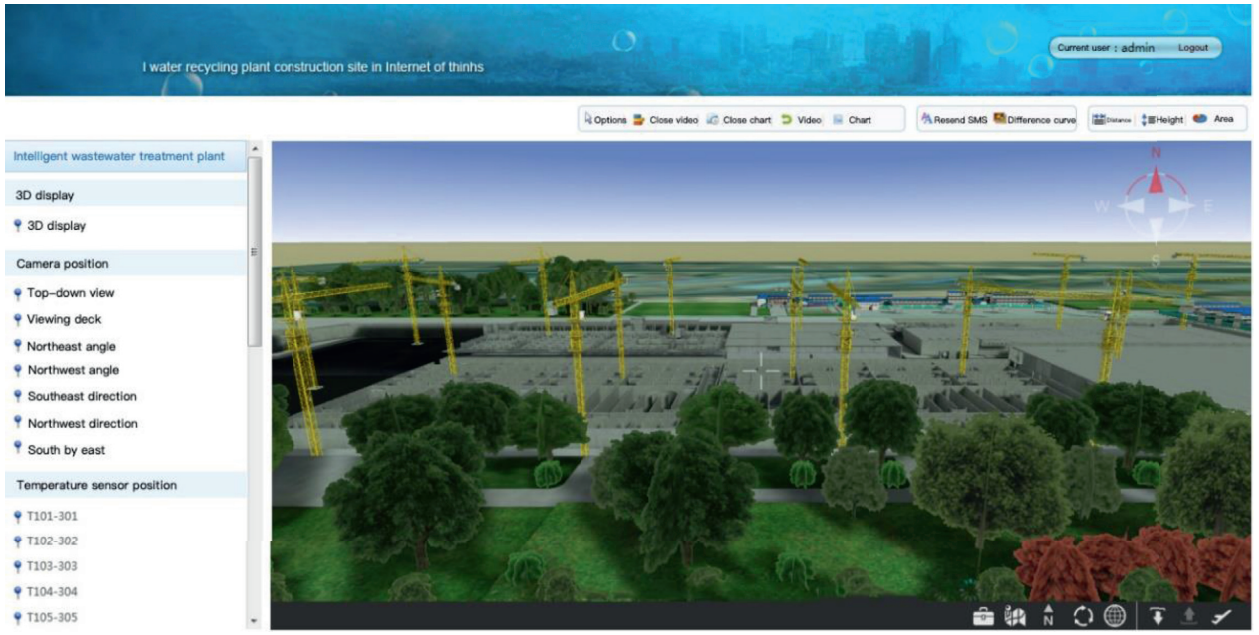


(a)

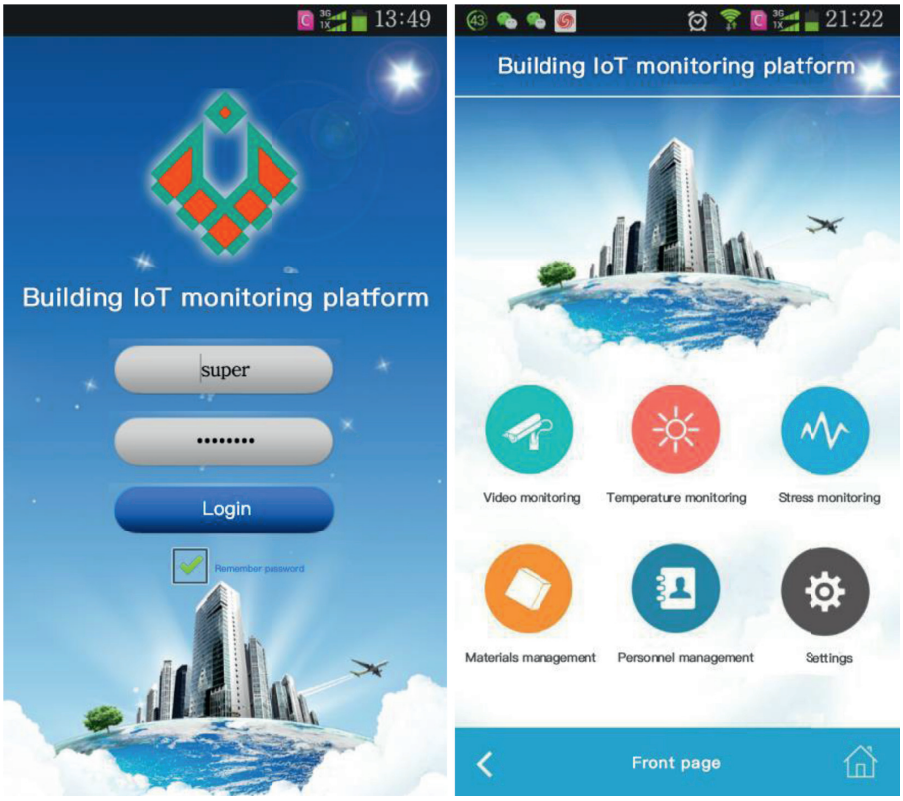


(b)

Figure 4: IoT management platform: (a) web terminal; (b) smartphone app mobile terminal.

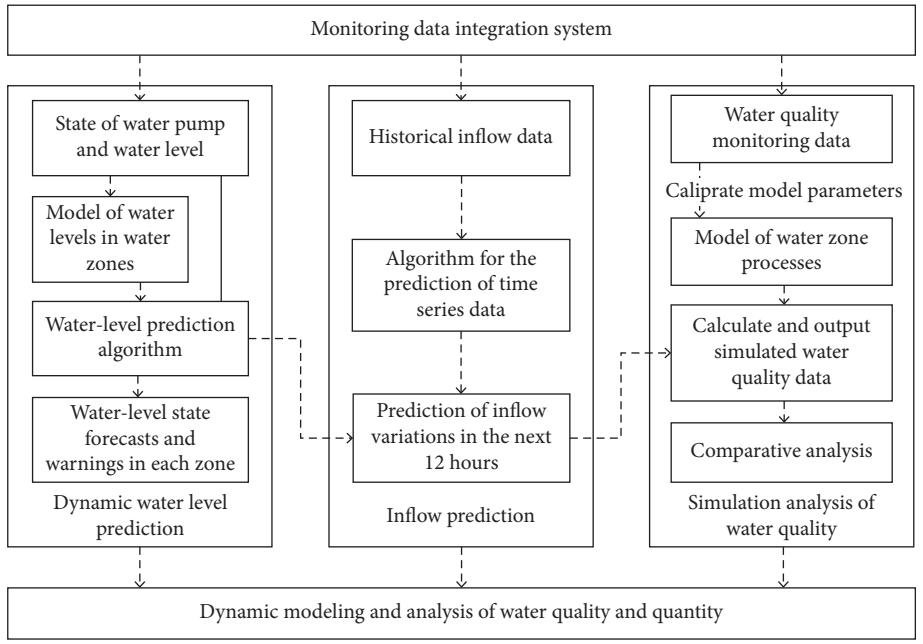


Figure 5: Dynamic water-quality and water-quantity modeling and analysis.

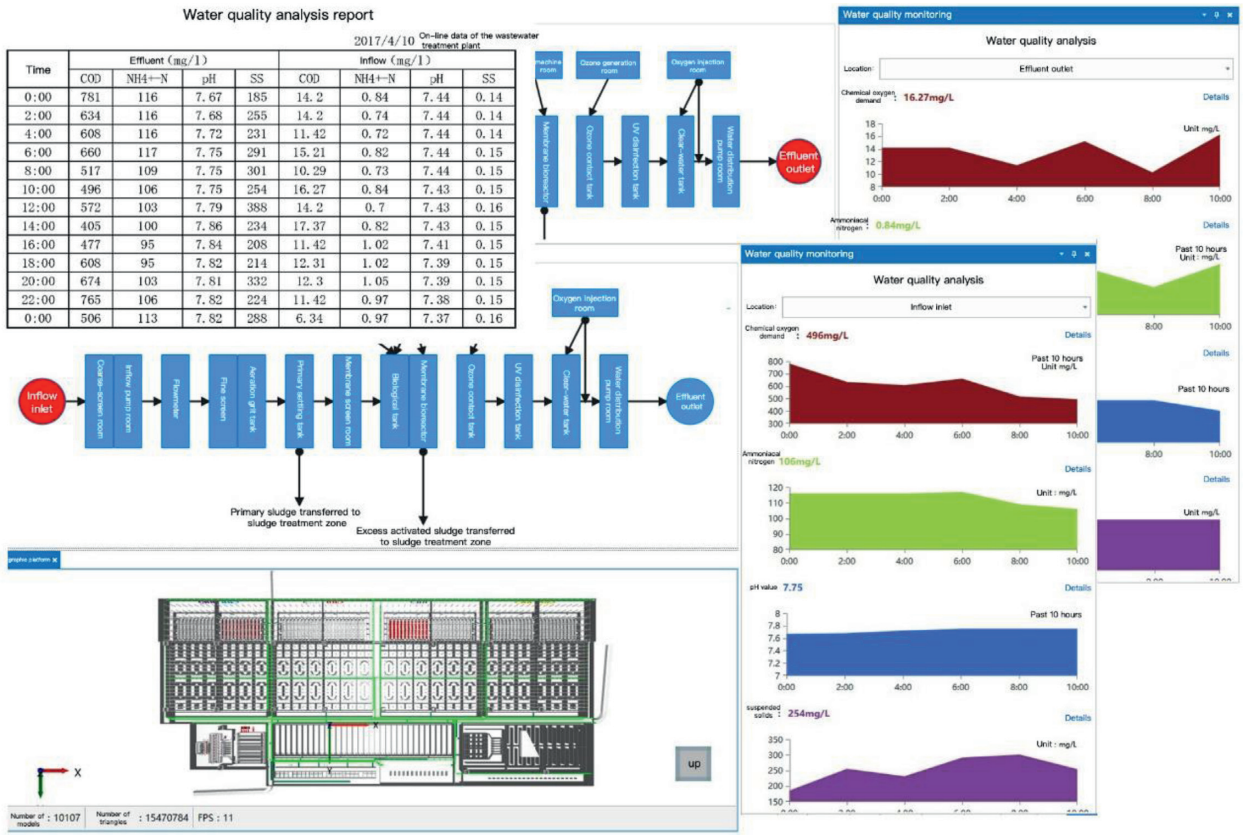


Figure 6: Effluent water-quality monitoring and report output.

multiprotocol dynamic-monitoring systems by employing messaging-based distributed architecture, plug-in-based multiprotocol extension, time-series data processing, in-memory database-based real-time data management, time-series database-based historical data management, and RESTful-based data-query services. Using extended attributed sets, the IFC protocol was extended to enable expression of the sensor entity information, sensor features,

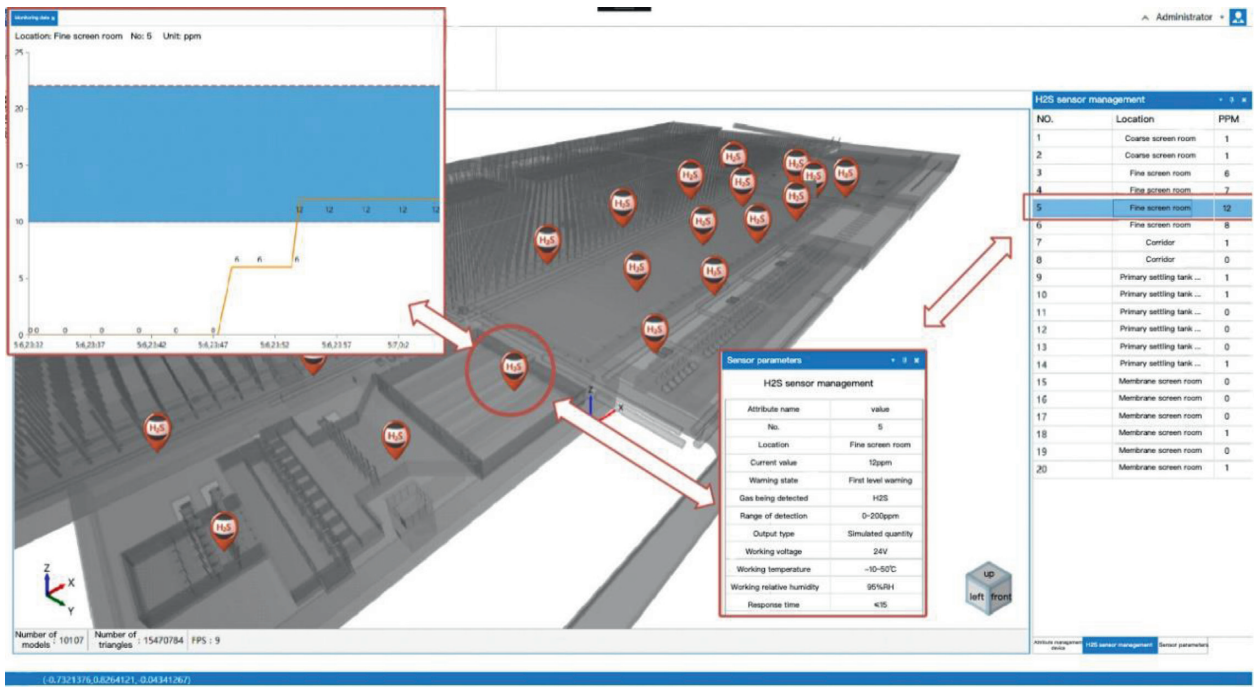


Figure 7: Querying the $H_2S$ sensor-value trends.

transmission-protocol information, relative positioning data, and historical data to enable storage of monitoring data from the O&M management processes. In addition, we virtualized the dynamic physical and environmental monitoring data of HWTP and thus developed an O&M safety management method based on the integration of its physical environment with virtual computing. This method was then supplemented with environmental monitoring and early warning techniques. An early warning and disaster mitigation system for HWTP was thus constructed (Figure 7), which also provided comprehensive analysis and intelligent decisions for O&M safety. Through the provision of early warning, emergency management, disaster simulations, and disaster guidelines, this system could effectively reduce the probability of disaster occurrence and minimize losses in life and property.

## 5. Conclusions and Future Work

The engineering case for the WTP BIM implementation was based on not only specific features of the construction project but also implicit assumptions about the nature of the industry and its work. In the key stages of 3D modeling, operation monitoring, as well as design options comparison and construction simulation, this project makes full use of BIM technology for visual expression, performance analysis, digital simulation, and high-efficiency information transfer. Under the framework of smart engineering design, the project quality, construction management level, and later operational efficiency have been significantly improved. During the design phase, the BIM model was used to perform specialized simulations of the key nodes to help optimize its design and the BioWin simulator was used to simulate and optimize the WTP processes and provide technical support for the O&M processes. During the construction phase, a BIM- and IoT-based construction platform was established which effectively improved the ability of fine management and control of the project. During the O&M phase, the WTP realized scientific management and intelligent O&M based on BIM and IoT technology, such as automatic monitoring and analysis of water quality and quantity and environment. Therefore, the project realized the transmission and sharing of data in the whole life cycle and maximized the cooperation of all participants, which played an important role in improving production efficiency, saving cost, and shortening construction period. In the end, the project became a model of a smart underground wastewater-treatment plant.

In addition to the papers presented in the literature review, this paper is one of the first developments of BIM applied in the WTP construction and O&M. Considering the evolution of the IoT and development of the digital twin and artificial intelligence, we believe that the construction of intelligence WTP should be further developed in the following two aspects.

First, future WTP developments should incorporate deep learning. Currently, the combination of advanced software and hardware has enabled partial automation and "intelligentization" of the WTP construction and O&M. However, a large amount of human input is still needed, and we have yet to solve the root causes of the issues associated with the experience-based approaches for the control of wastewater-treatment processes, which are often slow, risky, and wasteful. As we continue to accumulate data from the WTP operation, artificial-intelligence techniques such as deep learning will be needed to create predictive models for

WTP operations, which will greatly increase the accuracy of these predictive models.

Second, intelligent control systems should be developed for WTP operations. Although some works have been done on the monitoring and prediction of input water quality and operation control at HWTP, human intervention remains necessary for sewage treatment. Therefore, in the future, we should aim to create a cyber physical system that will enable systematic and intelligent control of wastewater-treatment systems.

## Data Availability

The data used to support the findings of the study are included in the article.

## Conflicts of Interest

The authors declare that they have no conflicts of interest.

## Acknowledgments

The authors would like to acknowledge the Consulting research project of Chinese Academy of Engineering and the Beijing Science and Technology Project for financially supporting this work under contract number 2016-XZ-14 and Z151100002115054 and thank the contractor and project staff who participated.

## References

[1] IEA, *The 2019 Global Status Report for Buildings and Construction*, United Nations Environment Programme, Nairobi, Kenya, 2019.

[2] P. J. Davies, S. Emmitt, and S. K. Firth, "Delivering improved initial embodied energy efficiency during construction," *Sustainable Cities and Society*, vol. 14, pp. 267–279, 2015.

[3] I. Z. Bribian, A. V. Capilla, and A. A. Uson, "Life cycle assessment of building materials: comparative analysis of energy and environmental impacts and evaluation of the eco-efficiency improvement potential," *Building and Environment*, vol. 46, no. 5, pp. 1133–1140, 2011.

[4] J. P. Xu, Y. W. Deng, Y. Shi et al., "A bi-level optimization approach for sustainable development and carbon emissions reduction towards construction materials industry: a case study from China," *Sustainable Cities and Society*, vol. 53, pp. 1–15, 2020.

[5] M. Honic, I. Kovacic, and H. Rechberger, "Improving the recycling potential of buildings through Material Passports (MP): an Austrian case study," *Journal of Cleaner Production*, vol. 217, pp. 787–797, 2019.

[6] N. Wang, "The role of the construction industry in China's sustainable urban development," *Habitat International*, vol. 44, pp. 442–450, 2014.

[7] U. Berardi, "Clarifying the new interpretations of the concept of sustainable building," *Sustainable Cities and Society*, vol. 8, no. Complete, pp. 72–78, 2013.

[8] R. M. Pulselli, E. Simoncini, F. M. Pulselli, and S. Bastianoni, "Emergy analysis of building manufacturing, maintenance and use: em-building indices to evaluate housing sustainability," *Energy and Buildings*, vol. 39, no. 5, pp. 620–628, 2007.

[9] UNEP, *Sustainable Building and Construction: Facts and Figures*, United Nation Environment Programme: Industry And Environment, Nairobi, Kenya, pp. 5–8, 2003, Online] Available from http://www.uneptie.org/media/review/vol26no2-3/005-098.pdf (Accessed: 19 March 2017.

[10] Y. Xing, N. Hewitt, and P. Griffiths, "Zero carbon buildings refurbishment--A Hierarchical pathway," *Renewable and Sustainable Energy Reviews*, vol. 15, no. 6, pp. 3229–3236, 2011.

[11] G. Ali, T. John, G. Amirhosein et al., "Building Information Modelling (BIM) uptake: clear benefits, understanding its implementation, risks and challenges," *Renewable & Sustainable Energy Reviews*, vol. 76, pp. 1046–1053, 2017.

[12] M. Oraee, M. R. Hosseini, E. Papadonikolaki, R. Palliyaguru, and M. Arashpour, "Collaboration in BIM-based construction networks: a bibliometric-qualitative literature review," *International Journal of Project Management*, vol. 35, no. 7, pp. 1288–1301, 2017.

[13] I. Othman, Y. Y. Al-Ashmori, Y. Rahmawati et al., "The level of building information modelling (BIM) implementation in Malaysia," *Ain Shams Engineering Journal*, vol. 12, pp. 455–463, 2020.

[14] B. Ilhan and H. Yaman, "Meta-analysis of building information modeling literature in construction," *International Journal of Engineering and Innovative Technology*, vol. 3, no. 4, pp. 373–379, 2013.

[15] N. Bui, C. Merschbrock, and B. E. Munkvold, "A review of building information modelling for construction in developing countries," *Procedia Engineering*, vol. 164, pp. 487–494, 2016.

[16] D. Migilinskas, V. Popov, V. Juocevicius, and L. Ustinovichius, "The benefits, obstacles and problems of practical bim implementation," *Procedia Engineering*, vol. 57, pp. 767–774, 2013.

[17] Y. Y. Al-Ashmori, I. B. Othman, Y. Rahmawati et al., "BIM benefits and its influence on the BIM implementation in Malaysia," *Ain Shams Engineering Journal*, vol. 11, pp. 1013–1019, 2020.

[18] S. Azhar, M. Khalfan, and T. Maqsood, "Building information modeling (BIM): now and beyonds," *Australasian Journal of Construction Economics and Building*, vol. 12, no. 4, pp. 15–28, 2012.

[19] J. L. Li, *Key Technologies and Engineering Applications of Smart construction*, China Construction Industry Press, Beijing, China, 2017, in Chinese.

Hindawi
Advances in Civil Engineering
Volume 2021, Article ID 8811684, 13 pages
https://doi.org/10.1155/2021/8811684

*Research Article*

# An Experiment-Based Simplified Method for the Model of Building Groups in CFD Simulation

**Hongling Guo**,[1] **Ying Zhou**,[1] **Yingxin Li**,[1] **Zhihui Zhang**,[1] **and Heng Li**[2]

[1]*Department of Construction Management, Tsinghua University, Haidian District, Beijing 100084, China*
[2]*Department of Building and Real Estate, The Hong Kong Polytechnic University, Hung Hom, Hong Kong, China*

Correspondence should be addressed to Hongling Guo; hlguo@tsinghua.edu.cn

Received 1 August 2020; Revised 9 December 2020; Accepted 28 March 2021; Published 14 April 2021

Academic Editor: Luigi Aldieri

Copyright © 2021 Hongling Guo et al. This is an open access article distributed under the Creative Commons Attribution License, which permits unrestricted use, distribution, and reproduction in any medium, provided the original work is properly cited.

Computational Fluid Dynamics (CFD) has been widely used in the simulation and analysis of community or urban wind environments. However, the CFD-based wind simulation of large-scale building groups usually consumes a lot of computing resources with high computing costs. To improve the efficiency of CFD-based wind simulation, this paper presents an experiment-based simplified method for the model of building groups. Two rectangular buildings are adopted as the basic unit and four control parameters ($B/L$, $W/L$, $H/L$, and $D/L$) are selected as the experiment factors to analyze the geometrical relationship of the two buildings. Note that $L$, $W$, and $H$, respectively, represent the windward edge length, width, and height of a building, $B$ is building interval distance, and $D$ is the distance between two building center axes. Then, a single factor experiment and an orthogonal experiment are designed and performed to determine the reasonable value range of each factor. Based on the experiment results and actual situation, the value ranges of four factors for the simplification of building group models are determined as follows: $B/L \in \{0, 1.5\}$, $W/L \in \{0, 2\}$, $D/L \in \{0, 0.25\}$, and $H/L \in \{0, 1\}$. Furthermore, a real case is presented to evaluate the performance of the proposed simplified method. The results indicate that the simplified method is able to improve the efficiency of CFD-based wind simulation of building groups, with the number of buildings decreasing from 620 to 395 (by 36.3%), and the number of tetrahedral grids decreasing from 8,832,199 to 7,766,778 (by 12.1%). Thus, this research contributes to the CFD-based wind simulation method of large-scale building groups and the analysis of the urban wind environment.

## 1. Introduction

Urban wind environment has attracted growing attention from urban planners. Previous research has shown that outdoor temperature is increased by 1.9°C with the wind speed decreasing from 1 m/s to 0.3 m/s, and the wind speed for thermal comfort in subtropical cities in summer is about 1.6 m/s [1]. Besides, the planning of urban wind environment has a significant impact on urban climate issues such as urban heat island effect, pollutant diffusion, usage of wind energy, and air quality [2–4]. Good wind environment contributes to a pleasant human living environment and plays an important role in constructing green ecological cities.

Simulation methods and technologies are being used in the analysis of urban wind environment. Particularly, Computational Fluid Dynamics- (CFD-) based simulation methods are attracting urban planners. Early CFD was developed for spacecraft design under special conditions. In the late 1970s, NASA designed experimental aircraft Highly Operational Aircraft Technology (HIMAT) [5] with CFD technology. With the improvement of computational performance, the application of CFD has been expanded to different industries, such as automobile and engine design, shipbuilding, civil engineering, and environmental engineering. In the study on urban wind environment, compared with traditional research methods (e.g., field measurement and wind tunnel test), CFD is more cost-effective, time-saving, and information-detailed. It can also simulate different spatial dynamics like hurricanes. Otherwise, CFD simulation can be applied to promote the accurate recognition of urban wind environment in the urban planning

stage, thus improving the quality of architectural design and urban planning.

However, in the CFD-based wind simulation of large-scale building groups, millions of grids need to be generated to describe the flow field exactly and completely, which requires high computational performance. In addition, CFD needs to rebuild the model of building groups and thus slow down relevant simulation as design alterations take place in urban planning. Therefore, it is obvious that the reasonable simplification of geometric models of building groups can enhance the efficiency of CFD-based wind simulation. To solve the aforementioned problem, this paper proposes a simplified method for the model of a cluster of buildings to reduce the computational cost from the perspective of a geometric model by the reasonable consolidation (simplification) of building models. It also considers the balance between computational efficiency and accuracy to promote the application of CFD in urban wind environment simulation.

## 2. Literature Review

The research on the CFD-based simulation of urban wind environment can be generally classified into two categories, i.e., the wind simulation of a single building and that of building groups. The former is mainly about the analysis of airflow inside or around a single building, focusing on the relationship between the building structure and wind environment. The wind environment mainly refers to indoor and outdoor natural ventilation and airflow. According to different types of structures, there are atrium buildings [6], sunroof buildings [7], serrated roof buildings [8], and other structures [9–12]. Reasonable building exterior design and elevation layout can facilitate air exchange, improve thermal comfort, and reduce building energy consumption. Thus, the research on the wind environment of a single building becomes more and more popular in the design of green buildings.

Moreover, the CFD-based wind simulation of building groups focuses on airflow among city streets, public places, and different buildings. According to the scale, building groups in an urban area can be classified into urban (up to 10 or 20 km), neighborhood (up to 1 or 2 km), and street scale (less than 100–200 m), to which different simulation accuracy and modeling methods are applicable [1]. In the street scale, Omar et al. analyzed the outdoor ventilation of different buildings combination structures in different wind directions and concluded that the central space formed by adjacent buildings and the building facing main wind are conducive to airflow [13]. Wang et al. used CFD to study the relationship between wind and orthogonal building layout and found that orthogonal building layout has higher wind energy density than a single building [2]. James explored the effects of building disturbances on natural ventilation by comparing airflow efficiency under conventional and misaligned rows; the results indicate that reasonable alternate distribution and building orientation can improve ventilation efficiency [14].

As for the neighborhood scale, previous research shows that the layout of streets has a great impact on the wind environment. Cao et al. analyzed the relationship between street direction and wind speed to show the impacts on urban thermal environment, which is significant to the street design [15]. Ramponi et al. [16] did the CFD simulation of wind environment in equal width or unequal width parallel streets in different areas and concluded that ventilation reduces in the downwind districts [3]. In addition, some researchers studied the wind environment of building groups with different properties. Huang et al. used 2D CFD to analyze the impact of gable roofs on airflow and pollutant diffusion in urban street canyons [3]. Hang compared the natural ventilation of different wind directions in open and semiopen urban spaces [17]. Yuan et al. developed a model with CFD to simulate air pollution dispersion and natural ventilation in high-density areas and found that reasonable urban planning can improve the air quality indoor and in street canyons [18]. Furthermore, Yuan et al. applied the semiempirical model to simulate the wind environment of high-density urban areas and developed a modeling-mapping approach to balancing modeling cost with result accuracy, which is statistically significant to evaluating wind speed in large-scale districts but lacks the theoretical support of physics [18].

At the urban scale, there is little research, particularly on the simplified method of building models. Tominaga et al. specified the boundary condition in the CFD simulation of a single building by substituting some simplified geometries for a cluster of buildings [19]. Other relevant research did not propose a quantifiable method to simplify the model of building groups. In order to simulate the urban wind environment, Wu et al. built a simplified model, in which the ratio of building space to building height and the ratio of separation distance to building length were selected as key parameters for the analysis of environmental effects [20]. However, the comparative analysis was not quantified. Moreover, the model is more ideal and thus limited to a certain of buildings because the selection and analysis of parameters are not comprehensive. For instance, the axis offset of staggered layout buildings is neglected and the influence of some parameters on the simplification of building models not analyzed.

Based on the current research, this research will develop a simplified method for the model of building groups with comprehensive parameters by simulating and analyzing the relationship between buildings and the mechanism of the wind environment without affecting the general trend of regional airflow.

## 3. Methodology

*3.1. Definition of Model Simplification.* It is difficult to comprehensively analyze the impact of building layout on wind environment as the layout of building groups varies from one to another. Previous research found that the differences in building layout [21] and elevation [22] had obvious effects on the wind environment. Therefore, two identical rectangular buildings in parallel are extracted as the ideal basic unit before the simplification to represent the layout of adjacent buildings in most building groups. As

shown in Figure 1, the simplification in this research means that the basic unit can be replaced with a parallelogram formed by the contour line of the building group. European Cooperation in the Field of Science and Technical Research (COST) suggests that an initial choice should be at least 10 cells per building side and 10 cells per cube root of building volume in CFD simulation [23]. Under the resolution requirements of COST, the simplification of the model will theoretically reduce the number of grids with consuming less time and labor. Besides, the reduction of strange-shaped space can also improve grid quality and save computational cost.

*3.2. Selection of Control Parameters.* The simplification of building groups needs to comply with certain rules. Control parameters are used to determine whether or not the model of a building group can be combined or simplified. Control parameters are specific quantitative expressions of complicated model space relationships and can reflect the characteristics of the complex shape to a certain extent. Some researchers used the ratio of building spacing and offset distance to the size of building to express the characteristics of building groups, while others used the ratio of windward area and projected area to building area as control parameters. The spatial relationship of a group of buildings is also selected as the control parameters of the simplified method in this research, but neglecting those factors difficult to quantify, such as complex topography, water, and vegetation. To determine the control parameters, we propose a basic building unit consisting of two identical rectangular buildings arranged along the wind direction, involving five variables, i.e., the dimensions of a building model (windward edge length ($L$), width ($W$), and height ($H$)) and the building group offsets (building interval distance ($B$) and distance between two building center axes ($D$)) (see Figure 2). To make control parameters dimensionless and universal, we used the ratios of different variables as the control parameters. Considering that the windward edge length ($L$) has a great impact on the range of the wind shadow area behind a building, in order to reduce the system error caused by wind shadow, the ratios of $W$, $H$, $B$, and $D$ to $L$ (i.e., $B/L$, $W/L$, $H/L$, and $D/L$) are selected as the control parameters for subsequent experiments.

*3.3. Determination of Value Ranges of the Control Parameters.* Single factor experiment and orthogonal experiment are performed in this research to determine the appropriate value range of each control parameter for the model simplification of building groups. Figure 3 illustrates the entire process of experiments from a technical perspective. Note that $[\alpha, \beta]$ and $[\alpha', \beta']$ are to, respectively, represent the results (i.e., the value ranges of control parameters) of single factor experiment and orthogonal experiment, and P represents the selected parameters (i.e., $B/L$, $W/L$, $H/L$, and $D/L$), thus meaning $\alpha \le \alpha' \le P \le \beta' \le \beta$. Only one factor is changing in the single factor experiment, with other factors remaining fixed to analyze the specific effect of the changing factor on experimental results. Besides, as the preparation of

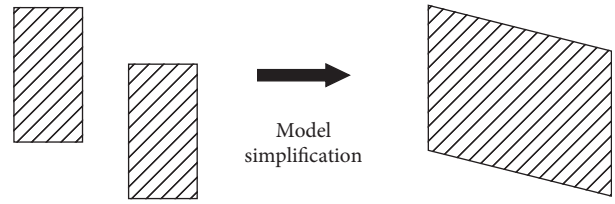


Figure 1: Schematic diagram of model simplification (plan view).

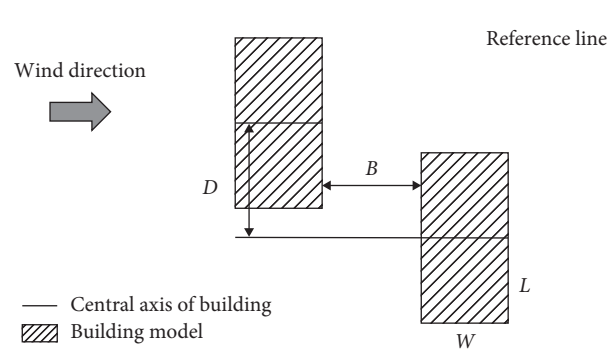


$D$: Distance between two building center axes
$B$: Building interval distance
$L$: Windward edge length of a building
$W$: Width of a building

Figure 2: Variables in the basic unit (building group).

the orthogonal experiment, the single factor experiment explores the function of each parameter to figure out the appropriate value range of each control parameter in the design process of the orthogonal experiment.

Orthogonal experiment using orthogonal tables for multifactor analysis can reliably infer the conclusion of a comprehensive experiment through a small number of selected representative tests with an optimized experimental scheme. Based on the results of the single factor experiment, the orthogonal experiment can not only analyze the interaction between different factors but also significantly reduce test times. And the effects of different control parameters on experimental results are ordered by intuitive analysis and variance analysis to select the optimal value and the suboptimal value as the optimal value range of each control parameter. Finally, the coordinated control indexes are verified by suitability verification.

## 4. Experiment Setup

*4.1. Design of Single Factor Experiment.* Four groups of single factor experiment were designed to analyze the four factors ($B/L$, $W/L$, $H/L$, and $D/L$). Considering the actual size of general buildings, $L$ was set to 30 m. Besides, the control parameters of the initial model in the single factor experiment were set as follows: $B/L = 0.5$, $W/L = 1$, $H/L = 1$, and $D/L = 0$. Figure 4 shows the initial model for the single experiment, in which $L * W * H = 30\,\text{m} * 30\,\text{m} * 30\,\text{m}$, $B = 15\,\text{m}$, and $D = 0\,\text{m}$. In the same way, the upper limit values of $B/L$, $W/L$, and $H/L$ were all set to 3, with six levels in equidistant distribution. As the projected area of the upwind building to the

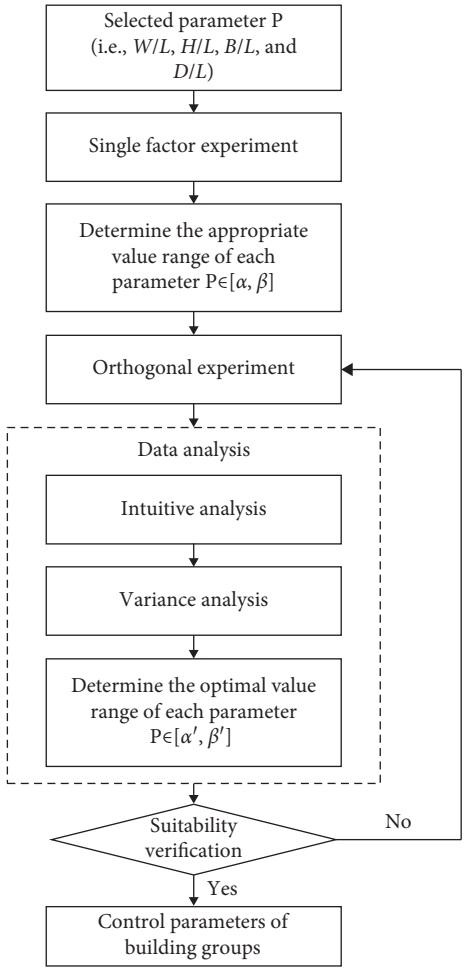


Figure 3: Technical roadmap of the entire experiment.

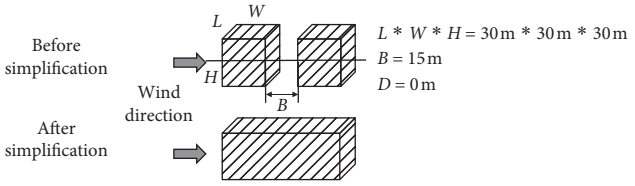


Figure 4: The initial model of the single factor experiment.

downwind building is greater than or equal to 0, which meant $D \leq L$, the upper limit of $D/L$ was 1 and set to six levels with the equidistant distribution. The corresponding control parameters of the single factor experiment are shown in Table 1, while other control parameters stay the same as those of the initial model.

*4.2. Design of Orthogonal Experiment.* The value ranges of four factors obtained from the single factor experiment were set to 4 levels in the following orthogonal experiment. According to the selection principle of the orthogonal table (i.e., to select a smaller experiment table based on the number of factors less than that of the column in an orthogonal table and the number of factor levels same as that of the orthogonal table), for the 4-factor-4-level experiment, a 5-factor-4-level orthogonal experiment table L16 ($4^5$) was selected (see Table 2). In comparison with the number of comprehensive tests, that of the test was effectively decreased from 256 ($4^4$) to 16.

Table 1: The level of control parameters of the single factor experiment.

| Level | $B/L$ | $W/L$ | $H/L$ | $D/L$ |
|---|---|---|---|---|
| 1 | 0.5 | 0.5 | 0.5 | 0 |
| 2 | 1 | 1 | 1 | 0.2 |
| 3 | 1.5 | 1.5 | 1.5 | 0.4 |
| 4 | 2 | 2 | 2 | 0.6 |
| 5 | 2.5 | 2.5 | 2.5 | 0.8 |
| 6 | 3 | 3 | 3 | 1 |

*4.3. Result of the Calculation Method.* In this research, deviation, as the criterion to evaluate experiments, refers to the speed changes at the reference line after simplification and consolidation.

*4.3.1. Selection of Reference Line.* As the basis of the deviation analysis, the reference line was selected as follows:

(1) The line located at 20 m behind the building group is in a general distance behind the model to show the influence of the front buildings on the rear buildings

(2) The line is 1.5 m height (pedestrian level), in which wind speed is a primary indicator of wind comfort in wind environment evaluation

(3) The line's length is as long as that of the calculation field, and the wind speed change in the entire computational domain was assessed

*4.3.2. Deviation Calculation.* The deviation is defined as

$$\Delta = \frac{\int_a^b \left| f_1 x - f_2(x) \right| \mathrm{d}x}{\int_a^b f_1(x) \mathrm{d}x}, \quad (1)$$

where $a$ and $b$ are the range of computational domain; $b - a = l$ is the length of the computational domain along the reference line; $f_1(x)$ and $f_2(x)$ are the fitting curves, respectively, for pre- and postconsolidation wind speed along the reference line.

Since the output value of CFD software is the wind speed at the reference line, it is difficult to form relevant fitting functions. To simplify this, this research inserted 1000 interpolation points into the initial data points according to the interpolation algorithm to get the following two sets of data points:

$f_1(x)$: $y_1, y_2, \ldots, y_{1000}$

$f_2(x)$: $z_1, z_2, \ldots, z_{1000}$

Then,

Table 2: Orthogonal experiment table L16 ($4^5$).

| Test number | Column number | | | | |
|---|---|---|---|---|---|
| | 1 | 2 | 3 | 4 | 5 |
| 1 | I | I | I | I | I |
| 2 | I | II | II | II | II |
| 3 | I | III | III | III | III |
| 4 | I | IV | IV | IV | IV |
| 5 | II | I | II | III | IV |
| 6 | II | II | I | IV | III |
| 7 | II | III | IV | I | II |
| 8 | II | IV | III | II | I |
| 9 | III | I | III | IV | II |
| 10 | III | II | IV | III | I |
| 11 | III | III | I | II | IV |
| 12 | III | IV | II | I | III |
| 13 | IV | I | IV | II | III |
| 14 | IV | II | III | I | IV |
| 15 | IV | III | II | IV | I |
| 16 | IV | IV | I | III | II |

$$\Delta = \frac{|y_1 - z_1| * \Delta x + |y_2 - z_2| * \Delta x + \cdots + |y_m - z_m| * \Delta x}{y_1 * \Delta x + y_2 * \Delta x + \cdots + y_m * \Delta x} = \frac{\sum_{i=1}^{m} |y_i - z_i|}{\sum_{i=1}^{m} y_i}. \quad (2)$$

*4.4. CFD Simulation Settings.* ANSYS Fluent 16.1 was used for CFD simulation and the simulation settings are shown in Table 3.

Considering a large number of simulation experiments required in the research, the standard $k$-$\varepsilon$ model was used for the advantage of low computing cost, little fluctuation, high accuracy in calculation, and extensive application in low-speed turbulence. Computational domain and the settings of boundary condition and grid resolution referred to the CFD simulation standard of Architectural Institute of Japan (AIJ) [19]. To decrease the systematic error created by model simplification and coordination, the simplified model had the same grid expansion ratio, grid resolution, and boundary condition as the original model.

## 5. Data Analysis

*5.1. Analysis of Single Factor Experiment.* Figure 5 displays the changes of experiment deviation $\Delta$ in different levels in the four single factor tests (i.e., $B/L$, $W/L$, $D/L$, and $H/L$). Some findings are presented as follows.

Deviation $\triangle$ has a positive correlation with $B/L$ and $D/L$ (see Figures 5(a) and 5(c)), which indicates that the velocity difference in the reference line after simplification expands with the increase of $B/L$ and $D/L$. This is because the space formed by consolidating the two buildings becomes larger and larger with the increase of building distance B and offset distance $D$, thus further blocking the downdraft and transverse airflow in the building gaps to increase the change of wind speed.

Deviation $\triangle$ has an approximate negative correlation with $W/L$ (see Figure 5(b)), and the difference in velocity decreases as $W/L$ increases. The reason is that the width of buildings has less influence on the wind shadow area, and with the increase of W, the relative change of volume of building group before and after consolidation decreases, thus reducing disturbance on air ventilation.

Deviation $\triangle$ has an overall positive correlation with $H/L$ (see Figure 5(d)) and the fluctuation of data point is due to the scale change of the wind shadow area. When $H/L = 0$, there is no barrier in front of the reference line; consolidation has no effect on the results. With the increase of $H/L$, the wind shadow area that is directly proportional to the building height becomes larger and thus, the difference of velocity is more affected by $H/L$.

In summary, the results of all single factor experiments indicate that factor $D/L$ has a great effect on the wind speed deviation followed by $B/L$, $H/L$, and $W/L$. The exact order of the influence is further confirmed by the following orthogonal experiment. Moreover, the experiment results are basically consistent with the theoretical prediction, thus being able to be a reference for the orthogonal experiment.

*5.2. Supplemental Design of Orthogonal Experiment.* According to the results of the single factor experiment, the monotonous zone of each factor was selected as its value range in the orthogonal experiment as follows: $B/L$: 0–2, $W/L$: 0–2, $H/L$: 0–2, and $D/L$: 0-1. The value ranges of all factors were set to four levels with equal intervals and the levels were selected randomly to avoid systematic errors caused by human factors. The levels of the factors in the orthogonal experiment are presented in Table 4.

All of the four factors and four levels mentioned above were substituted to Table 2, thus getting Table 5 including 16 tests. The fifth column in Table 5 was retained as an error column for the interaction test. $L$ in the orthogonal experiment was 30 m, the same as that in the single factor experiment. The parameters of 16 orthogonal tests were converted according to the horizontal distribution of the

Table 3: Simulation settings in ANSYS Fluent.

| | |
|---|---|
| Grid generation | Unstructured grid<br>Grid expansion ratio: 1.2<br>Grid resolution: ≤ 1/10 of each edge of the building |
| Computational domain | The distance between the building outer boundary and the computational domain edge: ceiling ≥5$H$, inflow boundary ≥5$H$, cross-range ≥5$H$, outflow boundary ≥15$H$<br>$X * Y * Z$: 2000 m * 1500 m * 600 m |
| Boundary condition | Inflow boundary and ceiling boundary: velocity-inlet—$v = U_{10} * (Z/10)^{0.3}$<br>Outflow boundary: pressure-outlet—101325 Pa<br>Lateral boundary: symmetry<br>Ground and building surface: wall |
| Operation pressure | 101325 Pa |
| Model | Standard $k$-$\varepsilon$ model |
| Near wall treatment | Enhanced wall functions |
| Solving algorithms | SIMPLEC |

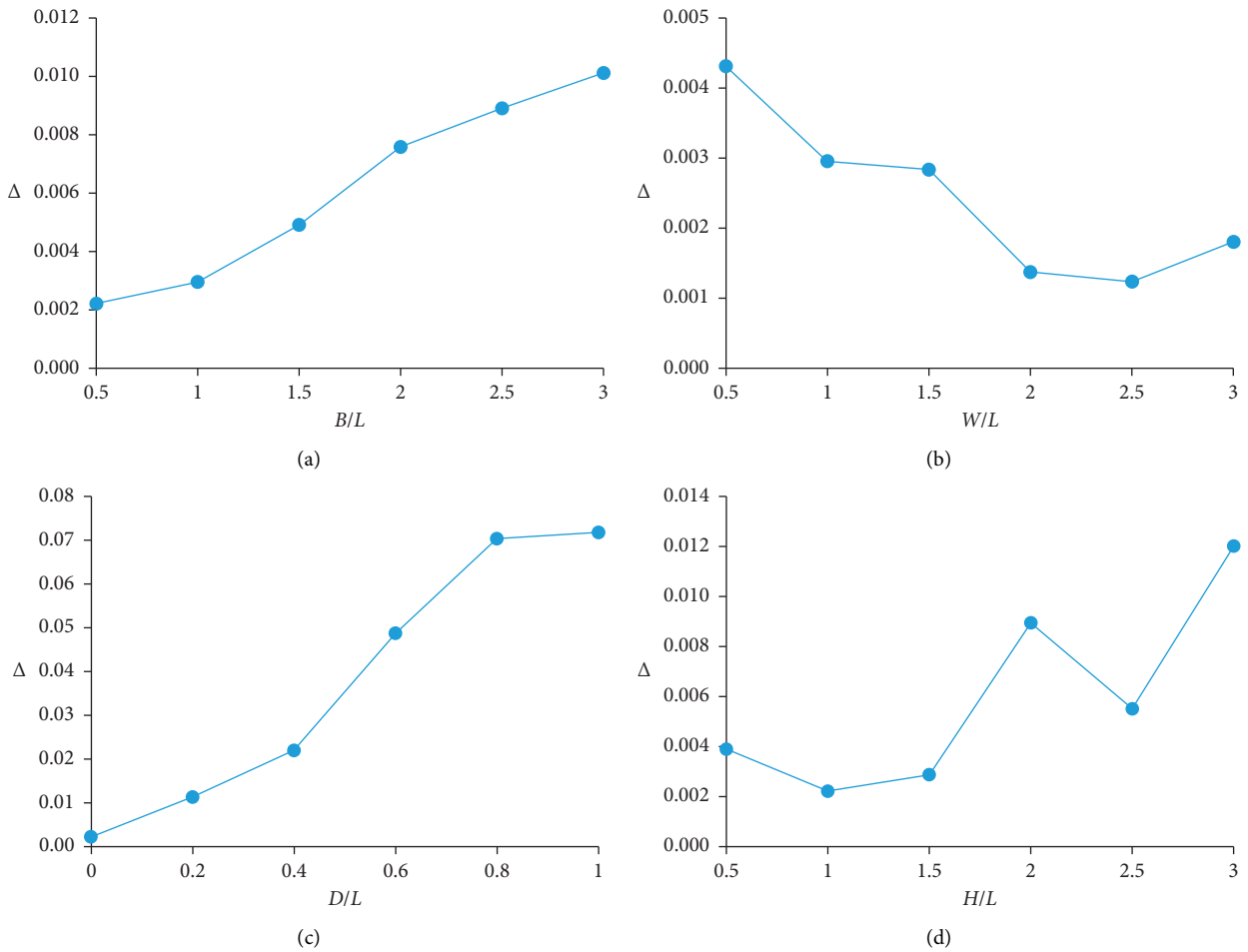


Figure 5: Changes of experiment deviation in different levels in four single factor tests. (a) Experiment deviation with $B/L$ changing from 0.5 to 3. (b) Experiment deviation with $W/L$ changing from 0.5 to 3. (c) Experiment deviation with $D/L$ changing from 0 to 1. (d) Experiment deviation with $H/L$ changing from 0.5 to 3.

Table 4: Level of the factors in the orthogonal experiment.

| Level | ① ($B/L$) | ② ($W/L$) | ③ ($D/L$) | ④ ($H/L$) |
|---|---|---|---|---|
| I | 1 | 0.5 | 1 | 1.5 |
| II | 0.5 | 1.5 | 0.5 | 2 |
| III | 2 | 1 | 0.25 | 0.5 |
| IV | 1.5 | 2 | 0.75 | 1 |

Table 5: The orthogonal experiment design.

| Experiment number | ① ($B/L$) | ② ($W/L$) | ③ ($D/L$) | ④ ($H/L$) | ⑤ |
|---|---|---|---|---|---|
| 1 | 1 | 0.5 | 1 | 1.5 | I |
| 2 | 1 | 1.5 | 0.5 | 2 | II |
| 3 | 1 | 1 | 0.25 | 0.5 | III |
| 4 | 1 | 2 | 0.75 | 1 | IV |
| 5 | 0.5 | 0.5 | 0.5 | 0.5 | IV |
| 6 | 0.5 | 1.5 | 1 | 1 | III |
| 7 | 0.5 | 1 | 0.75 | 1.5 | II |
| 8 | 0.5 | 2 | 0.25 | 2 | I |
| 9 | 2 | 0.5 | 0.25 | 1 | II |
| 10 | 2 | 1.5 | 0.75 | 0.5 | I |
| 11 | 2 | 1 | 1 | 2 | IV |
| 12 | 2 | 2 | 0.5 | 1.5 | III |
| 13 | 1.5 | 0.5 | 0.75 | 2 | III |
| 14 | 1.5 | 1.5 | 0.25 | 1.5 | IV |
| 15 | 1.5 | 1 | 0.5 | 1 | I |
| 16 | 1.5 | 2 | 1 | 0.5 | II |

orthogonal experiment table with the same CFD simulation settings.

*5.3. Analysis of Orthogonal Experiment.* Based on the CFD simulation, the deviations of the 16 orthogonal tests were obtained (see Table 6).

*5.3.1. Intuitive Analysis.* $K_i$ is the sum of the test results corresponding to level $i$ ($i$ = I, II, III, and IV) in the same column of Table 5. According to the experiment results, $K$ values were obtained (see Table 7). The changes of $K$ values with the factor levels in the orthogonal experiment are shown in Figure 6.

The effect of each factor on the experiment result can be represented as

$$\text{Range } (R) = \max\{K_{\text{I}}, K_{\text{II}}, K_{\text{III}}, K_{\text{IV}}\} - \min\{K_{\text{I}}, K_{\text{II}}, K_{\text{III}}, K_{\text{IV}}\}. \quad (3)$$

Then, $R_{③} > R_{①} > R_{④} > R_{②} > R_{⑤}$ is found in Table 7. This indicates that $D/L$ has the most influence on the results, followed by $B/L$ and $H/L$, and $W/L$ is minimal; there is no interaction between different factors as well.

*5.3.2. Variance Analysis.* Furthermore, variance analysis was performed on the experiment results to accurately assess the effect of each factor. This is summarized in Table 8.

As shown in Table 8, under $\alpha = 5\%$ significance level, the effect of each factor on the experiment results is significant. For the error column, $F_{③} > F_{①} > F_{④} > F_{②} > F_{⑤}$; the greater the $F$ value is, the more significant its impact on the results is. It can be found that this result is consistent with that of intuitive analysis.

*5.4. Suitability Verification.* The suitability verification is to verify whether the results of the optimal scheme in the orthogonal experiment are consistent with the actual situations. According to the above results of the orthogonal experiment, the optimal values of four control parameters were determined as $B/L = 1.5$, $W/L = 2$, $H/L = 0.5$, and $D/L = 0.25$, substituted into CFD simulation with the optimized deviation $\triangle = 0.007687$, which is smaller than that of other 16 tests (see Table 6).

## 6. Results and Discussion

*6.1. Determination of Control Parameters.* Based on the above analysis, the optimal and suboptimal values of the four control parameters are presented in Table 9. Furthermore, by considering the significance of each factor ($D/L > B/L > H/L > W/L$), the value ranges of control parameters were determined as follows.

$B/L$: according to the single factor experiment, $B/L$ was positively correlated with $\triangle$, the optimal value $B/L = 1.5$. However, building groups should already be adjusted when $B/L = 0$; thus, the value range of $B/L$ is 0–1.5.

$W/L$: according to the single factor experiment, $W/L$ was positively correlated with $\triangle$, the optimal value $W/L = 2$. The effect of $W/L$ on the experiment results was not significant and the value of $W/L$ in actual building groups may be small; thus, the value range of $W/L$ can be extended to 0–2.

$D/L$: according to the single factor experiment, $D/L$ was positively correlated with $\triangle$, the optimal value $D/L = 0.25$, and with the most significant effect on the experiments. Therefore, the optimal value was set as the upper limit of $D/L$; its value range is 0–0.25.

$H/L$: according to the single factor experiment, $H/L$ was positively correlated with $\triangle$, the optimal value $H/L = 0.5$. The effect of $H/L$ on the experiment results was not too significant; thus, the suboptimal value was selected as the upper limit of $H/L$, and its value range is 0-1.

Although the simplified method proposed in this research is based on two building groups, its application can be extended to multiple-building groups when their relationships satisfy the constraints of the control indexes. Besides, the control indexes should be adjusted appropriately according to the actual scale of building groups and the demand accuracy of CFD simulation.

Table 6: Deviations of the orthogonal experiment.

| Experiment number | 1 | 2 | 3 | 4 | 5 | 6 | 7 | 8 |
|---|---|---|---|---|---|---|---|---|
| Deviation △ | 0.067892 | 0.038909 | 0.021115 | 0.047969 | 0.026526 | 0.059733 | 0.05444 | 0.007824 |
| Experiment number | 9 | 10 | 11 | 12 | 13 | 14 | 15 | 16 |
| Deviation △ | 0.017716 | 0.021564 | 0.050074 | 0.014583 | 0.03658 | 0.011816 | 0.020159 | 0.016482 |

Table 7: $K$ value of the orthogonal experiment.

| $K_i$ | ① ($B/L$) | ② ($W/L$) | ③ ($D/L$) | ④ ($H/L$) | ⑤ |
|---|---|---|---|---|---|
| $K_{\mathrm{I}}$ | 0.175884509 | 0.148714 | 0.1941814 | 0.148731 | 0.117439 |
| $K_{\mathrm{II}}$ | 0.148523534 | 0.132021 | 0.100177 | 0.133387 | 0.127546 |
| $K_{\mathrm{III}}$ | 0.103936222 | 0.145787 | 0.0584707 | 0.085687 | 0.132011 |
| $K_{\mathrm{IV}}$ | 0.085036869 | 0.086859 | 0.160552 | 0.145576 | 0.136385 |
| Range ($R$) | 0.09084764 | 0.061856 | 0.1357107 | 0.063045 | 0.018945 |

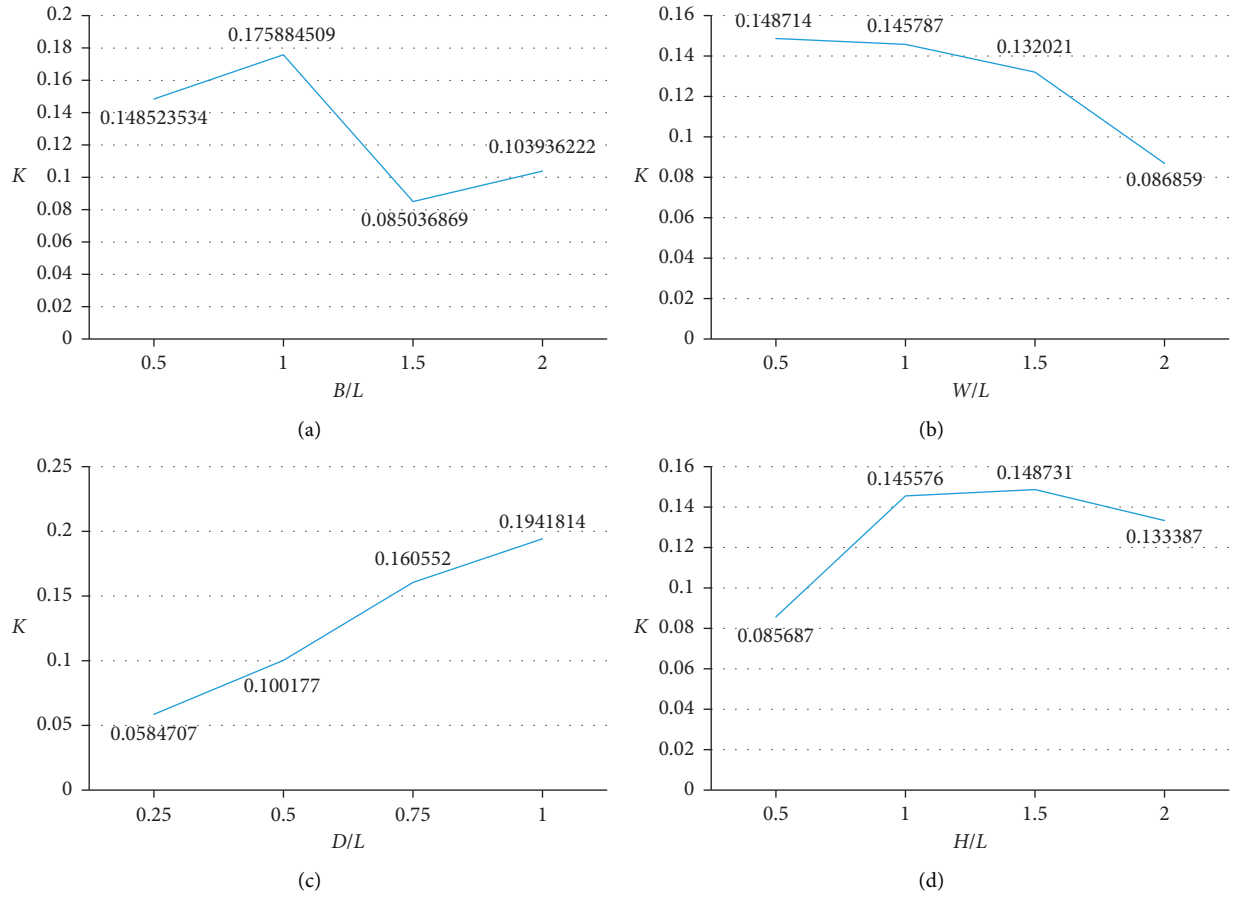


Figure 6: Changes of $K$ value with the factor levels in the orthogonal experiment. (a) Changes of $K$ value with different $B/L$ levels. (b) Changes of $K$ value with different $W/L$ levels. (c) Changes of $K$ value with different $D/L$ levels. (d) Changes of $K$ value with different $H/L$ levels.

Table 8: Variance analysis of the orthogonal experiment.

| Column no. | SS | d$f$ | MS | $F$ | Significance ($\alpha = 0.05$) |
|---|---|---|---|---|---|
| ① | 0.00128464 | 3 | 0.0004282 | 25.99792 | Outstanding |
| ② | 0.000613442 | 3 | 0.0002045 | 12.41453 | Outstanding |
| ③ | 0.002761893 | 3 | 0.0009206 | 55.89385 | Outstanding |
| ④ | 0.000639416 | 3 | 0.0002131 | 12.94018 | Outstanding |
| ⑤ | $4.94132E-05$ | 3 | $1.647E-05$ | 1 | |

Note: $SS_j$ is the sum of the square of deviations on the same column $j$ ($j$ = ①, ②, ③, ④, and ⑤) in the orthogonal table, representing the difference of experiment results; $df_j$ represents the degree of freedom, equal to the number of factor levels with minus 1; $MS_j$ is the average value of $SS_j$, equal to $SS_j/df_j$; $F$ equal to $MS_j/MS_⑤$ is to evaluate the significance of each factor.

Table 9: Optimal and suboptimal value of the control parameters.

| | $B/L$ | $W/L$ | $D/L$ | $H/L$ |
|---|---|---|---|---|
| Optimal value | 1.5 | 2 | 0.25 | 0.5 |
| Suboptimal value | 2 | 1.5 | 0.5 | 1 |

*6.2. Discussion.* According to data analysis, the changing trend of $B/L$ in the orthogonal experiment was different from that in the single factor experiment; this may be caused by the interaction between $B/L$ and other factors. Although, as an independent factor, the effect of $B/L$ on deviation was clear, the relationship might change after introducing the other factors. In the orthogonal experiment, the ratios of $B$, $W$, $H$, and $D$ to $L$ were selected as the factors which are not completely independent of each other. However, this kind of interaction can be verified by introducing other types of parameters in future experiments to figure out more reasonable and accurate control parameters.

## 7. Case Study

To verify the proposed simplified method, the model of a building group containing a total of 620 buildings with a height from 3 m to 78 m at Tsinghua University in Beijing was built (see Figure 7), with the size of 1,855 m along the east-west direction and 2,255 m along the south-north direction. The buildings whose control parameters met the requirements in Table 9 with identical height and regular arrangement were selected to test the validity of the control indexes. The appropriate building models were first simplified (consolidated); then, the simulation of the wind environment was conducted.

*7.1. Model Simplification.* To simplify the building group model, we considered the following two principles:

(1) The simplified objects were rectangular building groups, in which the buildings had similar shapes and their three-dimensional variances were less than 3. Especially, the buildings with less than 10 m height had a few effects on the overall wind field and thus could be consolidated directly. However, considering the effect of the uniqueness of buildings on the wind field, special-shaped or super high-rise buildings were not simplified in this research.

(2) The spatial planning of land use and the function of buildings should be considered when they were simplified. The buildings in different use of land could not be simplified, such as roads, parks, and rivers.

According to these principles, the simplification process of the building group model using the simplified method and the control parameters is shown in Figure 8.

As shown in Figure 9, the simplified building models cover many areas decreasing the number of buildings from 620 to 395 (by 36.3%).

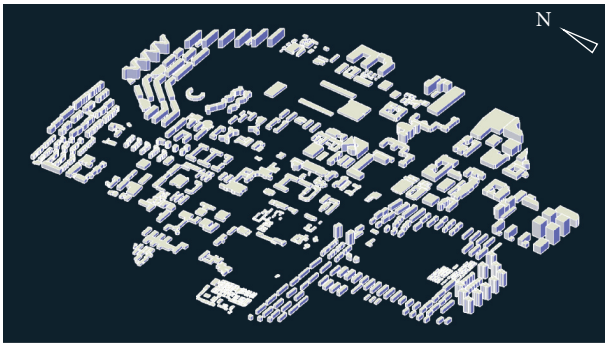


Figure 7: The original 3D model of the building group.

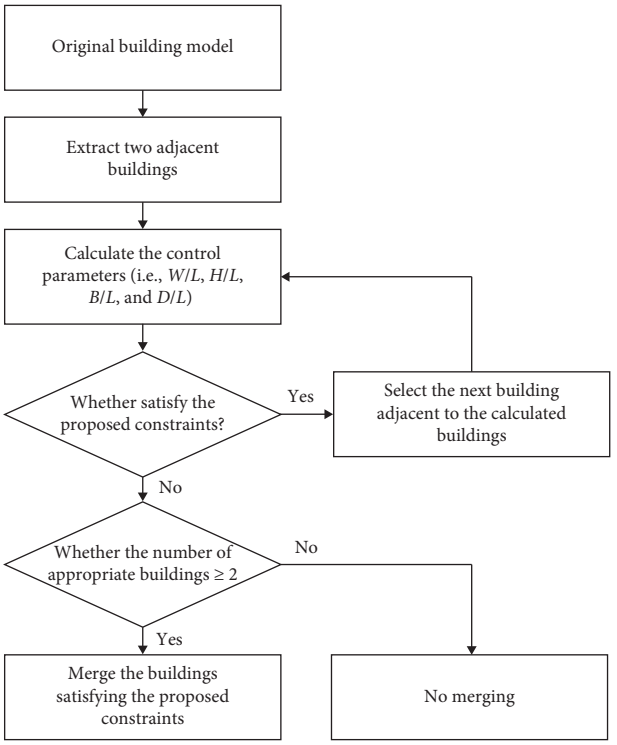


Figure 8: The simplification process of the building group model.

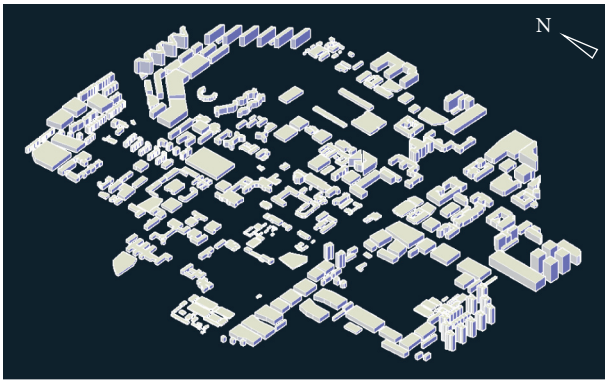


Figure 9: The simplified 3D model of the building group.

Table 10: The settings of various simulations in ANSYS Fluent.

| Items | Contents |
|---|---|
| Simulation software | ANSYS fluent 16.1 |
| Grid generation | Unstructured grid: the building grid size is 4 m, the ground grid size is 10 m, and the global grid size is 100 m; the size of the simplified building grid becomes 8 m, while other dimensions remain unchanged |
| Computational domain | The distances between the building outer boundary and the computational domain edge: ceiling = $5H$, inflow boundary = $5H$, cross-range = $5H$, and outflow boundary = $15H$; $X * Y * Z$: 2635 m * 3815 m * 468 m |
| Boundary condition | Inflow boundary and ceiling boundary: velocity-inlet——v = $v0 * (Z/10)^{0.3}$<br>Outflow boundary: pressure-outlet——101325 Pa<br>Lateral boundary: symmetry<br>Ground and building surface: wall |
| Pressure | 101325 Pa |
| Model | Standard $k$-$\varepsilon$ model |
| Near wall treatment | Standard wall treatment |
| Solving algorithms | SIMPLEC |
| Convergence criteria | The speed of the monitoring point reaches a steady value |

### 7.2. CFD Simulation

*7.2.1. Settings of CFD Simulation.* Considering the characteristics of local climate, model size and complexity, computing capability, etc., the settings of CFD simulation modeling are presented in Table 10.

*7.2.2. Comparison of Grids.* The result of the CFD simulation indicates that the quantity of the grids in the flow field can be reduced by the proposed simplified method with improved quality. As shown in Figure 10, considering the complicated geometric configuration of the building group model, the Octree algorithm in ANSYS ICEM CFD instead of structured grids was applied to generate the tetrahedral unstructured grids whose size and quantity were subject to computing resources. Compared with the original grid size in Table 10, the size of the simplified building grid became 8 m with other dimensions unchanged to reduce the impact of different overall grid resolutions on the calculation results. In the end, the number of tetrahedral grids was reduced from 8,832,199 to 7,766,778 (by 12.1%).

The comparison of grid quality before and after simplification is shown in Figure 11. The closer the grid quality value is to 1, the better the grid quality is. It is obvious that the overall grid quality is improved after simplification. This is because the reduction of the narrow space in the simplified model can smooth the tetrahedral grid transition under a given size and reduce grid problems such as repeating units and unconnected vertices.

*7.2.3. Simulation Results.* Airflow direction, speed, and relevant changes in urban areas are the main factors affecting the simulation of the wind environment of building groups on a large scale. To satisfy the requirement of grid accuracy, a 10 m high plane above the ground was selected as the reference surface to analyze the flow field. The velocity contour cloud maps and velocity vector maps in the reference surface before and after simplification are shown in Figures 12 and 13. The following findings were achieved:

(1) Compared with the original model, there were few changes of cloud map in the open space and the street valley of the simplified model, except for unstable wind speed in the simplified area. Moreover, the distribution of wind speed in most areas (e.g., areas ①, ②, and ③ marked in Figure 12) after simplification was almost the same as that before simplification.

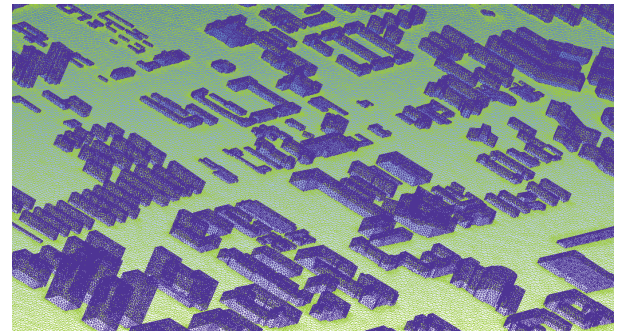

Figure 10: The grids of the original model.

(2) Merging adjacent buildings not only blocked original air passages but also caused a few changes in wind direction around the simplified building models. However, the overall distribution of wind direction in the flow field (e.g., areas ④, ⑤, and ⑥ marked in Figure 13) after simplification was also almost the same as that before simplification.

(3) Although the comparison of the wind fields before and after simplification indicated that the simplification of the building group model had an unavoidable impact on the local wind environment, the simulation results were acceptable at the urban level because there were no significant airflow changes in the main ventilation paths.

*7.2.4. Summary.* Compared with the original simulation, the quantity of the simplified grids was reduced by 12.1%. The simulation results indicated that the proposed simplified method with the exact control parameters was feasible for wind environment simulation on the urban scale but saved computational resources and improved computational efficiency. Besides, the improvement of computational

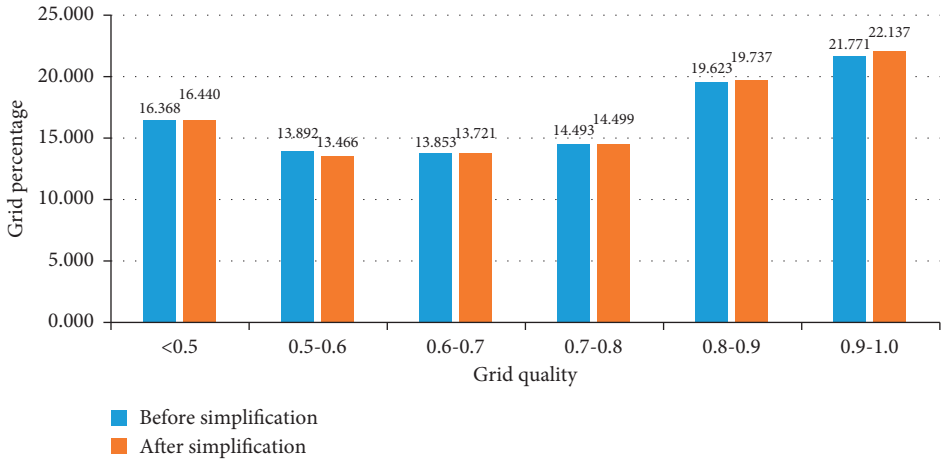


Figure 11: Comparison of grid quantity before and after simplification.

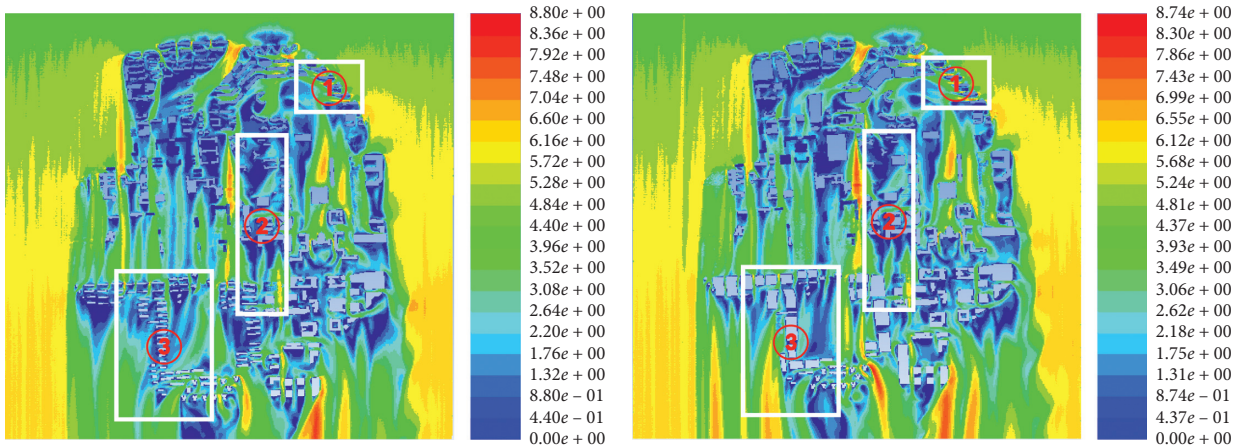


(a) (b)

Figure 12: Velocity contour cloud maps before and after simplification. (a) Velocity contour cloud map before simplification. (b) Velocity contour cloud map after simplification.

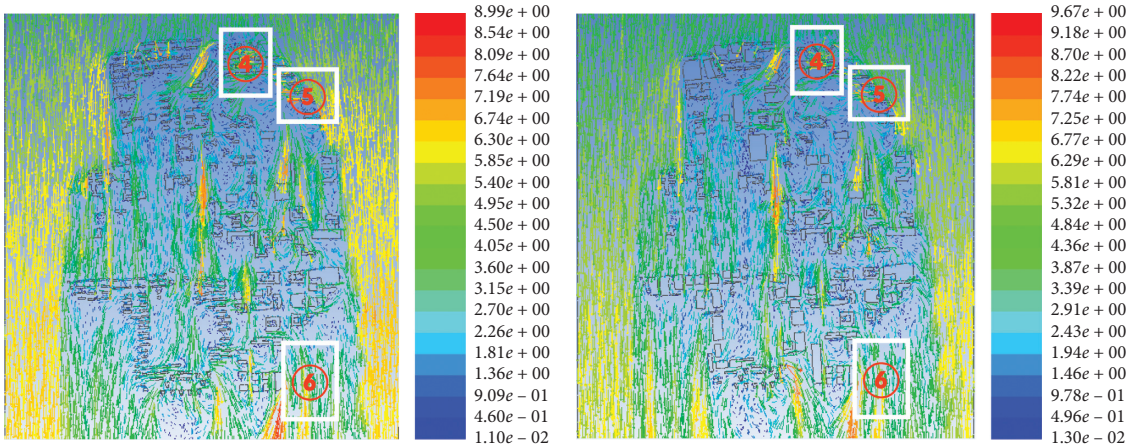


(a) (b)

Figure 13: Velocity vector maps before and after simplification. (a) Velocity vector map before simplification. (b) Velocity vector map after simplification.

efficiency in this research was subject to the strict selection criteria and simplification process for building group models. In the future practical applications, especially for the CFD simulation of building groups in an urban scale (size between 10 $km^2$ and 20 $km^2$) with denser areas (such as residential areas), higher grid accuracy, and more grids, the simplified method will be much more valuable and efficient.

## 8. Conclusion

A simplified method for the model of building groups in CFD simulation is proposed in this article and the appropriate value ranges of the four control parameters are determined as $B/L \in \{0, 1.5\}$, $W/L \in \{0, 2\}$, $D/L \in \{0, 0.25\}$, and $H/L \in \{0, 1\}$ using single factor experiment and orthogonal experiment. According to the variance analysis on the results of the orthogonal experiment, $D/L$ has the most effect on deviation $\triangle$, followed by $B/L$, $H/L$, and $W/L$. When the geometric relationship of a couple of buildings satisfies the control indexes, the simplified method is applicable. In order to verify the proposed method, the simulation model of the building group in Tsinghua University is built and analyzed in the case study. The results indicate that the proposed method can effectively reduce the number of grids generated in CFD simulation and improve the efficiency of simulation without decreasing the performance of simulation, especially in the simulation of a large scale of building groups. Therefore, it will extend the application of CFD simulation in the urban-level wind environment analysis.

However, there are also some limitations to this research. For example, the problems such as system errors, strong dissipativity, and low computational accuracy can be caused by the standard $k$-$\varepsilon$ turbulence model. It can be substituted with the LES model or tunnel test data for higher accuracy results in future research. Besides, as the selected factors are not completely independent of each other, there are some interactions between these factors. This can be verified by introducing other types of parameters such as topography, inflow angle, and building group layout in the future.

## Data Availability

The data used in this manuscript will be provided upon request.

## Disclosure

This article is an extension of the conference paper "*A Simplified Method for the Model of Building Groups in CFD Simulation*" published in the International Conference on Construction and Real Estate Management (ICCREM) 2017.

## Conflicts of Interest

The authors declare that they have no conflicts of interest.

## Acknowledgments

This work was supported by the NSFC-Zhejiang Joint Fund for the Integration of Industrialization and Informatization (Grant no. U1709212) and the Tsinghua University-Glodon Joint Research Centre for Building Information Model (RCBIM). The authors also thank Prof. Xinzheng Lu at Tsinghua University for providing the building data in the case study.

## References

[1] C. Yuan, L. Norford, R. Britter, and E. Ng, "A modelling-mapping approach for fine-scale assessment of pedestrian-level wind in high-density cities," *Building and Environment*, vol. 97, no. 15, pp. 152–165, 2016.

[2] B. Wang, L. D. Cot, L. Adolphe, S. Geoffroy, and J. Morchain, "Estimation of wind energy over roof of two perpendicular buildings," *Energy and Buildings*, vol. 88, no. 1, pp. 57–67, 2015.

[3] Y. Huang, X. Hu, and N. Zeng, "Impact of wedge-shaped roofs on airflow and pollutant dispersion inside urban street canyons," *Building and Environment*, vol. 44, no. 12, pp. 2335–2347, 2009.

[4] G. M. Stavrakakis, E. Tzanaki, V. I. Genetzaki, G. Anagnostakis, G. Galetakis, and E. Grigorakis, "A computational methodology for effective bioclimatic-design applications in the urban environment," *Sustainable Cities and Society*, vol. 4, pp. 41–57, 2012.

[5] J. D. Anderson, *Computational Fluid Dynamics: The Basics with Applications*, McGraw-Hill, New York, NY, USA, 1995.

[6] P.-C. Liu, H.-T. Lin, and J.-H. Chou, "Evaluation of buoyancy-driven ventilation in atrium buildings using computational fluid dynamics and reduced-scale air model," *Building and Environment*, vol. 44, no. 9, pp. 1970–1979, 2009.

[7] T. Kobayashi, T. Chikamoto, and K. Osada, "Evaluation of ventilation performance of monitor roof in residential area based on simplified estimation and CFD analysis," *Building and Environment*, vol. 63, pp. 20–30, 2013.

[8] J. I. Perén, T. van Hooff, B. C. C. Leite, and B. Blocken, "Impact of eaves on cross-ventilation of a generic isolated leeward sawtooth roof building: windward eaves, leeward eaves and eaves inclination," *Building and Environment*, vol. 92, pp. 578–590, 2015.

[9] R. Teppner, B. Langensteiner, W. Meile, G. Brenn, and S. Kerschbaumer, "Air change rates driven by the flow around and through a building storey with fully open or tilted windows: an experimental and numerical study," *Energy and Buildings*, vol. 80, pp. 570–583, 2014.

[10] C. M. Mak, J. L. Niu, C. T. Lee, and K. F. Chan, "A numerical simulation of wing walls using computational fluid dynamics," *Energy and Buildings*, vol. 39, no. 9, pp. 995–1002, 2007.

[11] B. Blocken, J. Carmeliet, and T. Stathopoulos, "CFD evaluation of wind speed conditions in passages between parallel buildings-effect of wall-function roughness modifications for the atmospheric boundary layer flow," *Journal of Wind Engineering and Industrial Aerodynamics*, vol. 95, no. 9–11, pp. 941–962, 2007.

[12] T. Ayata and O. Yıldız, "Investigating the potential use of natural ventilation in new building designs in Turkey," *Energy and Buildings*, vol. 38, no. 8, pp. 959–963, 2006.

[13] O. S. Asfour, "Prediction of wind environment in different grouping patterns of housing blocks," *Energy and Buildings*, vol. 42, no. 11, pp. 2061–2069, 2010.

[14] J. O. P. Cheung and C.-H. Liu, "CFD simulations of natural ventilation behaviour in high-rise buildings in regular and staggered arrangements at various spacings," *Energy and Buildings*, vol. 43, no. 5, pp. 1149–1158, 2011.

[15] A. Cao, Q. Li, and Q. Meng, "Effects of orientation of urban roads on the local thermal environment in Guangzhou city," *Procedia Engineering*, vol. 121, pp. 2075–2082, 2015.

[16] R. Ramponi, B. Blocken, L. B. de Coo, and W. D. Janssen, "CFD simulation of outdoor ventilation of generic urban configurations with different urban densities and equal and unequal street widths," *Building and Environment*, vol. 92, pp. 152–166, 2015.

[17] J. Hang, Z. Luo, M. Sandberg, and J. Gong, "Natural ventilation assessment in typical open and semi-open urban environments under various wind directions," *Building and Environment*, vol. 70, no. 15, pp. 318–333, 2013.

[18] C. Yuan, E. Ng, and L. K. Norford, "Improving air quality in high-density cities by understanding the relationship between air pollutant dispersion and urban morphologies," *Building and Environment*, vol. 71, no. 1, pp. 245–258, 2014.

[19] Y. Tominaga, A. Mochida, R. Yoshie et al., "AIJ guidelines for practical applications of CFD to pedestrian wind environment around buildings," *Journal of Wind Engineering and Industrial Aerodynamics*, vol. 96, no. 10-11, pp. 1749–1761, 2008.

[20] Z. Wu, T. Yan, and X. Fu, *CFD Simulation Technology Based Analysis on Urban Wind Environment of Shenzhen*, The 3rd China Construction Quality Forum, Shenzhen, China, 2009.

[21] L. Yang, *Green Building Design: Wind Environment of Building*, Tongji University Press, Shanghai, China, 2014.

[22] X. Y. Chen, B. Zheng, K. M. Hou, and D. K. Zhong, *Building Design and Natural Ventilation*, China Electric Power Press, Beijing, China, 2012.

[23] J. Franke, A. Hellsten, H. Schlünzen, and B. Carissimo, "The COST 732 best practice guideline for CFD simulation of flows in the urban environment: a summary," *International Journal of Environment and Pollution*, vol. 44, no. 1–4, pp. 419–427, 2011.

Hindawi
Advances in Civil Engineering
Volume 2021, Article ID 8898997, 14 pages
https://doi.org/10.1155/2021/8898997

*Research Article*

# Digital Twin in Computational Design and Robotic Construction of Wooden Architecture

**Ye Zhang, A. Meina, Xuhao Lin, Kun Zhang, and Zhen Xu**

*Department of Architecture, Tianjin University, Tianjin, China*

Correspondence should be addressed to Ye Zhang; yaapp2012@gmail.com

Received 5 August 2020; Revised 15 January 2021; Accepted 14 March 2021; Published 2 April 2021

Academic Editor: Jiansong Zhang

Copyright © 2021 Ye Zhang et al. This is an open access article distributed under the Creative Commons Attribution License, which permits unrestricted use, distribution, and reproduction in any medium, provided the original work is properly cited.

This study proposes a cyber-physical interconnection method for computational design and robotic construction in a wooden architectural realm. It aims to provide a highly efficient, flexible, and adaptive design-construction approach by continuously updating digital models and physical operations according to the locally sourced materials. A perception-modeling system to scan the source materials on-site and send their data simultaneously to design software was developed by using physical sensors and computational technologies in an innovative manner. The data was used for architectural programs to generate design outcomes and guide the robotic construction. The novelty of this study is to establish a real-time, bidirectional interaction mechanism between digital design and physical construction. The design outcome is no longer a fixed, predefined geometric model but a dynamic, data-driven model which would be updated by material conditions on-site. The construction robot is able to make synchronous adjustment automatically in coordination with the dynamic design. The success of the iterative perceiving-simulating-updating loop was demonstrated by building two pavilions.

## 1. Introduction

Robotic fabrication in the architectural field experienced a big leap since the beginning of the 21st century. Thanks to the expansion of the open-source program ecosystem and the development of programmable robotic machines (Kuka [1], ABB [2], etc.), an increasing number of digital fabrication projects are being conducted in which the designers are fully involved in the design-construction process from the beginning until completion. In most of these projects, digitalization technologies enable the design ideas to develop virtually by analyzing and managing a large quantity of data through different types of simulations.

In 2015, Menges introduced the concept of cyber-physical construction in architecture, which involves construction processes that intensively integrate the realm of physical production with the virtual domain of computation [3]. This concept helps robotic fabrication to become more intelligent, as various levels of predictions and new operation tests for a complex system are simulated before the system is applied in the real world [4].

In order to further develop this method, this research proposes an on-site robotic construction workflow that is based on real-time physical sensing and computational analysis instead of relying on explicit modeling and inalterable instructions. The construction environment of the architecture using local source materials is complex and dynamic. Natural materials vary in sizes and shapes; hence, they are difficult to predict and to be suitably used. Our on-site robotic construction system is endowed with the perception of its current environment and conditions of source materials. With the feedback information collected by the robot, the virtual plan is updated dynamically and physical robotic actuation is adjusted in coordination with the virtual plan in reverse. This research proposes another design-construction workflow; it is a recursive, informational data-driven paradigm, instead of a static, closed top-down decision-making process. It helps on-site robotic construction to remain optimal in terms of adaptiveness and feasibility.

In order to clarify the subject of discussion, this article aims to achieve the following objectives:

(1) A review of robotic fabrication and digital twin method applications

(2) An extension and realization of the perception-modeling system with sensing and transfer technologies so that the system is able to capture and store source materials' geometry in advance, assemble the components in Rhino/Grasshopper, and instruct on-site construction with real-time site information

(3) A redefinition of the novel design-construction workflow and data management, with a robust and integrated informational interaction of human-robot collaboration based on a digital twin model.

## 2. Background and Related Works

It was not until recently that the multifunctional industrial robots had their own test scenarios in the field of on-site architectural construction. In order to obtain remarkably efficient and accurate but automated fabrication output from robots, either of these experimental approaches tends to emerge as a series of parallel research fields to realize the novel architectural design-construction discipline, and, at the same time, a brand new concept of managing source data and operations over various fields as well as different phases in the design-construction workflow is raised.

*2.1. Robotic Fabrication for Wooden Architecture.* The application of digital technologies in wooden construction, including early joinery customization and the CNC process, started in the 1980s [5]. In less than 40 years, Mjøsa Tower, the tallest prefabricated timber frame high-rise building in the world, has been constructed with a maximum height of 85.4 m, demonstrating the potential of wood as one of the most sustainable universal construction materials. Due to the flexibility of its materialization nature, wood has also become one of the preferred robotic fabrication materials and has been used in more than 80% of the most projects in the current research field [6]. In earlier studies, two main aspects of robotic wood fabrication research were reported. Fabio et al. completed a series of large-scale robotic fabrication projects [5, 7], in which the wooden structural frame of the house was processed and assembled on-site. Alvarez et al. [8] and Schwinn et al. [9] from ICD University of Stuttgart introduced an integrative approach to build a sophisticated timber pavilion. However, both researches used processed timber components which is delicately produced and organized, and passively accepted errors occurred and accumulated during both fabrication and assembling processes. On the other hand, research studies also shed light on using unprocessed wood as the local components in a novel way, which may immensely improve the freedom and effectiveness of the system. Monier et al. developed a method for optimizing the use of native irregular shape wood pieces [10], although the method is still in the digital model phase. Schindler et al. worked on the potential of 3D scanning and the postprocessing of wooden branches by using CNC fabrication [11]. Obuchi et al. and their research pavilions [12, 13] from T-ADS in the University of Tokyo explored a series of raw material assembly logic by accumulating regular and irregular local components, pushing the limit of raw materials as proper constructible elements, and using the latest digitization technology and a sophisticated working process. Self et al. and their Wood Chip Barn minimized the preprocessing of the wooden elements, replacing wooden trunks with the pretreatment of the joints. The trunks were later 3D-scanned, all geometric information was collected to generate the final form, and part of the main structure was assembled beforehand and then transported to the site [6]. Nevertheless, for all of these unprocessed wooden construction researches, neither a fully integrated procedure from design to construction phases nor a synthesized data flow management method can be found.

*2.2. From Human-Robot Collaboration to Perception-Modeling Fabrication.* The component assembly task is considered to be of great significance in on-site construction. The main challenges of this task are handling complicated geometries and obtaining high production flexibility [14], which in turn reflects in the proportion of human and robot involvement in this process. With the ultimate objective of achieving a construction automaton, to indicate a clear boundary between human and robot is inevitable, which increases an additional layer to the system complexity. Research studies have been conducted on various methodologies and frameworks for human-robot collaboration, realizing a highly flexible and adaptable construction system. Almeida and Sousa operated a robotic arm to cut timber components and then assembled the pavilion with human effort [15]. Larsson et al. proposed a human-in-the-loop fabrication system for small-scale construction by using irregular wooden branches, a leverage digital scanning technology, and a 2.5 D CNC machine [16, 17]. It can be concluded that the division of labor between robot and human is relatively clear in the above cases; yet human involvement increases alongside the geometrical complexity, thereby resulting in a reduction in the effectiveness. By reconsidering such an increasing number of scenarios, the cases of implementing robotic perception-modeling fabrication intend to realize human involvement at the beginning of each informational input loop. Decision taken by the process of feeding physical environmental perception to the robot becomes possible with the support of the latest edge-computing technologies. Brugnaro et al. inspect the robotic fabrication of the woven bamboo structure in their robotic softness research, in which the real-time information is continuously shared with the decision maker [18]. Wu and Kilian conducted a research study on setting up a vision system to suggest assembly positions of the desired topological connections through real-time processed image information [19]. Jeffers discussed a method that a virtual model is built for persistent storage of material data and next built action can be computed accordingly [20].

In these cases, the robotic fabrication process includes interference either from the IoT devices or directly from

humans to achieve a more adaptable system attributed by the real-time informational update and adjustment, avoiding the gradually accumulated errors, while a master management method about the workflow has not yet been summarized or proposed. In order to develop this concept further, the distribution and management of the appropriate human-robot relationship for the whole lifecycle should be addressed prior to the description of the construction.

*2.3. The Digital Twin Paradigm.* Digital twin (DT), as a novel paradigm for realizing interaction and integration between the physical space and the virtual space, has been developed to manage complicated systems for the relevant academic circles and enterprises [21]. This method is considered to be able to provide an integral and material-behavior-driven construction paradigm for complex conditions in robotic fabrication process [22], aimed at bringing geometric and detailed design, structural simulation, 3D scanning, and on-site construction together.

The concept of the digital twin was first introduced by Grieves, who stated it as the "Conceptual ideal for product lifecycle management (PLM)" at the University of Michigan in 2002 [4], defined as "a set of virtual information" that describes the physical object of different scales. Due to the rapid development of IoT devices, the cloud-computing technology, and the machine learning algorithm, a multifunctional robotic arm is conferred with the capacity of retaining its digital twin, which receives real-time information through sensors, has access to the collected big data cloud, and triggers its physical twin to take actions after analyzing various design disciplines in the virtual world. This method was tested in the early space capsule prototype [23] and can be continuously developed in the manufacturing realm. In 1991, an idea called "simulation control" was proposed, which outlines a prototype system in which simulation is integrated into a CIM environment for manufacturing [24]. Thereafter, the concept and exploration of DT have seen rapid progress thanks to the advances in technology. The digital-twin-driven approach includes the following three parts: the physical layer, digital data exchange, and the virtual layer. The physical layer refers to the real production environment. The virtual layer refers to the digital model of the physical resources for carrying out both the manufacturing simulation and the real-time optimization of the systems. Digital data exchange refers to the data interaction between the physical layer and the virtual layer; it collects the real-time data from the physical layer and the feedback from the virtual layer and vice versa. Nowadays, the focus areas of digital twin applications are different from the product lifecycle, layout planning, process design, maintenance, PPC, etc. [25], and the inclusion of the digital twin model optimizes multiple aspects. Boschert and Rosen illustrated that the digital twin uses essential information to bridge over creation, production, operation, and disposal phases, thus resulting in a system available for succeeding in the phases in which almost everything within the system, including material geometry, structural performance, and raw data from fabrication, can be monitored and tracked [21]. Malik and Bilberg proposed a digital-twin-framework-based model that supports the design, development, and operation of human-robot collaboration in the manufacturing practice, illustrating the use of digital twin in the human-robot task allocation and the workplace setup [14]. Harper et al. in ABB focused on the development of digital twin standards in which the on-site virtual support can be achieved [26].

Taking advantage of the digital twin model, the negotiation and blurry boundary between the virtual and the physical space are erased, thus leaving a fully integrated cyber-physical construction environment for a real-time information feedback loop. The vision of the digital twin application is always emphasized; yet practical use is seldom tested or realized, especially for those robotic fabrication researches in architectural field.

## 3. Methodology

This research presents a digital twin framework (Figure 1) of the overall design-construction process, ensuring a smooth interconnected informational exchange back and forth linking the virtual and physical space. The framework consists of four phases: in the preparation phase, unprocessed wood branches are selected as source materials; the silhouette is selected and developed as the measuring method. In the material perception-modeling phase, the parameters and mathematical formulation of the real-time image acquisition and shape reconstruction system are calculated; corresponding programs are developed. In the dynamic design phase, material organization and the corresponding overall geometries are evolved using matching algorithm and positioning algorithm. In the flexible construction phase, robotic assembly is achieved using the executing program, monitoring program, and adjusting program. The digital twin framework enables up-to-date material information of the physical space to be reflected in the digital model with a high level of precision and synchronization, and the dynamic modifications of the digital model also provide an almost real-time change in the robotic assembly.

### *3.1. Preparation Phase*

*3.1.1. Material Selection.* Wood is considered to be a low-carbon, environmentally friendly material, and its unique texture is aesthetically favorable for architectural design. Straight tree trunks are widely used as they can be cut into standardized pieces for the building industry. However, small tree trunks and branches with diversified shapes are typically abandoned as they are difficult to use systematically due to their variability.

However, we believe that wood branches with natural variability demonstrate great potential in nonlinear architecture with complex geometry as they offer more approaches and possibilities in design. In the manufacturing processes, taking advantage of material variability rather than fabricating variable components out of standardized materials decreases processing operations, improves

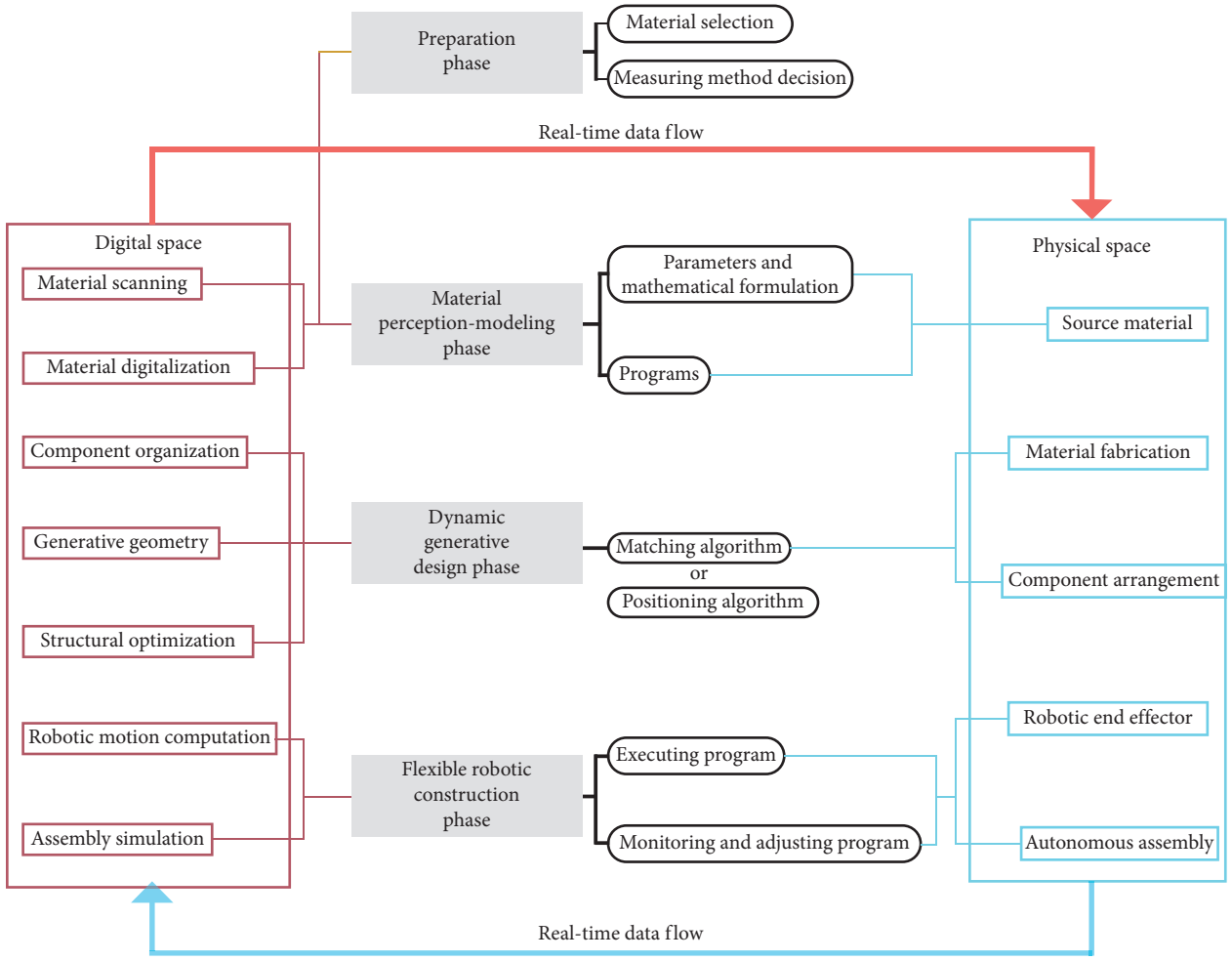


Figure 1: Digital twin framework for on-site construction.

fabricating efficiency, and transforms scrap materials into good account.

Our objective was to develop a real-time material information acquisition system that features variability recognition and shape awareness. Therefore, we used unprocessed wood branches collected from the trees on the construction site on the campus of Tianjin University. These branches were cut by the City Sanitation Department and were considered low valued and were to be chipped or burned if not used (Figure 2).

This study conducted pavilion-scale design-construction experiments. Consequently, we selected branches with lengths of 35–245 cm. Their diameters ranged from 4 cm to 20 cm, thick enough to be strong and thin enough to be easily used.

*3.1.2. Measuring Method Decision.* The existing measuring and modeling methods can be categorized into active and passive methods. The active methods primarily include moiré fringe, time-of-flight (ToF), structured lighting, and triangulation, whereas the passive methods primarily include shape from texture (SFT), shape from shading (SFS), multiview stereo (MVS), and silhouette methods. These methods rebuild objects with mathematical and physical principles. To be more specific, moiré fringe uses the interference of wave to deduce the shape; ToF measures the time taken by an object to travel a distance through a medium; SFT, SFS, and structured lighting mainly use perspective principles; and triangulation, MVS, and silhouette use the methods of deformations with triangular positioning. The attributes of each method are presented in Table 1 [14–18]. The "+" and "–" signs indicate strong and weak performances.

The perception-modeling system developed in this study was based on the silhouette method. We selected the silhouette method for the following reasons. 2D silhouettes from different views of the scanning material are able to rebuild a 3D digital model by Boolean intersection, and hence the method is feasible. Second, the hardware setup is convenient and suits for the environment of construction site. Third, the software is easy to operate and can be compatible with the popular design software Rhino/Grasshopper.

Based on the silhouette method, we introduced a simple algorithm to improve the speed and efficiency of the obtained outlines from wood branches and rebuild their visual replicas. The optimized perception-modeling system could

Figure 2: Material preparation.

Table 1: Measuring and modeling methods.

| | Name | Principle | Speed | Accuracy | Cost | Stability | Limitation |
|---|---|---|---|---|---|---|---|
| Active method | Moiré fringe | Diffraction and interference of light | ++ | +++ | + | + | Only available for objects with regular texture |
| | Time-of-flight (ToF) | Time taken for the wave to bounce back to the emitter | ++ | −− | −− | − | Low resolution and being easy to be disturbed |
| | Structured lighting | Encoding and decoding of light | + | ++ | + | ++ | Projection equipment required |
| | Triangulation | Solving trigonometric equation | + | − | + | + | Data sparseness |
| Passive method | Shape from texture (SFT) | Perspective distortion calculation | + | + | + | − | Surface texture information required |
| | Shape from shading (SFS) | Ray calculation | − | − | + | − | Light parameters required |
| | Multiview stereo (MVS) | Parallax principle | −− | −− | + | + | Image error being big |
| | Silhouette | Visible shell approximation | +++ | −− | ++ | ++ | Visible shell only |

quickly and easily build 3D digital models of all of the tested branches. The system could be embedded in the end effector of a construction robot for small-scale material components or fitted to a particular holder for large-scale components.

### 3.2. Material Perception-Modeling Phase

*3.2.1. Parameters and Mathematical Formulation.* The parameters of the perception-modeling system include camera angle, the size of the provided branches, the distance between the camera and the testing branch, the angle between two adjacent cameras, and the number of pixels in the corresponding direction. These parameters should be considered as a related set, and they would determine the precision and the cost of the system.

In this study, the radius of the branch range is set as $R$, the distance between the camera and the branch center is $d$, and the camera angle is set as $\alpha$. Hence, a relationship is formulated between these parameters as follows:

$$d = \frac{R}{\sin(\alpha/2)}. \tag{1}$$

Then, the number of pixels in the corresponding direction of the camera is set as $n$, and the resolution of the reconstructed model is set as $\gamma$. Then, a relationship is established between them using (1):

$$\gamma = 2R\cos\frac{(\alpha/2)}{n} = d\sin\frac{(\alpha)}{n}. \tag{2}$$

In regard to the error analysis, the uniform errors of the system are affected by two factors, as shown in Figure 3: one is the angle between two adjacent cameras, and the other is the radius of the projection on the plane of the camera group. In order to establish the error, the study sets the former as $\delta$, the latter as $r$, and the inherent error as $e$. Then, a relationship is formulated between these parameters as follows:

$$e = r\left(\csc\left(\frac{\delta}{2}\right) - 1\right). \tag{3}$$

An approach direction is that the performance of the equipment should be improved as much as possible, which means $e < \gamma$. Finally, the corresponding equipment configuration and the working range can be determined by solving the above equations.

For relatively smaller branches with a section radius of less than 10 cm, the perception-modeling system is embedded inside a Kuka KR60/HA Robot. Considering the robot arm span and the analysis of the above formular, the length of 165 cm was chosen as a safe threshold for the scanning branch. Actually, the threshold is a reference value with multiple idealizations. The measurement limit is related

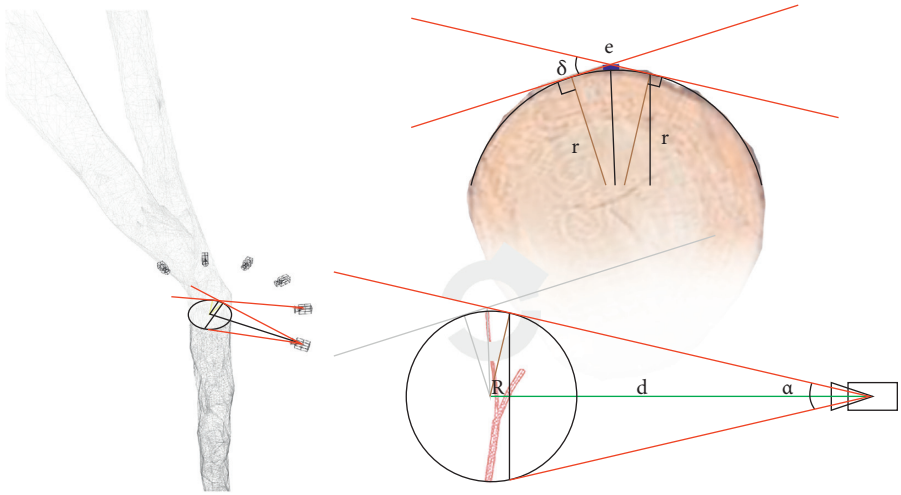


Figure 3: Parameter determination and error analysis.

to the shape of the branch, the position it is placed at, the lens parameters of the camera, and the position of the shot. The limit value is estimated from these parameters through a ternary function. Maintaining a balance between convenience and accuracy, this research finally uses $d = 100$ cm, $\alpha = 0.3\pi$, $\delta = 0.444\pi$, and $n = 720$. As shown in Figure 4, the robot would capture nine images from different perspectives as its end effort moves and shots in relevant positions.

For larger components exceeding the robotic scanning range, another strategy that controls several cameras to capture material images from different perspectives at the same time is applied by using a particular holder. With a similar calculation method, this study considers $d = 300$ cm, $\alpha = 0.3\pi$, $\delta = 0.667\pi$, and $n = 720$. Six cameras are fixed to a 600 cm long frame to shot the branch at the same time.

*3.2.2. Programs.* A calibration program for correcting dimensions is prepared before scanning the branches. The program establishes the mapping relationship between the contour pixels of the testing object in the measuring location and spatial points in the modeling software. The scaling parameter and the rotation parameter are calculated and examined. Meanwhile, scripts for reading information from multiple cameras are also developed. This calibration program only executes once at the beginning of the whole workflow and does not require recalculation once the branch is scanned.

After running the calibration program, the system begins to perceive physical branches and rebuild their 3D models virtually. Two programs are developed. One is an external program that captures different views of the branch images and extracts related data for the visual presentation. The other one is an interface program that synchronously receives the data and converts it into the corresponding digital model in the design software Rhino/Grasshopper.

The external program and the interface program run simultaneously. The external program extracts smooth contours of the branch, calculates three-dimensional coordinates of the points in the contours, and generates a file containing the data of all the points. The interface program receives array data, maps the spatial positions of the points, shapes outlines from different views, and generates the corresponding digital model by using the algorithm of the Boolean intersection (Figure 5).

The perception-modeling system developed in this study is endowed with flexibility, reliability, and usability. Firstly, flexibility implies that the material perception programs are applied in modular organizations, where each camera and its corresponding software layer can work independently. Therefore, researchers can add or reduce camera numbers to achieve different accuracy requirements. Additionally, the system displays a high tolerance for faults and hence is considered highly reliable. It considers the unstable operation of the sensor: when some cameras are broken, the other cameras can still work and maintain the system's function despite a reduced accuracy. Lastly, usability implies that the system is designed for easy operation, low cost, fast running, and high efficiency on most devices. The system has been optimized through appropriate image abstraction techniques that need less computational capacity, so that most computers are capable of running the program without considering the speed issue.

*3.3. Dynamic Generative Design Phase.* Source materials are recognized, digitalized, and analyzed in the perception-modeling phase and would be well organized in the design phase. They actively participate in generating the overall geometry of the architecture, and the outcome remains dynamic with the updating of the provided materials. This study provides two approaches to generate the dynamic design outcome based on the source materials.

*3.3.1. Matching Algorithm.* The first approach focuses on the matching algorithm; it generates geometry by optimizing the organization order of the provided branches. Based on connection rules, i.e., each fork of the branch should be connected with a fork of another branch; it firstly gets the results of different combination possibilities. If none of the

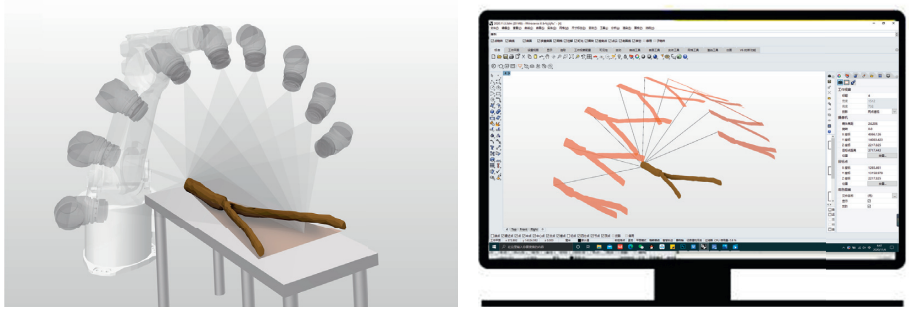

Figure 4: Perception-modeling system for small branches.

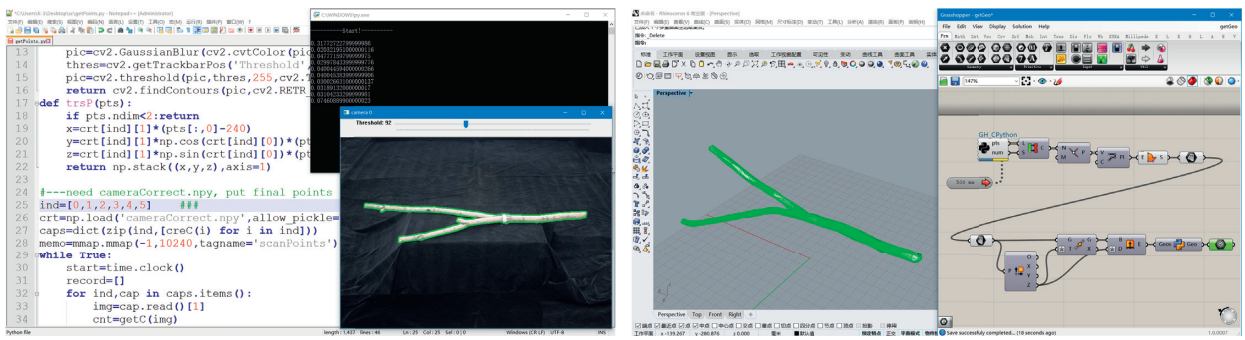

Figure 5: Scanning physical branches and building the corresponding digital models.

combinations can achieve the rule, more source branches should be provided until at least one option is resultful. After geometric simulations, material effectiveness of all resultful combinations is calculated and the most effective way is selected. Specifically, if the distance between two adjacent forks is too small, the extra parts beyond the intersection will not bear weight and will be ineffective. The total lengths of the ineffective parts of different combinations are calculated and their results are sorted. Finally, structural performance of generative geometry is simulated and optimized by finite element analysis in Grasshopper (Figure 6).

*3.3.2. Positioning Algorithm.* The other approach of generative design focuses on positioning algorithm, and the overall geometry evolves by scanning and assembling the source branches iteratively. The outcome is updated by continuously mirroring the current branch and putting it in a suitable position. A guiding curve is defined by the designer from an aesthetic perspective. The branch is assembled along the curve by anchor determination script and orientation determination script. The operation continues until no more branch is provided. In this approach, the overall geometry forms gradually, and the final outcome appears only after the last source branch is captured (Figure 7).

*3.4. Flexible Robotic Construction Phase.* After the material perception-modeling phase and the dynamic generative design phase, a flexible construction system is developed using real-time robotic communication techniques. The "flexible" term implies that the robotic fabrication system

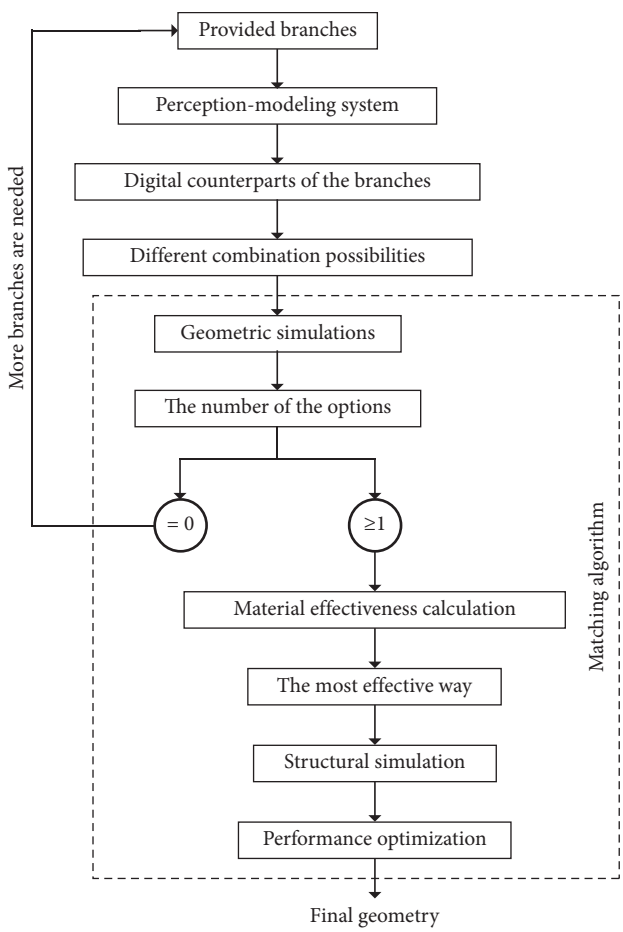


Figure 6: Workflow 1.

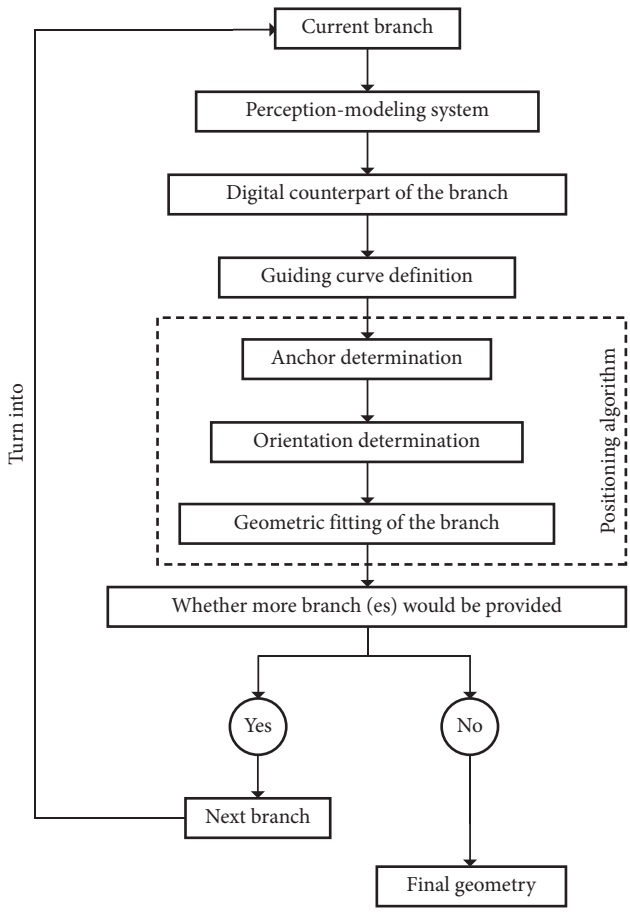


Figure 7: Workflow 2.

can react to new information acquired during the actual fabrication process rather than merely executing the previously compiled machine code.

*3.4.1. Executing Program.* Robotic executing program is developed in Grasshopper/KukaPrc. They output synchronous serial commands for the effector actuation in coordination with the dynamic design. Once the design model calculates the position of a branch, the robotic arm would move it to the corresponding location for assembly. In addition, a pause function and a forced-termination function are added to the program in order to prevent accidents.

*3.4.2. Monitoring and Adjusting Program.* The monitoring and adjusting program is developed using Grasshopper Python to quickly validate the assembly operation before its output in the real world. A monitoring module made of Kinect device is embedded in the end effector of the robotic arm to perform real-time skeletal detection. Quokka, a software tool for connecting Kinect with Grasshopper, is edited to use the Kinect as a 3D scanner. With the monitoring module, points and vectors could then be extracted from the centreline throughout the geometry of the branch, and then the actual status of the branch could be compared with the digital simulation. Adjusting codes are written in Grasshopper Python for modifying the assembling location if the difference between real geometry and digital geometry exceeds the threshold value.

## 4. Experimental Results and Discussion

Based on the above-discussed cyber-physical system, this research constructed two experimental pavilions to verify the feasibility. The processes and results are explained in the following sections.

*4.1. Experimental Case 1: "Robotic Knows" Pavilion.* The first experimental pavilion is called "Robotic knows." The pavilion is devised using a physical-virtual-physical procedure. Information extracted from the physical materials is processed to drive the digital design geometry and the digital model and, in turn, decides the robotic actuation in the physical space.

*4.1.1. Physical to Virtual: Material Perception and Design Generation.* In this pavilion, the abandoned "*Y*"-shaped branches with the length ranging from 75 cm to 245 cm are used, and their digital replicas are automatically built using the perception-modeling method developed in this study. The valuable data of the scanning branch are distilled, whereas the useless data that does not affect the design result, such as slight unevenness on the branch surface and the bending amplitude of each fork, are discarded. The valuable data include the following parameters: three-dimensional coordinates of the four points—P0, P1, P2, and P3—of the branch, the length between every two points, and the length and the thickness of each fork (Figure 8).

Then, the digital replicas of all the branches are used to generate the architectural design in Rhino/Grasshopper platform. Multiple screening is used to choose the organization method for all branches and to generate the corresponding architectural geometry. There are four levels of system screening: load-bearing screening, arrangement order screening, material effectiveness screening, and structural performance screening. In load-bearing screening, branches are sorted by volume, and the three largest branches are selected as the main supporting structure. In arrangement order screening, feasible arrangement orders are kept while incorrect arrangements are eliminated. As shown in Figure 9, for any two branches B and C, fix their P1 to P2 or P3 of branches A and check if they can intersect or not and then remove all the disjoint combinations. For the next layer, branches D and E connecting with branches B, repeat the logic. In material effectiveness screening, the total amount of useless material of every feasible arrangement is calculated and ranked. For all possible combinations, the intersection trajectory of branches B and C is an ellipse; choose the position that is closest to the central axis of branch A to ensure the overall stability, cut the useless parts of branches B and C, and repeat this process until all branches are linked to each other. Calculate the total cutting lengths of different options according to the information list of all the branches and rank all possibilities according to

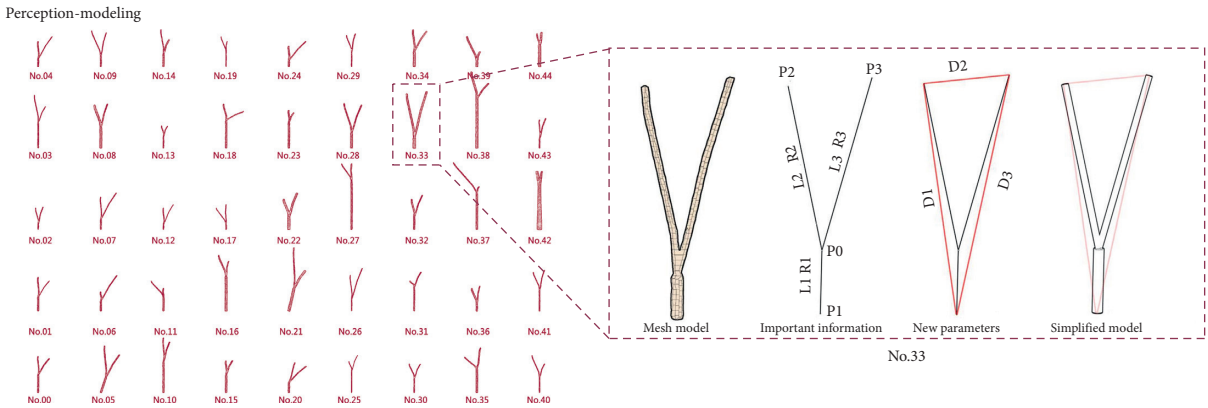


Figure 8: Information abstraction.

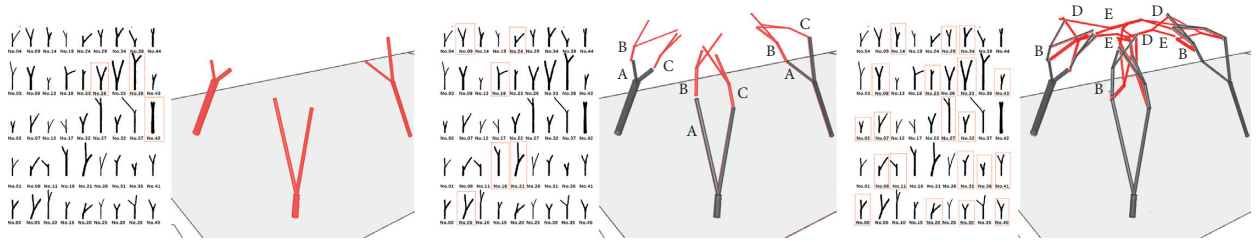


Figure 9: Computational generation process.

wasted materials. The top five options are selected. In structural performance screening, a plug-in of Grasshopper called "Millipedes" is used, and scripts are written in GH Python to test and optimize the structural performances of the five options. The best one is selected and optimized. The initial design sets three load-bearing branches from an empirical point of view. Nevertheless, the simulation results show that the shear force at the grounding points can be very strong and exceed their beating capacities. Therefore, modifications are proposed, and more small supporting branches are added. The upper part of the geometry is also regenerated to make the force distribution more uniform (see Figure 10).

*4.1.2. Virtual to Physical: Real-Time Data Flow and Robotic Construction.* Once the geometry is generated and optimized, data is transmitted from Grasshopper to the robot arm for creating a direct link between the digital design and the physical construction. Robotic construction includes the following two parts: localization and motion planning. In the localization part, a reference location is used to make the robot "know" its position. The results show that the position accuracy can be achieved within 2 cm. In the motion planning part, a plug-in called KukaPrc is used to control the robotic actuation. The program is written for computing the movement data based on the digital model (Figure 11).

The last step is joint designing for feedback error correction. At present, two methods are available for removing the errors: reducing errors by higher precision control and designing structures with larger error redundancy to directly absorb the errors. Considering the complexity and reliability, this experiment adopts the latter strategy. A special node with universal joints, three-way pipes, and jackscrews is designed to fix the major error. The universal coupling is very flexible and can freely adjust the distance and the angle of the two connection points. Before positioning the branches, the cardans are fixed on each branch. Each pipe with a universal joint is fixed with a fork, and there are three universal joints in each node that are connected by prefabricated metal pipes instead of the traditional shaft. The branch is autonomously moved to the corresponding position by the robot, whereas the cardans are manually welded, and the node is manually locked by the architects. The newly designed joints ensure structural stability and local adjustment (Figures 12 and 13).

*4.2. Experimental Case 2: "Robotic Eye-Brain-Hand Coordination" Pavilion.* The second experimental pavilion is referred to as the "robotic eye-brain-hand coordination." The pavilion is evolved by cyber-physical iteration with sensor-actuator feedback. The perception-modeling system is embedded in the end effector of a robot and is considered as the "eye" (the sensing end) of the iteration system, which reads the characteristics of the scanned branch and transfers the data to Rhino/Grasshopper on a PC. The "brain" (the calculation end) analyzes the data to calculate the position of the scanned branch. The "hand" (the action end), i.e., the robotic end-effector, assembles the branch autonomously without programming its motion code in advance. The "eye-brain-hand" program loop operates continuously, gradually evolving and unfolding the overall geometry of the pavilion (Figure 14).

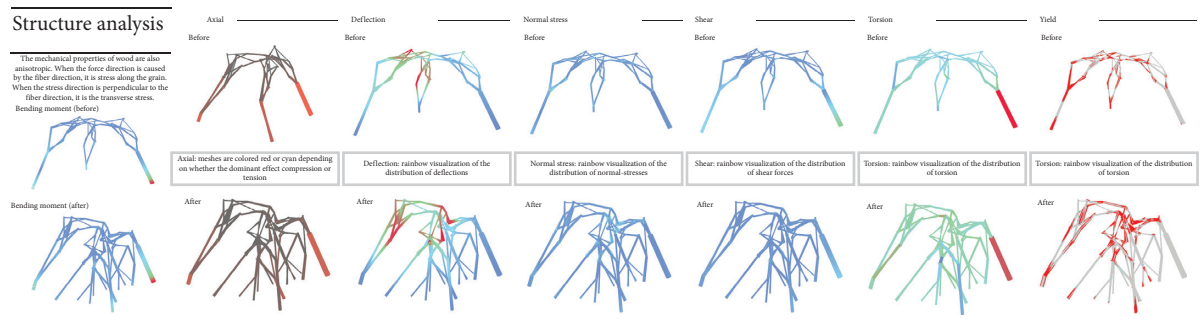


Figure 10: Structural performance analysis.

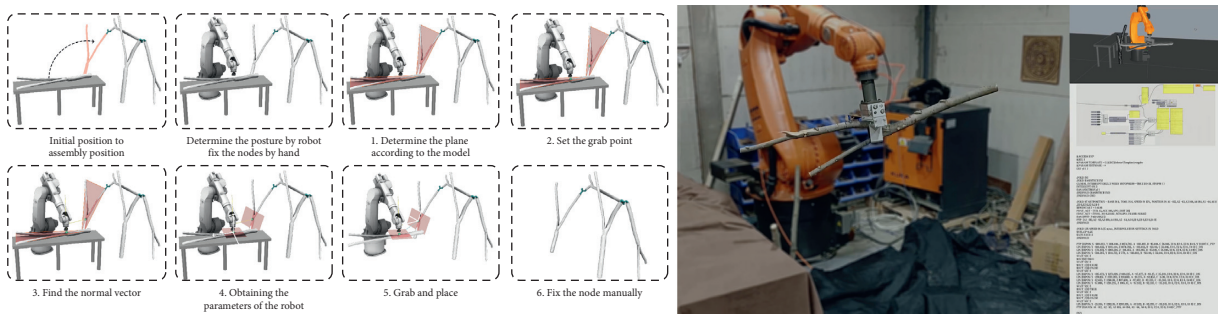


Figure 11: Robotic motion planning.

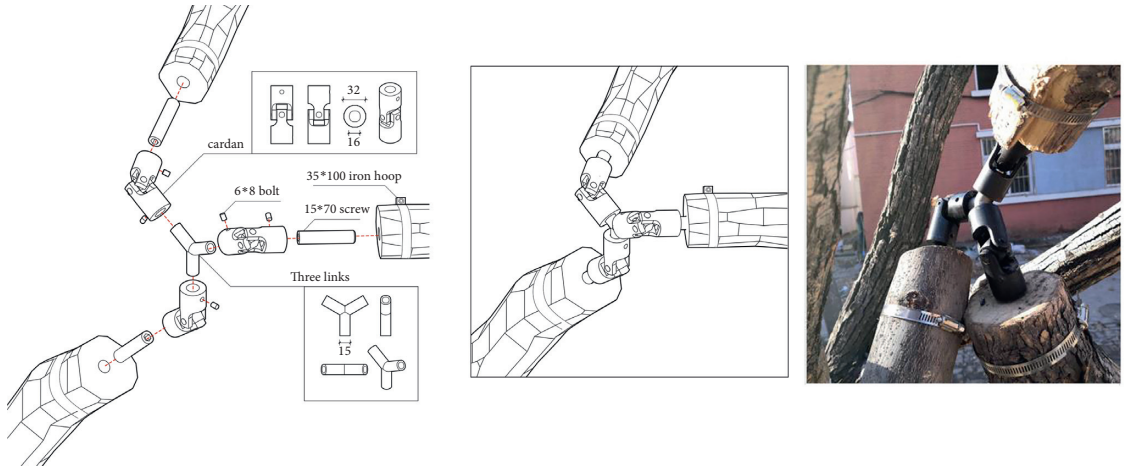


Figure 12: Joints.

Figure 13: "Robotic knows" pavilion.

The source materials of this pavilion are "*V*"-shaped branches with lengths ranging from 35 cm to 100 cm. The shape and size of the source material are different from those of the former pavilion for testing the adaptability of the perception-modeling system. The results show that it works well.

The positioning algorithm is programmed according to the aesthetic tendency, structurability, and structure performance. First, a guiding curve is defined by the designer. The space function and site conditions would affect the designer's conception. The site of this pavilion is flat, where

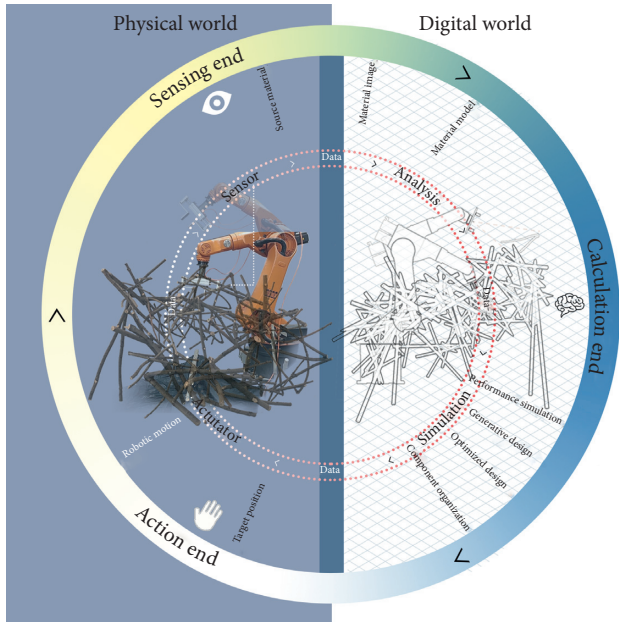


Figure 14: Cyber-physical construction.

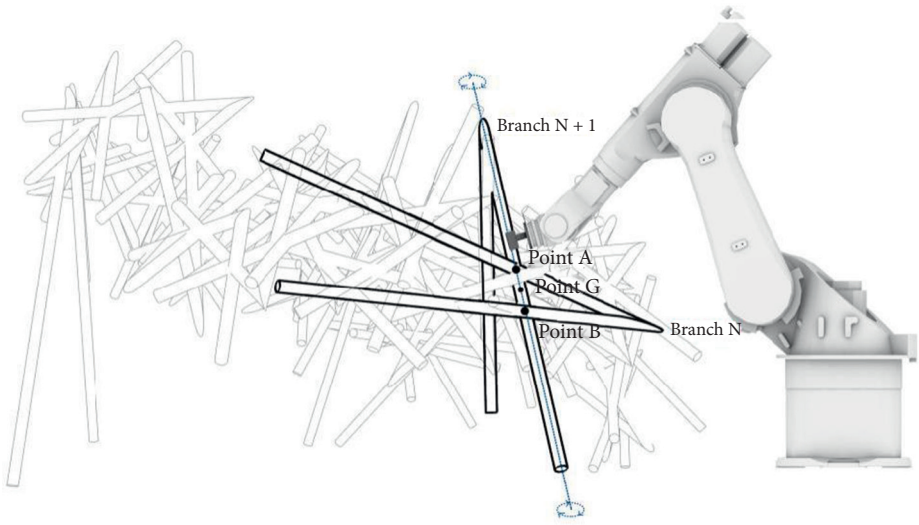


Figure 15: Branch assembly.

there are no roads or obstacles. Hence, a decreasing spiral guiding curve is defined, expecting that a closed shield is formed with an entrance hole. Then, the number of joints and joint positions are set based on the structurability and structure performance. Before the actual construction, testing experiments were conducted, and the results showed the following logic ensured feasibility and stability: the position of the current branch is determined by itself and the previous one. When assembling branch $(N+1)$, its midpoint G of the longer fork is found and then one-third of points near the branch attachment points A and B of branch N are computed; the midpoint of line AB coincides with the point G, and the longer fork in branch $(N+1)$ is passed through points A and B so that the joint position of branches $(N+1)$ and branch N is known. At this time, branch $(N+1)$ can be rotated along the AB axis and its rotation angle is determined by the tangent direction of branch $(N+1)$ to the nearest point of the guiding curve so that the assembly location of branch $(N+1)$ is determined (Figure 15).

The monitoring programs and adjusting programs are developed to prevent the problems before they even occur. Codes are written in Grasshopper and KukaPrc to allow real-time rectifications. In the digital model, the closest point selected each time is compared to the former one. If the current closest point grows in the opposite direction of the generating surfaces, the former point replaces it. This loop continues until the generating surface moves beyond the guiding curve. If there is any problem during the

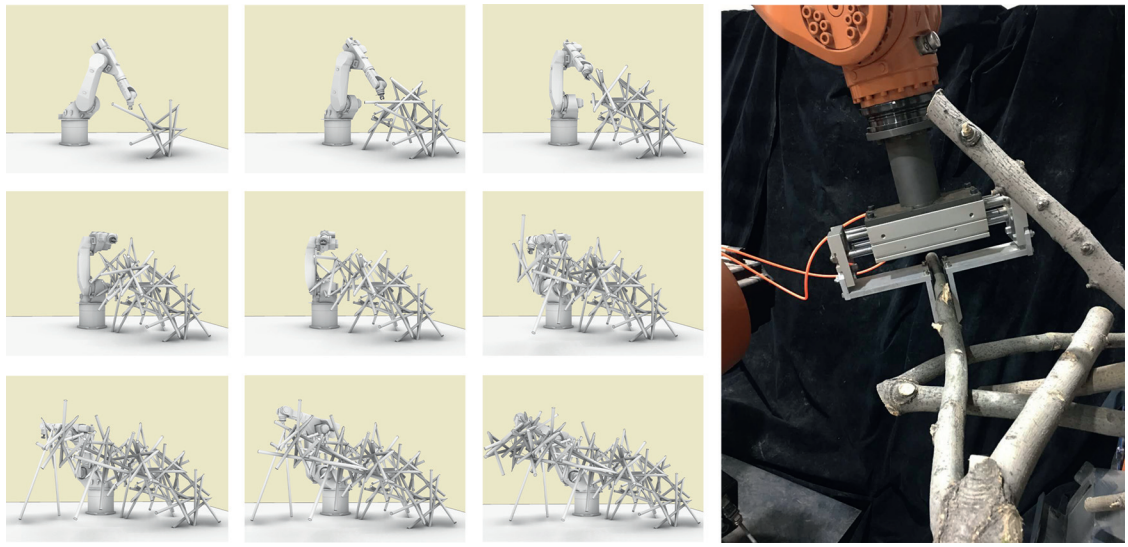

Figure 16: Robotic construction process.

(a) (b)

Figure 17: Digital simulation and physical construction.

construction process, the data are fed back to the digital model in Grasshopper for a real-time adjustment (Figures 16 and 17).

The end effector of the robotic arm is custom-designed and is supposed to hold the branch firmly and be available for the different surface qualities of all the provided wood branches. First, an electronically controlled claw is used. By using the AFMotor library in Arduino, the opening and closing states, running speed, and rotation direction of the gripper can be controlled in real time. However, such a claw has the following limitations: its opening and closing range is only 0–90 mm, and its maximum force weight is only 16 kg, so it is considered suitable for grabbing only light and thin branches. In order to improve the grabbing ability, the pneumatic parallel open/close claw is finally selected and modified. The size between the parallel plates is adjusted to match the diameter of the branch. The contacting surface of the plates is coated with a special rubber material for increasing the coefficient of friction so that the branch is not twisted. The features of this developed pneumatic claw are as follows: (1) wide opening and closing range, (2) greater grabbling ability, (3) being suitable for branches with different sizes and weights, and (4) the capability of being connected to the GH function and controlled by the generative digital model.

*4.3. Discussion.* The main advantages of the digital twin paradigm presented by the two pavilions are as follows.

First, the design-construction system becomes more adaptive and flexible. The traditional approaches usually present design by using static modeling and are not able to manage the challenges of dynamic conditions and the changing demands on the construction site. In the digital twin paradigm, generative design with updating information can optimize the output in real time in response to the source materials and unpredictable changes on the site.

Second, collecting and sending the data simultaneously improves the efficiency of handling complex material information and allows better use of each resource. Significant benefits of reduced managing time and cost can be achieved by the virtual experimentation of the generating and assembling process.

Lastly, the digital twin model is continuously updated with all the evolutionary changes and modifications in the physical system, and design and construction are no longer

disconnected and rather collaborate in a digital loop, offering a reasonable design and achieving a more efficient and precise actual realization.

Although these two pavilions focus on wood branches, the digital twin paradigm for generative design and robotic construction is applicable to other local source materials. By using the cyber-physical system, material scanning can be combined with a digitally arranged and robotically assembled continuous real-time workflow. Similar to the presented experimental cases, the final design and appearance emerge only after analyzing and responding to the geometric variability of the material.

## 5. Conclusion and Future Work

In this research work, a real-time perception-modeling system is explored for digitizing wooden branches of variable shapes, and the generated data is deployed later in both generative design and robotic construction phases. Using this system, material data were obtained and transformed from the physical space to the digital space. The data were subjected to geometrical optimization and structural simulation. In coordination with the digital model, the robot simultaneously outputs synchronous serial commands for the effector actuation. The following contributions of this research can be concluded.

First, a stable, robust, and easy-to-use material scanning method is explored. By implementing this method in perception-modeling phase, the unique geometrical information of each unprocessed wooden branch can be digitalized and abstracted so that all of the data is stored in a master digital twin model. This component information is later used in both generative design phase and robotic construction phase for different purposes.

Second, this research focuses on reusing unprocessed wooden branches as the basic components for two on-site constructed pavilions, in which the solutions are oriented toward the source material and the changing environment instead of a predefined workflow. The system is established with the capacity of integrating all data from preparation to construction phases and being updated according to real-time data.

Third, two practical construction cases are built and studied under guidance of the digital twin paradigm. All of the process data is stored and extracted back and forth from a master model, ensuring the data consistency and providing excellent efficiency in dealing with complicated geometry cases. Besides, the developed paradigm can reversely benefit the traditional discrete construction system with the method of adaptive process that copes with inevitable construction errors by feeding real-time information and making alternative decision iteratively.

In this report, a series of potential improvements are presented. First of all, the material sensing part can be improved. Different types of sensors are installed, and the analysis algorithms can be optimized. Therefore, the system is able to perceive and utilize other kinds of material information, such as strength and toughness. Second, the cyber-physical iteration part can be further optimized to deal with physical construction errors. In the robotic arm assembly part, errors inevitably exist between the real and the ideal environments, which may degrade the performance. Further improvement can be achieved by developing a global monitoring system together with the local joint scanning scheme, which provides necessary overall geometric modifying indications towards the ideal form. According to the difference between real geometry and digital geometry, a new strategy should be generated in real time for adjusting the assembling location of the next component.

The theory and method of this study can be used in future research. The digital twin paradigm opens up the possibility of integrating material variability by using highly customized analysis, calculation, and fabrication process [27]. Irregular timber panels or trunks can be analyzed for geometric fitting in large-scale constructions.

## Data Availability

The data used to support the findings of this study are included within the article.

## Conflicts of Interest

The authors declare that there are no conflicts of interest regarding the publication of this paper.

## Acknowledgments

This study was funded by Tianjin Science Foundation (agreement no. 19JCQNJC07300).

## References

[1] KUKA, http://www.kuka.com/.
[2] ABB, http://global.abb/.
[3] A. Menges, "The new cyber-physical making in architecture: computational construction." *Architectural Design*, vol. 85, no. 5, pp. 28–33, 2015.
[4] M. Grieves and J. Vickers, "Digital twin: mitigating unpredictable, undesirable emergent behavior in complex systems," in *Transdisciplinary Perspectives on Complex Systems*Springer, Berlin, Germany, 2017.
[5] S. Christoph, "Ein architektonisches periodisierungsmodell anhand fertigungstechnischer kriterien, dargestellt am beispiel des holzbaus," Ph.D. thesis, ETH Zurich, Zurich, Switzerland, 2019.
[6] M. Self, Z. Mollica, and P. Devadass, "Exploiting inherent material form," in *Proceedings of the 36th Annual Conference of the Association for Computer Aided Design in Architecture*, pp. 220–225, Ann Arbor, MI, USA, October 2016.
[7] P. Eversmann, F. Gramazio, and M. Kohler, "Robotic prefabrication of timber structures: towards automated large-scale spatial assembly," *Construction Robotics*, vol. 1, 2017.
[8] M. Alvarez, H. J. Wagner, A. Groenewolt, and O. D. Krieg, "The BUGA wood pavilion," in *Proceedings of the 36th Annual Conference of the Association for Computer Aided Design in Architecture*, pp. 490–499, Austin, TX, USA, October 2019.
[9] T. Schwinn, O. D. Krieg, and A. Menges, "Robotic sewing," in *Proceedings of the 39th Annual Conference of the Association*

*for Computer Aided Design in Architecture*, pp. 224–233, Austin, TX, USA, October 2019.

[10] V. Monier, J.-C. Bignon, and G. Duchanois, "Use of irregular wood components to design non-standard structures," *Advanced Materials Research*, vol. 671, pp. 2337–2343, 2013.

[11] C. Schindler, M. Tamke, A. Tabatabai, M. Bereuter, and H. Yoshida, "Processing branches: reactivating the performativity of natural wooden form with contemporary information technology," *Architectural Computing*, vol. 12, pp. 101–116, 2014.

[12] T/ADS, "STIK-DFL pavilion 2014," 2014, http://t-ads.org/blog/2014/11/18/stik-dfl-pavilion-2014/.

[13] T/ADS, "Pavilion: computational clay," 2017, http://t-ads.org/blog/2017/01/05/pavilion-computational-clay/.

[14] A. A. Malik, A. Bilberg, "Digital twins of human robot collaboration in a production setting," in *Proceeding of the 28th International Conference on Flexible Automation and Intelligent Manufacturing(FAIM2018)*, pp. 278–285, Columbus, OH, USA, June 2018.

[15] D. Almeida and J. P. Sousa, "Tradition and innovation in digital architecture reviewing the serpentine gallery pavilion 2005," in *Proceedings of the 35th eCAADe Conference*, pp. 267–276, Rome, Italy, September 2017.

[16] M. Larsson, H. Yoshida, and T. Igarashi, "Upcycling tree branches as architectural elements through collaborative design and fabrication," in *Proceedings of the 13th International Conference on Tangible, Embedded, and Embodied Interaction*, pp. 589–593, Tempe, AZ, USA, March 2019.

[17] M. Larsson, H. Yoshida, and T. Igarashi, "Human-in-the-loop fabrication of 3D surfaces with natural tree branches," in *Proceedings of the ACM Symposium on Computational Fabrication*, pp. 1–12, New York, NY, USA, June 2019.

[18] G. Brugnaro, E. Baharlou, L. Vasey, and A. Menges, "Robotic softness," in *Proceedings of the 36th Annual Conference of the Association for Computer Aided Design in Architecture*, pp. 154–163, Ann Arbor, MI, USA, October 2016.

[19] K. Wu and A. Kilian, "Design natural wood log structures with stochastic assembly and deep learning," in *Robotic Fabrication in Architecture, Art and Design*, pp. 16–30, Springer, Berlin, Germany, 2018.

[20] M. Jeffers, *Autonomous Robotic Assembly with Variable Material Properties*, Springer Press, Berlin, Germany, 2016.

[21] S. Boschert and R. Rosen, "Digital twin—the simulation aspect," in *Mechatronic Futures*, pp. 59–74, Springer, Berlin, Germany, 2016.

[22] A. Menges, "Integrative design computation: integrating material behaviour and robotic manufacturing processes in computational design for performative wood constructions," in *Proceedings of the 31th Conference of the Association For Computer Aided Design In Architecture (ACADIA)*, pp. 72–81, Banff, Canada, February 2011.

[23] M. Shafto, M. Conroy, and R. Doyle, *Modeling, Simulation, Information Technology & Processing-TA11*, National Aeronautics and Space Adminidtration, Washington, WA, USA, 2010.

[24] A. Bilberg and L. Alting, "When simulation takes control," *Journal of Manufacturing Systems*, vol. 10, no. 3, pp. 179–193, 1991.

[25] W. Kritzinger, M. Karner, G. Traar, J. Henjes, and W. Sihn, "Digital twin in manufacturing: a categorical literature review and classification," *IFAC PapersOnLine*, vol. 51, pp. 1016–1022, 2018.

[26] K. E. Harper, C. Ganz, and S. Malakuti, "Digital twin architecture and standards," *IIC Journal of Innovation*, 2019.

[27] P. Eversmann, "Robotic fabrication techniques for material of unknown geometry," in *Humanizing Digital Reality*, K. De Rycke, Ed., Springer, Berlin, Germany, 2018.

Hindawi
Advances in Civil Engineering
Volume 2021, Article ID 8824613, 17 pages
https://doi.org/10.1155/2021/8824613

*Research Article*

# A New Framework to Address BIM Interoperability in the AEC Domain from Technical and Process Dimensions

**Ran Ren and Jiansong Zhang**

*Automation and Intelligent Construction (AutoIC) Lab, School of Construction Management Technology, Purdue University, West Lafayette, IN 47907, USA*

Correspondence should be addressed to Jiansong Zhang; jiansong-zhang@purdue.edu

Received 7 August 2020; Revised 9 December 2020; Accepted 14 December 2020; Published 4 January 2021

Academic Editor: Emanuele Brunesi

Copyright © 2021 Ran Ren and Jiansong Zhang. This is an open access article distributed under the Creative Commons Attribution License, which permits unrestricted use, distribution, and reproduction in any medium, provided the original work is properly cited.

Building information modelling (BIM) is an integrated informational process and plays a key role in enabling efficient planning and control of a project in the architecture, engineering, and construction (AEC) domain. Industry foundation classes- (IFC-) based BIM allows building information to be interoperable among different BIM applications. Different stakeholders take different responsibilities in a project and therefore keep different types of information to meet project requirements. In this paper, the authors proposed and adopted a six-step methodology to support BIM interoperability between architectural design and structural analysis at both AEC project level and information level, in which (1) the intrinsic and extrinsic information transferred between architectural models and structural models was analyzed and demonstrated by a business process model and notation (BPMN) model that the authors developed; (2) the proposed technical routes with different combinations and their applications to different project delivery methods provided new instruments to stakeholders in industry for efficient and accurate decision making; (3) a new material-centered invariant signature with portability can improve information exchange between different data formats and models to support interoperable BIM applications; and (4) a newly developed formal material information representation and checking method was tested on a case study where its efficiency was demonstrated to outperform (i) proprietary representations and information checking method based on a manual operation, and (ii) the model view definition (MVD)-based information checking method. The proposed invariant signature-based material information representation and checking method brings a better efficiency for information transfer between architectural design and structural analysis, which can have significant positive effects on a project delivery due to the frequent and iterative update of a project design. This improves the information transfer and coordination between architects and structural engineers and therefore the efficiency of the whole project. The proposed method can be extended and applied to other application phases and functions such as cost estimation, scheduling, and energy analysis.

## 1. Introduction and Background

Nowadays, building information modelling (BIM) supports the critical data exchange in the architecture, engineering, and construction (AEC) domain among different models, applications, phases, and stakeholders. BIM can integrate geometric representations with a variety of semantic information of buildings. This contributes significantly to a shift in the method of information documentation and exchange among different types of models in the AEC domain. BIM acts as an innovative technology that connects two-dimensional drawings with three-dimensional models to integrate different lifecycle phases of a building or infrastructure in the AEC domain. The BIM interoperability problem is both a technical issue and a process issue. The technical dimension is reflected in the software workflows using various BIM applications. In the architectural design and structural analysis domains, this mounts to the importation and exportation compatibilities of various BIM authoring tools and engineering analysis software, and the interpretations and analyses of the imported/exported information in these software packages. The process

dimension is reflected in the actual use of modelling information between the architectural design and engineering analysis processes. The technical dimension focuses on the model (i.e., how the model is processed during importation/exportation from different software platforms) and the process dimension focuses on people (i.e., how people exchange information through the use of the models).

An engineering model is currently preferably created from scratch rather than adapting the building information models (BIMs) generated previously in a different software platform, because of the information missing and information inconsistency problems between directly converted architectural models and structural models. Missing information can cause uncertain or erroneous structural analysis results. Information inconsistency can cause confusions and misunderstandings between different stakeholders. In order to support interoperability between BIM applications, any missing or inconsistent information during the information exchange must be addressed. Existing research that explored BIM interoperability between architectural design and structural analysis heavily focused on the technical dimension with little or no consideration of the process dimension [1, 2]. There is a lack of a systematic methodology to develop BIM interoperability solutions based on demand analysis. To address that, in this paper, the authors proposed a new methodology that combined the consideration of the (1) technical information transfer process in the project delivery background context, and (2) analysis of information need and gaps, to lay the foundation of application-oriented BIM interoperability investigation. The information gap and need analyses focus on how the information flows between architectural design and structural analysis. An architectural model mainly describes building geometric information and appearance representation of a building. A structural model simulates the performance of structural elements under different types of loads. Both architectural design and structural analysis are key tasks in the process of constructing a building. Business process model and notation (BPMN) provides a set of constructs to support the representation of a business process. It is a notation scheme especially good for high level/domain level process analysis [3]. A BPMN diagram provides a graphical representation, therefore, facilitates an easier understanding of the process among different units within an organization [4]. In this paper, a BPMN model is used to capture the technical information transfer process. Segment-based technical interoperability routes are developed in the context of project delivery methods. The authors identified an urgently needed research task in helping with facilitating the provision of material information. To address that, the authors studied three main types of materials commonly used in a construction project, investigated how they could be provided in BIM, and proposed a new invariant signature-based [5–8] formal material information representation and checking method. A case study was conducted where the material information representation and checking method was applied to a 12-storey concrete frame model. The case study results demonstrated the efficiency of the proposed material information representation and checking method to support information transfer between architectural design and structural analysis, based on its comparison with a manual method.

## 2. Literature Review

*2.1. BIM and IFC Model View Definitions (MVDs) Application.* BIM has been theorized by Dr. Chuck Eastman, 45 years ago [8]. In the AEC domain, a widely accepted and matured technical platform, which is based on an open standard, can enable communication and collaboration among different stakeholders without requiring them to have specific skills or proprietary applications. BIM provides the platform to transform the communication of participants in the AEC area from a one-to-one paradigm to a many-to-one paradigm. While BIM interoperability of a system with itself and/or with other systems is a constantly challenging issue in the AEC domain; it needs to be investigated both in the technical dimension and the process dimension [9].

Industry foundation classes (IFC) have been developed by an industry consortium since 1994. Since then, industry context, standardization organization, resource availability, and technology development of BIM applications have exposed the standardization process to a dynamic environment centered around IFC [10]. IFC model view definitions (MVDs) are specification documents that define exchange protocols between different BIM applications, by specifying a set of concepts and relationships needed for the exchange. Therefore, MVD can help BIM developers incorporate IFC compatibility into their software development [11]. An MVD has two main parts: definitions and configurations. Definitions refer to the range of the possible concepts and relationships, whereas configurations refer to how the definitions should be used in a specific application context. For example, in the quantity take-off application context, the model of a concrete wall requires the following three possible relationships to be defined between 3D objects: disjoint, nested, or overlapping [12]. MVD is a useful construct for information checking of IFC data. Using MVD, entity instances (e.g., "IfcMaterial") could be checked, and a validation report will be created that lists entity instances and their numbers of occurrences [13]. MVD tools provide a platform to implement MVD definitions and concepts. However, attributes of entity instances usually could not be directly checked using the MVD tool (e.g., IfcDoc software).

*2.2. BIM Interoperability from Technical and Process Dimension Analyses.* From the technical dimension, BIM interoperability indicates the ability to exchange data with other systems without major modifications [14]. BIM enables visualization techniques, such as augmented reality, to be applied to the AEC domain, for goals such as defect management, facility management, and preview of a built environment before construction [15–18]. BIM can be applied to energy modelling and energy simulation as well,

where it has been identified that there is a gap in conversations between BIM applications and energy modelling tools during construction management [19, 20]. The integration of geographical information system (GIS) with other techniques (e.g., real-time location system) for BIM applications can improve the interoperability of different data types. For example, the IFC model can be imported into GIS to be further processed [21, 22]. In spite of the fast development of BIM, the AEC domain is still facing the problem of information missing between different BIM models, applications, and systems.

From the process dimension, BIM supports project management in procurement, construction, prefabrication, and facility management, among others [23, 24]. Although BIM-based construction networks improved the communication among geographically separated participants, how to maintain collaboration that comes from multiple disciplines and organizations is still a problem to solve [25–27]. With the development of a growing number of universities beginning to offer BIM-related courses in their AEC related programs, BIM becomes a promising vehicle for the education sector to introduce new information technology [28, 29]. To catalyze the development and harnessing of benefits mentioned above, information inconsistency between different stakeholders needs to be addressed to meet the BIM interoperability goal.

*2.3. BIM for Architectural Design and Structural Analysis within the Context of Project Delivery Method.* The integration of data, processes, and functions in a construction project is a major challenge that makes a technical development restrained by its process context [30, 31]. In construction, there are many different types of project delivery methods which sets the tone of a process context such as design-bid-build (DBB), design-build (DB), construction management at risk (CMR), construction management agency (CMA), construction management multiprime (CMMP), and integrated project delivery (IPD). At the high level, these methods can be organized into two categories based on whether the design and construction contracts are combined or separated, which dictate if the interaction between architectural design and structural analysis can be direct: (1) in DB and IPD, the design and construction contracts are combined, which allow architectural design and structural analysis to have direct and frequent interactions, whereas (2) in DBB, CMR, CMA, and CMMP, the design and construction contracts are separated, which render the interactions between architectural design and structural analysis indirect and less frequent. In practice, the selection of the best project delivery method depends on many factors such as the type of project (e.g., residential, commercial, and industrial), the experience and preference of the owner and other stakeholders on different types of design and construction contracts (e.g., combined or separated), the weights of construction cost, schedule, quality, and financial risk in their considerations, the available physical and intellectual resources, etc. [32, 33]. In the existing project delivery practice, an architectural model could not be directly used as a structural model. Structural engineers need to abstract useful information from the architectural model (or from the architects) to support the development of a structural model [34]. In addition, among all project delivery methods, the collaboration between architects and structural engineers is important, and their interactions are most likely to be frequent and iterative [35, 36].

*2.4. Limitations of Previous Research.* From the technical dimension, although BIM has shown profound positive effects in the AEC domain, information missing and inconsistency between different software, platforms, systems, or applications remain challenging. How to quickly identify the missed information and how to bridge the gaps between different information representation methods are essential for BIM interoperability, which request new approaches to support interoperable BIM both at the information level and at the application level. From the process dimension, different project delivery methods have different contract and organizational structures, which in turn forms different information communication/interaction loops. How to effectively integrate interoperable BIM technologies into such communication/interaction loops need to be considered at any phase of the lifecycle of a building or infrastructure project, the result of which could provide a new instrument for decision making to support BIM interoperability.

## 3. Research Methodology

At the information level, the BIM interoperability problem revolved around identifying information missing and information inconsistency between different data formats, platforms, and applications. At the processing level, BIM interoperability problem focuses on how to leverage techniques, skills, and methodologies to develop roadmaps for interoperable BIM applications. At the service level, the BIM interoperability problem requests user-friendly solutions for stakeholders in the industry to use for supporting their efficient and accurate decision making. To address the BIM interoperability problem by combining considerations in both the technical dimension and the process dimension, the authors propose a six-step method as explained below:

*Step 1:* (*BIM Application Phases/Functions Selection*). This step defines two application phases/functions between which BIM interoperability will be studied. Example application phases/functions include architectural design, structural analysis, cost estimation, and energy simulation, among others.

*Step 2:* (*BPMN Generation*). This step identifies the needed information transfer and communication between different stakeholders (e.g., architects and structural engineers) and creates a BPMN correspondingly for project delivery. In this step, the intrinsic and extrinsic information transferred between different models (e.g., architectural model and structural model) are demonstrated and analyzed to support BIM interoperability at the information level. In

generating the BPMN, procedures to produce both models will be investigated.

*Step 3:* (*Technical Routes Analysis for BIM Interoperability*). This step analyzes the BPMN and literature from the technical angle of view and identifies possible route segments for BIM interoperability between selected phases/functions. The developed technical routes with different combinations provide a new instrument for decision making from the process dimension for the purpose of information transfer. The proposed technical routes provide the backbone of the information transfer to support interoperable BIM applications.

*Step 4:* (*Information Need and Gap Analysis*). Information missing and inconsistency takes a central position in the BIM interoperability problems that need to be solved between different formats, platforms, and applications. Therefore, this step focuses on information missing and information inconsistency analysis (i.e., gap analysis) during the information transfer between different phases/functions based on data analysis, and identifies information representation and checking needs for IFC-based BIM interoperability. In this step, the authors analyze the information acquisition of different types of models and set the tone of the BIM interoperability solution.

*Step 5:* (*Solution Development)*. This step develops an augmented model view definition (MVD) model with customized algorithms to help check an IFC model for meeting specific information requirements to fill in the gap identified in Step 4. In addition, an invariant signature-based information representation method and its application on different project delivery methods help define augmented model view definitions (MVDs) with customized algorithms to fulfill information checking and validation goals. It provides an information representation and checking environment to process information between different models, which facilitates information communication efficiency and accuracy.

*Step 6:* (*Case Study Evaluation*). This step evaluates the information representation and checking method by implementing developed checking MVDs/algorithms and applying them to a case study. The use of the developed checking MVDs/algorithms will be comparatively evaluated with a pure manual approach. The evaluation helps demonstrate if the proposed method will bring benefits to BIM applications from efficiency and accuracy perspectives.

## 4. Experimental Results and Discussion

*4.1. Step 1: BIM Application Phases/Functions Selection.* BIM information is exchanged between different applications at different phases of a project. There are different types of building information models (BIMs) for different applications at the design stage of a construction project, including architectural models, structural models, MEP models, energy analysis models, and cost estimation models, among others. In this paper, the authors selected two application tasks at the design phase-architectural design and structural analysis, because of the following: (1) both applications belong to the design phase, and therefore, it is expected to be easier for collaboration to happen comparing to two application tasks that belong to different phases such as the architectural design in the design phase and facility management in the operation phase; (2) the collaboration between architectural design and structural analysis is usually the first collaboration that happens in a project team; and (3) an effective collaboration between architectural design and structural analysis lays the foundation for other further collaborations (e.g., collaboration between architectural design and cost analysis) to succeed. Architectural design plays an essential role in creating the representational model (i.e., BIM) for a construction project [37]. Structural analyses explore the various stresses, strains, and displacements of the building elements. Currently, it is easier to create a structural analysis model from scratch rather than adapting from the corresponding architectural model [38]. Seamless information exchange between architectural design and structural analysis models could improve coordination effectiveness between architects and structural engineers and bring benefits in time and cost savings to the project team.

*4.2. Step 2: BPMN Generation.* The authors analyzed the information transfer and communication between architectural design and structural analysis applications and summarized a BPMN that describes steps for creating an architectural model and a structural model, with information exchange between the two models (Figure 1). Solid-line arrows represent step sequences for model creation processes. Dashed lines show information transfer between different steps or models. Information from earlier steps in each model will be saved and delivered to the following steps. The shaded area (i.e., create architectural columns-create doors-create windows-create floors-create ceilings-create stairs) in the process of creating an architectural model represents composite subprocesses, where detailed components of an architectural model are developed. A structural model will be created based on the information from the architectural model, such as geometric information and material information. For example, walls and roofs from an architectural model provide geometric information that can be used as references in the creation of the corresponding structural model. The first step in the process of creating a structural model is a composite subprocess, which includes simplifying geometric information and maintaining material information from an architectural model. For example, a beam or column is represented by simplifying its geometry into a straight line in the structural model without losing beam or column material features. The other information not readily transferred from the architectural model is then added. The nodes connection information is shown by points in the structural model while specifying the connection types. Geometric information and material information will be saved and delivered to later steps. Material

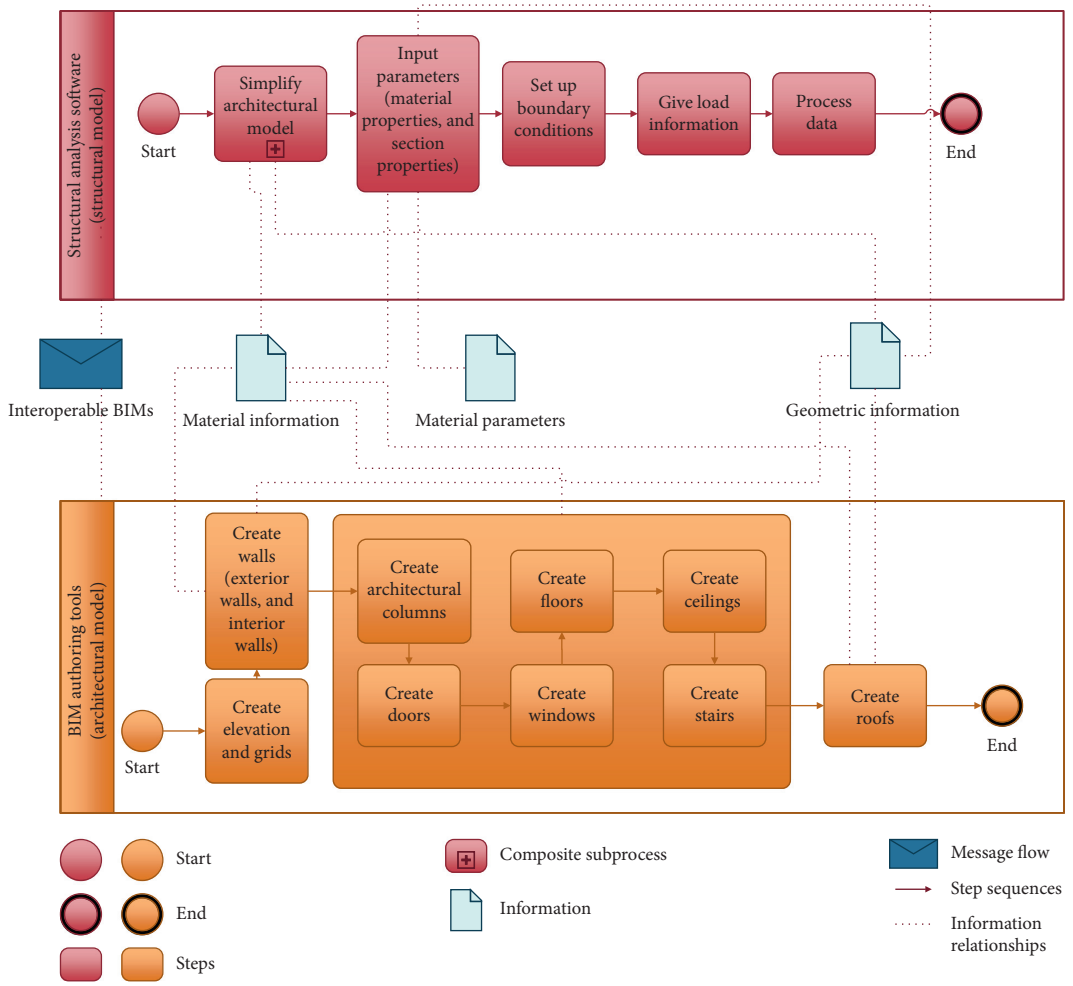


Figure 1: A BPMN representation of geometric and material information transfer.

parameters may need to be inputted manually to conduct structural analysis. An "envelope" symbol represents the overall message flow between an architectural model and a structural model. The BPMN represents the information transfer between different models and demonstrates that the intrinsic information of an architectural model can be the extrinsic information of a corresponding structural model (e.g., material information), which reflects potential BIM interoperability problems at the information level. The two model-development processes are usually conducted in different software by different personnel. Efficient information exchange between the architectural software and structural software and between the architect and structural engineer is, therefore, important.

*4.3. Step 3: Technical Routes Analysis for BIM Interoperability.* Based on analysis of most recent existing literature regarding BIM interoperability between architectural model and analysis model from technical and process perspectives (Table 1), it was found that most of the existing research only focused on developing roadmaps from the technical perspective, for example, developing software tools, system architectures, and information transfer mechanisms to support interoperable BIM applications [39–41, 9]. Other researchers solely focused on collaboration and integration framework of AEC projects to improve BIM interoperability [42–44]. There is a lack of systematic investigations in solving the information transfer problems from the technical dimension in the context of the process dimension to support BIM interoperability. To address the BIM interoperability issue that is initiated from the technical dimension in the context of the process dimension, the authors identified and proposed the following six technical route segments of interoperability between architectural design and structural analysis (Figure 2). A route for BIM interoperability would be a combination of one or more route segments to form a closed loop for information transfer. For example, *1-4-3* is one such technical route where information can be directly transferred from a proprietary architectural BIM to a proprietary structural analysis model; then, the structural analysis model can be exported to IFC and read back to the proprietary architectural BIM platform. To illustrate that an architecture model can be developed and saved in architectural design software (e.g., Autodesk Revit), in which the information could be directly read by compatible structural analysis software (e.g., Autodesk Robot); then, the structural analysis model that is developed based

Table 1: Sample work on BIM interoperability between architectural model and analysis model from technical and process dimensions.

| Literature | Main contribution | Technical dimension | Management dimension |
|---|---|---|---|
| [9] | Tested BIM interoperability in structural application among different AEC software platforms and found information missing and information inconsistency issues among BIM models | Yes | No |
| [39] | A new semantic approach to improve interoperability between BIMs and semantic model data | Yes | No |
| [40] | Integrated modelling and application interfaces to architectural design and specific analysis | Yes | No |
| [41] | An interpreted information exchange mechanism of IFC-based BIMs for information transformation from BIM design models to BIM application models | Yes | No |
| [42] | Addressed the interaction type and geographic range needs for BIM interoperability at the management level. | No | Yes |
| [43] | A decision-making tool and sustainability metrics to improve data sharing among various building models | No | Yes |
| [44] | Recommendations for BIM interoperability from the modular construction perspective | No | Yes |
| [45] | A CAD workflow for precast façade design to help BIM data exchange and use in project collaboration | Yes | Yes |
| [46] | Presented issues in visualization for IFC-based BIM interoperability | Yes | No |
| [47] | A method that combined IFC-based BIM conversion algorithms to convert architectural models to structural models while overcoming inconsistencies in data structures to improve BIM interoperability | Yes | Yes |
| [48] | Analyzed the interoperability between architectural design and structural analysis | Yes | No |

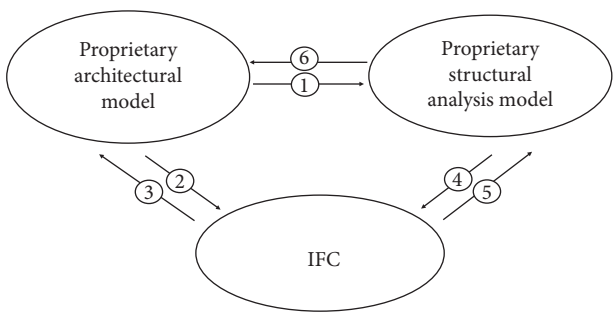


Figure 2: Six technical route segments of interoperability between architectural design and structural analysis.

on the information from the architectural model can be saved and exported as an IFC model, which can be read back to the architectural software. In this process, for instance, the dimensional information of a beam element in the architectural model can be transferred as values of $x$, $y$, and $z$ coordinates to the corresponding developed structural analysis model; then, the dimensional information in a structural analysis model can be exported as an entity instance "IfcCartesianPoint" in an IFC file, which can be imported and read back as dimensional information to architectural design software (e.g., Autodesk Revit).

In project delivery methods CMR and IPD, because the built-in collaboration enables architects and structural engineers to work together with other stakeholders as one team, the communication and negotiation between them and with the owners at an early stage of a project make it possible to identify/select architectural and structural software to use so that Route *1-6* becomes possible. For example, in CMR and IPD project delivery methods, the architects and structural engineers could work together to select compatible software both for architectural design and structural analysis (e.g., Autodesk Revit/Robot). In this process, a developed architectural model could be saved as a DWG format model and imported directly into the analysis software for structural analysis. In project delivery methods DBB and CMMP, however, because the owner or owner's representative establishes contracts with the different stakeholders separately, it is more difficult to specify compatible architectural or structural software to use for the architects and structural engineers. Therefore, the Route *2-5* is more feasible. For example, an architectural model created by an architect could be saved and exported to IFC format. Structural engineers could import the IFC file into a structural analysis tool to get the information (e.g., geometric information and material information) to conduct further analysis. In this process, the exported IFC file can be a bridge between architectural model/architectural design and structural model/structural analysis to support information transfer of interoperable BIM applications. For project delivery methods DB and CMA, although the owner does not hold all contracts individually and directly, Route *2-5* is still feasible. Therefore, *2-5* could be a potential solution for all project delivery methods if the quality of information transfer in this route can be guaranteed.

*4.4. Step 4: Information Need and Gap Analysis.* Based on analysis regarding information need and provision for architectural design and structural analysis at the model level, the authors summarized the following types of information needed in structural analysis/structural model: geometric

information, loads information, material information, connection type information, and boundary conditions.

Example types of information provided in architectural design/architectural model are elevation and grids information, geometric information (e.g., interior/exterior wall, columns, doors, windows, floors, roofs, and stairs), and material information (e.g., material name, colour, and texture information).

Between information missing and information inconsistency, the authors focus on the information missing problem, because this problem originates from (and roots in) the information generation process, e.g., designer or the BIM authoring tool (information provider) did not include the information, rather than coming from proprietary software or processing algorithms. In contrast, information inconsistency is more of a software implementation problem. Therefore, the information inconsistency problem needs to be solved software by software, whereas the information missing problem is possible to solve with automation and intelligent methods. According to Eastman et al. [49], there are three information providers in BIM: designer, derived data, and simulation or analysis. At the model level, material and geometric information are the essential parts of building elements based on the above-mentioned analyses. The authors argue that the information provider of the material information should be the designer/architect during the architectural design phase, either directly or indirectly together with geometric information of building objects for further use (e.g., structural analysis). Geometric information has been well studied in the literature, and material information representation and analysis is identified as a gap [41, 45].

*4.5. Step 5: Solution Development.* To support material information representation and coverage, the authors analyzed selected AEC software in terms of their material property settings in IFC based-BIMs (Table 2), which is a necessary step in both architectural design and structural analysis. In some software, materials can be selected directly, such as SolidWorks, which, however, is not specifically designed for civil structural analysis. In some software, only limited materials can be selected, for example, Graytec Advanced and SCIA software only include steel, concrete, and timber materials. Although some finite element analysis (FEA) software, such as ANSYS and ABAQUS, have been widely used for structural analysis, they have certain limitations when used for civil structural analysis. E.g., they can only be used to analyze small structures. In addition, the graphical user interface and application programming interface of FEA software need improvement in terms of information representations in civil engineering to be better used for civil structural analysis purposes [50, 51].

To successfully represent material information in the BIMs, the authors analyzed the needed material information in different analysis scenarios and summarized the needed material properties in each scenario into the authors' developed invariant material signature: mass, cross-sectional area, volume, mass density, stress, strain, shear stress, shear strain, shear modulus, Young's modulus, thermal expansion coefficient, and Poisson's ratio [48].

Based on the proposed material signature concept, the authors developed invariant material signatures for three main types of materials–steel, concrete, and wood. Figure 3 illustrates the detailed properties of these invariant material signatures.

From the process dimension, in different project delivery methods, the architects and structural engineers may choose software that may or may not be directly interoperable. Different interoperability scenarios will affect the possible technical routes to be used. For example, Route *1-6* (i.e., proprietary architectural model - > proprietary structural analysis model - > proprietary architectural model) become possible if the negotiations between architects and structural engineers and with the owners at an early stage of a project successfully identify selected architectural and structural software to use. In Route *1-6*, compatible software platforms provide proprietary channels to enable information and model transfer, but the limitations regarding material information missing and inconsistency still need to be addressed (Table 2). Otherwise, the Route *2-5-4-3* (i.e., proprietary architectural model - > IFC - > proprietary structural analysis model - > IFC - > proprietary architectural model) is more feasible. In Route *2-5-4-3*, the IFC model works as an intermediate data representation to support information and model transfer, which provides a new way to bridge architectural design and structural analysis tasks at the design phase.

The proposed material information representation method (i.e., the invariant material signatures) can be implemented for both Route *1-6* and Route *2-5-4-3*. The authors further leveraged technical BIM interoperability Route *2-5-4-3* to develop an IFC-based implementation, as providing solutions to direct information transfer between proprietary software (i.e., Route *1-6*) has to be conducted by the corresponding software companies. Similarly, the information inconsistency problem also has to be addressed by corresponding software companies even if an IFC-based workflow is used, by refining their exportation/importation to/from IFC or other formats to make sure it is error-free.

An IFC file not only contains geometric information of building elements, such as beams, columns, slabs, and walls, but also contains attributes for each object describing their physical and functional properties such as material properties and occupancy types. Figure 4 shows an example of a partial IFC file. In Figure 4, each line is representing an IFC entity and each argument in the parenthesis represents an attribute of this entity. For example, line #80 is one entity in the IFC file that represents material properties. In this entity, "#80" is its data line number, and "IfcExtendedMaterialProperties" is the name of the entity. "STD-Concrete" is one attribute value that is representing the name of an associated material. Material information such as material name can be extracted from such entities in the IFC physical file through analysis of a building element. For example, an "IfcBeam" can be linked to its related material entity (i.e., "IfcMaterial" in IFC file), which can be further related to other entities using "IfcRelAssociatesMaterial" [52]. Detailed material properties in the IFC files are defined by the entity "IfcPropertySingleValue." There

Table 2: Material property setting in different software platforms.

| Software | Software type | Choose material directly | Define new material | Comments |
|---|---|---|---|---|
| Tekla structure | Structural | √ | | |
| Autodesk Revit structure | | √ | | Besides materials, it also contains graphics, appearance, physical, and thermal properties. |
| ETABS | | √ | √ | |
| SAP 2002 | | √ | √ | |
| Graytec advanced | | √ | | Only cover steel, concrete, and timber materials. |
| SCIA | | √ | | If the material names in an IFC file are not in accordance with code names, it is necessary to define a material conversion table in the import dialogue. |
| CypeCAD | | √ | | Only cover steel, concrete, composite steel and concrete, and timber. |
| STAAD | | √ | √ | |
| PKPM | | √ | | The menu provides the diagram and calculation results of model rich graphics, and a template and reinforced material list. |
| MIDAS | | √ | √ | Cover concrete, steel, wood, and other types of material that a user defined. |
| ArchiCAD | Architectural | √ | √ | |
| ANASYS | FEA | √ | √ | |
| ABAQUS | | √ | √ | |
| Solid works | Engineering design | √ | √ | Concrete material parameters could not be defined. |

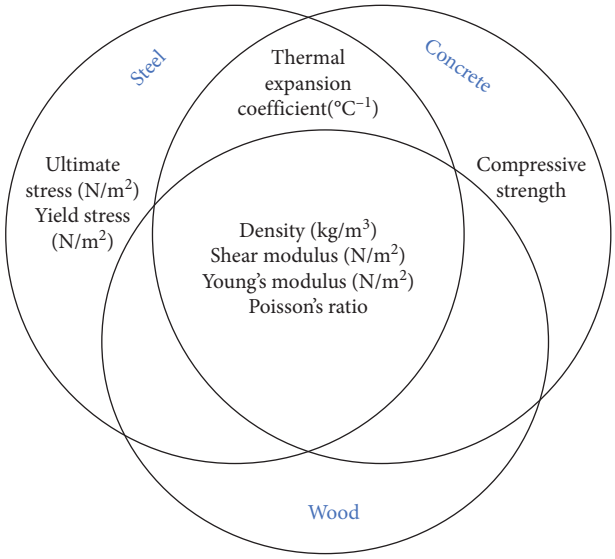


Figure 3: Material signature for different material types.

are four attributes of "IfcPropertySingleValue": "Name," "Description," "NominalValue," and "Unit."

Figure 5 shows a material property representation implementation diagram of a 12-storey building model in IFC, which was tested in the case study (Figure 6). It shows that, in this IFC file, any information related to material properties is rooted in an "IfcExtendedMaterialProperties" entity. There are four directly related entities which are "IfcMaterial," "IfcPropertySingleValue," "IfcText," and "IfcLabel" to represent material property details. There are four different types of material properties representations (attributes) in the entity of "IfcPropertySingleValue," they are "IfcIdentifier," "IfcText," "IfcValue," and "IfcUnit," which represent the material name, material description, nominal value of material property, and unit of value, respectively. Through the proposed invariant material signatures, IFC representation could represent material information in both the architectural model and the structural model in a consistent way.

The authors analyzed the IFC model regarding material information representation implementation in two versions: IFC2X3 and IFC4, and developed corresponding MVDs in IfcDoc software [52]. Attributes of the same entity (e.g., "IfcMaterialProperties") could be different between the two versions, e.g., in the IFC2X3 version, only the attribute "Name" is included in the "IfcMaterialProperties," whereas in the IFC4 version, it has "HasExternalReferences," "Name," "Description," "Properties," and "Material," five attributes in total. There is no relationship between attributes of the "IfcPropertySingleValue" entity and the "IfcMaterialProperties" entity in the IFC2X3 version. Whereas, in the IFC4 version, attribute "Properties" is the connection between the "IfcPropertySingleValue" entity and the "IfcMaterialProperties" entity (Figures 7 and 8). However, information from these different versions of IFC could all converge in our invariant material signatures.

Furthermore, because the IFC2X3 version has its limitations for model representation, some of the entities could not be used in the IFC2X3 version (Figure 9). As Figure 9 shows, some entities such as "IfcExtendedMaterialProperties" could not be defined in the IFC2X3 or IFC4 versions. Some entities such as "IfcMaterialProfile" and "IfcMaterialDefinition" could not be defined in the IFC2X3 version but could be defined in the IFC4 version. Its structure and relationships were also

```
ISO-10303-21;
HEADER;
FILE_DESCRIPTION (('ViewDefinition [CoordinationView]'), '2;1');
FILE_NAME ('Model 1 updated xz diaphragm p delta.ifc','2015-09-01T01:05:39',('Miqdad'),('gg'),'15.2.2','ETABS 2015','None');

FILE_SCHEMA(('IFC2X3'));
ENDSEC;

DATA;
#1=IFCRELAGGREGATES('0nViTsTdvAih6qtPD70Hxd',#3,$,$,#4,(#5));
#2=IFCRELAGGREGATES('1ZBISaGP5AAuDmjUWsOILr',#3,$,$,#5,(#6));
#3=IFCOWNERHISTORY(#7,#8,$,.NOCHANGE.,1441069539,$,$,1441069539);
#4=IFCPROJECT('0bepq99WH6SPBtaUQvpxcj',#3,'Model 1 updated xz diaphragm p delta.$et',$,$,$,$,(#9),#10);
#5=IFCSITE('3dLvXUwrbB7Q9q0FWDCaP$',#3,'Default Site',$,$,$,$,$,.ELEMENT.,$,$,$,$,$);
#6=IFCBUILDING('0pYH7FsGP18gLYtfcLzLR8',#3,'Default Building',$,$,$,$,$,.ELEMENT.,$,$,$);
#7=IFCPERSONANDORGANIZATION(#11,#12,$);
#8=IFCAPPLICATION(#13,'15.2.2','ETABS 2015','ETABS 2015');
#9=IFCGEOMETRICREPRESENTATIONCONTEXT('Project World','Model',3,$,#14,$);
#79=IFCCOLUMN('3zWBvyzd5BgQ6Z_5MwzlJl',#83,'1',$,$,#84,#85,$);
#80=IFCEXTENDEDMATERIALPROPERTIES(#86,(#87,#88,#89,#90,#91,#92),$,'STD-CONCRETE');
#81=IFCRELASSOCIATESMATERIAL('03Qfl2zgj5eBwGF3FEEjJP',#3,$,$,(#79),#86);
```

Figure 4: Sample IFC entities representation.

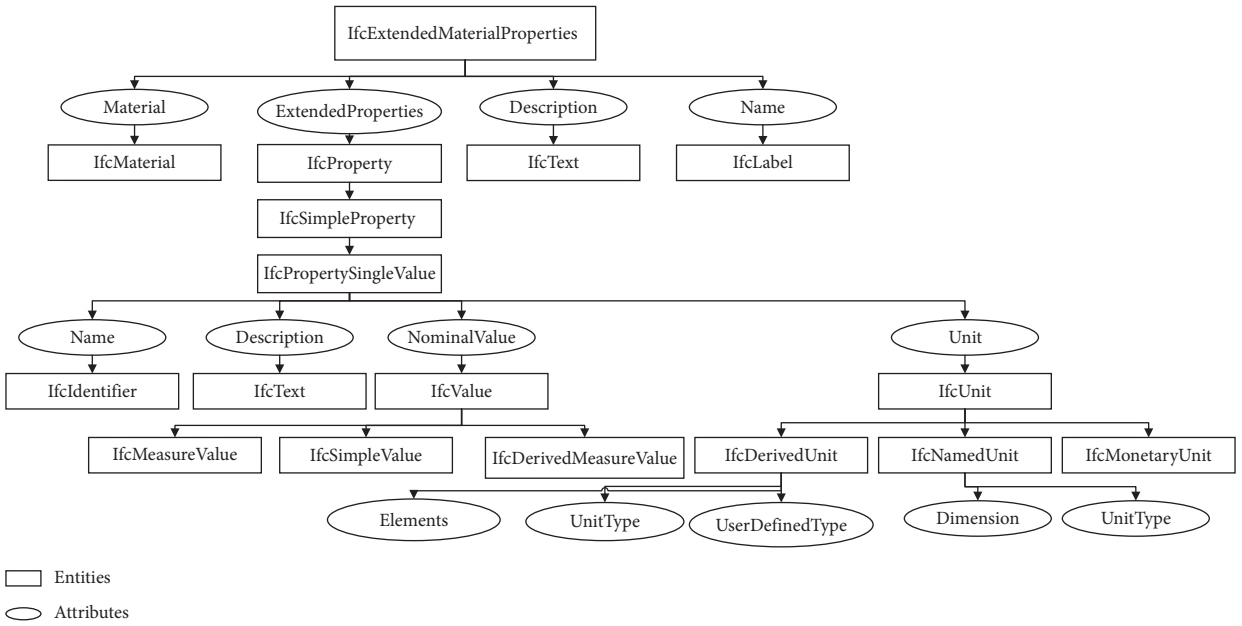


Figure 5: Common material property representation based on IFC schema.

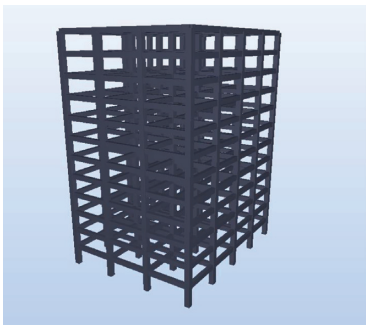

IFC 2 × 3 concrete

Material signature
(i) Mass density
(ii) Thermal expansion coefficient
(iii) Shear modulus
(iv) Poisson's ratio
(v) Compressive strength
(vi) Young's modulus

Figure 6: The 12-storey concrete building used in case study.

different from the IFC4 version. For example, there were three attributes "Name," "HasRepresentation," and "ClassifiedAs" for the entity "IfcMaterial" in the IFC2X3 version. But there were nine attributes "AssociatedTo," "HasExternalReferences," "HasProperties," "Name," "Description," "Category," "HasRepresentation," "IsRelatedWith," and "RelatesTo" for the entity "IfcMaterial" in the IFC4 version. Based on the structure of IFC4, it could represent more information because it incorporated more abundant entity attributes than IFC2X3.

The authors proposed a framework of material information checking based on augmenting the above MVD models with customized algorithms, as well as based on the proposed invariant material signatures. Among the three main types of materials discussed in this paper, the only difference in their MVD validating results would be the number of entities, because the detailed material information is contained in the "Name" and "NominalValue" attributes of the "IfcPropertySingleValue" entity. E.g., for steel material, seven required entities are checked that contained seven parameters: MassDensity, PoissonRatio, ShearModulus, ThermalExpansionCoefficient, UltimateStress, YieldStress, and

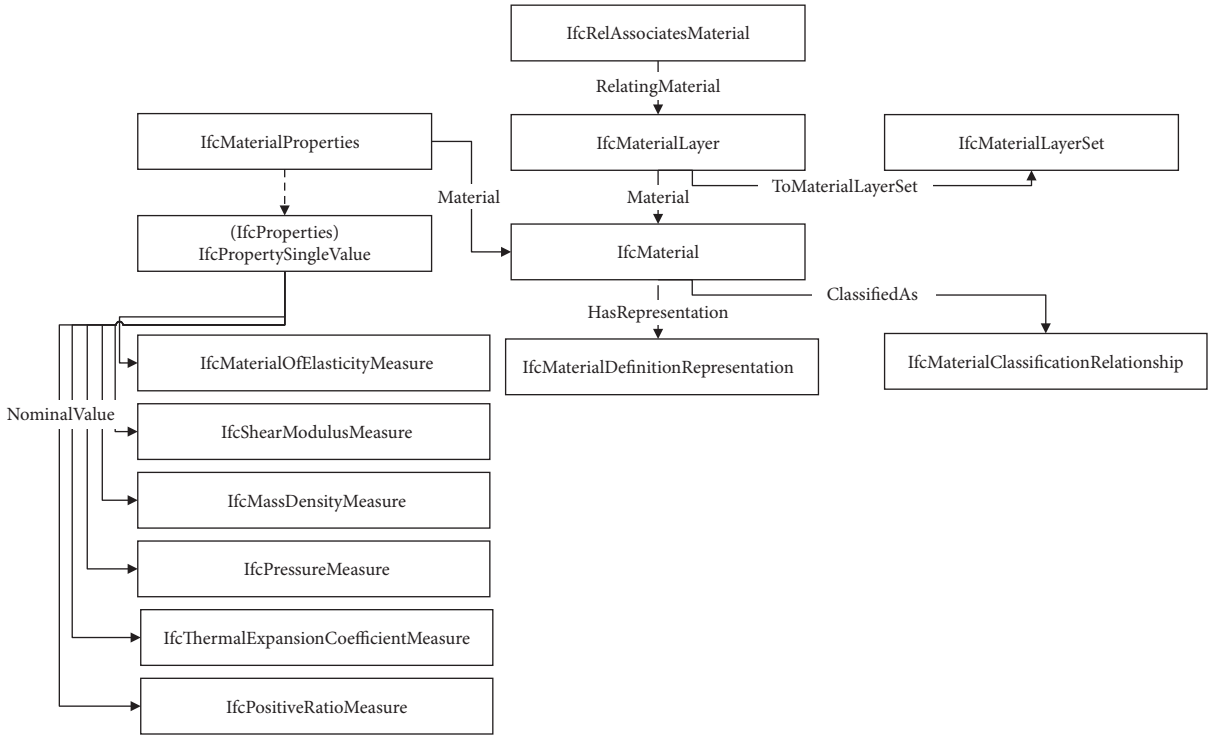


Figure 7: Structure of the IFC2X3 version of MVD.

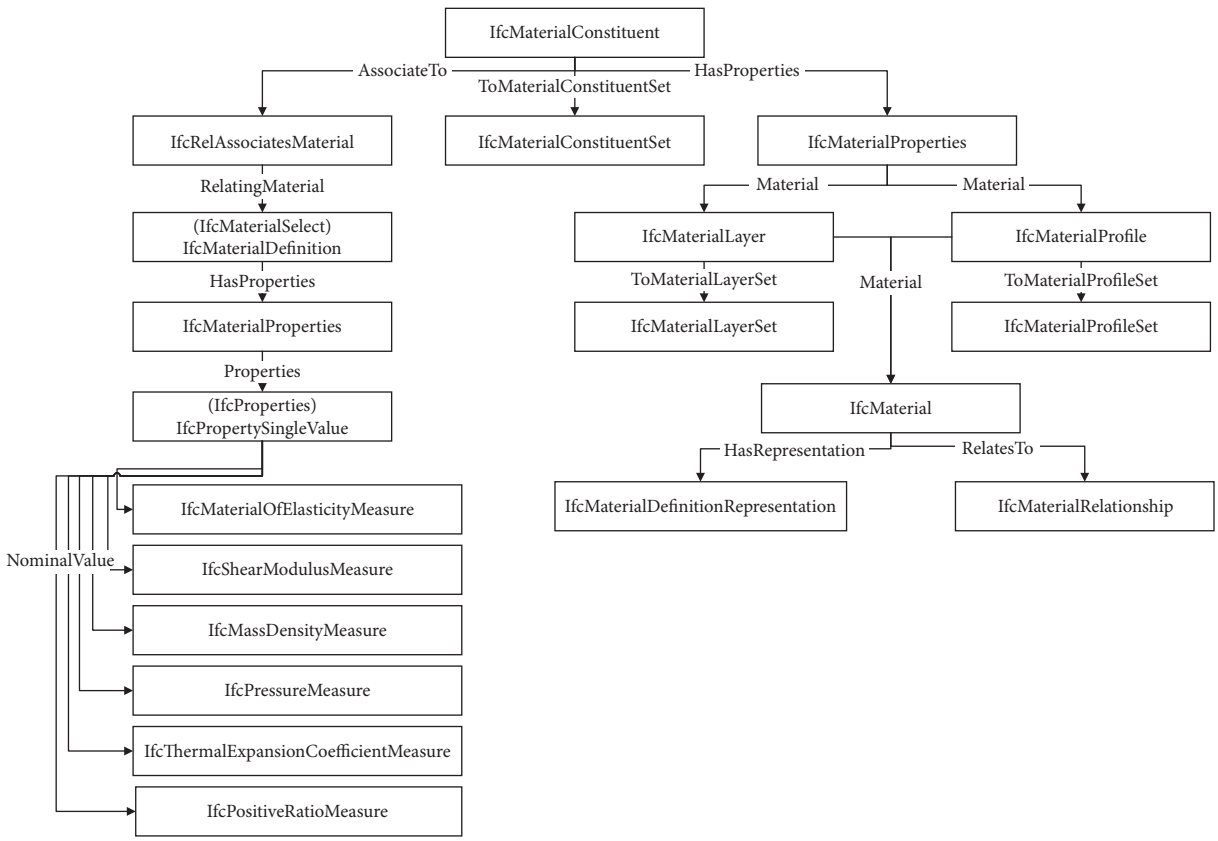


Figure 8: Structure of the IFC4 version of MVD.

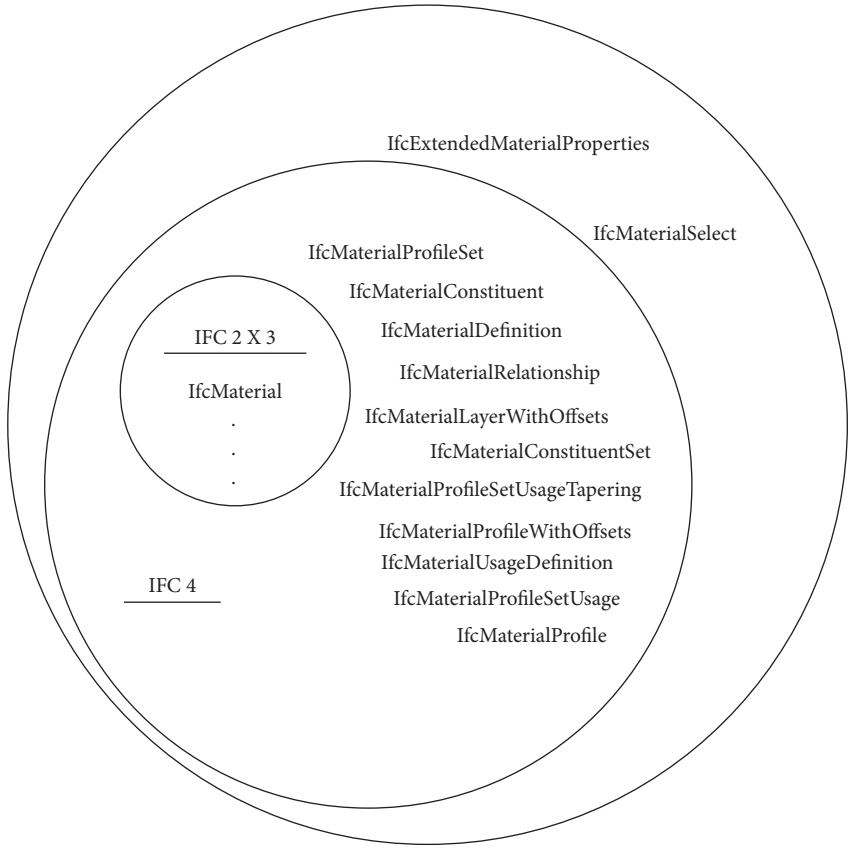


Figure 9: Examples of comparisons of information representation between IFC2X3 and IFC4 MVD versions.

YoungsModulus. For concrete material, six required entities are checked for six corresponding parameters: MassDensity, PoissonRatio, ShearModulus, ThermalExpansionCoefficient, CompressiveStrength, and YoungsModulus. Therefore, the authors picked one (i.e., concrete material) as an example. As part of the material information checking framework, the authors developed an IFC-based material information checking algorithm, with a special focus on checking "IfcExtendedMaterialProperties," "IfcMaterialSelect" entities and detailed parameters of steel, concrete, and wood materials in the AEC domain. Figure 10 shows the flow diagram of this customized material information checking algorithm for augmenting MVD-based checking. The algorithm runs three main steps as follows: (1) check IFC entity instances (i.e., "IfcExtendedMaterialProperties", and "IfcMaterialSelect") based on MVD constraints; (2) extract material types based on "IfcMaterial" entity instance; (3) check specific material parameters from "IfcPropertySingleValue" entity instances based on different material types. This algorithm will terminate after all the material parameters are checked. The results regarding what specific entity information and material parameter information exists or does not exist will be printed out in a report. Through the developed material information checking algorithm, the missing material information could be identified and used to inform the IFC model developer and user.

*4.6. Step 6: Case Study Evaluations.* The authors chose a 12-storey concrete model (Figure 6) as the case study model to test the material information representation and checking method. There were three types of material information entities in the IFC model: "IfcMaterial," "IfcExtendedMaterialProperties," and "IfcPropertySingleValue." The results (Figure 11) showed how the six-detailed material parameters of the concrete material in our invariant material signatures were represented, where the highlighted contents showed such material parameter representation details.

Depending on the software in use, manual information transfer may cover all required information, but it is time-consuming and error-prone. Model size is another factor that will affect the information transfer results and a larger model size could significantly increase the needed manual information transfer time. To evaluate the proposed method in facilitating information transfer between architectural design and structural analysis, the authors compared the proposed method with manual information transfer from

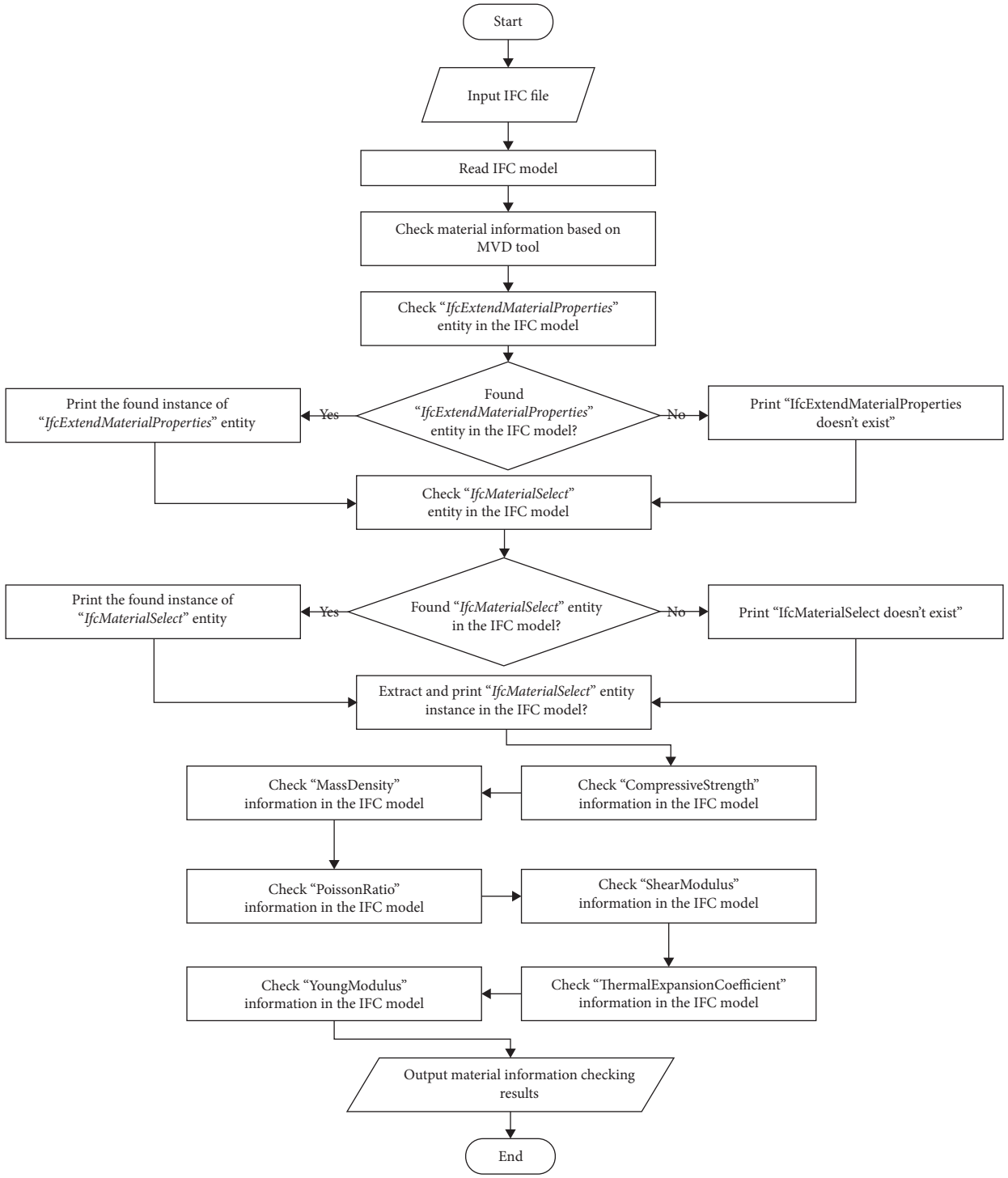


Figure 10: Material information checking algorithm augmenting MVD.

```
#80=IFCEXTENDEDMATERIALPROPERTIES(#86,(#87,#88,#89,#90,#91,#92),$,'STD-CONCRETE');
#86=IFCMATERIAL('STD-CONCRETE');
#87=IFCPROPERTYSINGLEVALUE('CompressiveStrength',$,IFCPRESSUREMEASURE(4.0000000E+003),#26);
#88=IFCPROPERTYSINGLEVALUE('MassDensity',$,IFCMASSDENSITYMEASURE(2.2481827E-004),#23);
#89=IFCPROPERTYSINGLEVALUE('PoissonRatio',$,IFCRATIOMEASURE(1.7000000E-001),$);
#90=IFCPROPERTYSINGLEVALUE('ShearModulus',$,IFCSHEARMODULUSMEASURE(1.3461538E+006),#30);
#91=IFCPROPERTYSINGLEVALUE('ThermalExpansionCoefficient',$,IFCTHERMALEXPANSIONCOEFFICIENTMEASURE(5.5000000E-006),#33);
#92=IFCPROPERTYSINGLEVALUE('YoungModulus',$,IFCMODULUSOFELASTICITYMEASURE(3.1500000E+006),#31);
```

Figure 11: Material information representation implementations in IFC file.

Table 3: IFC-based invariant material signatures representation implementations.

| Parameters name | Unit information | Material type | IFC representations of "NominalValue" |
|---|---|---|---|
| Mass density | kg/m3 | Steel, concrete, and wood | IfcMassDensityMeasure |
| Young's modulus | $N/m^2$ | Steel, concrete, and wood | IfcModulusOfElasticityMeasure |
| Shear modulus | $N/m^2$ | Steel, concrete, and wood | IfcShearModulusMeasure |
| Poisson's ratio | | Steel, concrete, and wood | IfcPositiveRatioMeasure or IfcRatioMeasure |
| Thermal expansion coefficient | °C-1 | Steel and concrete | IfcThermalExpansionCoefficientMeasure |
| Ultimate stress, yield stress, and compressive strength | $N/m^2$ | Steel and concrete | IfcPressureMeasure |

the time efficiency perspective. A manually developed gold standard was used as ground truth in the evaluation, which included the material information input for structural analysis from an architectural model. The proposed invariant material signatures were implemented in IFC2X3 representations based on the IFC model that was exported from a BIM application software, to transfer material information and their parameters to the corresponding material signature. In this case, the model was exported to the IFC2X3 version to follow industry practice. Although IFC4 is a more advanced version comparing to IFC2X3 as discussed in Step 5, IFC 2X3 still dominates practical use in the industry, due to its massive market penetration and applications that follow it. The Coordination View 2.0 of IFC2X3 is split into two MVDs in IFC4: (1) the Reference View, which is mainly for viewing and coordination purposes and referencing domain models to each other; (2) the Design Transfer View, which is for exchanging IFC models to be used for further design and evaluation tasks. In practice, the Design Transfer View for IFC4 is not fully available, and Coordination View 2.0 for IFC2X3 cannot be fully replaced by the Reference View of IFC4 per se [53]. To address that, the authors proposed the material signature for which IFC2X3 and IFC4 versions of BIMs could be converged. Table 3 shows the IFC-based invariant material signatures as the destination representations of the conversion process. The first and last columns in Table 3 represent "Name" and "NominalValue" attributes for each parameter in IFC data, which are related to material definitions. It was not necessary to define every attribute in the entity based on the IFC schema when the model was created. But the "Name" and "NominalValue" attributes must be defined in the IFC file of a model (i.e., an instantiated physical file).

The authors compared the time consumption of the proposed method with that of a manual information transfer. In the manual information transfer, the interfaces of Solibri Model Viewer and Autodesk Revit 2018 were used. The authors imported the test case model in the software and clicked through each element to add their material information in the property panel. The manual information transfer took 11 minutes to finish. The time could be further increased significantly with model size and complexity because the engineers need to click through each element to identify and assign the detailed material parameters to them and then document the material information for further analysis. In comparison, the proposed method enables automated and efficient conversion and transfer of the material information between architectural models and structural models, based on invariant material signature representations using IFC. In the IFC format, the model could use "Name" attribute of "IfcMaterial" entity instance to represent/store material types (e.g., steel, concrete, and wood) and use "Name" and "NominalValue" of "IfcPropertySingleValue" entity instance to represent/store material parameters (e.g., mass density and Young's modulus). Using the proposed method, all the material information (i.e., material type and its parameters) could be successfully represented, processed, and analyzed (e.g., structural analysis). Table 4 shows the performance comparison of these two methods.

Table 4: Performance comparison of the proposed method with manual transfer.

| Method | Time consumption (min) |
|---|---|
| Manual transfer | 11 |
| Proposed method | 2 |

Figure 12 shows the IFC model validation/checking results using the MVD augmenting algorithm. The authors implemented the algorithm using IfcOpenShell library, which is an open-source library for accessing and processing IFC data. The results showed that the six-detailed material parameters of the concrete material were successfully checked by the MVD augmenting algorithm. The highlighted content showed that "IfcMaterialSelect" entity was not found, whereas "IfcExtendedMaterialProperty" and six material parameters were successfully found and extracted in the IFC model. The total time

```
[Data] #80=IfcExtendedMaterialProperties(#86,(#87,#88,#89,#90,#91,#92),$,'STD-CONCRETE')
[Info] IfcMaterialSelect doesn't exist
[Data] #86=IfcMaterial('STD-CONCRETE')
[Info] CompressiveStrength exists
[Info] MassDensity exists
[Info] PoissonRatio exists
[Info] ShearModulus exists
[Info] ThermalExpansionCoefficient exists
[Info] YoungModulus exists
[Data] #87=IfcPropertySingleValue('CompressiveStrength',$,IfcPressureMeasure(4.0000000E+003),#26)
[Info] CompressiveStrength
[Info] ['4.0000000E+003']
[Info] PSI
[Data] #88=IfcPropertySingleValue('MassDensity',$,IfcMassDensityMeasure(2.2481827E-004),#23)
[Info] MassDensity
[Info] ['2.2481827E-004']
[Info] ( KILOGRAM ^ 1 ) * ( MILLIMETRE ^ -3 )
[Data] #89=IfcPropertySingleValue('PoissonRatio',$,IfcRatioMeasure(1.7000000E-001),$)
[Info] PoissonRatio
[Info] ['1.7000000E-001']
[Info] None
[Data] #90=IfcPropertySingleValue('ShearModulus',$,IfcShearModulusMeasure(1.3461538E+006),#30)
[Info] ShearModulus
[Info] ['1.3461538E+006']
[Info] ( MILLIMETRE ^ -2 ) * ( NEWTON ^ 1 )
[Data] #91=IfcPropertySingleValue('ThermalExpansionCoefficient',$,IfcThermalExpansionCoefficientMeasure(5.5000000E-006),#33)
[Info] ThermalExpansionCoefficient
[Info] ['5.5000000E-006']
[Info] KELVIN ^ -1
[Data] #92=IfcPropertySingleValue('YoungModulus',$,IfcModulusOfElasticityMeasure(3.1500000E+006),#31)
[Info] YoungModulus
[Info] ['3.1500000E+006']
[Info] ( MILLIMETRE ^ -2 ) * ( NEWTON ^ 1 )
```

Figure 12: Report of material information checking results by customized algorithm.

Table 5: Performance comparison of the proposed information checking method with manual checking method.

| Method | Time consumption (min) |
|---|---|
| Manual checking | 4.2 |
| Proposed method | 0.8 |

consumption of running augmented algorithm was 48 seconds in a computer with core i5 dual-core processer and 8 GB RAM, which could be further reduced with a more powerful machine. In contrast, the manual information checking process took 4.2 minutes even after leveraging the search function in a text editor. Table 5 shows the performance comparison of these two methods.

## 5. Conclusions

In this paper, the authors proposed a six-step research methodology to analyze and address BIM interoperability problems and used it to analyze BIM interoperability between architectural design and structural analysis. Six common project delivery methods were taken into account as the background context, and a BPMN diagram was created based on the transfer and use of modelling information between architectural models and structural models in the architectural design and structural analysis processes. Six technical route segments were summarized to explain any BIM interoperability application between the architectural design and structural analysis processes. To facilitate such interoperability, the authors devised invariant material signatures and developed material signatures for three common construction materials. Then, they developed a formal material information representation and checking method in a systematic way to help solve the material information gap identified through the experiment. The advantage of the proposed material information representation and checking method was demonstrated in a comparative experiment with manual information transfer and checking through a case study. It shows that applying the proposed material information representation and checking method to a construction project could improve information exchange between the architectural models and the structural models for facilitating communication efficiency between architects and structural engineers, therefore, bringing the time and cost benefits to the entire project delivery process. In the process dimension, the proposed technical routes with different combinations and their applications to different project delivery methods provide new instruments for stakeholders in the industry to use for supporting their decision making. As a result, it enables the interaction between architects and structural engineers to be more efficient and therefore more

frequent to contribute practical impact in a project process not only for a shorter schedule and faster information delivery but also for a better design and safer structure.

*5.1. Contributions to the Body of Knowledge.* This research is one of the first systematic explorations of BIM interoperability between architectural design and structural analysis following a new six-step research methodology that was targeted at supporting BIM interoperability research and development. This research contributes to technical routes by summarizing six-route segments of BIM interoperability between architectural design and structural analysis. A combination of one or more route segments could form a closed loop for information transfer to support BIM interoperability, which is what the AEC industry ultimately needs. From the process dimension, the technical route segments with different combinations for information transfer and their applications to specific project delivery methods provide new instruments to stakeholders in the industry for efficient and accurate decision making. The gap analyses regarding information missing and information inconsistency between architectural models and structural models were conducted to find that, in some situations, such as the technical route from proprietary architectural BIM to IFC and from IFC to proprietary structural analysis model, material information could be missing. The authors developed gap analyses of material information between architectural models and structural models and proposed a new set of invariant material signatures and a corresponding material information representation and checking method. The proposed material information representation and checking method could improve information transfer between architectural design and structural analysis to support BIM interoperability in different project delivery methods. The case study results showed that the proposed method could improve information exchange efficiency between architectural design and structural analysis to facilitate BIM interoperability. In addition, the proposed method can be adapted to facilitate the information flow between any two stages of the lifecycle of a building or infrastructure (e.g., roadway, bridge, and culvert) project (e.g., between preconstruction stage and postconstruction stage to deal with the maintenance issues).

The impact of applying this research in the AEC domain could be far-reaching. This research provides a formal invariant signature-based material information representation and checking method to support BIM interoperability. This method facilitates information exchange between architectural models and structural models, which helps improve the information transfer and coordination between architects and structural engineers and therefore the efficiency of the whole project. The proposed method can be extended and applied to other application phases and functions such as cost estimation, scheduling, and energy analysis.

*5.2. Limitations and Future Work.* The authors acknowledge the following limitation of the proposed formal information representation and checking method in its current shape. Although the proposed method was tested in representing and checking required material information for information transfer between an architectural model and a structural model, how it will perform in representing and checking other types of information, such as analysis results information, needs to be further explored. In future work, the authors plan to expand the proposed method in representing and checking other types of information such as logistic information and in different interoperability scenarios such as between architectural design and energy simulation.

## Data Availability

All data generated or analyzed during the study are available from the corresponding author upon request.

## Disclosure

The opinions, findings, and conclusions or recommendations expressed in this material are those of the authors and do not necessarily reflect the views of the National Science Foundation (NSF).

## Conflicts of Interest

The authors declare that there are no conflicts of interest regarding the publication of this paper.

## Acknowledgments

The authors would like to thank the National Science Foundation (NSF). This material is based on work supported by the NSF under Grant No. 1745374.

## References

[1] C. Wong Chong, K. Baker, J. Afsari, Zhang, and M. Roach, "Integration of BIM processes in architectural design, structural analysis, and detailing: current status and limitations," in *Proceedings of the ASCE Construction Research Congress, ASCE*, pp. 1203–1212, Tempe, AZ, USA, 2020.

[2] R. Ren and J. Zhang, "Comparison of BIM interoperability applications at different structural analysis stages," in *Proceedings of the ASCE Construction Research Congress, ASCE*, pp. 537–545, Tempe, AZ, USA, 2020.

[3] R. M. Dijkman, M. Dumas, and C. Ouyang, "Semantics and analysis of business process models in BPMN," *Information and Software Technology*, vol. 50, no. 12, pp. 1281–1294, 2008.

[4] S. A. White, "Introduction to BPMN," *IBM Cooperation*, vol. 2, no. 0, p. 1, 2004.

[5] H. L. Wu, R. Sadraddin, J. Ren, Zhang, and X. Shao, "Invariant signatures of architecture, engineering, and construction objects to support BIM interoperability between architectural design and structural analysis," *Journal of Construction Engineering and Management*, vol. 147, no. 1, Article ID 04020148.

[6] J. Wu, H. L. Sadraddin, R. Ren, J. Zhang, and X. Shao, "New automated BIM object classification method to support BIM interoperability," *Journal of Computing in Civil Engineering*, vol. 33, no. 5, Article ID 04019033, 2020.

[7] J. Wu and J. Zhang, "Introducing geometric signatures of architecture, engineering, and construction objects and a new

BIM dataset," in *Proceedings of the 2019 ASCE International Conference on Computing in Civil Engineering, ASCE*, pp. 264–271, Atlanta, GA, USA, June 2019.

[8] B. Daniotti, A. Pavan, S. L. Spagnolo, V. Caffi, C. Pasini, and C. Mirarchi, "Benefits and challenges of bim in construction," *BIM-Based Collaborative Building Process Management*, pp. 143–165, Springer, Cham, Switzerland, 2020.

[9] R. Ren, J. Zhang, and H. N. Dib, "BIM interoperability for structural analysis," in *Proceedings of the ASCE Construction Research Congress, ASCE*, pp. 470–479, New Orleans, LA, USA, April 2018.

[10] M. Laakso and A. O. Kiviniemi, "The IFC standard: a review of history, development, and standardization information technology," *ITcon*, vol. 17, no. 9, pp. 134–161, 2012.

[11] T. Akanbi, J. Zhang, and Y. C. Lee, "Data-driven reverse engineering algorithm development (D-READ) method for developing interoperable quantity takeoff algorithms using IFC-based BIM," *Journal of Computing in Civil Engineering*, vol. 34, no. 5, Article ID 04020036, 2020.

[12] J. Hietanen, *IFC Model View Definition Format*, 2nd Version International Alliance for Interoperability, 2006, https://www.standard.no/Global/PDF/ISO-TC59-SC13/N_287_Integrated_IDM-MVD_Process_for_IFC-formats.pdf.

[13] R. Ren and J. Zhang, "Model information checking to support interoperable bim usage in structural analysis," *Computing in Civil Engineering 2019: Visualization, Information Modeling, and Simulation*, pp. 361–368, American Society of Civil Engineers, Reston, VA, USA, 2019.

[14] S. Shirowzhan, S. M. E. Sepasgozar, D. J. Edwards, H. Li, and C. Wang, "BIM compatibility and its differentiation with interoperability challenges as an innovation factor," *Automation in Construction*, vol. 112, p. 103086, 2020.

[15] H.-L. Chi, S.-C. Kang, and X. Wang, "Research trends and opportunities of augmented reality applications in architecture, engineering, and construction," *Automation in Construction*, vol. 33, pp. 116–122, 2013.

[16] C.-S. Park, D.-Y. Lee, O.-S. Kwon, and X. Wang, "A framework for proactive construction defect management using BIM, augmented reality and ontology-based data collection template," *Automation in Construction*, vol. 33, pp. 61–71, 2013.

[17] H. Bae, M. Golparvar-Fard, and J. White, "High-precision vision-based mobile augmented reality system for context-aware architectural, engineering, construction and facility management (AEC/FM) applications," *Visualization in Engineering*, vol. 1, no. 1, 2013.

[18] X. Wang, M. J. Kim, P. E. D. Love, and S.-C. Kang, "Augmented Reality in built environment: classification and implications for future research," *Automation in Construction*, vol. 32, pp. 1–13, 2013.

[19] G. Gourlis and I. Kovacic, "Building Information Modelling for analysis of energy efficient industrial buildings - a case study," *Renewable and Sustainable Energy Reviews*, vol. 68, pp. 953–963, 2017.

[20] E. Kamel and A. M. Memari, "Review of BIM's application in energy simulation: tools, issues, and solutions," *Automation in Construction*, vol. 97, pp. 164–180, 2019.

[21] U. Isikdag, J. Underwood, and G. Aouad, "An investigation into the applicability of building information models in geospatial environment in support of site selection and fire response management processes," *Advanced Engineering Informatics*, vol. 22, no. 4, pp. 504–519, 2008.

[22] P.-C. Lee, Y. Wang, T.-P. Lo, and D. Long, "An integrated system framework of building information modelling and geographical information system for utility tunnel maintenance management," *Tunnelling and Underground Space Technology*, vol. 79, pp. 263–273, 2018.

[23] D. Bryde, M. Broquetas, and J. M. Volm, "The project benefits of building information modelling (BIM)," *International Journal of Project Management*, vol. 31, no. 7, pp. 971–980, 2013.

[24] O. W. Chong and J. Zhang, "Game simulation to support construction automation in modular construction using BIM and robotics technology – stage I," in *Proeedings of the 2019 ASCE International Conference on Computing in Civil Engineering, ASCE*, pp. 376–383, Atlanta, GA, USA, 2019.

[25] R. Volk, J. Stengel, and F. Schultmann, "Building information modeling (BIM) for existing buildings — literature review and future needs," *Automation in Construction*, vol. 38, pp. 109–127, 2014.

[26] Y. Liu, S. Van Nederveen, and M. Hertogh, "Understanding effects of BIM on collaborative design and construction: an empirical study in China," *International Journal of Project Management*, vol. 35, no. 4, pp. 686–698, 2017.

[27] M. Oraee, M. R. Hosseini, E. Papadonikolaki, R. Palliyaguru, and M. Arashpour, "Collaboration in BIM-based construction networks: a bibliometric-qualitative literature review," *International Journal of Project Management*, vol. 35, no. 7, pp. 1288–1301, 2017.

[28] C. M. Clevenger, M. Ozbek, S. Glick, and D. Porter, "Integrating BIM into construction management education," *EcoBuild Proceedings of the BIM-Related Academic Workshop*, vol. 8, Washington, DC, USA, 2010.

[29] A. Abbas, Z. U. Din, and R. Farooqui, "Integration of BIM in construction management education: an overview of Pakistani Engineering universities," *Procedia Engineering*, vol. 145, pp. 151–157, 2016.

[30] H.-L. Chi, X. Wang, and Y. Jiao, "BIM-enabled structural design: impacts and future developments in structural modelling, analysis and optimisation processes," *Archives of Computational Methods in Engineering*, vol. 22, no. 1, pp. 135–151, 2015.

[31] A. L. C. Ciribini, S. Mastrolembo Ventura, and M. Paneroni, "Implementation of an interoperable process to optimise design and construction phases of a residential building: a BIM Pilot Project," *Automation in Construction*, vol. 71, pp. 62–73, 2016.

[32] J. K. Larsen, G. Q. Shen, S. M. Lindhard, and T. D. Brunoe, "Factors affecting schedule delay, cost overrun, and quality level in public construction projects," *Journal of Management in Engineering*, vol. 32, no. 1, Article ID 04015032, 2016.

[33] B. C. Lines, K. T. Sullivan, J. B. Smithwick, and J. Mischung, "Overcoming resistance to change in engineering and construction: change management factors for owner organizations," *International Journal of Project Management*, vol. 33, no. 5, pp. 1170–1179, 2015.

[34] E. Ulkeryildiz, *A Model for Evaluating the Absorptive Capacity of Architectural Design Teams*, Graduate School of Engineering and Science of zmir Institute of Technology, Urla, Turkey, 2015.

[35] P. Mujumdar and J. U. Maheswari, "Design iteration in construction projects - review and directions," *Alexandria Engineering Journal*, vol. 57, no. 1, pp. 321–329, 2018.

[36] S. Beazley, E. Heffernan, and T. J. McCarthy, "Enhancing energy efficiency in residential buildings through the use of BIM: the case for embedding parameters during design," *Energy Procedia*, vol. 121, pp. 57–64, 2017.

[37] A. J. C. Penabad, "Picking up where we left off the typological diagram as a fundamental tool for a conscious architectural design process," *Journal of Geography*, vol. 6, no. 1, pp. 11–18, 2018.
[38] McGraw-Hill Construction, *The Business Value of BIM for Construction in Major Global Markets: How Contractors Around the World Are Driving Innovation with Building Information Modeling*, Smart Market Report, Bedford, MA, USA, 2014.
[39] Q. Z. Yang and Y. Zhang, "Semantic interoperability in building design: methods and tools," *Computer-Aided Design*, vol. 38, no. 10, pp. 1099–1112, 2006.
[40] P. Sanguinetti, S. Abdelmohsen, J. Lee, J. Lee, H. Sheward, and C. Eastman, "General system architecture for BIM: an integrated approach for design and analysis," *Advanced Engineering Informatics*, vol. 26, no. 2, pp. 317–333, 2012.
[41] I. J. Ramaji and A. M. Memari, "Interpretation of structural analytical models from the coordination view in building information models," *Automation in Construction*, vol. 90, pp. 117–133, 2018.
[42] A. Grilo and R. Jardim-Goncalves, "Value proposition on interoperability of BIM and collaborative working environments," *Automation in Construction*, vol. 19, no. 5, pp. 522–530, 2010.
[43] L. C. Bank, M. McCarthy, B. P. Thompson, and C. C. Menassa, "Integrating BIM with system dynamics as a decision-making framework for sustainable building design and operation," in *Proceedings of the First International Conference on Sustainable Urbanization (ICSU)*, Hong Kong, December 2010.
[44] R. L. Solnosky, A. M. Memari, and I. J. Ramaji, "Structural BIM processes for modular multi-story buildings in design and construction," in *Proceedings of the 2nd Residential Building Design & Construction Conference (201-215)*, State College, PA, USA, 2014.
[45] R. Sacks, I. Kaner, C. M. Eastman, and Y.-S. Jeong, "The Rosewood experiment - building information modeling and interoperability for architectural precast facades," *Automation in Construction*, vol. 19, no. 4, pp. 419–432, 2010.
[46] J. Steel, R. Drogemuller, and B. Toth, "Model interoperability in building information modelling," *Software & Systems Modeling*, vol. 11, no. 1, pp. 99–109, 2012.
[47] Z.-Z. Hu, X.-Y. Zhang, H.-W. Wang, and M. Kassem, "Improving interoperability between architectural and structural design models: an industry foundation classes-based approach with web-based tools," *Automation in Construction*, vol. 66, pp. 29–42, 2016.
[48] M. Aldegeily, J. Zhang, Y. Hu, and X. Shao, "From architectural design to structural analysis: a data-driven approach to study building information modeling (BIM) interoperability," in *Proceedings of the 54th ASC Annual International. Conference, ASC*, pp. 537–545, Fort Collins, CO, USA, April 2018.
[49] C. Eastman, J.-m. Lee, Y.-s. Jeong, and J.-k. Lee, "Automatic rule-based checking of building designs," *Automation in Construction*, vol. 18, no. 8, pp. 1011–1033, 2009.
[50] F. Fu, *Advanced Modelling Techniques in Structural Design*, pp. 11–14, John Wiley and Sons, Hoboken, NJ, USA, 2015.
[51] X. Y. Deng and T. Y. Chang, "Creating structural model from IFC-based architectural model," in *Proceedings of the Joint International Conference on Computing and Decision Making in Civil and Building*, p. 3, Montreal, Canada, June 2006.
[52] *IfcDoc Software, Building SMART*, Mar 2020, https://technical.buildingsmart.org/resources/ifcdoc/.
[53] Retrieved from: https://www.b-cert.org/Documentation/e6d094e3-7245-45e5-3154-08d500137b53, Oct 2020.

Hindawi
Advances in Civil Engineering
Volume 2020, Article ID 8858322, 16 pages
https://doi.org/10.1155/2020/8858322

*Research Article*

# Joint Investigation and 3D Visual Evaluation of Rock Mass Quality

**Haiping Yuan,[1] Chenghao Chen,[1] Yixian Wang,[1,2] Hanbing Bian,[3] and Yan Liu[2]**

[1]*School of Civil Engineering, Hefei University of Technology, Hefei 230009, China*
[2]*State Key Laboratory of Explosion Science and Technology, Beijing Institute of Technology, Beijing 100081, China*
[3]*Laboratoire de Génie Civil et Géoenvironnement, Université de Lille, Lille 5900, France*

Correspondence should be addressed to Yixian Wang; wangyixian2012@hfut.edu.cn

Received 1 May 2020; Revised 10 December 2020; Accepted 14 December 2020; Published 30 December 2020

Academic Editor: Jia-Rui Lin

Copyright © 2020 Haiping Yuan et al. This is an open access article distributed under the Creative Commons Attribution License, which permits unrestricted use, distribution, and reproduction in any medium, provided the original work is properly cited.

In order to realize the high efficiency quality classification and three-dimensional visualization of engineering rock mass and to solve the technical difficulties of the traditional rock mass quality evaluation method such as high labor intensity, long process time consumption, many intervention processes such as scale measurement and manual calculation, and nonintuitive classification results, this paper puts forward a 3D visual rock mass quality evaluation method and system based on close-range photography, which optimizes the traditional rock mass quality evaluation method, makes the rock mass classification three-dimensional and visible, and realizes the estimation of unrevealed rock mass quality evaluation index. The research results show the following: (1) The method of storing joint information by close-range photography and extracting joint information by human-computer interaction improves the working efficiency and the process is safe and controllable compared with the traditional method of collecting fracture parameters. (2) Based on the statistical analysis of 97 groups of roadway survey data, the comprehensive statistical regression formula between BQ value of Chinese national standard and RMR value is given, and there is a good correlation between BQ value and RMR value of rock mass quality index. (3) Based on the power-inverse ratio method, the three-dimensional model of rock mass classification of the mine was established, and the cutting model obtained the current distribution diagram of rock mass quality grade, providing scientific reference for drilling, blasting, support, and other production design optimizations.

## 1. Introduction

Gu Dezhen has established the concept of rock mass structure in the early 1960s [1]. It is suggested that the characteristics of rock mass mainly depend on the internal structure of rock mass [2, 3]. Fine description, rapid measurement, and visual representation of the structure of rock mass and its spatial distribution of quality grade are the foundation and key to solve many underground engineering problems. Geological survey of traditional joints and fractures is complicated and cumbersome. The observation points are determined by the surveyor's line first, and then the joint measurement is carried out one by one on the site of the bad working environment by means of a scale and geological compass, and the data of the nature, occurrence, length, width and spacing of each joint fracture, and the position of the intersection point between the structure surface and the measuring line are recorded. It is obvious that the traditional collection methods with high labor intensity, low efficiency, high risk, and high accuracy affected by human and environmental factors need to be improved and innovated urgently. At present, there are many comprehensive evaluation methods of rock mass quality at home and abroad. The evaluation factors and evaluation criteria of grading methods of rock mass quality evaluation are different, and different evaluation methods for the same evaluation object may have different evaluation results [4, 5]. Therefore, it is very important to study the correlation between different rock mass quality evaluation and grading methods. With the rapid development of science and technology, 3D imaging technology in the 21st century has shown significant development potential. The 3D classification of rock mass quality will guide engineering construction more intuitively and concretely, which is the development trend of rock mass quality classification.

The method of manual field contact measurement [6–10] usually uses geological compass, geological hammer, measuring rope, tape gauge, and other tools to investigate and measure joints and fractures one by one. The accuracy of this method is greatly influenced by human and environmental factors, which is time-consuming, laborious, and inefficient, and the proportion of labor cost is high. Normally, 200–300 fractures can be measured in pairs a day. Fracture information collectors have long been exposed to the field environment, affected by weather, section exposure, and other environmental factors, and sometimes may be threatened by geological disasters such as landslides. Borehole survey is an important part of geophysical logging technology. This method has special requirements for drilling technology and quality, and the interpretation accuracy is sometimes difficult to guarantee. Though the ANN (Artificial Neural Network) combined with fuzzy logic [11] and RMD index [12] is used to study the distribution of fracture density, it is still difficult to reflect the characteristics of structural anisotropy of rock mass. And the method is not suitable for obtaining and collecting the profile information in large quantities. Photogrammetry is a technique to reconstruct the space position and three-dimensional shape of the object by using the image of the subject, and its history is comparable to that of photographs, dating back to the mid-19th century (Ross-Brown and Atkinson, 1972 [13]). Compared with other methods, the digital image of field rock is obtained by digital camera equipment, and then image processing is carried out by computer, and the relevant fracture data can be obtained. This method can transfer a large number of field works to the indoor to complete, with the advantages of precision, high efficiency, practicality, comprehension, and few environmental disturbances, which effectively solve the disadvantages and shortcomings of the traditional method, provide a new idea for obtaining geometric information of rock mass structure surface, and have been favored by the majority of scholars [14–19]. Wu [20] introduced the information processing scheme of digital image of beach rock mass developed according to modern computer vision theory; Fan [21] studied the intelligent recognition of digital images of rock mass fractures based on image processing and recognition technology to realize automatic interpretation of fractures; Li et al. [22] realized the evaluation of radial differences and axial prediction of tunnel rock mass structure based on the sequence palm surface image and then realized the effective agreement between the quantitative index of rock mass structure and the engineering purpose; Galdames et al. [23] classified and processed segmented rock images using hyperspectral sensors, laser range finders, and color cameras.

The early rock mass classification methods were proposed based on the experience of tunnel engineering with shallow buried depth, such as Protodyakonov classification method, Terzaghi classification method, and RMR classification method (Method of Rock Mass Rating). At present, the development trend of surrounding rock classification method is from qualitative-based classification method to qualitative-quantitative combination method. Moreover, the classification index has been developed from single index to multi-index evaluation system. The most widely influential methods are BQ method (Chinese standard for engineering classification of rock mass), $Q$ system classification, and RMR classification method. With the development of human engineering technology and the requirement of modern engineering, more and more deep-buried extra-long tunnels are needed. The geological conditions of these tunnels are often complex and the crustal stress conditions are prominent, while the early methods have less consideration on the influence of crustal stress, especially high ground stress, on tunnel stability, which limits their application in modern tunnel design. Tan [24] modified the traditional $Q$ system method and established a method suitable for the evaluation of surrounding rock quality in deep engineering, based on the influence of high ground stress, high temperature, and high osmosis on surrounding rock quality. RMR method did not consider the effect of crustal stress or groundwater on the stability of rock mass and supporting structure [25]. Since both RMR and $Q$ systems use RQD (rock quality designation) value as basic parameters, the defects in the description of joint state by the values themselves inevitably lead to the deviation of the final rock mass quality score. Chen et al. [26] researched on three-dimensional accurate division method of structural homogenization in underground mines for the problems of weak detailed identification ability of existing homogenization methods; Su and Ning [27] used the maximum interval classifier to judge the surrounding rock level; Cong et al. [28] considered the influence of tunnel span on the stability of surrounding rock, adjusting and improving the basic quality index of surrounding rock, so that the quantitative and qualitative classification results of surrounding rock are basically consistent. At present, the research and improvement of rock mass quality evaluation by researchers at home and abroad mainly focus on these directions, such as the research and development of special measuring equipment and supporting procedures, the improvement or supplement of classical rock mass quality evaluation methods, and the simple development of rock mass quality rating procedures. However, there is less research on the method of intervention in rock mass investigation by simple, fast, efficient, and economical ordinary photographic camera suitable for engineering.

Driven by new theories and technologies such as big data, cloud computing, artificial intelligence, and the strong demand of economic and social development, big data driving knowledge learning, cross-media collaborative processing, man-machine collaborative enhancing intelligence, and other aspects have become the focus and hot spot of geotechnical engineering development. It is a matter of great urgency to innovate the traditional low efficiency technology means and solve the multidisciplinary and common problems of fine description, rapid measurement, and visual representation of rock mass structure and its quality grade. In order to improve the geological survey of traditional joints and fractures, to realize the high efficiency automation and 3D visualization of rock mass quality classification, the fracture photos are obtained by close-range photography [29–33], and the key characteristic

parameters of joint fractures are extracted by computer processing. According to all kinds of published documents related to rock mass quality classification and interconversion of basic parameters for quality classification of rock mass, the rock mass quality classification is completed quickly. At the same time, a program automatically processes the collected basic information and directly gives the rock mass quality evaluation results of each set of information according to the relevant classification methods. The correlation between RMR and BQ is analyzed and discussed on the basis of engineering example [34–36]. Finally, a three-dimensional model of rock mass classification is established based on the distance power-inverse ratio method. The research idea is shown in Figure 1. On the basis of MATLAB platform, the intelligent evaluation system of image fracture AI identification and rock mass quality is developed, the quality grade of rock mass and the dynamic distribution of regional rock mass under mining disturbance are finely described, rapidly measured, and directly visualized, and the digital, intelligent transition and 3D visual management of quantification of rock mass and rock mass quality identification are realized.

## 2. Basic Information Acquisition of Rock Mass Quality Classification

*2.1. Close-Up Photo Collection of Joints and Cracks.* The close-up photography is used to collect the joint fissure images of the rock mass in the small area. The quality of the collected photographs is affected by factors such as lighting, shooting distance, shooting angle, and surrounding environment. Therefore, the specified parameters are uniformly adopted for the controllable factors. Combining with the field situation, four Dongzhisheng DS-900 LED bulbs are used as light sources; each bulb has a maximum luminous flux of 2000 LM and a light source of scattering light. To ensure a moderate light intensity, the linear distance between the bulb and the outcropping plane of joint cracks should be 1~2 meters, and the same shooting distance should be 1~2 meters. Degree will result in different scales in different areas of the image. In order to ensure the same scales in different parts of the image, we should try to ensure that the lens plane is parallel to the rock wall plane. Lighting arrangement adopts the way of 45 degrees angle between the lamp position and the outcrop plane of joints and fissures. The plane of joints and fissures is often uneven, so the upper and lower left sides of the camera should be arranged as far as possible. A lamp position is arranged in the four directions of the upper right and the lower right, as shown in Figure 2. In order to determine the scale of the close-up photographic photograph, a reference object of a known regular shape of the sheet is placed at a position within the photographing area and does not affect the integrity of the joint fissure; a sheet-like reference object, a photographic area plane, and a camera lens should be in a parallel state to avoid scale deviation, photographic photos shown in Figure 3.

The close-range photographs obtained by this method have soft and uniform light and clear joints.

*2.2. Collection of Rock Strength Indicators.* Strength of rock generally includes compressive strength (uniaxial compressive strength and triaxial compressive strength), tensile strength, and shear strength, among which shear strength and compressive strength are often the main factors to determine the stability of rock engineering. This paper uses a portable point loader to measure the compressive strength of rock; the rock sample after destruction is shown in Figure 4; at the anchor point of each close-up photography, no less than 12 rock samples are taken and the sampling point sampling position is recorded, and the uniaxial compressive strength of the rock is obtained according to the following equation [37]:

$$R_c = 22.82 I_s^{0.75}. \quad (1)$$

*2.3. Engineering Factors Affecting Rock Mass Strength.* The basic quality of rock mass is the inherent characteristic of rock mass, which reflects the most basic mechanical properties of rock mass. Based on the actual project of a metal mine in south China, the rock mass quality is classified according to the rock mass quality evaluation method, and the information such as the strike inclination angle, structural surface conditions, groundwater conditions, and field coordinates of the dominant joint group at the close shot should be collected in the field. In this paper, roadway investigation and statistical analysis are carried out in the range of −540 m~−455 m in a metal mine in south China, 97 joint pictures and 97 groups of corresponding index data are obtained, and a total of 6048 fractures and related parameters are obtained. Information collection of engineering factors affecting rock mass strength is shown in Table 1. The structure surface conditions A, B, C, D, and E, respectively, mean "discontinuous, closed, very rough, and the unweathered rock cliff," "<1 mm, slightly rough wall, width slightly weathered rock," "<1 mm, slightly rough wall, width serious weathering rock," "surface smooth or soft interlayer thickness <5 mm, the width of 1~5 mm, continuous," "surface smooth or soft interlayer thickness >5 mm or opening >5 mm, continuous." The groundwater conditions A, B, C, D, and E, respectively, mean "completely dry," "wet," "wet cave wall," "dripping water," and "running water."

After the on-site statistical data are recorded in this form, the rock mass quality information database on the computer side is input uniformly for storage and retention (the information database on the computer side has been made into a software form that can be dynamically changed at any time), paving the way for the automatic rock mass quality classification calculation by the self-programmed program later. This form of data statistics can be supplemented or deleted at any point in the mine and can change a single piece of data in the data group, thus realizing the dynamic grading of rock mass quality in the mine.

## 3. Basic Information-Related Processing and Rock Mass Quality Classification

*3.1. Extraction of Crack Information in Close-Up Photographs.* The geological survey of traditional joint fissures is mainly carried out by measuring personnel to determine the

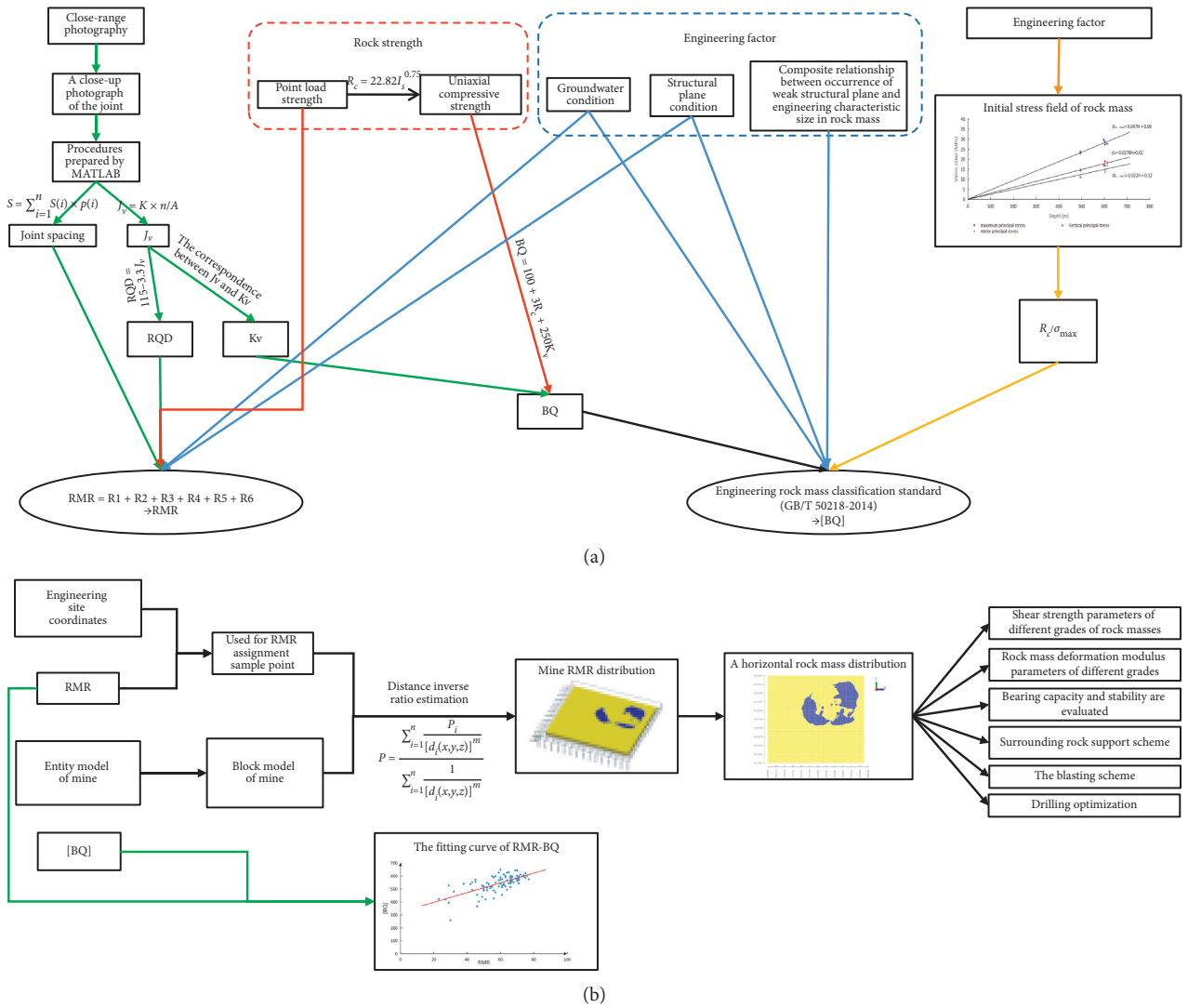


Figure 1: Overview of 3D visual rock mass quality evaluation method and system based on close-up photography: (a) the first part and (b) the second part.

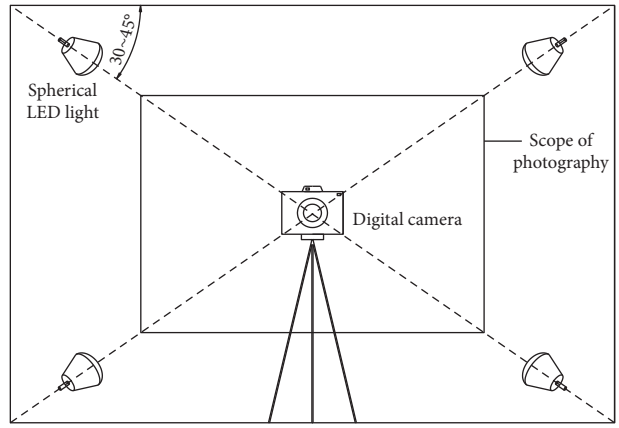


Figure 2: Schematic diagram of light source layout.

observation points, then manually measuring the nature, occurrence, and trace of each joint fissure by means of a tape measure, geological compass, and other tools on the site of the harsh working environment. Data such as length, width, spacing, structural plane, and intersection position of the survey line are summarized and entered into the Joint

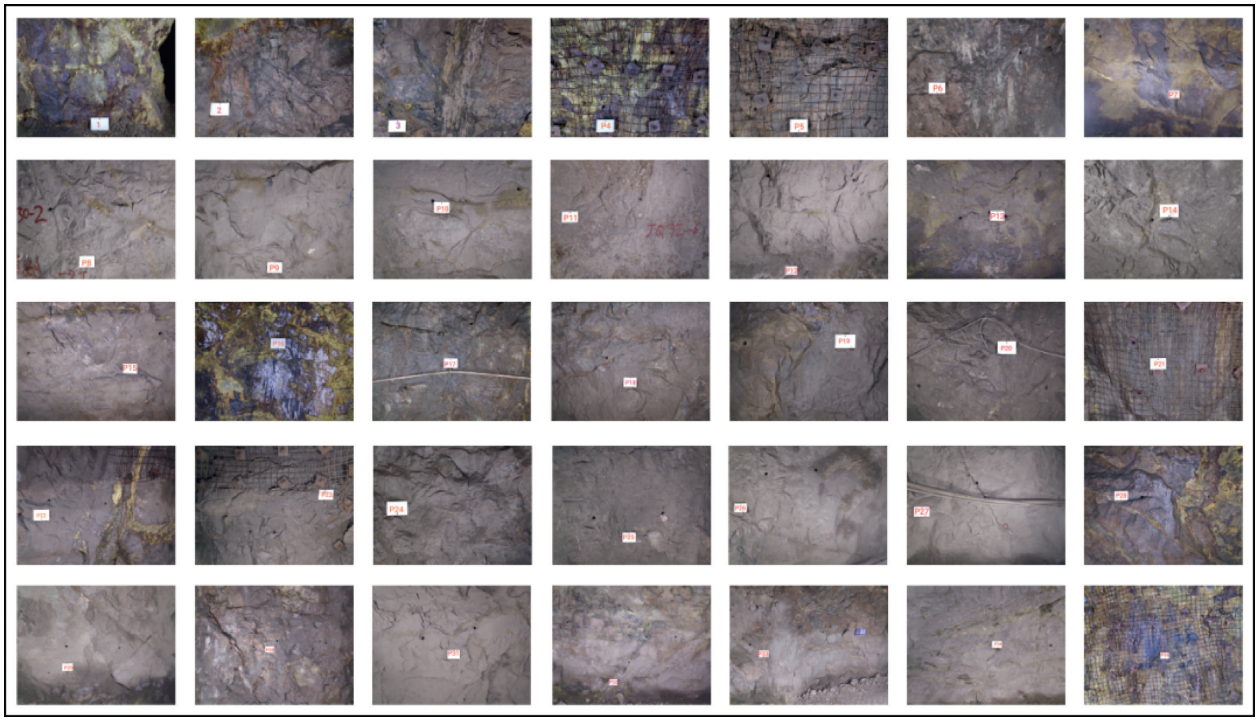

Figure 3: Close shot photography of joints and cracks.

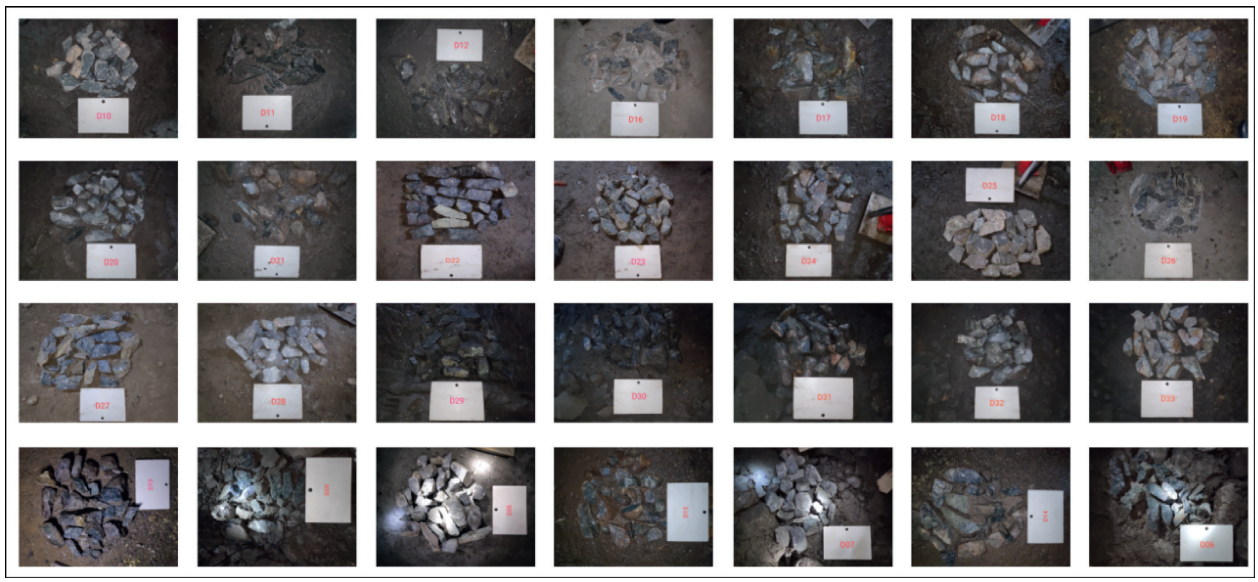

Figure 4: Site point load test after rock damage.

Fracture Information Statistics Table. It is urgent to improve and innovate the traditional collection method, which is characterized by high labor intensity, low efficiency, high risk, and high accuracy under the influence of human and environmental factors. This paper processes the close-up photographs of the joints and cracks on the computer through self-programming and identifies and obtains the basic information of each fissure.

In this paper, the self-compiled MATLAB program is used to obtain the pixel-length scale (cm/pixel) of the photos by selecting the flaky reference objects in each close-up photography picture. Click the two end points of the crack to read the coordinate values of the two end points from the current coordinate system. According to the coordinates of the two end points and the scale, the centroid coordinates, length, and inclination angle of the crack can be obtained. However, for different ranges within the close-up photography digital image, the scale is deviated and needs to be corrected.

As shown in Figure 5, the length and width of the shooting plane area $ABCD$ are, respectively $a$, $b$, and the linear distance from the lens $O$ to the shooting plane area $ABCD$ $|OO'| = L$, where $O'((1/2)a, (1/2)b)$ is the shooting

Table 1: Engineering factors affecting rock mass strength.

| Photo ID | Date of the photo | Tunnel strike (°) | Dominant joint 1 | | | Dominant joint 2 | | | Dominant joint 3 | | | Structural plane condition | Groundwater condition | Photo site location | | |
|---|---|---|---|---|---|---|---|---|---|---|---|---|---|---|---|---|
| | | | Joint strike (°) | Joint orientation (°) | Joint inclination (°) | Joint strike (°) | Joint orientation (°) | Joint inclination (°) | Joint strike (°) | Joint orientation (°) | Joint inclination (°) | | | $x$ | $y$ | $z$ |
| *P*1 | 190516 | 169 | 332 | 54 | 82 | 336 | 64 | 82 | 325 | 64 | 88 | *C* | *B* | 531030 | 3433204 | −540 |
| *P*2 | 190504 | 50 | 176 | 264 | 64 | 176 | 255 | 62 | 170 | 260 | 73 | *B* | *B* | 531038 | 3433206 | −540 |
| *P*3 | 190504 | 170 | 80 | 170 | 61 | 270 | 352 | 65 | 252 | 350 | 57 | *B* | *B* | 531053 | 3433182 | −540 |
| *P*4 | 190702 | 159 | 87 | 354 | 48 | 10 | 344 | 44 | 37 | 358 | 50 | *B* | *B* | 530948 | 3433215 | −540 |
| ⋮ | ⋮ | ⋮ | ⋮ | ⋮ | ⋮ | ⋮ | ⋮ | ⋮ | ⋮ | ⋮ | ⋮ | ⋮ | ⋮ | ⋮ | ⋮ | ⋮ |
| *P*95 | 190709 | 169 | 169 | 259 | 80 | 170 | 260 | 82 | 173 | 152 | 75 | *B* | *B* | 530787 | 3432805 | −508 |
| *P*96 | 190709 | 133 | 31 | 114 | 82 | 32 | 116 | 90 | 30 | 112 | 74 | *B* | *B* | 531012 | 3432799 | −508 |
| *P*97 | 190709 | 133 | 133 | 223 | 45 | 135 | 250 | 42 | 130 | 212 | 41 | *C* | *B* | 530994 | 3432822 | −508 |

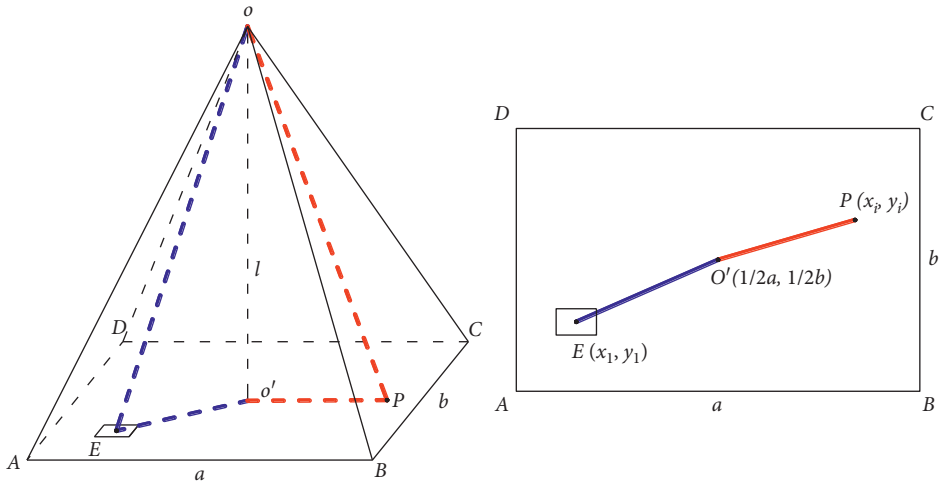


Figure 5: Schematic diagram of scale deviation correction.

plane area $ABCD$ center point, the center point of the reference object is $E(x_1, y_1)$, and the point $P(x_i, y_i)$ is any point in the shooting plane area $ABCD$; then, the line segment $O'E$ and the line segment $O'P$ length are shown in the following equations:

$$|O'E| = \sqrt{\left(x_1 - \frac{a}{2}\right)^2 + \left(y_1 - \frac{b}{2}\right)^2}, \tag{2}$$

$$|O'P| = \sqrt{\left(x_i - \frac{a}{2}\right)^2 + \left(y_i - \frac{b}{2}\right)^2}. \tag{3}$$

Assuming that the standard scale $\lambda$ is taken at O′ point along the $OO'$ direction, the scale $\lambda_E$ at the reference object should be corrected by the correction coefficient $k_1$; that is, $\lambda_E = k_1\lambda$, and $\lambda = \lambda_E/k1$, as shown in the following equation:

$$\lambda = \left(\frac{\lambda_E}{k_1}\right) = \lambda_E \frac{L}{\sqrt{(x_1 - (a/2))^2 + (y_1 - (b/2))^2 + L^2}}. \tag{4}$$

When shooting at point $P$, the scale $\lambda_P$ should be multiplied by the correction factor $k_2$, and the scale $\lambda$ at point $P$ is as shown in the following equation:

$$\lambda_P = k_2\lambda = \frac{\sqrt{(x_i - (a/2))^2 + (y_i - (b/2))^2 + L^2}}{L}\lambda. \tag{5}$$

The following equation can be obtained from (4) and (5):

$$\lambda_P = \frac{\sqrt{(x_i - (a/2))^2 + (y_i - (b/2))^2 + L^2}}{\sqrt{(x_1 - (a/2))^2 + (y_1 - (b/2))^2 + L^2}}\lambda_E. \tag{6}$$

That is, $\lambda_P = K\lambda_E$, and using $K$ to correct the scale when the coordinates of any point in the photo $P(x_i, y_i)$ are obtained, the results are shown in Table 2.

The spacing of two fractures can be calculated by using the coordinate of fracture endpoint (if the fractures do not intersect, the trapezoidal shape of the quadrangle of the fracture endpoint is approximately used to calculate the spacing; if fracture intersection exists, use the centroid distance as the crack spacing), single photo within group according to the angle of joints, and average of two adjacent fracture spacing in the group as a group of crack spacing; take fissure number that accounts for more than 10% of the total number of single photo fissures for effective group, on the basis of effective crack spacing $S(i)$ according to the weight $P(i)$ photos total distance $S$, as shown in the following equation. Manual review of 20 groups of fissure spacing was conducted, and the results are shown in Table 3. The results show that the error rate of fissure spacing calculated by fissure endpoint coordinates is less than 15%:

$$S = \sum_{i=1}^{n} S(i) \times P(i). \tag{7}$$

*3.2. Index of Rock Mass Incompleteness.* The strength of rock mass is significantly different from that of rock. The strength of rock mass is lower than that of rock, and only in a few cases is the strength of rock mass close to that of rock. The reason for this difference is that there are many large-scale structural planes and weak interlayers in rock mass. In engineering practice, rock mass is generally classified according to various specifications, and then parameters such as bearing capacity are selected correspondingly according to the quality classification. Rock mass incompleteness index generally refers to volume joint number $J_v$, rock quality designation RQD, and rock mass integrity index $K_v$. It is an index reflecting the number and scale of various structural planes and weak interlayers in rock mass and has an important impact on rock mass quality.

*3.2.1. Volume Joint Number $J_v$.* The joint number of rock mass volumes is the number of structural planes per cubic meter of rock mass volume. The $J_v$ value calculated by Spacing Method should be calculated according to joint

Table 2: Crack parameters in close-up photographs.

| Photo ID | Joint ID | Centroid $x$ | Centroid $y$ | Joint length (cm) | Joint dip angle (°) | Left endpoint $X$ of line segment | Left endpoint $Y$ of line segment | Right endpoint $X$ of line segment | Right endpoint $Y$ of line segment |
|---|---|---|---|---|---|---|---|---|---|
| 1 | 1 | 3.902368613 | 31.66493389 | 17.13418358 | 91.78991061 | 3.634777623 | 23.10202219 | 4.169959604 | 40.22784559 |
| 1 | 2 | 10.45834788 | 56.68469152 | 14.50432034 | 119.8759927 | 6.845869511 | 50.39630324 | 14.07082626 | 62.9730798 |
| 1 | 3 | 13.26805329 | 71.66978699 | 15.48563651 | 108.1218602 | 10.85973437 | 64.31103475 | 15.6763722 | 79.02853924 |
| 1 | 4 | 17.81710013 | 94.68261219 | 18.53345324 | 94.96974073 | 17.01432715 | 85.45072301 | 18.6198731 | 103.9145014 |
| ⋮ | ⋮ | ⋮ | ⋮ | ⋮ | ⋮ | ⋮ | ⋮ | ⋮ | ⋮ |
| 97 | 79 | 133.5649822 | 127.8110631 | 15.18768713 | 117.7185016 | 130.0328734 | 121.0886627 | 137.0970909 | 134.5334636 |
| 97 | 80 | 111.1190009 | 154.244909 | 13.81812699 | 76.65127289 | 109.5238551 | 160.9673095 | 112.7141468 | 147.5225086 |
| 97 | 81 | 127.8680326 | 137.4958774 | 17.35616609 | 93.76403486 | 127.2983377 | 128.836514 | 128.4377276 | 146.1552407 |

Table 3: Manual review of crack spacing.

| Photo ID | $P1$ | $P2$ | $P3$ | $P4$ | $P5$ | $P6$ | $P7$ | $P8$ | $P9$ | $P10$ | $P11$ | $P12$ | $P13$ | $P14$ | $P15$ | $P16$ | $P17$ | $P18$ | $P19$ | $P20$ |
|---|---|---|---|---|---|---|---|---|---|---|---|---|---|---|---|---|---|---|---|---|
| Weighted spacing of joints (cm) | 41.1 | 27.3 | 38.6 | 37.1 | 24.8 | 32.2 | 42.7 | 22.1 | 28.3 | 25.1 | 25.4 | 32.5 | 37.9 | 32.0 | 29.1 | 20.0 | 26.0 | 18.3 | 11.9 | 23.0 |
| Joint spacing checked manually (cm) | 38.7 | 26.4 | 33.9 | 38.6 | 29.1 | 35.6 | 39.1 | 18.9 | 25.3 | 28.4 | 29.5 | 31.7 | 39.8 | 28.2 | 28.9 | 17.6 | 27.7 | 20.3 | 13.6 | 25.4 |
| Error rate (%) | 6.22 | 3.52 | 14.00 | 3.80 | 14.71 | 9.45 | 9.15 | 12.42 | 11.83 | 11.59 | 13.90 | 2.37 | 4.80 | 13.52 | 0.58 | 13.46 | 6.09 | 9.91 | 12.45 | 9.63 |

statistics in the following Equation [37], where $J_v$ is the joint number of rock mass volumes (bars/m$^3$). $N$ is the number of structural plane groups in the statistical region; $S_i$ refers to the number of structural planes of the $i$th group along the normal direction per meter long. $S_0$ is the number of nongroup joints per cubic meter of rock mass. The $J_v$ value calculated by Direct Method should directly count the number of joints in unit volume rock mass:

$$J_v = \sum_{i=1}^{n} S_i + S_0, \quad i = 1, \ldots, n. \tag{8}$$

Generally, when the joints are evenly distributed, $J_v$ is changed from one-dimensional (in the borehole or a single survey line) to a three-dimensional multiplicative coefficient $K = 1.35$~$6.0$, and $J_v$ is changed from being two-dimensional (joint number per unit area) to three-dimensional. The coefficient $K$ should be 1.15~1.35 [38]. In this paper, the two-dimensional $J_v$ can be obtained from the number of joints and the size of the photograph in a close-up photograph. Convert the two-dimensional coefficient to the three-dimensional coefficient, as shown in the following equation, where $K$ is the conversion factor; $n$ is the number of joints in a single photo; $A$ is the photo size (cm$^2$):

$$J_v = K \times \frac{n}{A}. \tag{9}$$

*3.2.2. Rock Quality Index RQD.* RQD (rock quality designation) was proposed and developed by Deere (1964) at the University of Illinois, USA. It is an internationally accepted method for identifying the quality of rock engineering and is a quantitative parameter reflecting the integrity of engineering rock mass [39]. The method uses the corrected core take-up rate of the borehole to evaluate the quality of the rock; that is, the diamond drill bit with a diameter of 75 mm and the double-layer core tube are drilled in the rock, and the core is taken continuously, and the drill is taken back. In the core, the ratio of the sum of the lengths of the core segments greater than 10 cm in length to the return stroke is expressed as a percentage. Palmstrom [38] proposed three estimation methods of rock quality index RQD, namely, Farmer Joint Density Estimation Method, Volume Joint Counting Estimation Method, and Precision Line Estimation Method. In this paper, Volume Joint Counting Estimation Method is adopted. The calculation of RQD value is shown in te following equation; when $J_v < 4.5$, RQD = 100; RQD is equal to 0 when $J_v \geq 35$:

$$\mathrm{RQD} = 115 - 3.3J_v. \tag{10}$$

*3.2.3. Rock Mass Integrity Index $K_v$.* The rock mass integrity coefficient, also known as the fissure coefficient, indicates the integrity of the rock mass, which is the square of the ratio of the longitudinal wave velocity of the rock mass to the rock. The integrity factor can be determined by the dynamic method. The calculation method is shown in the following equation, where $K_v$ is the integrity coefficient of rock mass; $V_{\mathrm{pm}}$ is the longitudinal wave velocity of rock mass; $V_{\mathrm{pr}}$ is the longitudinal wave velocity of indoor rock (or rock block). Engineering Rock Mass Grading Standard (GB/T

50218–2014) [37] indicates that when the measured value is unconditionally obtained, $K_v$ value can be determined by the rock mass volume joint number $J_v$ according to Table 4:

$$K_v = \left(\frac{V_{pm}}{V_{pr}}\right)^2. \quad (11)$$

*3.3. Surrounding Rock Strength Stress Ratio.* According to the specification, when the engineering rock mass has the initial stress state represented by the strength stress ratio, the influence of the initial stress state on the correction coefficient $K_3$ should be considered. According to the surrounding rock mass strength stress ratio, $K_3$ is selected to modify the basic quality index of rock mass BQ, as shown in Table 5 [37]. In the stability analysis of underground engineering structures such as roadways and stopes, the original rock stress is an initial stress boundary condition, and the original rock stress is the force source causing the deformation and destruction of underground engineering structures. The source of mine pressure is closely related to the original rock stress. Before calculating the stress distribution around any excavated rock mass, the stress state before excavation must be measured or estimated. The original rock stress is the sum of gravity stress and tectonic stress.

The mine completed the original rock stress measurement in 2011. According to the information provided by the metal mine, seven ground stress holes were arranged by the hollow inclusion strain gauge [40–44], and the hollow inclusion stress relief data collection was performed using YJL-16 type intelligent data static. The resistance strain gauge collects data every 3 cm when the hole stress is released, as shown in Figures 6 and 7. According to the data obtained by the measurement, the ground stress measurement results of each measuring point are as follows: ① the maximum principal stress is located in the horizontal direction, and its value is 1.2~1.8 times of the dead weight stress; ② the maximum horizontal principal stress ($\sigma_{h,\max}$), minimum horizontal principal stress ($\sigma_{h,\min}$), and vertical principal stress ($\sigma_v$) all show approximately linear growth with the increase of depth. By using linear regression theory, the relationship between each principal stress and depth is shown in the following equations. The linear regression relationship between maximum horizontal principal stress, minimum horizontal principal stress, and vertical principal stress with depth is shown in Figure 8. The strength-stress ratio of surrounding rock can be calculated from the relationship between principal stress and depth and rock uniaxial compressive strength *Rc*:

$$\sigma_{h,\max} = 0.06 + 0.047H, \quad (12)$$

$$\sigma_{h,\min} = 0.12 + 0.022H,$$
$$\sigma_v = 0.02 + 0.0278H. \quad (13)$$

From the value of the stress measurement results, the distribution of the in situ stress field at the three horizontal measurement points in the mining area has the following laws: (1) the results of each measurement point have two principal stresses close to the horizontal direction and the angle between

Table 4: Correspondence between $J_v$ and $K_v$.

| $J_v$ (bar/m$^3$) | <3 | 3~10 | 10~20 | 20~35 | ≥35 |
|---|---|---|---|---|---|
| $K_v$ | >0.75 | 0.75~0.55 | 0.55~0.35 | 0.35~0.15 | ≤0.15 |

Table 5: Effect of initial stress state on correction factor $K_3$.

| Surrounding rock strength stress ratio ($R_c/\sigma_{\max}$) | BQ | | | | |
|---|---|---|---|---|---|
| | >550 | 550~451 | 450~351 | 350~251 | ≤250 |
| <4 | 1.0 | 1.0 | 1.0~1.5 | 1.0~1.5 | 1.0 |
| 4~7 | 0.5 | 0.5 | 0.5 | 0.5~1.0 | 0.5~1.0 |

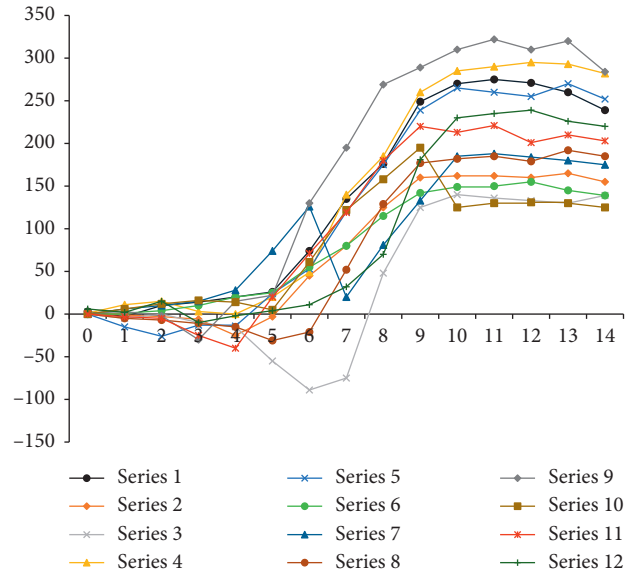


Figure 6: −455 m stress relief process curve of measuring point 7# in the horizontal middle section.

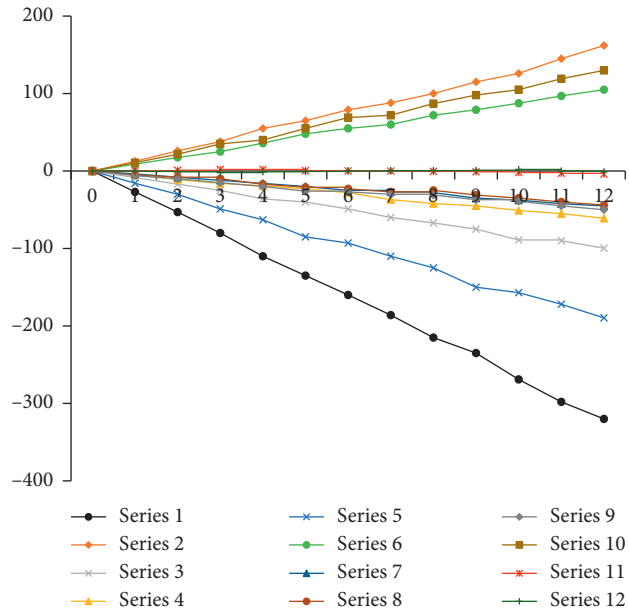


Figure 7: −455 m horizontal middle section 7# measuring point confining pressure constant curve.

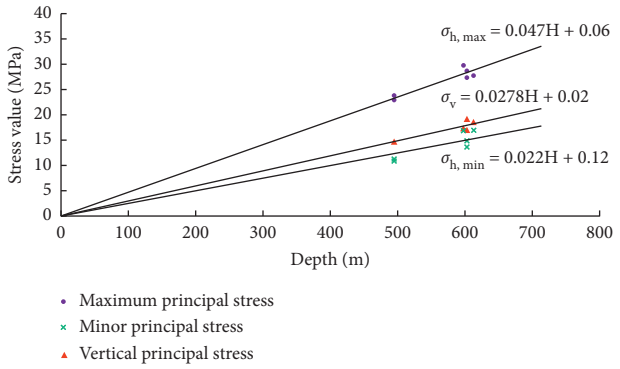


FIGURE 8: Relationship of$\sigma_{h,\max}$, $\sigma_{h,\min}$, and $\sigma_v$ to depth.

the maximum principal stress and the horizontal plane. The average is 12° and the maximum is 25°, indicating that the horizontal tectonic stress is the dominant stress; the direction of the intermediate principal stress is close to the vertical direction; (2) the maximum principal stress is located in the horizontal direction, and its value is 1.2–1.8 times the weight stress; (3) the direction of the maximum principal stress except for the 6# measuring point is in the northeast-southwest direction as a whole; the minimum principal stress is in the north-northwest direction, and the maximum horizontal principal stress is 1.7–2.2 times the minimum principal stress; (4) the vertical stress value is basically equal to or slightly greater than the weight of the upper strata; (5) the maximum horizontal principal stress ($\sigma_{h,\max}$), the minimum horizontal principal stress ($\sigma_{h,\min}$), and the vertical principal stress ($\sigma_v$) all show an approximately linear growth relationship with the increase of depth. Using linear regression theory, the relationship between each principal stress and depth is obtained in (12) and (13). The regression coefficient in (12) is 0.0278 and the coefficient in the average bulk density of the overburden (2.7–2.8) × 104 N/m$^3$ is very close, reflecting the fact that the vertical stress is basically equal to or slightly greater than the self-weight stress.

*3.4. Rock Mass Quality Classification.* Rock mass quality classification is a comprehensive reflection of the characteristics of engineering rock mass. In engineering practice, the rock mass is generally classified according to various specifications, and then the bearing capacity and other parameters are selected according to the quality classification. Rock mass classification provides scientific reference for production optimization design, such as drilling, blasting, and support. The accuracy of rock mass classification is of great significance to rock mass engineering. The commonly used rock mass quality classification is based on RMR classification method and BQ classification method, etc. In this paper, combined with RMR method and BQ method, the rock mass around the mine level of −540 m is, respectively, carried out.

RMR (rock mass rating) method was proposed by Bieniawski [45] in 1973 as a method to determine the quality level of rock mass, and it has been modified for 4 times successively, which is now based on the 1989 version [46]. The system considers the uniaxial compressive strength ($R1$) of the rock mass, the rock quality index RQD ($R2$), the structural plane spacing ($R3$), the structural surface condition ($R4$), the groundwater condition ($R5$), and the structural surface occurrence and engineering. The relationship of the trend ($R6$), a total of six indicators as basic parameters, and the main factors affecting the stability of the rock mass is scored, and the sum value is taken as the RMR value of the rock mass, as shown in

$$\mathrm{RMR} = R1 + R2 + R3 + R4 + R5 + R6. \tag{14}$$

Engineering Rock Mass Grading Standard (GB/T 50218–2014) [37] is the most commonly used rock mass quality evaluation method in China. This standard adopts the comprehensive index method composed of multiple parameters. Taking the quantitative indexes $R_c$ and $K_v$ of the two grading factors as parameters, the basic quality index of rock mass (BQ) is calculated according to the formula, and BQ is used as the quantitative index of the classification level, as shown in the following equation. When $R_c > 90K_v + 30$, take $R_c = 90K_v + 30$. When $K_v > 0.04R_c + 0.4$, take $K_v = 0.04R_c + 0.4$:

$$\mathrm{BQ} = 100 + 3R_c + 250K_v. \tag{15}$$

In this paper, the self-programming process is used to process and calculate the above-mentioned indicators. According to the specification, the scores of 97 groups of data are given. After the BQ is modified according to the specifications, the underground engineering rock mass quality index [BQ] is obtained, and the BQ is calculated according to the maximum score of 100. The value is approximately the same as the RMR score of the percentile system, and the average error rate is 8.26%. The results are shown in Table 6. Among the 97 graded test sections, 20 of them had the same grade, with an agreement rate of 20.6%, and 63 of them had a grade difference, accounting for 64.9%.

According to the information in Table 5, the distribution statistics of the RMR values of 97 groups of data can be obtained. As shown in Figure 9, the level IV rock mass in the measurement block is the largest, accounting for 54.6%, while the rest are level II and III rock mass, without any level I or V.

Software has been developed to make the grading evaluation process automatic. Only the database files prepared in the early stage need to be updated, and then the rock mass quality rating results and distribution statistical charts at the sampling measuring points in the mine can be obtained through rapid computer calculation.

BQ and RMR classification methods are comprehensive consideration of various factors of rock mass, and there is a certain correlation between them in essence. In order to learn from the successful experience of foreign engineering design based on rock mass classification, it is necessary to establish the relationship between the basic quality index of national standard rock mass BQ and foreign classification. In 2001, Cai Bin et al. performed statistical analysis on the measured data of different engineering sites to establish the relationship between [BQ] (corrected value of BQ) and RMR [47]. In 2004, Jiang Ping analyzed the relationship between BQ and RMR by combining 54 measured values of highway

Table 6: Rock mass quality rating at the sampling point of the mine.

| Photo ID | Joint weighted spacing (cm) | Volume joint number $J_v$ (bar/m$^3$) | Point load (MPa) | RQD (%) | Joint condition | Groundwater conditions | RMR score | RMR level | Rock integrity index $K_v$ | Uniaxial strength (MPa) | BQ score | Underground engineering rock mass quality index [BQ] | [BQ] conversion score (%) | BQ level |
|---|---|---|---|---|---|---|---|---|---|---|---|---|---|---|
| *P*1 | 41.107 | 21.8 | 11.3 | 43.1 | C | Moist | 49 | III | 0.33 | 140.67 | 603.6 | 523.6 | 62.3 | II |
| *P*2 | 27.3281 | 23.2 | 11.3 | 38.6 | B | Moist | 59 | III | 0.31 | 140.67 | 599.0 | 519.0 | 61.5 | II |
| *P*3 | 38.6462 | 29.4 | 11.3 | 18.1 | B | Moist | 50 | III | 0.23 | 140.67 | 578.3 | 498.3 | 58.0 | II |
| *P*4 | 37.134 | 25.2 | 8.4 | 31.7 | B | Moist | 56 | III | 0.28 | 112.16 | 506.5 | 426.5 | 46.1 | III |
| ⋮ | ⋮ | ⋮ | ⋮ | ⋮ | ⋮ | ⋮ | ⋮ | ⋮ | ⋮ | ⋮ | ⋮ | ⋮ | ⋮ | ⋮ |
| *P*95 | 53.2338 | 7.1 | 11.3 | 91.5 | B | Moist | 63 | II | 0.63 | 140.67 | 680.0 | 600.0 | 75.0 | I |
| *P*96 | 30.4314 | 9.2 | 11.3 | 84.8 | B | Moist | 74 | II | 0.57 | 140.67 | 665.5 | 605.5 | 75.9 | I |
| *P*97 | 28.75 | 25.8 | 11.3 | 29.7 | C | Moist | 52 | III | 0.27 | 140.67 | 590.0 | 490.0 | 56.7 | II |

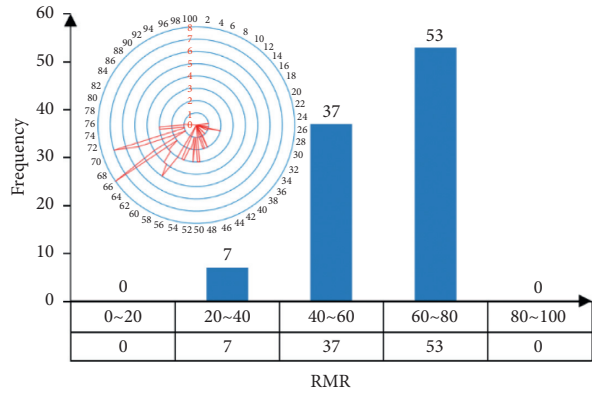


Figure 9: Rock mass RMR distribution statistics at the sampling point.

slope in Yixing section of Ninghang expressway [48]. In 2009, Yan combined other materials with the actual measurement data of the surrounding rock of the underground cavern of Dagangshan Hydropower Station, and the relationship between the BQ correction value and RMR and Q was obtained [49]. In this paper, 97 groups of BQ and RMR values and [BQ] and RMR values were linearly and exponentially fitted respectively, and the correlation between BQ and RMR and [BQ] and RMR was established. The results are shown in Figure 10.

The results show that there is a good correlation between BQ and RMR and [BQ] and RMR, and their linear fitting relationship is more appropriate than the exponential fitting relationship. The rock mass quality level is roughly in the range of II~IV, and the correlation between the BQ $\longrightarrow$ RMR, RMR $\longrightarrow$ BQ, and other indicators can be converted.

## 4. 3D Visualization of Engineering Rock Mass Quality Indicators

Through the above methods and steps, the indicators and conclusions for evaluating rock mass quality can be obtained automatically according to the collection of rock mass information to be evaluated and the related processing of computer programs. In order to meet the convenience of the project, a three-dimensional rock mass model is established and interpolated to give the rock mass quality evaluation index, so that the rock mass quality information can be obtained intuitively and conveniently. By directly or slice-observing the assigned three-dimensional rock mass model, it is possible to understand and predict the quality of the rock mass near a certain coordinate, which is of great significance for judging the safety and construction feasibility of mines, tunnels, slopes, and other projects.

In the actual project, the data collected by the drilling data and the trench data are limited. To obtain the internal information of the rock mass, a reasonable geological variable estimation method must be used. In the field of geology, rock mass quality indicators and deposit grades have a certain correlation in space; that is, variables within a certain range have mutual influences. The power-inverse ratio method is one of the most commonly used spatial interpolation methods. When calculating the value of an interpolation point, according to the principle that the larger the distance is, the larger the weight value is, the linear weighting of several adjacent points is used to fit the value of the estimated point. Assume that the point to be estimated in the three-dimensional space is $P$ point, the coordinates $(x_p, y_p, z_p)$, and a series of discrete points around it are unevenly distributed sample points, coordinates $(x_i, y_i, z_i)$, sample point attribute values $P_i$ $(i = 1, 2, \ldots n)$, the distance between the point to be estimated and the sample point is recorded as $d_i$, and the attribute value $P$ of the distance to be estimated by the power-inverse ratio method is as shown in the following equation [50]. In the formula, $m$ is the power value of the power-inverse ratio method. The larger the power, the greater the weight of the nearest point to the estimated point. In this paper, the power is 2:

$$P = \frac{\sum_{i=1}^{n} \left(P_i / \left[d_i(x, y, z)\right]^m\right)}{\sum_{i=1}^{n} \left(1 / \left[d_i(x, y, z)\right]^m\right)}. \tag{16}$$

In this paper, RMR value is selected as attribute value to get rock mass grade distribution at −540 m level. According to the horizontal geological plane map of each level, the boundary information of rock mass can be obtained, and the solid model of rock mass can be established preliminarily by importing the boundary information into the 3DMine software as a constraint condition, as shown in Figure 11.

Combining the acquired RMR values with the photo field locations in Table 1 yields a set of $(x, y, z, \text{RMR})$ data sets that will be used as sample points for block model assignment. Firstly, a solid model of the cube containing the estimated area was established to observe the rock mass distribution near the level of −540 m more intuitively [51–55]. The $z$ direction of the cube was −560~−450 m, and the $x$ and $y$ directions were 529500~532099 m and 3431599~3433849 m, respectively; Secondly, the solid model is converted into a block model. The size of the block is 10 m × 10 m × 10 m, and the new block attribute RMR is created. Finally, using the power-inverse ratio method to assign values to the block based on the sample point data, a block model with an RMR attribute value for each block is obtained. The rock mass distribution of −560~−450 m can be visually observed, as shown in Figure 12. Slice the block with plane $Z = -540$ to obtain the rock mass grading distribution at the level of −540 m, as shown in Figure 13. Taking the rock mass near the level of −540 m as the research object, the comprehensive research on the three-dimensional visual classification of rock mass quality can provide scientific reference for the design optimization of rock drilling, blasting, and support and reduce the production cost.

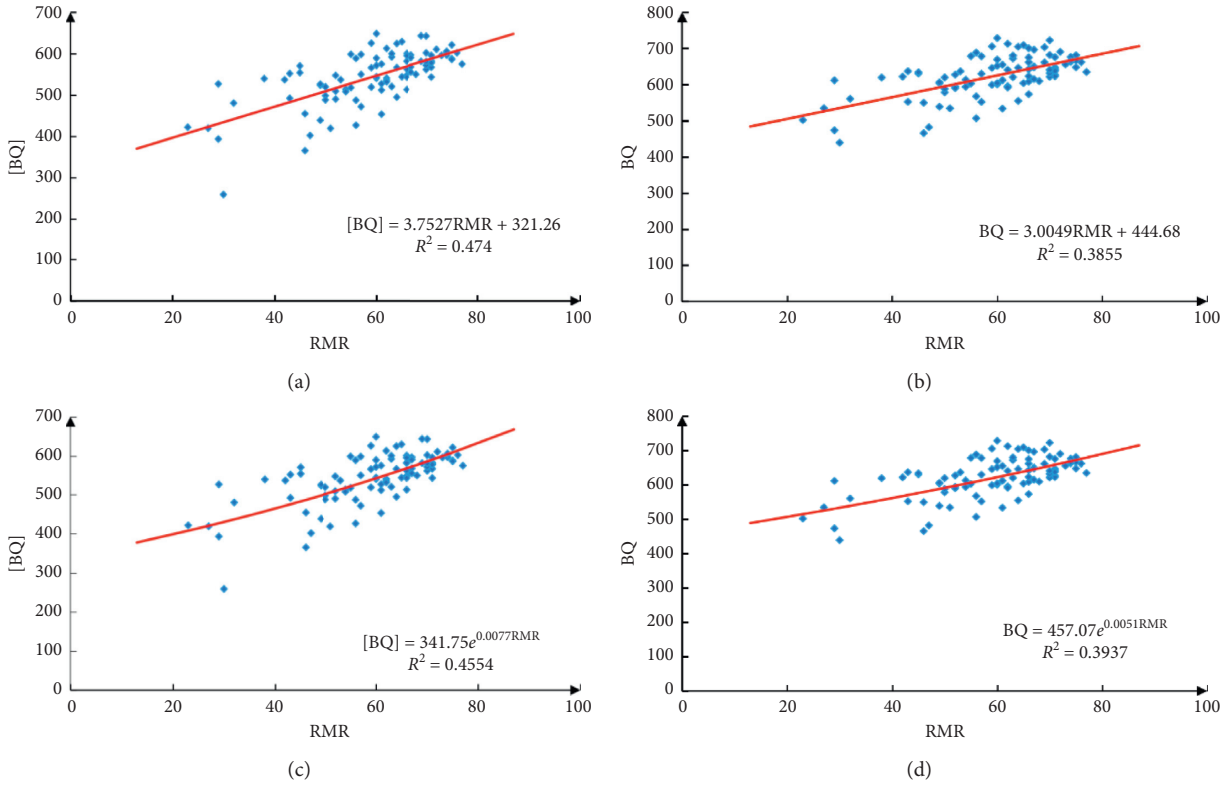


Figure 10: Fitting curve of [BQ]/BQ and RMR, (a) RMR-[BQ] linear fitting straight line, (b) RMR-BQ linear fitting straight line, (c) RMR-[BQ] exponential fitting curve, and (d) RMR-BQ index fitting curve.

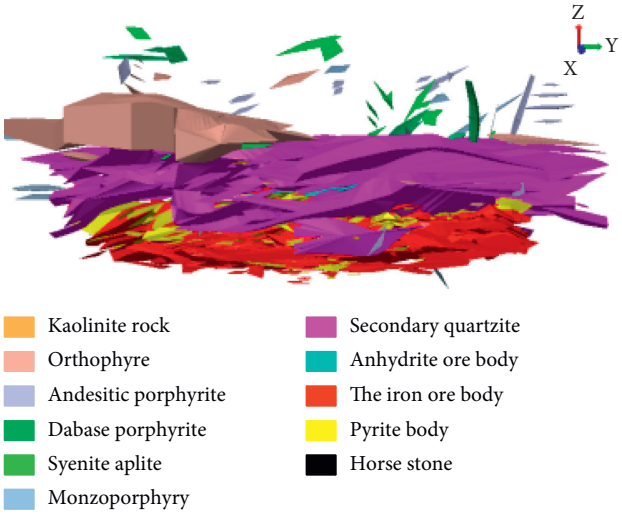


Figure 11: Ore body and rock mass model.

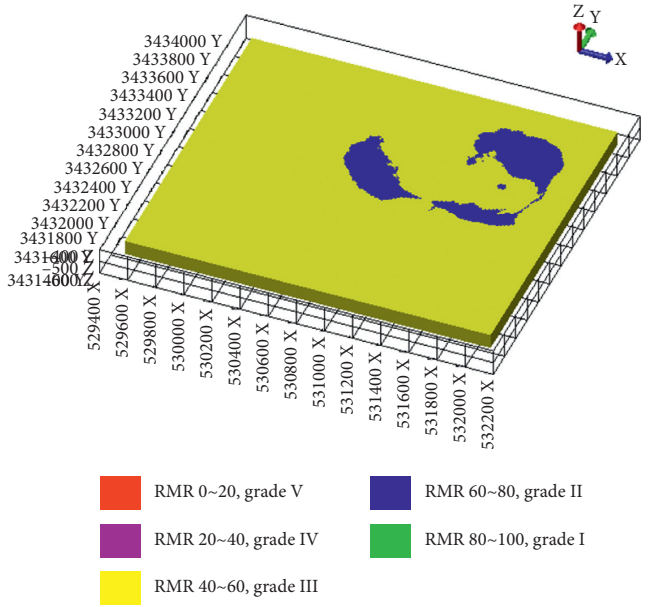


Figure 12: −560~−450 m RMR index rock mass classification 3D model.

The classification method and visualization system proposed in this paper have been automated in most aspects. Simple updates to data can be made at any time, being convenient and fast. It takes only a few tens of minutes to input the data to the map of the status quo of the rock mass distribution at all levels. After obtaining the distribution diagram of each level rock mass class, the support design, blasting scheme setting, and drilling scheme optimization can be carried out as a whole for different levels of rock mass regions.

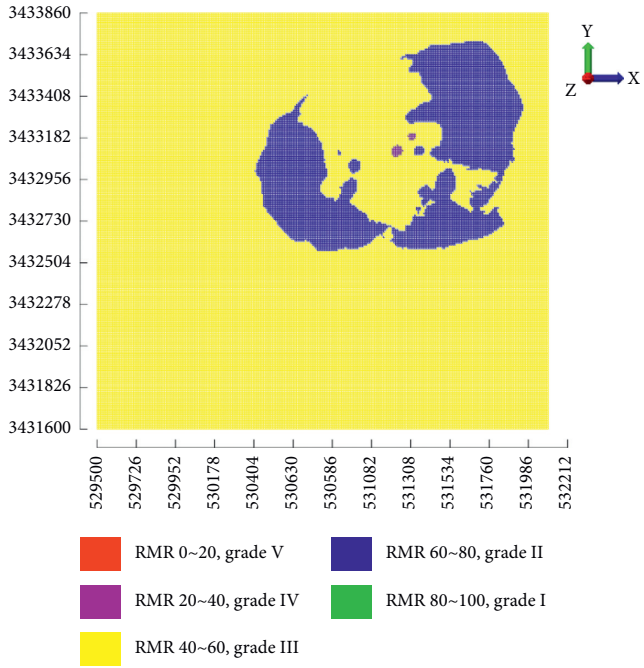


Figure 13: Current status map of horizontal grading distribution of −540 m horizontal rock mass.

## 5. Conclusion

Put forward the optimization of traditional rock mass quality evaluation method based on 3D visualization of rock mass quality evaluation method of close shot photography and system, solve the traditional method of adverse operating environment manual labor intensity big, long time consuming, and accomplish three-dimensional visual; the rock mass classification problem uncovered rock mass quality classification valuation grade and achieved good effect. The main conclusions are as follows:

(1) A method for acquiring key feature parameters of joints based on close-range photography is proposed. The method extracts key characteristic parameters such as length, inclination, centroid position, spacing, and quantity of cracks in close-range photography photos by self-programming.

(2) Based on various literature achievements related to RMR method and BQ method as well as the research and analysis of 97 groups of data measured in a mine field in south China, the engineering practice effect of RMR method and BQ method and their correlation are studied and summarized. The research shows that the two rock mass classification methods have perfect engineering adaptability and correlation.

(3) A 3D visualization method for rock mass quality classification is presented. The method establishes a three-dimensional block model suitable for a particular mine based on entity model such as ore bodies and surrounding rocks. The rock mass quality index (RMR/BQ) of each survey point was combined with the field coordinates to create the sample points of rock mass quality index of the area to be estimated. The three-dimensional block model is endowed through the power-inverse ratio method to get the three-dimensional rock mass classification model of mine, and the three-dimensional visualization of rock mass quality classification is finally realized.

In conclusion, the 3D visualization rock mass quality evaluation method and system based on photographing technology have great application advantages, such as saving time, improving the evaluation accuracy by weakening manual intervention, reducing the engineering economic cost, and ensuring the safety of human work. It provides a new idea for modern rock mass quality evaluation and monitoring and is worth popularizing.

## Data Availability

All data generated or analyzed during this study are included within this article.

## Conflicts of Interest

The authors declare no conflicts of interest.

## Acknowledgments

The authors gratefully acknowledge support for this research from the National Natural Science Foundation of China (51874112, 51774107, and 42077249) and the Open Program of State Key Laboratory of Explosion Science and Technology (Beijing Institute of Technology) (KFJJ20).

## References

[1] D. Gu, *Foundation of Rock Mass Engineering Geomechanics*, Science Press, Beijing, China, 1979.

[2] W. Mingdong, F. Dai, N. Xu, T. Zhao, and Y. Liu, "An experimental and theoretical assessment of semi-circular bend specimens with chevron and straight-through notches for mode I fracture toughness testing of rocks," *International Journal of Rock Mechanics and Mining Sciences*, vol. 99, pp. 28–38, 2017.

[3] F. Peng, F. Dai, Y. Liu, N. Xu, and P. Fan, "Effects of coupled static and dynamic strain rates on the mechanical behaviors of rock-like specimens containing preexisting fissures under uniaxial compression," *Canadian Geotechnical Journal*, vol. 55, no. 5, pp. 640–652, 2018.

[4] W. Mingdong, F. Dai, N. Xu, Y. Liu, and T. Zhao, "A novel chevron notched short rod bend method for measuring the mode I fracture toughness of rocks," *Engineering Fracture Mechanics*, vol. 190, pp. 1–15, 2018.

[5] W. Mingdong, F. Dai, N. Xu, T. Zhao, and K. Xia, "Experimental and numerical study on the fracture process zone and fracture toughness determination for ISRM-suggested semi-circular bend rock specimen," *Engineering Fracture Mechanics*, vol. 154, pp. 43–56, 2016.

[6] P. H. S. W. Kulatilake and T. H. Wu, "Estimation of mean trace length of discontinuities," *Rock Mechanics and Rock Engineering*, vol. 17, no. 4, p. 215, 1984.

[7] J. Hu, B. Yu, and L. Guo, "Using the geological structure survey method to determine the direction of the minimum resistance line of fractured rock mass blasting," *China Mining*, vol. 21, no. 9, pp. 122–124, 2012.

[8] C. Chen and G. Wang, "Discussion on the correlation of various rock mass quality evaluation methods," *Journal of Rock Mechanics and Engineering*, vol. 21, no. 12, pp. 1894–1900, 2002.

[9] D. Zhang and S. Bai, "Measurement method of joint fracture surface opening in rock mass," *China Testing Technology*, vol. 29, no. 3, pp. 33-34, 2003.

[10] G. Lei, C. Yang, G. Wang et al., "Geometrical characteristics and evaluation of rock mass joints in the new site of Beishan preselected area," *Chinese Journal of Rock Mechanics and Engineering*, vol. 35, no. 5, pp. 896–905, 2016.

[11] J. Zhang, Y. Xing, and L. Zheng, "Research on fracture identification using artificial intelligence technology," *Logging Technology*, vol. 29, no. 1, pp. 52–55, 2005.

[12] C. Wang, P. Hu, and W. Sun, "Rock mass integrity evaluation method based on borehole camera technology," *Rock and Soil Mechanics*, vol. 31, no. 4, pp. 1326–1330, 2010.

[13] D. M. Ross-Brown and K. B. Atkinson, "Terrestrial photogrammetry in open-pits: 1-descripion and use of the Phototheodolite in mine surveying," *Instution of Mining & Metallurgy*, vol. 81, no. 1, pp. 7–11, 1972.

[14] S. Tian, X. Ge, and Z. Tu, "Experimental study on digital close-range photogrammetry of tunnel and underground space structure deformation," *Chinese Journal of Rock Mechanics and Engineering*, vol. 25, no. 7, pp. 1309–1315, 2006.

[15] F. Wang, J. Chen, X. Fu et al., "Research on acquiring geometric information of rock mass structural plane based on VirtuoZo," *Chinese Journal of Rock Mechanics and Engineering*, vol. 27, no. 1, pp. 169–175, 2008.

[16] C. Zhou, H. Zhu, and W. Zhao, "Non-contact measurement method for the appearance of rock mass structural plane with binocular system," *Chinese Journal of Rock Mechanics and Engineering*, vol. 29, no. 1, pp. 111–117, 2010.

[17] Y. Wang, S. Wang, M. Guo et al., "Fast digital recognition and stability analysis of joint information on tunnel face," *Chinese Journal of Geotechnical Engineering*, vol. 33, no. 11, pp. 1734–1739, 2011.

[18] Y. Liu, F. Dai, L. Dong, N. Xu, and P. Feng, "Experimental investigation on the fatigue mechanical properties of intermittently jointed rock models under cyclic uniaxial compression with different loading parameters," *Rock Mechanics and Rock Engineering*, vol. 51, no. 1, pp. 47–68, 2018.

[19] Y. Liu, F. Dai, P. Fan, N. Xu, and L. Dong, "Experimental investigation of the influence of joint geometric configurations on the mechanical properties of intermittent jointed rock models under cyclic uniaxial compression," *Rock Mechanics and Rock Engineering*, vol. 50, no. 6, pp. 1453–1471, 2017.

[20] Z. Wu, D. Nie, X. Li et al., "Research on acquisition and processing of rock mass structure information based on digital image," *Chinese Journal of Rock Mechanics and Engineering*, vol. 22, no. S2, pp. 2568–2571, 2003.

[21] L. Fan and L. Ning, "Research on intelligent interpretation method of rock mass fracture image based on pattern recognition technology," *Progress in Natural Science*, vol. 14, no. 2, pp. 236–241, 2004.

[22] S. Li, H. Liu, L. Li et al., "Quantitative characterization method and engineering application of rock mass structure based on digital image," *Journal of Rock Mechanics and Engineering*, vol. 36, no. 1, pp. 1–9, 2017.

[23] F. J. Galdames, C. A. Perez, P. A. Estévez, and M. Adams, "Classification of rock lithology by laser range 3D and color images," *International Journal of Mineral Processing*, vol. 160, pp. 47–57, 2017.

[24] W. Tan, Y. Wu, J. Liu et al., "Improvement of Q system for deep rock mass quality classification," *China Mining*, vol. 29, no. 2, pp. 161–165, 2020.

[25] L. Wang, J. Li, J. Li et al., "Correction and engineering application of RMR evaluation system," *Chinese Journal of Rock Mechanics and Engineering*, vol. 32, no. S2, pp. 3309–3316, 2013.

[26] Q. Chen, T. Yin, and Y. Gao, "Study on the three-dimensional division method of the homogeneous region of the fissured rock mass structure in underground mines," *Rock and Soil Mechanics*, vol. 40, no. 8, pp. 3181–3188, 2019.

[27] Y. Su and M. Ning, "Method for judging surrounding rock grades based on maximum interval classifier," *Chinese Journal of Underground Space and Engineering*, vol. 28, no. 5, pp. 803–805, 2008.

[28] Y. Cong, H. Guo, Y. Zheng et al., "Research on surrounding rock classification method for rock subway engineering," *Modern Tunnelling Technology*, vol. 53, no. 3, pp. 33–41, 2016.

[29] M. A. Aguilar, F. J. Aguilar, and F. Agüera, "Mapping small areas using a low-cost close range photogrammetric software package with aerial photography," *The Photogrammetric Record*, vol. 20, no. 112, p. 16, 2005.

[30] S. Martínez, J. Ortiz, M. L. Gil, and M. T. Rego, "Recording complex structures using close range photogrammetry: the cathedral of santiago de compostela," *The Photogrammetric Record*, vol. 28, no. 144, pp. 375–395, 2013.

[31] S. Huang, Z. Zhang, T. Ke, M. Tang, and X. Xu, "Scanning photogrammetry for measuring large targets in close range," *Remote Sensing*, vol. 7, no. 8, pp. 10042–10077, 2015.

[32] S. K. Ghosh, "A close-range photogrammetric system for 3-D measurements and perspective diagramming in biomechanics," *Journal of Biomechanics*, vol. 16, no. 8, pp. 667–674, 1983.

[33] D. C. Brown, "Unflatness of plates as a source of systematic error in close-range photogrammetry," *Photogrammetria*, vol. 40, no. 4, pp. 343–363, 1986.

[34] S. S. Kang, H. Y. Kim, and B. A. Jang, "Correlation of in situ modulus of deformation with degree of weathering, RMR and Q-system," *Environmental Earth Sciences*, vol. 69, no. 8, 2012.

[35] S. Y. Choi and H. D. Park, "Comparison among different criteria of RMR and Q-system for rock mass classification for tunnelling in Korea," *Tunnelling and Underground Space Technology*, vol. 17, no. 4, pp. 391–401, 2002.

[36] A. Laderian and M. A. Abaspoor, "The correlation between RMR and Q systems in parts of Iran," *Tunnelling & Underground Space Technology Incorporating Trenchless Technology Research*, vol. 27, no. 1, p. 0, 2012.

[37] GB/T 50218—2014, *Engineering Rock Mass Grading Standard*, China Planning Press, Beijing, China, 2015.

[38] A. Palmstrom, "Measurements of and correlations between block size and rock quality designation (RQD)," *Tunnelling and Underground Space Technology*, vol. 20, no. 4, pp. 362–377, 2005.

[39] G. L. Xu, "Estimation method of rock quality index RQD," *Hydrogeology & Engineering Geology*, vol. 6, pp. 43–45, 1991.

[40] B. Amadei, "In situ stress measurements in anisotropic rock," *International Journal of Rock Mechanics and Mining Sciences & Geomechanics Abstracts*, vol. 21, no. 6, pp. 327–338, 1984.

[41] X. Yang, J. Pang, H. Lou, and L. Fan, "Characteristics of in situ stress field at Qingshui coal mine," *International Journal of*

*Mining Science and Technology*, vol. 25, no. 3, pp. 497–501, 2015.

[42] F. Dai, B. Li, N. Xu et al., "Deformation forecasting and stability analysis of large-scale underground powerhouse caverns from microseismic monitoring," *International Journal of Rock Mechanics and Mining Sciences*, vol. 86, pp. 269–281, 2019.

[43] A. Li, Y. Liu, F. Dai, K. Liu, and M. Wei, "Continuum analysis of the structurally controlled displacements for large-scale underground caverns in bedded rock masses," *Tunnelling and Underground Space Technology*, vol. 97, Article ID 103288, 2020.

[44] Y. Wang, H. Zhang, H. Lin, Y. Zhao, and Y. Liu, "Fracture behaviour of central-flawed rock plate under uniaxial compression," *Theoretical and Applied Fracture Mechanics*, vol. 106, Article ID 102503, 2020.

[45] Z. T. Bieniaski, "Engineering classification of jointed rock masses," *Transaction of the South African Institution of Civil Engineering*, vol. 15, no. 12, pp. 335–344, 1973.

[46] Z. T. Bieniawski, *Engineering Rock Mass Classification*, pp. 180–250, Science Press, New York, NY, USA, 1989.

[47] B. Cai, Y. Yu, and X. Wu, "Relationship between "classification standard of engineering rock mass" and Q classification and RMR classification and deformation parameter estimation," *Journal of Rock Mechanics and Engineering*, vol. 20, no. z1, pp. 1677–1679, 2001.

[48] C. Wang, D. Li, and W. Zhao, "Discussion on the overall stability of the high slope of Lanyoushan deep road cutting in Yixing, Nanjing-Hangzhou expressway," *Journal of Disaster Prevention and Mitigation Engineering*, vol. 4, pp. 417–422, 2004.

[49] T. Yan, X. Wu, and L. Wu, "Correlation study and engineering application of the classification of surrounding rocks in underground caverns," *Chinese Journal of Underground Space and Engineering*, vol. 5, no. 3, pp. 41–47, 2009.

[50] P. Duan, Y. H. Sheng, J. Li, L. V. Haiyang, and S. Zhang, "Adaptive IDW interpolation method and its application in air temperature field," *Geographical Research*, vol. 33, no. 8, pp. 1417–1426, 2014.

[51] F. Wu, R. Gao, Q. Zou, J. Chen, W. Liu, and K. Peng, "Long-term strength determination and nonlinear creep damage constitutive model of salt rock based on multistage creep test: implications for underground natural gas storage in salt cavern," *Energy Science & Engineering*, vol. 8, pp. 1592–1603, 2020.

[52] H. Lin, H. Yang, Y. Wang, Y. Zhao, and R. Cao, "Determination of the stress field and crack initiation angle of an open flaw tip under uniaxial compression," *Theoretical and Applied Fracture Mechanics*, vol. 104, Article ID 102358, 2019.

[53] H. Yuan, C. Chen, Z. He, and Y. Wang, "Numerical simulation of fluid-solid coupling in surrounding rock for river stope mining," *Shock and Vibration*, vol. 2020, no. 4, 11 pages, Article ID 9786182, 2020.

[54] Y. Zhao, Y. Wang, W. Wang et al., "Modeling of rheological fracture behavior of rock cracks subjected to hydraulic pressure and far field stresses," *Theoretical & Applied Fracture Mechanics*, vol. 101, 2019.

[55] B. X. Yuan, L. Xiong, L. Zhai et al., "Transparent synthetic soil and its application in modeling of soil-structure interaction using optical system," *Frontiers in Earth Science*, vol. 7, p. 276, 2019.

Hindawi
Advances in Civil Engineering
Volume 2020, Article ID 8865107, 22 pages
https://doi.org/10.1155/2020/8865107

*Research Article*

# A Novel HDF-Based Data Compression and Integration Approach to Support BIM-GIS Practical Applications

**Zeyu Pan, Jianyong Shi, and Liu Jiang**

*Department of Civil Engineering, Shanghai Jiao Tong University, Shanghai 200240, China*

Correspondence should be addressed to Jianyong Shi; shijy@sjtu.edu.cn

Received 5 August 2020; Revised 23 November 2020; Accepted 4 December 2020; Published 22 December 2020

Academic Editor: Qian Wang

Copyright © 2020 Zeyu Pan et al. This is an open access article distributed under the Creative Commons Attribution License, which permits unrestricted use, distribution, and reproduction in any medium, provided the original work is properly cited.

Constructing a fully mapped virtual world is the premise of establishing the digital twin system; thus, the integration of BIM (Building Information Modeling) and GIS (Geographic Information System) constitutes a fundamental part of the mature digital twin. Although quite a few theoretical unified data models of BIM and GIS integration have been presented in precedent research, the practical web-based applications and software support for real-world city information modeling are still difficult to achieve. One of the challenges is storage inefficiency. It thence leads to burdens in exchange and analysis, which hugely impede the realization of virtual-real fusion. To address that issue, in this research, we contribute to exploring an HDF- (Hierarchical Data Format-) based, innovative, and synthesized scheme with three significant technical processes. First, data reorganization trims the original data with efficient redundancy elimination and reordering for IFC-SPF (IFC STEP Physical File) and XML-encoded CityGML (City Geography Markup Language). Next, bidirectional transformation methods for BIM and GIS modeling data, images, and analytical data into HDF are proposed. They retain the entities and relationships in modeling data and can further improve the compactness and accessibility by ultimately 60%–80% which saves 497,612 KB from 565,152 KB in the test of ZhongChun transformation substation. Finally, data aggregation enhances the bond of the integrated model and heterogeneous data resources from the transformed HDF files. The case studies show that the approach proposed in this paper could reach high efficiency for practicability of the BIM + GIS integration model. This light-weight integration method can further improve the front-end service responsiveness in digital twin applications.

## 1. Introduction

There is a trend that the researchers and the governments are putting increasing emphasis on the multisource associated event-driven city planning and management, from regular facility maintenance to evacuation and rescue operations for city-level disasters such as flood, wildfire, and earthquake. In our perspective, the premise of making such an event-based decision is to create the digital twin, literally a thorough, dynamic digital reflection of the real urban environment which should be capable of (1) containing as many city features as possible, (2) synchronizing with its host dynamically through multiple urban data resources, and (3) forming a real-time and integrated response to the events. Functionally, two renowned kernel technologies are integrated as the core foundation of the digital twin to support the city features, known as BIM (Building Information Modeling) at the microlevel and GIS (Geographic Information System) at the macrolevel [1]. Previous attempts for BIM and GIS integration often focus on the semantic mapping of both information models in static cases [2–5], which is inadequate for practical digital twin applications. Generally speaking, for the web services which generate gigabytes of data per second like urban online services, the data to be processed at the edge can retain shorter response time, more efficient processing, and smaller network pressure [6]. It spawns a demand to explore an efficient, cooperative, and heterogeneity-friendly approach for data exchange, query, and integration in practical situations to relieve computing and storage burden. Thence, we

conduct this research to deal with the merging of heterogeneous data formats, compact data storage and exchange, and efficient response to urban events.

BIM excels at dealing with data storage and exchange for 3D models, especially the specific interior components of structures, including buildings, tunnels, and bridges. Meanwhile, GIS masters at managing the potential topological relationships between the entities and events in exterior geographic spaces, while the interior information is usually quite limited. The concept of merging BIM and GIS is naturally reasonable. Borrmann et al. state that integrating BIM and GIS tools is essential for planning extensive infrastructure facilities [2]. Ninić et al. [7] also pointed out that it is indispensable to integrate BIM and GIS when solving multiple scalar issues of planning, designing, and analyzing infrastructure projects [7]. Based on comprehensive BIM-GIS integration, in the future, the urban stakeholders, including governments or single residents, will be able to create a sustainable living environment [1] through more intelligent and approachable management patterns for energy management or lifecycle management. To realize this schema-level forge, plenty of researchers [3–5, 8–13] have been endeavoring for years on analyzing and refactoring those two notable vendor-neutral data standards, IFC and CityGML. IFC (Industry Foundation Classes) is designed to describe the indoor building environment, and complementarily, CityGML (City Geography Markup Language) conveys the outdoor urban environment as more powerful. They have great potential in storage, manipulation, organization, and exchange of urban data. For the sake of serving as stable, open, and consensus standard data models, both of them are vendor-neutral.

However, there are two main challenges during the attempt at integrating those two technologies. The first one is about conceptual data models. The incompatibilities in IFC and CityGML schema, especially the geometric representation [8] and the entity ambiguity, are so aggravating for BIM-GIS integrated applications. The other one is about the scale of integrated data. When the project scale grows, the data complexity, heterogeneity, and volume will explosively increase. Even for a simple city application, gigabyte-level data storage, transmission, and analysis are quite ubiquitous.

At present, pertinent researchers have spent much attention enhancing or extending the concepts of data models, which is undoubtedly essential. However, in comparison, the necessity of developing an efficient storage and exchange format for integrated information has been long overlooked. To make up for the conceptual incompatibilities in both data structures, the researchers have generally followed two respective measures: embedding BIM to GIS or merging them into a uniform, customized data structure. The first attempts include geometric representation transforming [8, 9, 13], georeferencing [10], property mapping [11], multiscale geometric semantic modeling [2], and geometric translation through an indirect path [12]. At the same time, the second attempt involves developing an integrated data model for underground utility management [3] and presenting an ontology-based general data model for integration [4, 5].

When transforming the geometries and semantics from IFC into the target CityGML, no matter which schemes to use, it is inevitable to encounter the inherent defects of CityGML listed by Yang and Eastman [14]. The defects inheriting from XML (Extensible Markup Language), GML (Geographic Markup Language), and from CityGML itself include high parsing cost, too many possible variations of geometric representation, verbiage, and hence massive storage burden. Deng et al. [15] succeeded in mapping partial geometrical representations, Brep (Boundary Representation), Sweptsolid, and CSG (Constructive Solid Geometry) of IFC into Brep of CityGML for LoD1~LoD4 (LoD: Level of Detail). However, the storage size of LoD4 in CityGML will grow to 250%~400% compared with the original IFC files [15]. Additionally, even a low level-of-detail (LoD2) of a single city might be easily over 2 GB (without compression). These phenomena will cause disastrous effects on those high storage-dependent applications in BIM-GIS integration, such as urban-level visualization and big data analysis. As a result, they will reduce the reusability and the capacity of processing the data.

This paper aims to find a practical solution to relieve the storage burden, which can improve data mining capacity in urban data and solve the insufficiency of existent data formats of BIM and GIS for digital twin development. We conduct this research to settle this issue from pretransform, transform, and posttransform processes. More specifically, it is divided into first the refinement of source data such as IFC-SPF, XML-encoded CityGML, pictures, and so on (without format change), then the transformation into a compact, unified data format (Hierarchical Data Format, HDF [16]) (with format change), and finally the enhancement of the bond between each data resource. Thus, three crucial procedures are proposed: (1) data reorganization of IFC-SPF and XML-encoded CityGML files; (2) data transformation for IFC-SPF, CityJSON, photos, time history functions, and so on; and (3) data aggregation of the transformed heterogeneous data.

To facilitate understanding, the rest of this paper is organized as follows. In Section 2, the fundamental features and defects of current BIM-GIS integrated data management will be analyzed. It will then introduce the candidate data format HDF and two experimental, inspiring light-weight data formats (IFC-HDF and CityJSON). In Section 3, the following stuff elaborates on this research's principal methodologies, including data refinement, data transformation, and data aggregation. Next, in Section 4, we will present result evaluation and case validation in integrating BIM and GIS through HDF. In Section 5, the main contributions in current research are summarized. Finally, in Section 6, a few directions in the further study are presented.

## 2. Background

*2.1. Basic Features of BIM-GIS Projects.* It is genuinely common to have multiple sources of data files in one BIM-GIS application, such as emergency response [17], leading to two unignorable challenges: storage burden and data

heterogeneity issues. On the one hand, in a typical AEC (Architecture, Engineering, and Construction) project, the relevant information resources might involve not only building information models but also 2D drawings, documentation, photographs, point cloud data, FEM (Finite Element Method) data, etc. On the other hand, there are also multiple geographic data resources, such as maps, texture, oblique photogrammetry data, and so forth. Although BIM and GIS technologies have been endeavoring to merge their relevant data into their respective open consensus data models, it is impossible to cover and transform all other data models with massive preliminary preparation.

*2.2. Defects of Current Official Data Formats of IFC and CityGML in Data Sharing.* Data serialization is a term in computer science that represents the process of converting structured data to a format that allows the sharing of the data in a form that can recover its original structure [18]. The most prevalent IFC format is IFC-SPF (STEP Physical File, STEP is STandard for the Exchange of Product Model Data, with the extension of ".ifc"). Concurrently, there are also several variations such as IFC-XML (Extensible Markup Language) for cross-domain information exchange, IFC-JSON (JavaScript Object Notation) [19] for web-based applications, and IFC-OWL (Web Ontology Language) [20] for linked data services. In contrast, CityGML owns one specific official data format referred to as XML-encoded CityGML. Besides, there are some experimental alternatives for both data standards, namely, IFC-HDF and CityJSON. A detailed discussion of both formats will be presented later in this article.

Here are some issues in BIM-GIS transformation. The data formats mentioned above might have one or more following disadvantages.

(1) Text-based: it is a tricky feature of a data format, as it can be profitable for increasing human readability but needs massive labor work when being parsed. The data formats in BIM are text-based. Their entity instances tend to be laid out in files since their implicit relationships are established by references such as #45 = IFCAXIS2PLACEMENT3D (#42, #43, and #44) in IFC-SPF. It is difficult for highly efficient random information access. Therefore, it induces poor performance in cases with considerable building information. The parsing of CityGML, as mentioned before, has great difficulty in dealing with malformed XML. In contrast, in the binary format, HDF organizes the collected data with a predefined hierarchical structure. It allows the users to access the information randomly and isochronally by tracking the path reference link. Although HDF format is binary serialized, it is also self-described and highly readable after decoding. It enables the users without prior knowledge of HDF format to smoothly explore the file and retrieve data required because all information, such as data hierarchy and data types, is encoded in itself [21].

(2) Verbose (IFC-XML, IFC-JSON, IFC-OWL, and XML-encoded CityGML): those IFC formats explicitly translate the metadata hidden in IFC-SPF from relative schema specifications and repeat these attribute names in each instance declaration, as shown in Figure 1. It improves readability to some extent but will generally burden 13%, 48%, and even 1272% on storage for each format than the original IFC-SPF [22]. The same dilemma occurs in CityGML since the root format is XML, where related developers have long criticized the verbosity. On the other hand, a feature in HDF, the so-called compound data type, fixes both readability and verbosity issues. To illustrate, Figure 2 suggests that the attribute names will be declared only once as data types for each type instantiation of IFC, while the whole file remains easy to understand.

(3) Redundant: during the whole lifetime of each BIM or GIS project, no matter which schema version (IFC Schema Specification-buildingSMART Technical [23]; CityGML | OGC [24]) the model file complies with, data redundancy involving instance repetition and geometry complexity [25] is unintentionally generated, as depicted in Figure 3. Sometimes, it may even accumulate up to 60–70% in relatively large models [26]. To achieve further performance on BIM-GIS integrated applications, data redundancy eliminating pretreatments based on the original SPF file are inevitable.

In this paper, the pretreatment of IFC-SPF, which includes duplicate removal and instance reordering, will be introduced. It is noteworthy that this pretreatment process is also feasible during the translation to other data formats of IFC.

(4) Storage challenge: all the prevalent IFC formats have this issue, even for IFC-SPF. Meanwhile, using XML-encoded CityGML as a 3D urban data storage usually tends to cost massive file size [14], especially in high level-of-detail cases. In Krijnen's fundamental work on IFC-HDF, he has mentioned some vital conclusions that IFC-HDF is far more compact than the other formats and could have an alluring performance that saves around 50–70% size in comparison with IFC-SPF on large building models [27]. Unlike many different data formats, HDF allows the exploiters to randomly access information by indexing with decompressing the chunked datasets of interest rather than the whole file. The compact storage and random access capability of data archives will profoundly enhance data transmission and demonstration performance.

(5) Incomplete: IFC schema is designed extensible, which allows the professional developers to attach their findings or integrate information from other domains onto IFC schema as extensions, for instance, structural health monitoring [28], point cloud [29], design change management [30], and so

IfcJSON fragment

```
{
    "axis": {
        "instanceId": 43,
        "directionRatios": [0, 0, 1],
        "type": "IfcDirection"
    },
    "instanceId": 45,
    "location": {
        "instanceId": 42,
        "coordinates": [0, 0, 0],
        "type": "IfcCartesianPoint"
    },
    "refDirection": {
        "instanceId": 44,
        "directionRatios": [1, 0, 0],
        "type": "IfcDirection"
    },
    "type": "IfcAxis2Placement3D"
}
```

IFC-SPF fragment

```
#42=IFCCARTESIANPOINT((0.,0.,0.));
#43=IFCDIRECTION((0.,0.,1.));
#44=IFCDIRECTION((1.,0.,0.));
#45=IFCAXIS2PLACEMENT3D(#42,#43,#44);
```

Figure 1: Expression comparison between IfcJSON and IFC-SPF format.

| | id | type | GlobalId | OwnerHistory | Name | Description | ObjectType | ObjectPlacemer |
|---|---|---|---|---|---|---|---|---|
| 0 | 800342 | IfcBuildingElementPart | 1UVe6Ptx2FL1b1jcB2oTKc | EI_id_#22_If... | Gevel betimmering, hor... | None | None | EI_id_#799975_IfcL |
| 1 | 798896 | IfcBuildingElementPart | 1spECmAd1bUcY8PhxZPL$o | EI_id_#22_If... | Tengels | None | None | EI_id_#797823_IfcL |
| 2 | 851951 | IfcBuildingElementPart | 1A7qmCfNeypHA_a5Motcmj | EI_id_#22_If... | 400 Isolatie wand | None | None | EI_id_#851886_IfcL |
| 3 | 849108 | IfcBuildingElementPart | 3pdah9ZwyL6w_tkLtyfvj9 | EI_id_#22_If... | 400 Isolatie wand | None | None | EI_id_#849042_IfcL |
| 4 | 503 | IfcBuildingElementPart | 0CMdCMGf21$eLdXN0Q7yX6 | EI_id_#22_If... | Steen - Baksteen | None | None | EI_id_#432_IfcLoca |
| 5 | 409 | IfcBuildingElementPart | 0FMv1xIafTJKC69h0p1Vxj | EI_id_#22_If... | 410 Luchtspouw buiten | None | None | EI_id_#338_IfcLoca |

Figure 2: An exemplary dataset for type IfcBuildingElementPart of IFC in HDFViewer 3.1.0 as a demonstration of data simplicity in HDF.

IFC-SPF segment

```
#31 = IFCAXIS2PLACEMENT3D(#32, #33, #34);
#32 = IFCCARTESIANPOINT((0., 0., 0.));
#33 = IFCDIRECTION((0., 0., 1.));
#34 = IFCDIRECTION((1., 0., 0.));
#35 = IFCBUILDINGSTOREY('36_p3GiZXEHxQ3gWc
#36 = IFCLOCALPLACEMENT(#30, #37);
#37 = IFCAXIS2PLACEMENT3D(#38, #39, #40);
#38 = IFCCARTESIANPOINT((0., 0., 0.));
#39 = IFCDIRECTION((0., 0., 1.));
#40 = IFCDIRECTION((1., 0., 0.));
```

Figure 3: Simple data redundancy in IFC-SPF.

on. Likewise, CityGML also allows these kinds of Application Domain Extension (ADE) to increase the schema's extensibility. However, such extension development work might cost lots of human labor, and it usually relies on a particular version of the schema. Besides, to some extent, those schema extensions enrich the valuable information that the original schema can participate in specific applications, but, due to its domain-related features, the data it can store and present are still quite limited. Contrarily, HDF, the domain-neutral binary data format, is compatible with various kinds of data formats. Hence, it is essential for the efficient organization of heterogenetic data in complex projects.

Owing to its capacity in efficiently treating those heterogeneous data, the specific data format, Hierarchical Data Format (HDF), is chosen as the candidate format for relieving the storage burden and dealing with data heterogeneity issues in this research. The following paragraphs will make a brief introduction to HDF.

### 2.3. HDF's Basic Concepts

(1) Definition and function: vividly speaking, HDF is analogous to a powerful, portable synthesis of databases and organized file systems. As defined by its official organization, it is designed as a scientific binary data format capable of supporting an unlimited variety of data types and is portable and extensible for high volume and complex data [16, 31]. It is widely supported for creation, edition, and parsing by popular programming languages such as C, Fortran, C++, Java, Python, Matlab, IDL, etc. Besides, it also excels at hierarchical compartmentalization and self-descriptive compound data type [32].

(2) Characteristics: one of HDF's most attractive features for complicated projects is that it can be treated as a versatile file system and can hold various heterogeneous datasets, including images, tables, graphs, and even documents, including PDF or Excel besides the primary datasets.

(3) Specialty: HDF adopts a specific chunked compression storage method, through which the whole binary file can be decomposed intuitively into a customized or predefined number of data chunks with an inherent identification index. Due to the chunked compression feature, HDF is adept at storing considerable amounts of data with an astonishing rapid random information retrieval, which is truly precious for city-level data management.

In comparison to relational databases, the option of using HDF as a target repository to help incorporate the storage and manipulation of metadata and data in specific

applications can remarkably improve the portability and flexibility [33]. HDF meets the requirements of both light-weight data transmission and real-time interoperation with low delay in BIM-GIS integration applications.

*2.4. Two Enlightening Data Formats.* Referring to the latest studies [14, 27, 29, 32, 34], to develop a proper exchange data format for light-weight applications in BIM and GIS, respectively, two promising alternatives have been proposed, respectively, namely, CityJSON and IFC-HDF. Both have splendid features innately when serving as a potential compact variant. Hence, it is quite natural to come up with a scheme that assimilates them as two base data formats and make proper adjustments to develop an appropriate container for BIM-GIS integration. Before that, some essential characteristics of CityJSON and IFC-HDF will be discussed first.

*2.4.1. CityJSON.* CityJSON is developed to offer a compact and developer-friendly alternative data format, namely, JSON (JavaScript Object Notation), for storing 3D city models rather than the original inefficient CityGML, according to its website [35]. Although it remains experimental and underexamined by practical experiences, the characteristic it possesses is quite impressive [14]. In comparison with XML-encoded CityGML, CityJSON is much more compact (about one-sixth of equivalent XML-encoded CityGML), which is essential for serving as an acceptable exchange format. It is easier to deal with by developers since JSON is a long liable data format and more human-readable.

When XML-encoded CityGML is being parsed into CityJSON, some significant changes have been made. First, it removes the direct hierarchical relations (for instance, the component trunks contained in a particular city object) of CityGML. It rebuilds them into an implicit form: parent/children relation to realizing the aim of a relatively flattened data structure. This treatment is controversial because it will undoubtedly improve the random accessibility of minor components. Still, in another view, it might decrease the human readability and proficiency when searching for the composition relationships. Secondly, to enlarge the flexibility of the primary feature of numerous vertices' point storage due to Brep shape representation, the developers of CityJSON figured out a solution where the coordinates of vertices are segregated from the former slots in those primitive GML leaves and then rearranged with duplicate removal. The superior entities must reference the point through the index. Furthermore, in CityJSON, most object IDs embody 3D primitive geometric form element IDs except for city objects and semantic surfaces [14].

As a GIS-specific exchange data format, CityJSON will no doubt be powerful, but there are still some adjustments required to make for this research's purpose. LoD4 (the interior environment) of city objects in CityGML, including building, bridge, and tunnel modules, was not designed to be involved in CityJSON. Even if it were supported, it would affect data management (due to the index mapping) and data storage [22] itself to some extent. This omission might decrease the analysis dimension of this format for specific applications that need indoor data. For completeness, the interior data are compensated with IFC by converting both indoor and outdoor information into a particular compact exchange data format, namely, HDF, here, with a method to seamlessly transform the geometric and semantic information for both data structures. Besides, in the XML or JSON data format, the texture materials tend to be attached beyond the main file. It might cause some inefficiency when carrying on data transmission. The pretreatment of appearances is considered and will then be converted into the target HDF to improve the data completeness further.

*2.4.2. IFC-HDF.* The scientific binary data format, HDF, was first introduced to IFC in 2015 by Krijnen et al. [34]. This series of work about IFC-HDF [27, 29, 32, 34] revealed the possibility to develop a new variation of IFC for exchange, query, and storage with HDF's remarkable storage capacity, high compression, and random information retrieval ability of large volume data cases and its aptitude to be compatible with a wide range of heterogeneous data types.

Before being adopted in the AEC industry, HDF as an efficient exchange data format has already had great fame in different applications of all kinds of fields for many years, especially in those sensitive with data storage and query capacity such as web-based visualization and high-performance, parallel data analysis [36]. It is common sense that with the development of data acquisition methods, the data scale and data complexity for each field, involving BIM and GIS, have become an inspiring treasure and a severe issue simultaneously. As data scale and heterogeneity grow, plain text-based data formats will cause problems when processing substantial N-dimensional datasets. Then, the systems' scalability and flexibility will be challenged [37]. HDF, as a self-described, neutral data format, has some essential characteristics for web-based services, including efficient parallel I/O (Input/Output) for fast read/write, compact data storage, and storage and management of metadata and data provenance information to facilitate complex analysis workflows [36]. Hence, researchers or professionals tend to select HDF as the fundamental data archive format for high-performance real-time analysis and visualization systems owing to its splendid storage and access efficiency. For example, HDF has been exploited by nuclear physics [38], analytical chemistry [21], spaceborne altimetry [39], social science [40], meteorology [36], and so forth.

Krijnen 2019, stated that there are more inspiring facts about the effects of using HDF as the data format of the 3D building information [32]. Two critical conclusions can be derived: (1) for data storage, a well-padded HDF with its inherent compression will reach one-fifth (maximum 80% compression ratio in particular cases) of the original IFC-SPF and nearly the same or even better than IFC-SPF (gzip); (2) for processing and access time, IFC-HDF will be far more efficient than IFC-SPF in all cases and the query time surprisingly remains almost same for different scales of model thanks to its chunked compression algorithm. IFC-

ZIP also has great compression capacity, but when used for information extraction, the whole clumsy file needs to be decompressed first, while HDF need not be due to its chunked compression mechanism.

Analogous to CityJSON, IFC-SPF has been designed to present the content with flattening data mode. At the same time, unlike CityJSON, IFC-SPF spreads out almost all elements as entity instances in its model file (ISO 10303-21 : 2002 [41]).

For the sake of rebuilding the hierarchical system of the model through the implicit references, the whole text-based file must be parsed first, and the relationships must be retrieved. For large model files, this process based on IFC-SPF might be challenging. HDF provides a flexible alternative to search for interest without parsing the whole hierarchical system due to random access capability.

## 3. Methodology

The succeeding subsections are divided into three functional parts: data reorganization, data transformation, and data aggregation. We proposed a methodology that links up the above three procedures to support the storage, exchange, and retrieval of large-scale project data in practical digital twin applications. The processes of each part are summarized in Figure 4. They are set to be extensible and modular, which means components in this approach are flexible to embrace data processing efficiency.

Here is a brief explanation of the technology roadmap depicted in Figure 4. The first phase is the data reorganization. It processes the raw data from source files with respective pretreatment methods for each data resource, including IFC-SPF, CityJSON, images, and analytical data. We contribute to detecting and eliminating the duplicate redundancies and reference redundancies in IFC-SPF with high performance during the data reorganization. The next phase is the data transformation. It takes charge of transforming the pretreated data into HDF. In this phase, we try to maintain each source's data structure to realize the bidirectional transformation, which means it is feasible to regenerate the source file back from the transformed HDF. Besides, our contribution is to present a recursion solution to change the information embedded in CityGML/CityJSON to the target format HDF, and the reversal conversion is also realized. The final phase is data aggregation. It is responsible for establishing the semantic links between the objects in the transformed heterogeneous resources under the supervision of project ontologies derived from practical situations and experiences to enhance the bond between the transformed data.

Utilizing the comprehensive approach with data reorganization, data transformation, and data aggregation based on HDF proposed in this research, the BIM-GIS related data can be integrated at the storage and semantic level in a more practical way. Furthermore, there is another point to be mentioned. In each phase, the procedures' outcomes can be exported separately as the resource for other situations, which gives this scheme more flexibility to adapt to new applications.

*3.1. Data Reorganization.* To further promote the efficiency and performance of data exchange, storage, and analysis of BIM-GIS integration, some pretreatments for different primitive data resources are necessary. Compared to the modeling data studied in this paper, the reorganization of images and analytical data is relatively simple; this phase of those data is moved into the data transformation section. In this subsection, we emphasize the methods applied to IFC-SPF and XML-encoded CityGML.

*3.1.1. Procedures for IFC-SPF.* This procedure for IFC-SPF is composed of two functional parts: eliminating redundant information and reordering instances. Both are based on pure text processing and hence version-neutral with different IFC schema, which guarantees no information loss.

*(1) Elimination of Redundant Information.* Redundancy always occurs in each IFC file, no matter what the file size is. Additionally, there is a positive correlation between file size and data redundancy. A more intuitive demonstration of this phenomenon will be exhibited later with example files in Section 4.1.

Four procedures for the elimination of redundant information are proposed (Algorithm 1): Text separation*, Repetition detection*, Reference replacement*, and Reassembly*. There are three necessary containers to maintain the process which are CD (Content Dictionary) for storing instance content with its identifiers where the key is instance id (the value is the wrapped content), RR (Reference Relationship Dictionary) for storing reference relationships such as {'#30':['#24','#31']} in #30 = IFCLOCALPLACEMENT (#24,#31) case, RP (Repetition Pair Dictionary) for storing detected duplicates, and their replacements such as {'#40':'#34' or wrapped #34} in #40 = IFCDIRECTION (1.,0.,0.) and #34 = IFCDIRECTION (1.,0.,0.) case.

Main data flow (Figure 5): the BodySection retrieved through TextSplit will be transported to RepetionDetect to traverse each instance. During the traversal, the instance line will be split as ID-Content pair with a content repetition check to make sure whether it is redundant or not. After that, reference replacement will be executed to replace the redundant instances' ID with its initial sibling. Finally, all sections will be reassembled as the target output.

Note: it is generally impossible to get complete trimming for a redundant IFC-SPF with just one epoch, owing to its tree-like reference structure, which will generate recursive redundancy. An illustration is presented in Figure 6 to elaborate on this phenomenon.

Iteration of instance line generation is taken to refrain from insufficient trimming. The iteration would be terminated once the count of repetition pairs reaches zero. After several trials (Figure 7), patterns emerge that the duplicate removal process's epochs will come close to 11 or more, implicitly determined by the deepest branch of IFC structure (might be slightly different depending on the IFC schema version, here checked IFC2x3).

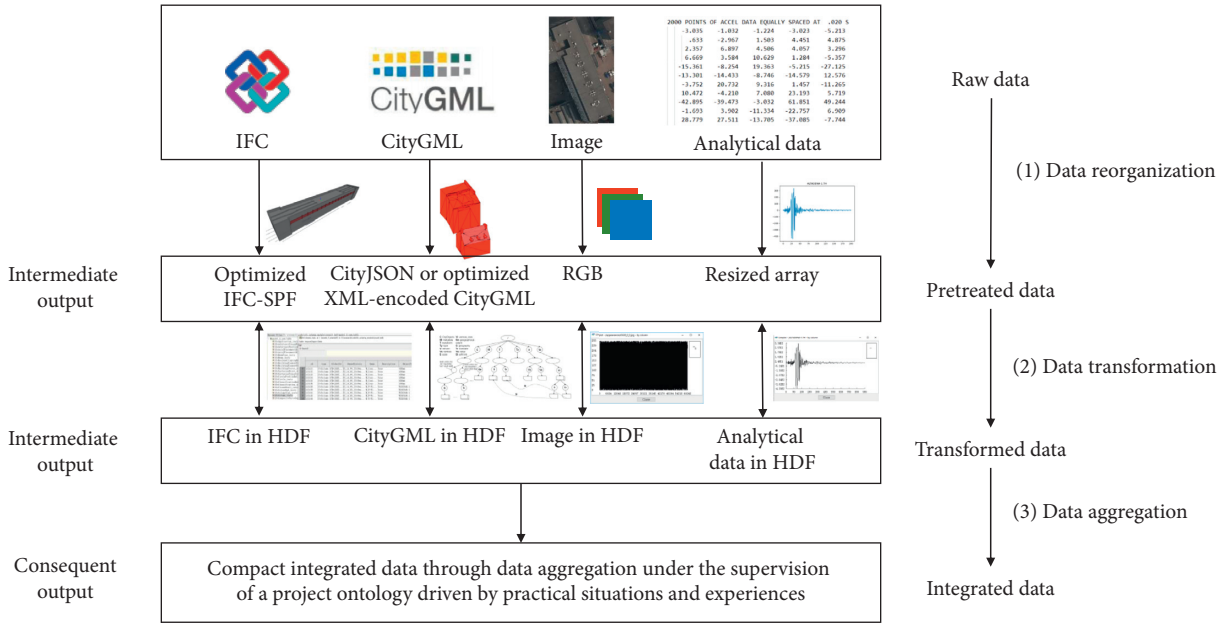


Figure 4: Methodology of this research.

**Input**: *File*: Original IFC Step Physical File
**Output**: *File* // Final trimmed file
(1) **function** DUPLICATEREMOVE(*File*)
(2) *Lines* ← *File.readlines*()
(3) // do Step 1
(4) *TextSpilt*(*Lines*) ⟶ *HeadSection*, *BodySection*, *FootSection*
(5) // do Step 2
(6) *RepetitionDetect*(*BodySection*) ⟶ *CD*, *RR*, *RP*
(7) // loop Step 3 until length[RP] = 0, where RP can be renewed by Step 2
(8) *ReferenceReplace*(*CD*, *RR*, *RP*) ⟶ $BodySection_{renew}$
(9) // do Step 4
(10) *Reassembly*(*Headsection*, $BodySection_{renew}$, *FootSection*) ⟶ $File_{new}$
(11) **return** $File_{new}$
(12) **end function**

Algorithm 1: Duplicate removal: remove the repetition occurred in IFC-SPF.

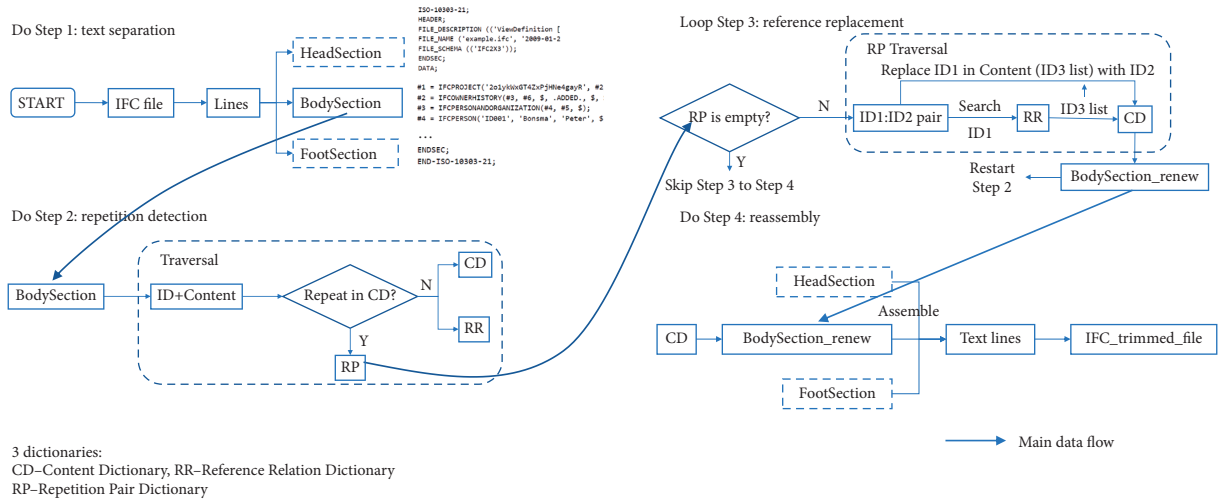


Figure 5: Data flowchart for duplicate removal of IFC-SPF.

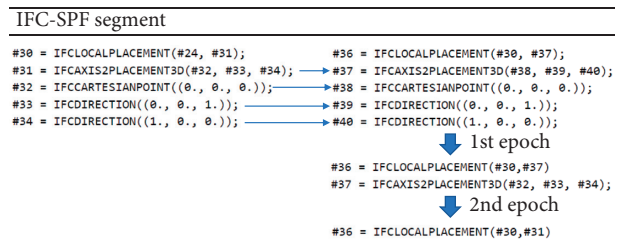


Figure 6: Recursive redundancy in IFC.

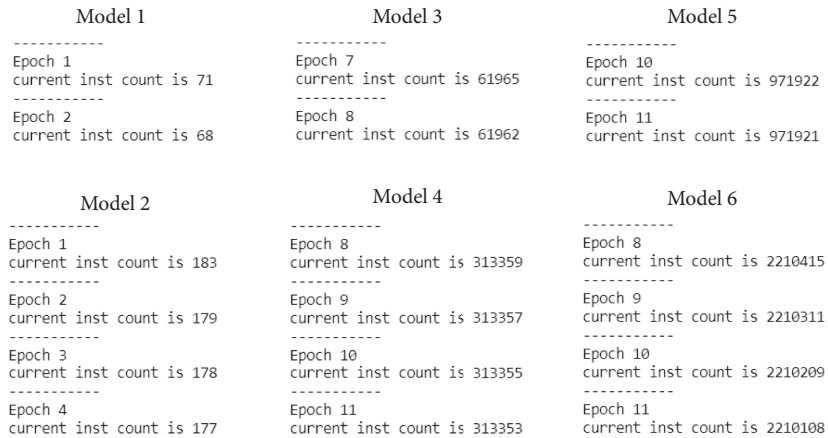


Figure 7: A demonstration of the epoch cost of each test model in this research (detailed information of each model will be discussed in Section 4).

**Input:** BodySection: List of Instances
**Output:** $File_{new}$
(1) **function** INSTANCEREORDER(*BodySection*)
(2) // do Step 1
(3) *ReferenceCount*(*BodySection*) $\longrightarrow$ *RC*, *CD*
(4) // do Step 2
(5) *IDSubstitute*(*RC*, *CD*) $\longrightarrow$ $BodySection_{renew}$
(6) // do Step 3
(7) *Reassembly*(*HeadSection*, $BodySection_{renew}$, *FootSection*) $\longrightarrow$ $File_{new}$
(8) return $File_{new}$
(9) **end function**

Algorithm 2: Instance reordering: reorder the instances based on the particular principle that the more frequently an instance is referenced, the smaller the referred identifier is assigned.

*(2) Reordering of the Instances*. This treatment aims to reset the instance order with one principle: the more frequently an instance is referenced, the smaller the referred identifier is assigned. Assigning frequently referenced objects with short identifiers can help decrease the byte cost of serialization. The compactibility can be further improved since the bytes for storage the references take decrease. Analogous to duplicate removal, the critical point is to find the appropriate substitutes for the target reference in "instance content." However, unlike duplicate removal, reordering does not need iterations. If this process begins right behind duplicate removal, then it can be simplified.

Instance reordering (Algorithm 2): Reference count*, ID substitution*, and Reassembly*. There are two necessary containers to maintain the process, which are RC (Reference Count Dictionary) and CD (Content Dictionary). CD here has almost the same capability as that in the Duplicate Removal section, while RC stores the frequency of each instance being referenced.

Main data flow (Figure 8): the retrieved BodySection will be split into ID-Content pairs. Meanwhile, the reference count will be recorded as the sorting principle. After that, reassign each instance's ID and further substitute the reference IDs in the instance contents. Finally, all sections will be reassembled as the target output.

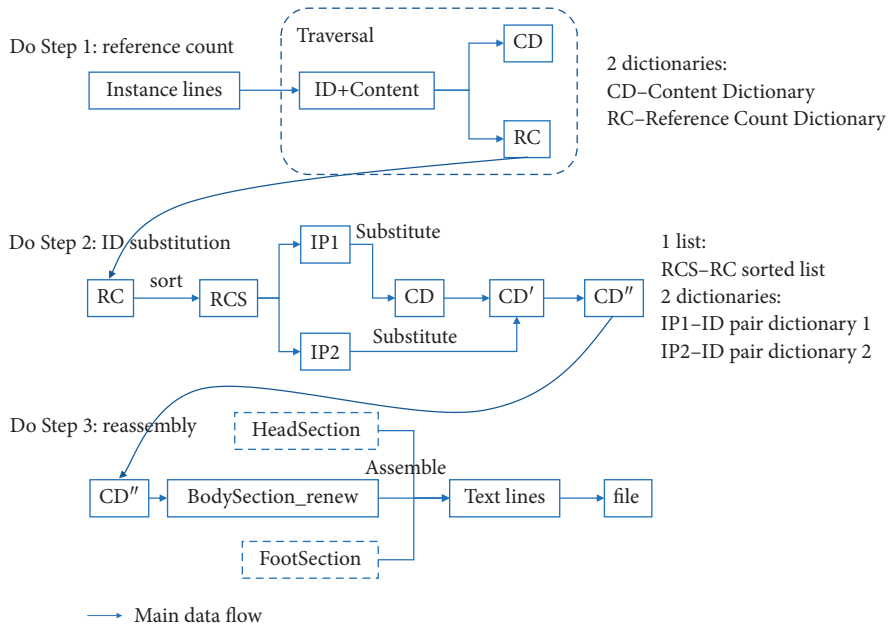


Figure 8: Data flowchart for instance reordering of IFC-SPF.

In Figure 9, part of the reference count statistics of each test model is demonstrated. It will be convenient for us to make the ID substitution process by extracting the original files' reference frequency.

### 3.1.2. Procedures for XML-Encoded CityGML

*(1) Removal of the Vertex Redundancy.* In XML-encoded CityGML, to guarantee its explicit hierarchical structure of city object instantiation, the geometric representations such as surfaces and vertices tend to be embedded deep and separately in related XML trees. That feature will generate geometric redundancy. Although the reference solutions based on x-link are proposed to relieve this dilemma, due to GML's versatile representation patterns, this problem can still not be radically solved. Contrarily, after converting the representations into CityJSON, all vertices are extracted, and the surfaces can remain connected to relevant vertices by a particular indexing mechanism inherited from Wavefront OBJ [14, 42]. With this isolated vertex container, the duplicates can be removed, and the reference can be refreshed completely. Besides, by now, CityJSON has supported the bidirectional conversion with XML-encoded CityGML. Hence, it is worthwhile to transform XML-encoded CityGML into CityJSON, which can be processed by an open-source toolkit citygml-tools [43] before merging data into HDF.

*(2) Pretreatment for Irregular Datasets.* Based on its process difficulty, the original data containers in CityJSON can be divided into three levels: regular, semiregular, and irregular. In contrast, because of its EXPRESS specialty, the IFC data can be all regarded as a regular level.

(a) Regular: in the regular cases, the original data are well formed with the fixed dimensional size of data, including vertices (x, *y*, and z table stored, as shown in Figure 10) and vertices-texture. Those kinds of data can be parsed directly into a highly compressed data form.

(b) Semiregular: for example, in the case of appearance in CityJSON, the textures are listed with verbose but regular map elements, which can be parsed as a compound 2D data table, as depicted in Figure 11.

(c) Irregular: the irregular data are an aggravating issue when making the transformation process. For instance, in CityJSON, inherited from GML, the boundaries can be composed of different kinds of patches, leading to dimension confusion and difficulty to be parsed as a compact data table in HDF. Hence, padding is added to the original container and the voids are filled with "−1" to solve this dilemma. This pretreatment contains three steps: detect irregular arrays, calculate the maximum scale for each dimension, and finally, resize the container with paddings filled with −1.

The result of padded irregular data in HDF is shown as follows (Figure 12). For convenience in presentation, the second and third dimensions are switched, but the data stored are still in dimension size of $10 \times 1 \times 6$.

*3.2. Data Transformation.* As being narrated above, due to its remarkable adaptability of supporting heterogeneous data sources and other strengths, HDF is chosen as the candidate storage and exchange data format in this research to support the integration of BIM and GIS. The following subsections put forward the bidirectional transformation for four kinds of data in BIM-GIS integration, including IFC, CityJSON, images, and analytical data.

Model 1

```
Reorder start
Five most referenced id and reference count:
ID      Count
#2      10
#22     7
#25     5
#20     4
#56     4
```

Model 3

```
Reorder start
Five most referenced id and reference count:
ID      Count
#22695  1961
#29     874
#52     171
#56     135
#27868  72
```

Model 5

```
Reorder start
Five most referenced id and reference count:
ID      Count
#41     21234
#511476 6966
#134747 4871
#131435 4734
#19     4483
```

Model 2

```
Reorder start
Five most referenced id and reference count:
ID      Count
#2      26
#22     14
#20     9
#87     7
#47     6
```

Model 4

```
Reorder start
Five most referenced id and reference count:
ID      Count
#22     12447
#49     1681
#519    1541
#45     1507
#174    1088
```

Model 6

```
Reorder start
Five most referenced id and reference count:
ID      Count
#41     34442
#19     6923
#38     3624
#31     2599
#10144  1909
```

Figure 9: A demonstration of reference count statistics extracted from the original files.

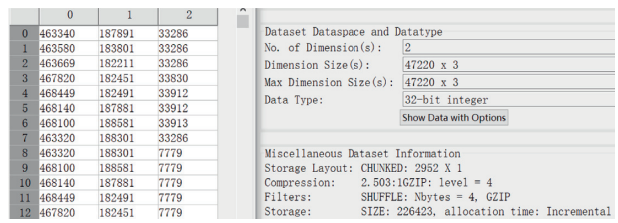

| | 0 | 1 | 2 |
|---|---|---|---|
| 0 | 463340 | 187891 | 33286 |
| 1 | 463580 | 183801 | 33286 |
| 2 | 463669 | 182211 | 33286 |
| 3 | 467820 | 182451 | 33830 |
| 4 | 468449 | 182491 | 33912 |
| 5 | 468140 | 187881 | 33912 |
| 6 | 468100 | 188581 | 33913 |
| 7 | 463320 | 188301 | 33286 |
| 8 | 463320 | 188301 | 7779 |
| 9 | 468100 | 188581 | 7779 |
| 10 | 468140 | 187881 | 7779 |
| 11 | 468449 | 182491 | 7779 |
| 12 | 467820 | 182451 | 7779 |



Figure 10: Regular vertex storage in HDF, with 2.503 compression ratio and 47220 vertices.

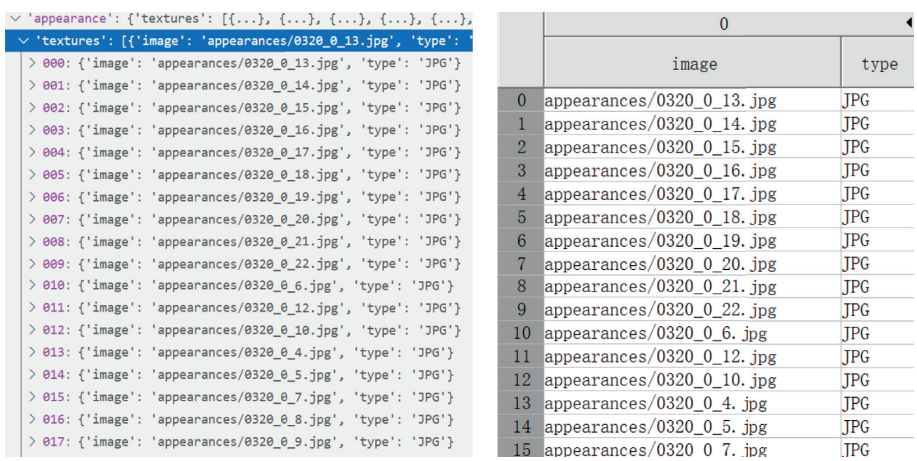

```
'appearance': {'textures': [{...}, {...}, {...}, {...}, {...},
'textures': [{'image': 'appearances/0320_0_13.jpg', 'type': '
  000: {'image': 'appearances/0320_0_13.jpg', 'type': 'JPG'}
  001: {'image': 'appearances/0320_0_14.jpg', 'type': 'JPG'}
  002: {'image': 'appearances/0320_0_15.jpg', 'type': 'JPG'}
  003: {'image': 'appearances/0320_0_16.jpg', 'type': 'JPG'}
  004: {'image': 'appearances/0320_0_17.jpg', 'type': 'JPG'}
  005: {'image': 'appearances/0320_0_18.jpg', 'type': 'JPG'}
  006: {'image': 'appearances/0320_0_19.jpg', 'type': 'JPG'}
  007: {'image': 'appearances/0320_0_20.jpg', 'type': 'JPG'}
  008: {'image': 'appearances/0320_0_21.jpg', 'type': 'JPG'}
  009: {'image': 'appearances/0320_0_22.jpg', 'type': 'JPG'}
  010: {'image': 'appearances/0320_0_6.jpg', 'type': 'JPG'}
  011: {'image': 'appearances/0320_0_12.jpg', 'type': 'JPG'}
  012: {'image': 'appearances/0320_0_10.jpg', 'type': 'JPG'}
  013: {'image': 'appearances/0320_0_4.jpg', 'type': 'JPG'}
  014: {'image': 'appearances/0320_0_5.jpg', 'type': 'JPG'}
  015: {'image': 'appearances/0320_0_7.jpg', 'type': 'JPG'}
  016: {'image': 'appearances/0320_0_8.jpg', 'type': 'JPG'}
  017: {'image': 'appearances/0320_0_9.jpg', 'type': 'JPG'}
```

| | 0 | |
|---|---|---|
| | image | type |
| 0 | appearances/0320_0_13.jpg | JPG |
| 1 | appearances/0320_0_14.jpg | JPG |
| 2 | appearances/0320_0_15.jpg | JPG |
| 3 | appearances/0320_0_16.jpg | JPG |
| 4 | appearances/0320_0_17.jpg | JPG |
| 5 | appearances/0320_0_18.jpg | JPG |
| 6 | appearances/0320_0_19.jpg | JPG |
| 7 | appearances/0320_0_20.jpg | JPG |
| 8 | appearances/0320_0_21.jpg | JPG |
| 9 | appearances/0320_0_22.jpg | JPG |
| 10 | appearances/0320_0_6.jpg | JPG |
| 11 | appearances/0320_0_12.jpg | JPG |
| 12 | appearances/0320_0_10.jpg | JPG |
| 13 | appearances/0320_0_4.jpg | JPG |
| 14 | appearances/0320_0_5.jpg | JPG |
| 15 | appearances/0320_0_7.jpg | JPG |

Figure 11: Original form in JSON (left) and resultant form in HDF (right), with 33.388 : 1 compression ratio in texture case; the source file is 3-20-DELFSHAVEN from [35].

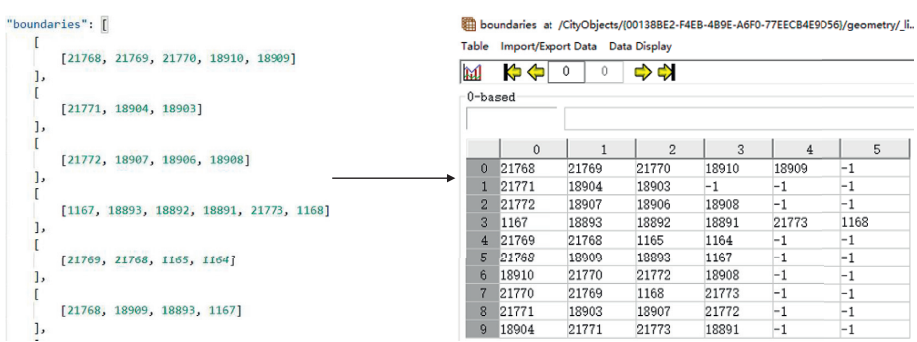

```
"boundaries": [
  [
    [21768, 21769, 21770, 18910, 18909]
  ],
  [
    [21771, 18904, 18903]
  ],
  [
    [21772, 18907, 18906, 18908]
  ],
  [
    [1167, 18893, 18892, 18891, 21773, 1168]
  ],
  [
    [21769, 21768, 1165, 1164]
  ],
  [
    [21768, 18909, 18893, 1167]
  ],
```



| | 0 | 1 | 2 | 3 | 4 | 5 |
|---|---|---|---|---|---|---|
| 0 | 21768 | 21769 | 21770 | 18910 | 18909 | -1 |
| 1 | 21771 | 18904 | 18903 | -1 | -1 | -1 |
| 2 | 21772 | 18907 | 18906 | 18908 | -1 | -1 |
| 3 | 1167 | 18893 | 18892 | 18891 | 21773 | 1168 |
| 4 | 21769 | 21768 | 1165 | 1164 | -1 | -1 |
| 5 | 21768 | 18909 | 18893 | 1167 | -1 | -1 |
| 6 | 18910 | 21770 | 21772 | 18908 | -1 | -1 |
| 7 | 21770 | 21769 | 1168 | 21773 | -1 | -1 |
| 8 | 21771 | 18903 | 18907 | 21772 | -1 | -1 |
| 9 | 18904 | 21771 | 21773 | 18891 | -1 | -1 |

Figure 12: Original form in JSON (left) and resultant form in HDF (right) in boundary case.

Two fundamental data units in HDF are group and dataset. Dataset is analogous to the table in relational databases, and group is similar to the directory in a file system. Besides, both data units can have attributes to store extra information, which is helpful when converting a complex data structure such as CityJSON.

*3.2.1. IFC-SPF to HDF.* This transformation work references an officially published ISO standard, ISO /TS 10303-26 : 2011 binary representation of EXPRESS-driven data [44]. Since IFC is a variant of EXPRESS, it is feasible to transplant EXPRESS-HDF into IFC-HDF. For interoperability, a promotion to the parsing process has been made so that the reverse transformation, namely, from HDF to IFC-SPF, can also be accomplished. Besides, through this algorithm, it will not be necessary to rely on a particular IFC-relevant toolkit in parsing or regenerating IFC-SPF. The critical point is to extract information such as explicit attributes directly from the original EXPRESS-based schema. It also allows us to parse the IFC-SPFs regardless of the version of the IFC schema. Furthermore, to get prepared for the data aggregation phase, an index map between IFC-SPF-based identifier and HDF-based identifier is deliberately appended to the main contents as can be seen in Figure 13. In Section 3.3, more details about the function of the index map will be explained.

As is represented in Algorithm 3, it is feasible to gain bidirectional transformation between IFC-SPF and HDF through those two functions. The metadata of the original file will be extracted and parsed as the HDF's attributes. It is critical to parse the raw instance text lines into the form of "inst_id = ifctype (paramList)" to wrap the instances with their relevant explicit attributes. The reverse transformation depends on unwrapping and reassembly.

Besides, after several tests, it is proved that the bidirectional transformation here is seamless, which means it will be much compacter and, more importantly, safe to store the source data.

*3.2.2. CityJSON to HDF.* IFC is a derivation of EXPRESS, making it possible to represent complicated data models with an object-oriented approach concisely [45]. Hence, the model information involved in IFC-SPF, due to its EXPRESS-like configuration, can be easily parsed as field-value datasets and then dumped into HDF. However, on the contrary, CityJSON tends to elaborate its contents with explicit hierarchical data structure with numerous, disperse, small lists, which is challenging to be parsed directly into HDF. So far, we have managed to realize the bidirectional transformation by tracking the whole hierarchical structure in CityJSON through recursion. The inefficient explicit hierarchy causes the major storage challenge here. In future work, we consider developing an object-oriented variant of CityGML/CityJSON to flatten the data structure further. The below graph (Figure 14) is an HDF diagram that represents a typical CityJSON file. It contains the transformed data resources and their relationships. The dashed line refers to reference redirecting in HDF.

Algorithms 4 and 5 show how to constitute the bidirectional conversion between CityJSON and HDF. Recursion is the key to the conversion processes here. The recursion process helps us to maintain the whole original hierarchy from CityJSON without grasping the complicated structure in advance.

In the positive conversion from CityJSON to HDF, a particular function named DictParse is designed to experience recursion. The inputs are (a) "hdfFile," the target HDF for writing, (b) "aDict," the recursive data units, and (c) "prev_path," the path of the parent group stored in the target HDF. It is essential to check the input dictionary's values, whether they are instances of a dictionary, list, or others, to further recurse or parse them into HDF datasets and attributes. Additionally, in the particular case that needs converting a list of objects into HDF data units, some subgroups are inserted in the form of "_list_item_#num" to remind the back-conversion process to translate the items into a list.

On the other hand, in the reversal conversion from HDF to CityJSON, similarly, another function designed to experience recursion is GroupWalk. The inputs contain (a) "group," the reversive data unit stored in HDF, (b) "grandParentNode," the grandparent node related to current data defined in target dictionary, (c) "parentNode," the parent node related to current data defined in target dictionary, and (d) "rootDict," the target output dictionary. This process is to assemble the target output dictionary with the data extracted from source HDF through recursion. Groups in HDF are iterated to find the attributes and datasets to parse them into the target dictionary. When dealing with datasets, if the datasets are detected as padded, it will be cleaned first before further transformation. Besides, a list is allocated here to prepare to hold the objects in the "list_item_#num" group and, finally, attach the list directly to the grandparent node if the list's length is not zero.

*3.2.3. Image to HDF.* Image is an indispensable part of practical digital twin projects. In this section, we will focus on the reorganization and transformation of images. With the help of OpenCV (an open toolkit for image processing) [46], the large source TIFF and BMP images, or processed PNG and JPG, will be feasible to be compressed with different qualities (0–100) into HDF and be regenerated to meet the need of specific applications. The images should be further encoded through OpenCV as streaming data in storage to increase storage efficiency; meanwhile, they can be decoded as real image files for formal utility. The algorithm of the processes above is summarized in Algorithm 6. Besides, the procedure of image processing might be followed by the flowchart in Figure 15. In the last process of Figure 15, it shows the result of decoding the stored image data in HDF and restitute to regular images.

*3.2.4. Analytical Data to HDF.* Most analytical data have a fine structure and primary data types, which can be easily parsed into HDF. Here is an example of time history functions. The input time history functions grouped with 1,

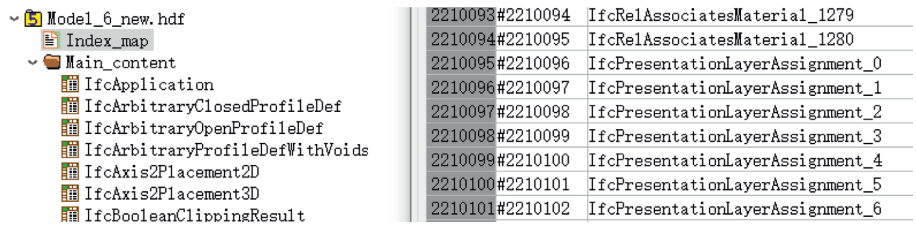


Figure 13: The demonstration of the index map (on the left side is the primary structure of IFC in HDF; on the right side is the index map dataset).

**Input:** *IFC-SPF*: The serialized IFC file with the extension of '.ife'
**Output:** *HDF*: The resultant serialized IFC file with the extension of '.hdf', *Back_IFC-SPF*: Reversal transformed IFC-SPF
(1) **function** IFC2HDF(*SPF*)
(2) // 0. Premise: Prepare explicit attributes of the corresponding version of EXPRESS Schema before start
(3) //1. Parse SPF into metadata and instance list with RegularExpression or others.
(4) *Lines* ← *SPF.readlines*()
(5) *Head_Section*, *Raw_inst_lines* ← *Extract*(*Lines*)
(6) *File_Description*, *File_Name*, *File_Schema* ← *MetaData*(*Head_Section*)
(7) *Parsed_insts* ← *IterAndParse*(*Raw_inst_lines*)
(8) // 2. Apply semantics to the instances based on relevant explicit attributes and classify them with IFC Entity, such as "IfcCartesianPoint"
(9) *Semantic_insts* ← *WrapAndClassify*(*Parsed_insts*)
(10) //3. Transform the semantic insts into array and further datasets in HDF by defining datatype
(11) *Datasets_in_hdf* ← *MainTransform*(*Semantic_insts*)
(12) // 4. Write HDF
(13) *HDF* ← *WriteToDisk*(*Datasets_in_hdf*)
(14) **end function**
(15) function HDF2IFC(*HDF*)
(16) // 1. Extract MetaData
(17) *File_Description, File_Name, File_Schema* ← *Extract*(*hdfFile.attrs*)
(18) *MetaData* ← *Repr*(*File_Descriptiion, File_Name, File_Schema*)
(19) //2. Parse Entity instances from datasets
(20) *Raw_inst_list* ← *Iter AndUnwrap*(*hdfFile*['*MainContent*'])
(21) //*Representwith*"*a* = *b*(*c*);" *for each instance where a is inst_id, b is i fcType, c is parameter_list*
(22) *Inst_text_list* ← *Repr*(*Raw_inst_list*)
(23) // 3. Reassemble and Write IFC-SPF
(24) *Back_IDC-SPF* ← *ReassembleAndWrite*(*MetaData*, *Inst_text_list*)
(25) **end function**

Algorithm 3: Bidirectional transformation between IFC-SPF and HDF.

2, and $Z$ directions will be resized and then serialized into HDF, as shown in Figure 16.

*3.3. Data Aggregation.* As is narrated at the beginning of the Methodology section, this phase, data aggregation, is critical to integrating the transformed heterogeneous data related to the digital twin by establishing semantic links between them under a practical project ontology's supervision. The ontology enables us to extract the partial, pertinent data from HDF in a particular logic. We consider the comprehensive of the transformed HDF files as a compact version of the BIM-GIS project repository, which can hold the necessary data for multiple urban simulations or other applications. This repository will include typical modeling data and relevant analytical data. The required data for a specific integrated application can be queried [27], extracted, or even linked (to save storage) directly from the repository.

There are two main reasons why we choose to import the integrated data model in the posttransformation phase rather than directly extract data from the original or, maybe, post-reorganized data. The first reason is reusability. The city objects are usually taken as static data in digital twin applications since these models' main contents do not change so frequently. It is efficient to manage the data in the same compact format which will be handy for retrieval. Bidirectional conversions have been developed between these data with HDF, which means it is safe to store the data in the compact format, HDF, for extracting and renewing the analytical data back to the original formats. The second reason is accessibility. Krijnen et al. [32] mentioned that due to the special chunking and compression mechanism when

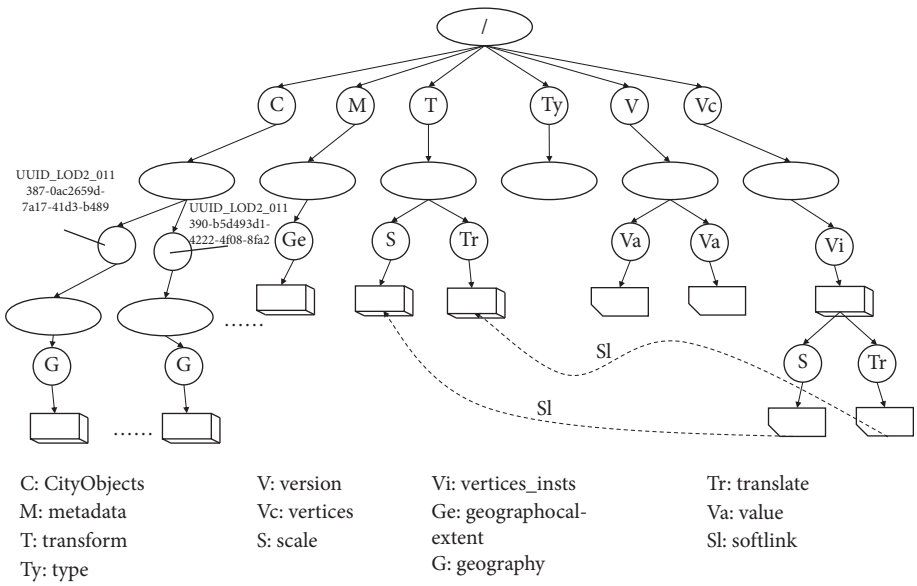


Figure 14: HDF diagram for an example CityJSON file.

**Input:** *CityJSON*: The serialized CityGML file with the extension of '.json'
**Output:** *HDF*: The resultant serialized CityJSON file with the extension of '.hdf'

```
(1) function DICTPARSE(hdfFile, aDirect, prew_path)
(2)    prev_prev_path ← prev_path
(3)    for key, valucinaDict.items() do
(4)       prev_path ← " {0}/{1}".format(prev_prev_path, key)
(5)       If type(value) ≡ dict then
(6)          DictParse(hdfFile, value, prev-path)
(7)       else
(8)          if type(value) ≡ list then
(9)             root_path ← prev_path
(10)            for i = 0 ⟶ len(value) do
(11)               item ← value[i]
(12)         if type(item) ≡ dict then
(13)            prev_path ← "{0}/_list_item_{1}".format(root_path, i)
(14)            DictParse(hdfFile, item, prev_path)
(15)         else
(16)            //Create datasets with pretreated array from regular/semiregular/irregular data
(17)         end if
(18)         end for
(19)      else
(20)         if type(value) ∈[str, int, float] then
(21)            // Convert these kinds of data into attributes
(22)         end if
(23)      end if
(24)   end if
(25)   end for
(26) end function
(27) function CITYJSON2HDF (CityJSON)
(28)   //1. Prepare source json and target hdf.
(29)   jDict ← CityJSON
(30)   hdfFile ← Open(name, mode = 'ω')
(31)   //2. Recurse DietParse function
(32)   DictParse(hdfFile, jDict,".")
(33)   //3. Write HDF
(34)   HDF ← WriteToDisk(Datasets_in_hdf)
(35) end function
```

Algorithm 4:Transformation from CityJSON to HDF.

```
Input: HDF: The resultant serialized CityJSON file with the extension of '.hdf'
Output: CityJSON: The serialized CityGML file with the extension of '.json'
(1) function GROUPWALK(group, grandParentNode, parentNode, rootDict)
(2)   for attr ∈ group.attrs do
(3)     // Attributes are parsed, respectively, according to their data type, such as string, int, and float
(4)   end for
(5)   specialList ← List()//Prepare to hold the objects in "_list_item_#num"
(6)  for elem ∈ group do
(7)     if IsStarWith(elem.name, "_list") then
(8)       newNode ← GroupWalk(elem, parentNode, {}, {})
(9)       specialList.append(newNode)
(10)    else
(11)      if type(elem) ≡ Dataset then
(12)        rawList ← Listify(elem)
(13)       // Remove the Paddings (-1) if the datasets are padded
(14)        treatedList ← checkAndParse(rawList)
(15)        parentNode[elem.Name] ← treatedList
(16)    else
(17)      if type(elem) ≡ Group then
(18)        grandParentNode ← parentNode
(19)        childNode ← parentNode[elem.Name] ← {}
(20)        parentNode ← childNode
(21)        rootDict ← GroupWalk(elem, grandParentNode, parentNode, rootDict)
(22)      end if
(23)    end if
(24)    end if
(25)  end for
(26)  if len(specialList) ≠ 0 then
(27)    grandParentNode[group.Name] ← specialList
(28)  end if
      return rootDict
(29)  end function
(30)  function HDF2CITYJSON(HDF)
(31)    //1. Prepare source hdf.
(32)    hdfFile ← Open(name, mode='r')
(33)    // 2. Recurse GroupWalk function
(34)    rootDict ← GroupWalk(hdfFile, {}, {}, {})
(35)    //3. Write json
(36)    json.dump(rootDict, CityJSON)
(37) end function
```

Algorithm 5: Transformation from HDF to CityJSON.

storing data in HDF, it costs much less both time and data size of reading. Since there are many requests for real-time analysis and response in BIM-GIS web-based applications, it is natural to choose the extraction steps with HDF.

The technique route to aggregate the related transformed city data can be followed as above (Figure 17). The content which is enclosed by the dashed block is still under experiment. The urban ontology for BIM-GIS integration is designed as shown in Figure 18. For simplicity, the relationships of the entities have been omitted in this figure. This ontology is composed of 7 subontologies, including Analysis, Facility, Feature, Geometry, PhysicalElement, SpatialElement, and Resource. Each subontology will maintain the essential elements for the BIM-GIS integrated applications. The ontologies' function is to organize the relevant, valuable data in a particular logic so that the relationship between the different kinds of pretreated source data can be revealed. It is efficient to retrieve the information from these HDFs and instantiate them through the ontology. The HDFPath entity is set in case some resource data are hard to instantiate. It records the link of the target file and the path to access the data. Moreover, in 3.2.1 IFC-SPF to HDF transformation, the index map appending to the main content was mentioned. It is beneficial for data retrieval. Since we have reordered the entity instances in the original IFC file, the identifiers have become consistent, which means it is able to get the target table and index through "Index_map [instance_id-1] [1]" in constant-time query with no relevance to the count of the instances in original IFC-SPF.

Section summary: the research's core purpose is to explore a practical solution to relieve the storage burden and improve the capacity of data mining of heterogeneous data in BIM-GIS cooperative domains. We propose the methodology based on developing a comprehensive of three

**Input:** *InputPath*: Folder path stores appearances, *OutputPath*: resultant hdfs' folder path
Output: *Files*: HDF Files

```
(1) function IMAGE2HDF(InputPath, OutputPath)
(2)     img_list ← List()
(3)     Create hdf File ⟶ f
(4)     f.create_group("appearances")
(5)     Get image file names ⟶ f
(6)     for i = 0 ⟶ len(name_list) do
(7)         image_name ← name_list[i]
(8)         image_dir ← path.join(path, image_name)
(9)         // openev.imread can read multiple image formats
(10)        img ← opencv.imread(dir_image)
(11)        // opencv.cvtColor can change the color matrix into another assigned form
(12)        img ←opencv.cvtColor(img, opencv.COLOR_BGR2YCR_CB)
(13)        // opencv.imencode can encode image matrix to a streaming array
(14)        //img_fps is the target image quality, range: (0, 100)
(15)        img_param ← [int(opencv.IMW RITE_JPEG_QUALITY), img_fps]
(16)        img_encode ← opencv.imencode(".JPEG," img, img, img-param) [1]
(17)        img_list.append(img_encode)
(18)        f["appearances"].create_dataset(name = img_name, dtype = unit8,
(19)        data = img_encode, compression = "gzip," chunks = true, shuffle = true)
(20)    end for
(21) end function
```

Algorithm 6: Image processing: save image to hdf and regenerate image from hdf (the image format can be JPG, PNG, BMP, and TIFF).

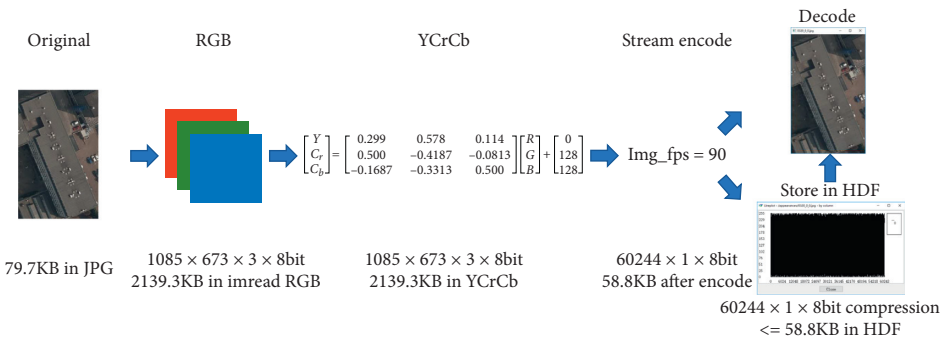


Figure 15: Flowchart of image processing with an exemplary image (image source from [35]).

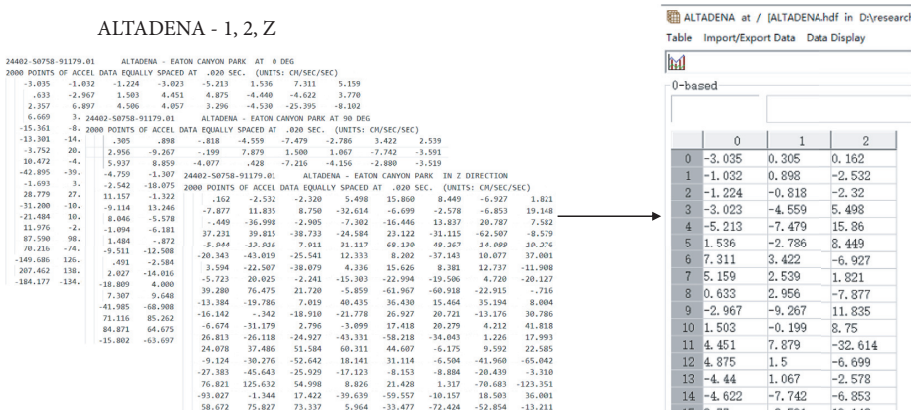


Figure 16: An example of transformed analytical data in HDF.

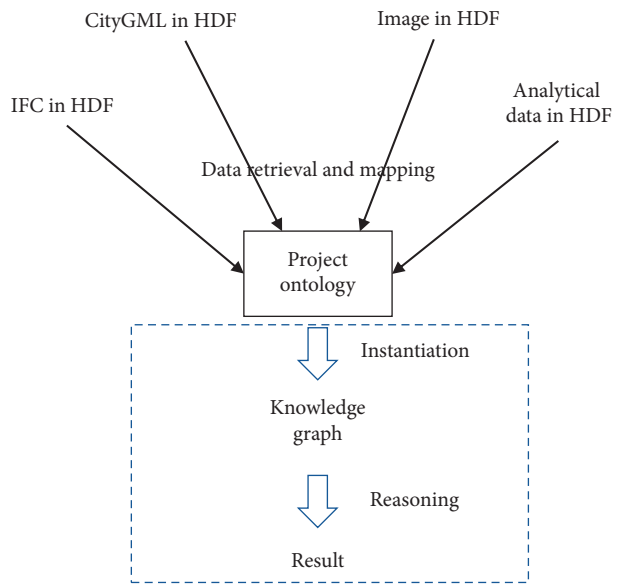


Figure 17: Technique route of data aggregation phase.

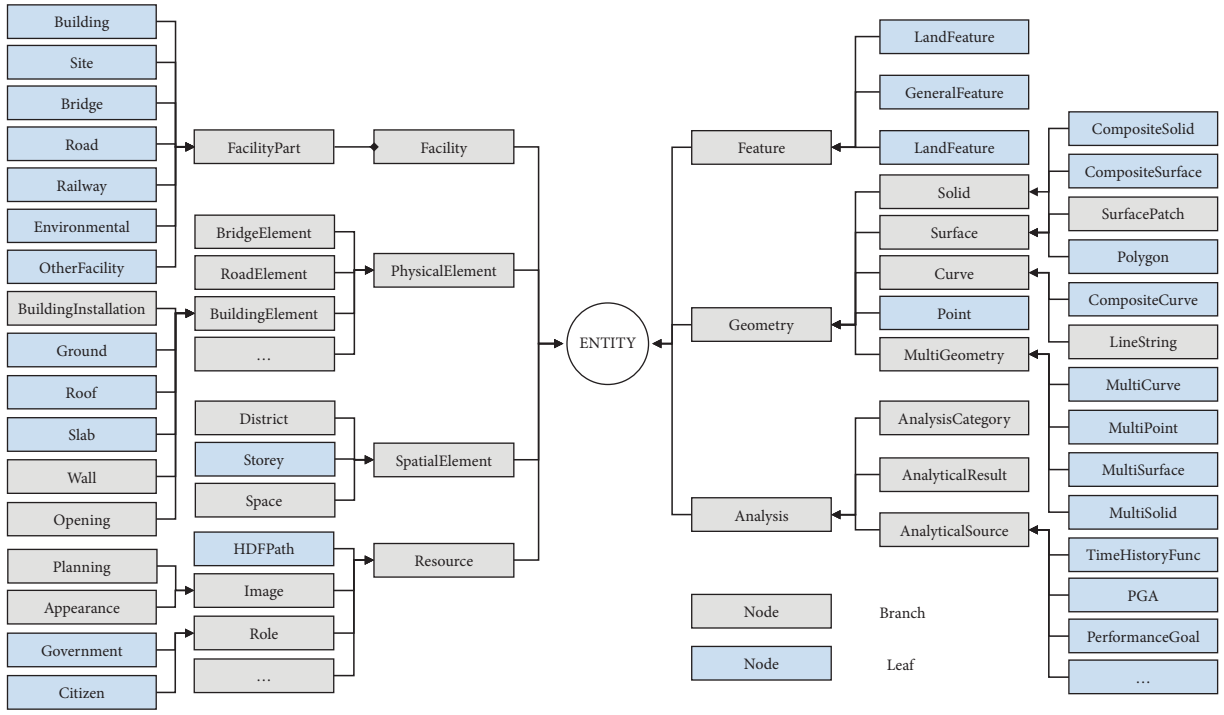


Figure 18: The experimental urban ontology designed to aggregate information from the transformed data.

essential procedures in this section. Through data reorganization and data transformation against data resources, the valuable data are reserved and eventually transformed into the candidate compact and highly efficient data format, so-called HDF, for further data mining processes. During data aggregation, a project ontology can be imported, and further retrieval and mapping from the transformed HDFs should meet the requirements of this ontology. Some adjustments have been made in previous phases like reordering and index maps to extract the desired information more efficiently.

## 4. Result Evaluation

*4.1. For IFC-SPF.* Seven test models were chosen to verify the feasibility and effectiveness of the proposed procedures. These models can be divided into three groups according to their volume as (1) group 1-tiny model: Model 1 and Model 2; (2) group 2-medium model: Model 3 and Model 4; (3) group 3-big model: Model 5, Model 6, and Model 7. The detailed information about the component count and file size of these models is listed in Figure 19. Model 6 and Model

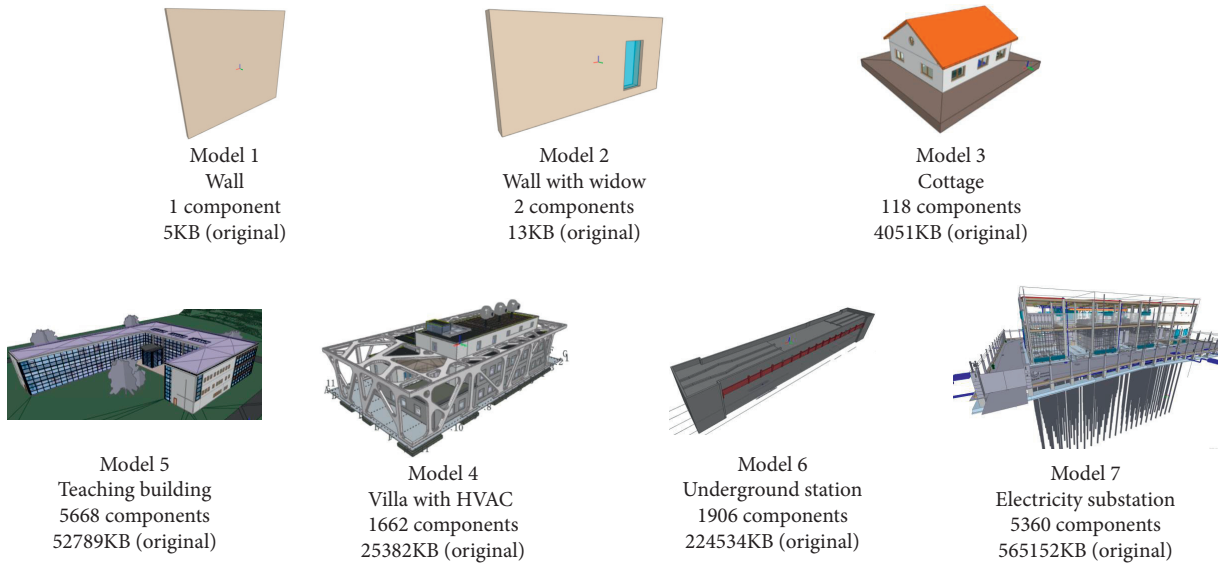


Figure 19: Detailed information of 6 test model cases in IFC-SPF.

7 are real-world infrastructure models that represent HongCaoLu underground station and ZhongChun electricity substation in Shanghai. The two models have involved the architecture and construction sections and the MEP (Mechanical, Electrical, and Plumbing) modeling data; herein, the corresponding IFC-SPF volumes reach 224534 KB and 565152 KB, respectively.

Primary data checks can be run in multiple IFC-SPF editors, including BIMVision (Figure 20). It can be checked whether the component count remains the same, whether components are well positioned or not, and whether the property sets are identical in the property section. It concludes that the redundant data will be eliminated without data loss after executing the proposed procedures.

The duplicate count table of the 3 topmost redundant types for 7 IFC-SPF cases (Table 1) was generated through the comparison before and after the pretreatment process. From this table, it can be found that, in most cases, IfcCartesianPoint is the most redundant type (in Model_7, its rank remains $4^{th}$ with 1145153 duplicates).

Figure 21 illustrates the result of the two procedures on IFC-SPF. It indicates that the process for transforming the original IFC-SPF into the targeted data format with reorganization pretreatment performs remarkably on giant models such as Models 5, 6, and 7. However, there might be some abnormal expansion in tiny models such as Models 1 and 2, which is probably caused by the intrinsic reserved space for each HDF. Fortunately, the number of those tiny models involved in urban-level data management is usually relatively low, so we focus on the performance of giant model data compression and further transmission.

Figure 21 also shows that it is possible to save even more transformation time and storage space due to duplicate removal and instance reordering compared to the previous study. The largest test model reaches 565,152 KB in size with 270,152 KB of the intermediate optimized model and 67,544 KB of the final output HDF. The optimization ratio comes to 88% of the original file and 75% of the optimized file, saving almost 300 MB after data reorganization and almost 500 MB after transformation. Furthermore, since the reverse transformation (from HDF to IFC) has been realized in this research, the resultant HDF can now be treated as the compact variant of IFC for efficient query and other data retrieval processes.

*4.2. For CityJSON.* The following table depicts the sizes of the regular datasets such as "vertices" and "transform" objects depending on JSON (compact version) and HDF, respectively, to testify HDF's efficiency in storing GIS information vividly (the source CityJSON files here originated from [35], and the resultant HDF cost savings can be detected in Table 2).

In this research, the bidirectional conversion of CityJSON and HDF has been accomplished. We verified the new resultant CityJSON files with cjio (a Python CLI to manipulate and validate CityJSON [47]) and got validated with the reversal transformation.

An example of the transformed HDF from CityJSON is demonstrated in Figure 22. This figure expresses almost all details when transforming CityJSON, including forming the basic hierarchical structure, dealing with simple datasets by using attributes, padding the irregular arrays, and deconstructing the object list into "_list_item_#num" subgroups.

So far, since we chose to migrate the whole explicit hierarchy into HDF, although it reserves the original structure, it might cause unpleasant inflation in storage. The redundancy of the original structure can be seen in, for instance, the identical expression for the same kind of city objects, as shown in Figure 22. This kind of hierarchical redundancy will significantly affect the performance of HDF storage. In future work, we consider learning experience from EXPRESS and introduce an object-oriented approach to CityGML/CityJSON to further simplify the expressions of

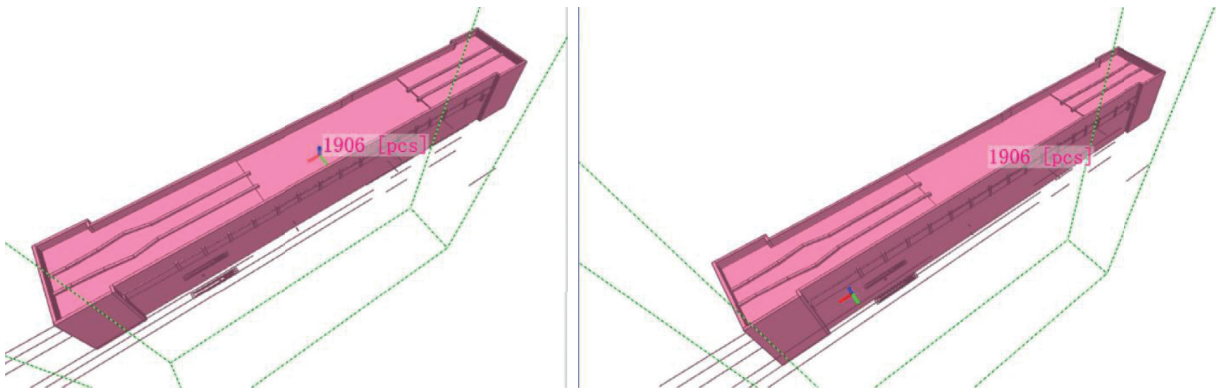


Figure 20: Comparison between original (left) and optimized (right) checked in BIMVision (a free viewer for IFC) (pcs means the count of components here).

Table 1: Partial duplicate count for 7 test IFC-SPFs.

| Model | Original size (KB) | 1st redundant type | Count | 2nd redundant type | Count | 3rd redundant type | Count |
|---|---|---|---|---|---|---|---|
| Model_1 | 5 | IfcCartesianPoint | 6 | IfcDirection | 6 | IfcAxis2Placement3D | 3 |
| Model_2 | 13 | IfcCartesianPoint | 15 | IfcDirection | 11 | IfcPropertySingleValue | 5 |
| Model_3 | 4051 | IfcCartesianPoint | 10160 | IfcPresentationStyleAssignment | 2612 | IfcSurfaceStyle | 2605 |
| Model_4 | 25382 | IfcCartesianPoint | 59628 | IfcPolyLoop | 28444 | IfcFaceOuterBound | 28376 |
| Model_5 | 52789 | IfcCartesianPoint | 9879 | IfcAxis2Placement3D | 7191 | IfcShapeRepresentation | 4992 |
| Model_6 | 224534 | IfcCartesianPoint | 1211164 | IfcAxis2Placement4D | 99665 | IfcShapeRepresentation | 99665 |
| Model_7 | 565152 | IfcPolyLoop | 1289515 | IfcFaceOuterBound | 1286657 | IfcFace | 1286632 |

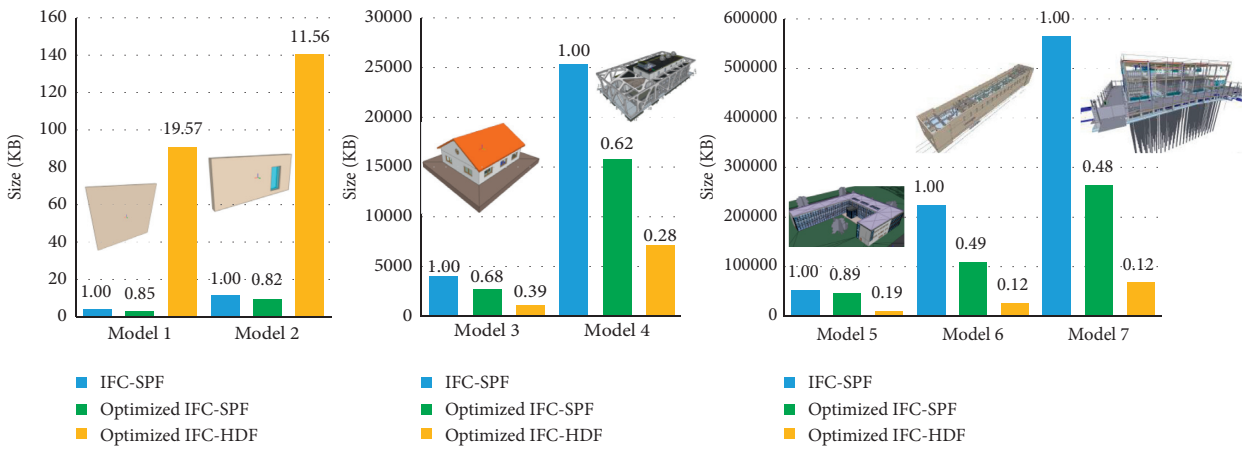


Figure 21: Comparison of the file size of IFC-SPF, optimized IFC-SPF, and IFC-HDF (optimized IFC-SPF means the intermediate IFC-SPF after data reorganization).

particular objects and make full use of HDF compound datasets.

## 5. Discussion

In our perspective, three main capacities of digital twin should be achieved: (1) containing as many city features as possible, (2) synchronizing with its host dynamically through multiple urban data resources, and (3) forming a real-time integrated response to the events. BIM and GIS, as two fundamental technologies of digital twin, aim at exploiting urban data from the micro and macro level. Previous studies have shown that further merging the micro and macro level urban data can bridge the cross-domain data analysis gap. A considerable number of studies have been conducted to integrate BIM and GIS technologies. Much effort was put on extending one original data structure to help embody the other or developing some novel integrated data structures. However, relatively little research focuses on the integrated storage and exchange format itself.

Table 2: Storage cost for vertices and transform objects in JSON and HDF.

| Vertices and transform object* | JSON (KB) | HDF (KB) | Compression ratio |
|---|---|---|---|
| Two buildings | 6 | 12 | 100% |
| 3-20-DELFSHAVEN | 506 | 158 | −69% |
| DenHaag_01 | 541 | 164 | −70% |
| LoD3_Railway | 1378 | 297 | −78% |
| VM05_2009 | 1512 | 368 | −76% |
| Vienna_102081 | 2066 | 485 | −77% |
| DA13_3D_Buildings_Merged | 29125 | 7460 | −74% |
| Zurich_Building_LoD2_V10 | 95239 | 22534 | −76% |

*Here, we compared the performance of the regular data containers which are mentioned in Section 3.1.2.

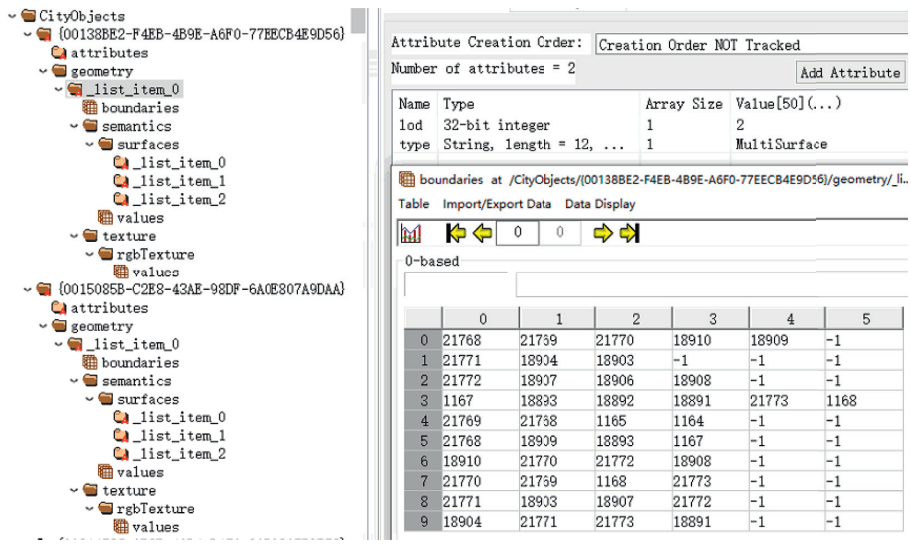


Figure 22: A demonstration of almost all details of the transformed CityJSON in HDF.

To help collect the valuable information from each field for further integral applications, it is also necessary to propose an appropriate scheme which should obtain high efficiency of integration under the premise of little information loss.

Both BIM and GIS have been ameliorating their own open official data standard. This paper analyzed the defects of currently prevalent official data formats when chosen as an alternative media for integration, including text-based, verbose, redundant, storage-challenging, and incomplete. To solve this dilemma, we propose an HDF-based comprehensive scheme of compact, vendor-neutral, and heterogeneity-friendly approach to support the integration of BIM-GIS. The scheme is constituted with three subprocedures: data reorganization, data transformation, and data aggregation.

First, in the data reorganization part, we contribute to proposing the duplicate removal and instance reordering with pure text processing no matter which programming language is chosen (we have succeeded in Python and C#) and which version of IFC schema is followed. It is fruitful to have the original file get slim (51% reduction in Model 6 and 52% reduction in Model 7) and relieve the burden of storage and exchange of detailed structural models in digital twin. Additionally, instance reordering improves the query efficiency through the index map since it is already consistent in identifiers. Moreover, we treat the data in CityJSON as regular, semiregular, and irregular and pretreat them separately to make them prepared for further transformation.

Next, in the data transformation phase, the bidirectional conversion to HDF of all four kinds of data is realized in city information modeling. For IFC-SPF, we add the index map and file metadata of the original IFC in HDF and then back-convert the data from HDF to IFC. Besides, the version-neutral transformation process can be fulfilled without importing a special IFC processor. The transformation efficiency is very satisfactory for IFC since it is EXPRESS-based and object-oriented. The test results show that the largest test model can be first optimized from 565,152 KB into 270,152 KB by data reorganization and finally transformed into 67,544 KB of HDF. For CityJSON, we also propose the bidirectional conversion algorithms with recursion to improve interoperability. All the hierarchical structures of the CityJSON are retained, and the redundancy of hierarchy is, to some extent, harmful for HDF storage since the datasets become small but numerous. For images, we apply the encode and decode process of a standard image. The bidirectional transformation is especially vital to the interoperability, representing the ability to convert the modified HDF (if it happens in further analysis) back into the original file format to make it entirely consistent.

Finally, in the data aggregation phase, a technique route is proposed to establish the semantic relationships between the objects in transformed heterogeneous resources under a project ontology's supervision. In most application scenarios, there is no need for all the related models' information to get analyzed. Populating all the instances from BIM and GIS of an integrated project into a unified urban ontology will induce storage waste. Thus, we consider an HDF-based project repository as the critical base waiting for data extraction to further instantiate only the required data with the target application ontology. By retrieving the relevant data from transformed HDF files, it is possible to further save query and storage costs. In the future, more practical experiments will be conducted to evaluate this phase.

## 6. Conclusion and Future Work

Being processed under the proposed comprehensive data reorganization, data transformation, and data aggregation, the potentially valuable information will be fully restored. The data storage will be saved about 60%–80% for IFC-SPF and 60%–70% for regular CityJSON contents, more for original CityGML files. The effect on semiregular and irregular data in CityGML deserves further research. We believe this light-weight processing and transformation for both data formats might be surprisingly profitable in further integrated BIM-GIS applications.

Until now, although the intrinsic information of both BIM and GIS has been extracted compactly and transformed together in storage and exchange level integration and partially semantic level integration, there are still two issues remained to be solved: (1) the organization of this proposed integrated data structure is still relatively loose and dispersed and (2) the semantic ambiguity of interfields might cause novel redundancy. To help guide the organization of the integrated data structure of BIM-GIS in HDF, in future research, more further efforts will be made to improve our project ontology. Besides, the next step to do is to examine the proposed ontology in more practical scenarios.

Additionally, through this research, it has been found out that the data transformation of CityGML usually takes more effort than that of IFC, which is caused by data regularity. IFC standard is derived from EXPRESS, and the physical file can be easily divided into defined entities. Each instance of a defined entity has the same attribute matrix, making it easier to be transformed into HDF datasets. In future work, we consider absorbing both the original JSON structure and object-oriented approach to simplify the expressions of specific objects in CityGML/CityJSON to achieve more satisfying results when parsing into HDF.

## Data Availability

The data used to support the findings of this study are available from the corresponding author upon request.

## Additional Points

*Highlights*. (i) Proposing an HDF based synthesized scheme towards the practical application of BIM-GIS integration with data reorganization, transformation, and aggregation processes. (ii) Executing efficient data reorganization with redundancy elimination and reordering for original IFC-SPF and CityGML. (iii) Presenting bidirectional and vendor-neutral data transformation methods to embody heterogeneous data formats including model data, images, and analytical datasets in urban projects. (iv) Delivering a compact representation for BIM-GIS integrated information based on HDF.

## Conflicts of Interest

The authors declare that they have no conflicts of interest.

## Acknowledgments

The research project presented in this paper was supported by Shanghai Science and Technology Innovation Plan (15DZ1203403) provided by Science and Technology Commission of Shanghai Municipality 15DZ1203403 and the Research Plan of Multidimensional Information Model System in Power Transmission and Transformation Engineering provided by State Grid Corporation of China.

## References

[1] H. Wang, Y. Pan, and X. Luo, "Integration of BIM and GIS in sustainable built environment: a review and bibliometric analysis," *Automation in Construction*, vol. 103, pp. 41–52, 2019.

[2] A. Borrmann, T. H. Kolbe, A. Donaubauer, H. Steuer, J. R. Jubierre, and M. Flurl, "Multi-scale geometric-semantic modeling of shield tunnels for GIS and BIM applications," *Computer-Aided Civil and Infrastructure Engineering*, vol. 30, no. 4, pp. 263–281, 2015.

[3] M. Wang, Y. Deng, J. Won, and J. C. P. Cheng, "An integrated underground utility management and decision support based on BIM and GIS," *Automation in Construction*, vol. 107, Article ID 102931, 2019.

[4] E. P. Karan, J. Irizarry, and J. Haymaker, "BIM and GIS integration and interoperability based on semantic web technology," *Journal of Computing in Civil Engineering*, vol. 30, no. 3, Article ID 04015043, 2015.

[5] C. Kuster, J.-L. Hippolyte, and Y. Rezgui, "The UDSA ontology: an ontology to support real time urban sustainability assessment," *Advances in Engineering Software*, vol. 140, Article ID 102731, 2020.

[6] W. Shi, J. Cao, Q. Zhang, Y. Li, and L. Xu, "Edge computing: Vision and challenges," *IEEE Internet of Things Journal*, vol. 3, no. 5, pp. 637–646, 2016.

[7] J. Ninić, C. Koch, and J. Stascheit, "An integrated platform for design and numerical analysis of shield tunnelling processes on different levels of detail," *Advances in Engineering Software*, vol. 112, pp. 165–179, 2017.

[8] J. Zhu, X. Wang, P. Wang, Z. Wu, and M. J. Kim, "Integration of BIM and GIS: geometry from IFC to shapefile using open-

source technology," *Automation in Construction*, vol. 102, pp. 105–119, 2019.

[9] J. Zhu, X. Wang, M. Chen, P. Wu, and M. J. Kim, "Integration of BIM and GIS: IFC geometry transformation to shapefile using enhanced open-source approach," *Automation in Construction*, vol. 106, Article ID 102859, 2019.

[10] A. A. Diakite and S. Zlatanova, "Automatic geo-referencing of BIM in GIS environments using building footprints," *Computers, Environment and Urban Systems*, vol. 80, Article ID 101453, 2020.

[11] T. W. Kang and C. H. Hong, "A study on software architecture for effective BIM/GIS-based facility management data integration," *Automation in Construction*, vol. 54, pp. 25–38, 2015.

[12] Z. Xu, L. Zhang, H. Li, Y.-H. Lin, and S. Yin, "Combining IFC and 3D tiles to create 3D visualization for building information modeling," *Automation in Construction*, vol. 109, Article ID 102995, 2020.

[13] A. Rafiee, E. Dias, S. Fruijtier, and H. Scholten, "From BIM to geo-analysis: view coverage and shadow analysis by BIM/GIS integration," *Procedia Environmental Sciences*, vol. 22, pp. 397–402, 2014.

[14] H. Ledoux, K. A. Ohori, K. Kumar, B. Dukai, A. Labetski, and S. Vitalis, "CityJSON: a compact and easy-to-use encoding of the CityGML data model," *Open Geospatial Data, Software and Standards*, vol. 4, no. 1, p. 4, 2019.

[15] Y. Deng, J. C. P. Cheng, and C. Anumba, "Mapping between BIM and 3D GIS in different levels of detail using schema mediation and instance comparison," *Automation in Construction*, vol. 67, pp. 1–21, 2016.

[16] "OGC Hierarchical Data Format Version 5 (HDF5®) Standard | OGC," 2020, https://www.opengeospatial.org/standards/HDF5.

[17] V. Zverovich, L. Mahdjoubi, P. Boguslawski, F. Fadli, and H. Barki, "Emergency response in complex buildings: automated selection of safest and balanced routes," *Computer-Aided Civil and Infrastructure Engineering*, vol. 31, no. 8, pp. 617–632, 2016.

[18] "Data Serialization – the Hitchhiker's Guide to Python," 2020, https://docs.python-guide.org/scenarios/serialization.

[19] K. Afsari, C. M. Eastman, and D. Castro-Lacouture, "JavaScript Object Notation (JSON) data serialization for IFC schema in web-based BIM data exchange," *Automation in Construction*, vol. 77, pp. 24–51, 2017.

[20] P. Pauwels and W. Terkaj, "EXPRESS to OWL for construction industry: towards a recommendable and usable ifcOWL ontology," *Automation in Construction*, vol. 63, pp. 100–133, 2016.

[21] O. Rübel, A. Greiner, S. Cholia et al., "OpenMSI: a high-performance web-based platform for mass spectrometry imaging," *Analytical Chemistry*, vol. 85, no. 21, pp. 10354–10361, 2013.

[22] "IFC formats – buildingSMART technical," 2020, https://technical.buildingsmart.org/%20standards/ifc/ifc-formats/.

[23] "IFC schema specification – buildingSMART technical," 2020, https://technical.buildingsmart.org/standards/ifc/ifc-schema-specifications/.

[24] "CityGML | OGC," 2020, https://www.opengeospatial.org/standards/citygml.

[25] Z.-Z. Hu, S. Yuan, C. Benghi et al., "Geometric optimization of building information models in MEP projects: algorithms and techniques for improving storage, transmission and display," *Automation in Construction*, vol. 107, Article ID 102941, 2019.

[26] G. Lee, C. M. Eastman, and R. Sacks, "Eliciting information for product modeling using process modeling," *Data & Knowledge Engineering*, vol. 62, no. 2, pp. 292–307, 2007.

[27] T. Krijnen and J. Beetz, "A SPARQL query engine for binary-formatted IFC building models," *Automation in Construction*, vol. 95, pp. 46–63, 2018.

[28] M. Theiler and K. Smarsly, "IFC Monitor - an IFC schema extension for modeling structural health monitoring systems," *Advanced Engineering Informatics*, vol. 37, pp. 54–65, 2018.

[29] T. Krijnen and J. Beetz, "An IFC schema extension and binary serialization format to efficiently integrate point cloud data into building models," *Advanced Engineering Informatics*, vol. 33, pp. 473–490, 2017.

[30] A. Jaly-Zada, C. Koch, and W. Tizani, "IFC extension for design change management," in *Proceedings of the 32nd CIB W78 Conference*, Eindhoven, The Netherlands, October 2015.

[31] "HDF5 documentation," 2020, https://portal.hdfgroup.org/display/HDF5/HDF5.

[32] T. F. Krijnen, *Efficient Storage and Retrieval of Detailed Building Models: Multi-Disciplinary and Long-Term Use of Geometric and Semantic Construction Information Eindhoven*, Technische Universiteit Eindhoven, Eindhoven, Netherlands, 2019.

[33] W. Duane, D. Livingstone, and D. Kidd, "Integrating environmental models with GIS: an object-oriented approach utilising a hierarchical data format (HDF) data repository," *Transactions in GIS*, vol. 4, no. 3, pp. 263–280, 2000.

[34] T. F. Krijnen, J. Beetz, S. Ochmann, R. Vock, and R. Wessel, "Towards extending IFC with point cloud data," in *Proceedings of the 22nd EG-ICE Workshop*, pp. 13–15, Eindhoven, The Netherlands, June 2015.

[35] H. – CityJSON, https://www.cityjson.org/, 2020.

[36] G.-K. Mbogo, S. V. Rakitin, and A. Visheratin, "High-performance meteorological data processing framework for real-time analysis and visualization," *Procedia Computer Science*, vol. 119, pp. 334–340, 2017.

[37] C. Vitolo, Y. Elkhatib, D. Reusser, C. J. A. Macleod, and W. Buytaert, "Web technologies for environmental big data," *Environmental Modelling & Software*, vol. 63, pp. 185–198, 2015.

[38] Y. Chen, F. Wang, S. Li, B. J. Xiao, and F. Yang, "The implementation of a data acquisition and service system based on HDF5," *Fusion Engineering and Design*, vol. 112, pp. 975–978, 2016.

[39] V. Nandigam, K. Lin, M. Phan, A. Borsa, S. J. S. Khalsa, and C. Crosby, "Rapid access and visualization of Spaceborne Altimetry data from ICESat and ICESat-2," in *Proceedings of the IGARSS 2018-2018 IEEE International Geoscience and Remote Sensing Symposium*, pp. 5270–5273, Valencia, Spain, July 2018.

[40] K. Ackermann and S. D. Angus, "A resource efficient big data analysis method for the social sciences: the case of global IP activity," *Procedia Computer Science*, vol. 29, pp. 2360–2369, 2014.

[41] ISO 10303-21, *Industrial Automation Systems and Integration—Product Data Representation and Exchange—Part 21: Implementation Methods: Clear Text Encoding of the Exchange Structure*, International Organization for Standardization, Geneva, Switzerland, 2002, https://www.iso.org/standard/33713.html.

[42] O. B. J. Wavefront, "Summary from the encyclopedia of graphics file formats," 2020, http://www.fileformat.info/format/wavefrontobj/egff.htm.

[43] "citygml4j/citygml-tools: collection of tools for processing citygml files," 2020, https://github.com/citygml4j/citygml-tools.
[44] ISO/TS10303-26:2011 Industrial automation systems-Product data representation and exchange-Part 26: Implementation methods: Binary representation of EXPRESS-driven data, https://www.iso.org/standard/50029.html.
[45] D. Yang and C. M. Eastman, "A rule-based subset generation method for product data models," *Computer-Aided Civil and Infrastructure Engineering*, vol. 22, no. 2, pp. 133–148, 2007.
[46] OpenCV, 2020, https://opencv.org/.
[47] CityJSON/io, "Python CLI to process and manipulate cityjson files," 2020, https://github.com/cityjson/cjio.

Hindawi
Advances in Civil Engineering
Volume 2020, Article ID 8824135, 21 pages
https://doi.org/10.1155/2020/8824135

*Research Article*

# Prediction of Highway Tunnel Pavement Performance Based on Digital Twin and Multiple Time Series Stacking

**Gang Yu**,[1,2] **Shuang Zhang**,[1,2] **Min Hu**,[1,2] **and Y. Ken Wang**[3]

[1]*SILC Business School, Shanghai University, Shanghai 201800, China*
[2]*SHU-SUCG Research Centre for Building Industrialization, Shanghai University, Shanghai 200072, China*
[3]*Computer Information Systems and Technology, University of Pittsburgh, Pittsburgh 15260, PA, USA*

Correspondence should be addressed to Shuang Zhang; zs_melodie@shu.edu.cn

Received 6 August 2020; Revised 3 November 2020; Accepted 10 November 2020; Published 4 December 2020

Academic Editor: Jia-Rui Lin

Copyright © 2020 Gang Yu et al. This is an open access article distributed under the Creative Commons Attribution License, which permits unrestricted use, distribution, and reproduction in any medium, provided the original work is properly cited.

The existing pavement performance prediction methods are limited to single-factor predictions, which often face the challenges of high cost, low efficiency, and poor accuracy. It is difficult to simultaneously solve the temporal, spatial, and exogenous dependencies between pavement performance data and maintenance, the service life of highways, the environment, and other factors. Digital twin technology based on the building information modeling (BIM) model, combined with machine learning, puts forward a new perspective and method for the accurate and timely prediction of pavement performance. In this paper, we propose a highway tunnel pavement performance prediction approach based on a digital twin and multiple time series stacking (MTSS). This paper (1) establishes an MTSS prediction model with heterogeneous stacking of eXtreme gradient boosting (XGBoost), the artificial neural network (ANN), random forest (RF), ridge regression, and support vector regression (SVR) component learners after exploratory data analysis (EDA); (2) proposes a method based on multiple time series feature extraction to accurately predict the pavement performance change trend, using the highway segment as the minimum computing unit and considering multiple factors; (3) uses grid search with the *k*-fold cross validation method to optimize hyperparameters to ensure the robustness, stability, and generalization ability of the prediction model; and (4) constructs a digital twin for pavement performance prediction to realize the real-time dynamic evolution of prediction. The method proposed in this study is applied in the life cycle management of the Dalian highway-crossing tunnel in Shanghai, China. A dataset covering 2010–2019 is collected for real-time prediction of the pavement performance. The prediction accuracy evaluation shows that the mean absolute error (MAE) is 0.1314, the root mean squared error (RMSE) is 0.0386, the mean absolute percentage error (MAPE) is 5.10%, and the accuracy is 94.90%. Its overall performance is better than a single model. The results verify that the prediction method based on digital twin and MTSS is feasible and effective in the highway tunnel pavement performance prediction.

## 1. Introduction

In early 2020, China proposed a plan to accelerate the modernization of urban governance with advanced application of technologies, such as the Internet, big data, and artificial intelligence to support the transformation and upgrading of traditional infrastructures, and merge into innovatively infrastructures, such as intelligent transportation infrastructures. According to government statistics, as of the end of 2019, the summed length of highway tunnels of China reached 18.9666 million meters. To comprehensively improve the management level of urban highway tunnels, academia and industry are paying great attention to the life cycle management of urban highway tunnels based on digital twins. A digital twin, proposed by Michael Grieves in 2002, is a mapping relationship between the physical space and virtual space and is intelligent. It maps, records, simulates, predicts, and manages the running track of the life cycle of objects in the physical world and digital virtual space. The life cycle management of urban highway tunnels emphasizes the transformation from traditional corrective maintenance to data-driven preventive maintenance, in which the accurate and timely prediction of highway pavement performance plays a crucial role.

There are two types of research methods in the field of pavement performance prediction. One type is based on traditional statistical models, and the other type is derived from modern machine learning models. Methods based on traditional statistical models are relatively extensive, including deterministic methods such as mechanical prediction models and mechanical-empirical prediction models [1–6], as well as probabilistic methods such as Markov probability models and Bayesian probability models [7–10]. The deterministic model is based on empirical classification, mechanical analysis, or mechanism analysis to predict the pavement performance. Eghbalpoor [1] et al. proposed a three-dimensional finite element model of asphalt pavement to study the damage to the pavement caused by high cyclic loads and their healing effect. Zhang [2] et al. proposed a research method based on morphological dynamics to predict the temperature stress change trend of long-term aging asphalt pavement materials. Shirzad [4] et al. explored the influence of the asphalt mixture ratio on pavement performance and established a mechanical experience model to predict rutting. The probabilistic model is an empirical model dominated by a large amount of measured data. Bianchini [8] et al. proposed an IF-THEN fuzzy neural inference model to predict pavement performance. Li [11] et al. used the method of *K*-means and type-2 fuzzy set to predict the long-term traffic volume. Chen [7] et al. used a Markov chain Monte Carlo (MCMC) simulation to analyze the failure probability of pavement prevention and treatment. Abed [10] et al. used the Monte Carlo simulation method to predict the change probability of pavement performance. The existing traditional statistical models are limited to single-factor predictions, in which single independent variables can hardly reflect the essence of pavement performance. They usually focus on the statistical inference and interpretability of a small sample under certain hypothesis testing conditions. They usually use a small sample size, mainly to represent the relationship between the data and the result variables and the importance of these relationships, and the calculation accuracy is limited. With the increase in the service life of urban highway tunnels, pavement performance is subjected to long-term coupling effects of loads, maintenance situations, environmental conditions, material properties, and other factors, and the resulting pavement diseases aggravate the uncertainty of the driving comfort and safety of the pavement. The predictive effect of traditional statistical methods is sometimes suboptimal in practical engineering.

Studies have shown that machine learning models are superior to traditional statistical methods, such as curve fitting, exponential smoothing, and the autoregressive moving average methods. The accuracy of prediction can be optimized through feature selection, hyperparameter tuning, and integrated learning technology. Gong [12] et al. developed a random forests regression (RFR) model to predict the international roughness index (IRI) performance of flexible pavement based on long-term historical time series data information of disasters, traffic, gas, and structure. The comparison found that it was significantly better than the regularized linear regression model. Xiao and Nie [13] used the regression model and time series GM (1, 1) to predict pavement performance. The maximum difference between the time series predicted value and the regression model predicted value can be reduced by 1%. Bi [14] et al. proposed a time series algorithm suitable for single-factor distributed version to predict the workload of the next stage. Lintonen and Raty [15] proposed a new self-learning stopping criterion for multivariate time series which is a positive-unlabeled (PU) learning case. Liu [16] et al. improved the accuracy of pavement temperature prediction by using a gradient boosting extreme learning machine (GBELM). Gong [17, 18] considered parameters such as materials, structure, traffic, and environment and successfully developed the Mechanistic-Empirical Pavement Design Guide (MEPDG) deep neural network model and GBM method for pavement rutting prediction, and the accuracy was improved. Hu [19] obtained risk indicators from a neural network prediction model and found that the application of data analysis improved the similarity of the predictive performance of the overall pavement safety level. Wang [20] et al. proposed a training method to automatically determine the parameters of network structure for the deep belief network (DBN) with transfer learning (TL-GDBN). Gao [21] et al. proposed 6 non-BP swarm intelligence search algorithms (BBO, PSO, GA, ACO, ES, and PBOL) for model training and developed a new dendritic neuron model (DNM) that considers nonlinearity. Wang and Kumbasar [22] used two swarm intelligence algorithms (PSO and BBBC) to optimize parameters. The machine learning model provides a new method for effectively dealing with multiple factors, ambiguity, randomness, and other issues. It can consider multiple factors and processes high-dimensional data at the same time. It focuses more on the balance between accuracy and complexity. The training set learns the predictive model, and the testset evaluates and verifies its accuracy. No hypothesis conditions are required. The larger the sample size is, the faster the model converges. The generalization integration framework [23], proposed by Wolpert in 1992, is a serial multilevel learning structure with flexibility and uncertainty that can achieve both bagging integration and boosting integration. Lin [24] et al. proposed a stacking model (SMVP) based on real datasets for predicting changes in public bicycle traffic flow. Compared with the traditional single model, the certainty level is increased by 25.58%. Zhai [25, 26] et al. predicted and analyzed the average daily polyvinyl acetate (PM2.5) concentration in Beijing, China, and developed a stacked ensemble model, including the stacking of LASSO, AdaBoost, XGBoost, the GA-MLP-optimized multilayer perceptron, and the support vector regression model (SVR). The results showed that the stacked combination model had high interpretability. Jiang [27] et al. also proposed a stacked ensemble model, which used RF, ERT, XGBoost, LightGBM, RNN, bidirectional RNN, LSTM, and GRU as basic learners, and used logistic regression as the second-level metalearner. In different application scenarios, the stacked models constructed by researchers such as Li [28], Yang [29], and Feng [30] et al. had good results, suggesting an idea for

establishing stacked models to predict pavement performance in the field of urban highway tunnel pavement performance prediction.

In the field of architecture, engineering, construction (AEC), BIM has proved to be an intelligent and parametric digital modeling method that can support the full life cycle of buildings. Since 2019, researchers have begun to conduct applied research on digital twins in the AEC field based on the BIM model [31, 32]. A digital twin refers to a virtual model that is completely consistent with physical entities in the real world and can simulate an entity's behavior and performance in a real environment in real-time. Digital twin technology has the characteristics of traceability, high integration, real-time, and high precision [33, 34]. In the design phase, digital twins can be used for model design, collision detection, pipeline synthesis, and hardcover design. Lu [35] et al. proposed a semiautomatic digital twin system based on images and CAD drawings, aiming at the time-consuming problem of BIM construction. In the construction phase, digital twins can be used for cost budgeting [36], quality management [37], construction collaboration [38], and schedule management [39]. In the operation and maintenance phase, digital twins can be used for equipment asset management [40], safety and prevention management, building space management, and building environment management. Shim [40, 41] et al. proposed a bridge maintenance program based on the concept of digital twins. The program combines a 3D information model-based maintenance information management system with a digital detection system that uses image processing to enhance the decision-making process in terms of the bridge maintenance process reliability.

Therefore, this paper proposes a tunnel pavement performance prediction method based on a digital twin + MTSS for the life cycle operation and maintenance management of urban highway tunnels. Considering many factors, such as the maintenance condition, the service life of highways, and the environment, along with the actual pavement performance data of urban highway tunnels, this method adopts machine learning methods to improve the prediction accuracy, which is conducive to extending the service life of urban highway tunnel pavement, and provides support for operational management. The remainder of this paper is organized as follows: the second section introduces the digital twin for pavement performance prediction and the MTSS prediction model. The third section applies the proposed method in practical engineering projects and compares it with the single model to evaluate the performance of the MTSS model and verifies the applicability of the method. Finally, the fourth section summarizes the whole paper.

## 2. Theoretical Basis of Regression Models

*2.1. EXtreme Gradient Boosting (XGBoost).* XGBoost is a highly scalable gradient boosted decision tree system. It has the advantages of good robustness and strong scalability. In recent years, it has shown excellent performance in many fields, such as information technology and software engineering [42], environmental science [30], and economics and finance [36]. XGBoost performs a second-order Taylor expansion on the loss function and uses a quadratic function to approximate the loss function. To prevent overfitting, regularization is introduced into the loss function to constrain the number and weight of leaf nodes, balance the complexity of the model, and optimize each iteration until the following equation is minimized [43].

$$L^{(t)} \simeq \sum_{i=1}^{n} \Big[ l\big(y_i, \widehat{y}^{(t-1)}\big) + \partial_{\widehat{y}^{(t-1)}} l\big(y_i, \widehat{y}^{(t-1)}\big) f_t(x_i) + \frac{1}{2} \partial^2_{\widehat{y}^{(t-1)}} l\big(y_i, \widehat{y}^{(t-1)}\big) f_t^2(x_i) \Big] + \Omega(f_t), \tag{1}$$

where $\Omega(f_t) = \gamma T + (1/2)\lambda \|\omega\|^2$, $\sum_{i=1}^{n} l(y_i, \widehat{y}_i)$ is the loss function, $\Omega(f_t)$ is the regularization term, $T$ is the number of leaf nodes, and $\gamma$ and $\lambda$ are the regularization parameters.

*2.2. Gradient Boosting Decision Tree (GBDT).* GBDT is an ensemble method of boosting. It uses the CART decision tree as the basic learner. The GBDT is different from RF that RF can be generated in parallel by the voting method, while GBDT is an ensemble of weight-based weak classifiers, which is the accumulation of the branch results of each tree, and can be generated only serially. Therefore, the GBDT is more concerned with reducing the bias in the training process, while the RF is more concerned with reducing the variance in the training process. At the same time, GBDT has good robustness and high scalability [44].

*2.3. Light Gradient Boosting Machine (LightGBM).* LightGBM is an open-source distributed gradient boosting framework based on the decision tree algorithm developed by the Microsoft Research Asia Distributed Machine Learning Toolkit (DMTK) team [45]. It is an improved decision tree integration model based on GBDT and XGBoost [46]. Two aspects are improved. (1) Gradient-based one-sided sampling (GOSS): GOSS algorithm sorts the gradients. Samples with a large gradient are selected by percentage, and those with a small gradient are randomly selected to optimize the sampling of the training sample set and reduce the sample points when calculating the gradient. (2) Exclusive feature bundling (EFB): mutually exclusive features are bound to reduce the feature dimension when selecting split points. In a data environment with large training samples and high-dimensional features, it exhibits a faster training speed and efficiency, requires lower memory usage, offers better accuracy, can handle larger-scale data, and supports parallel learning.

*2.4. Random Forest (RF).* RF is an ensemble bagging model proposed by Breiman [47] that combines the CART tree and random space method without assuming a prior distribution. Each tree is built by the independent random sampling method. The original data subset is sampled and generated by the bootstrap method, and a random subset of the feature attributes is randomly choosed according to a specific

criterion. The selection of the training set is random, and each training set is independent of the others. Random forests generally perform better than single decision trees because the results of random forests are determined by voting on the results of multiple decision trees. Each decision tree in a random forest has its own result, and the random forest selects the result with the largest number of votes as its final result by counting the results of each decision tree.

*2.5. Linear Regression.* The linear regression method assumes that the relationship between independent variables and target variables is linear. This simplicity often makes linear regression the best choice for small sample analysis and also makes these models relatively easy to interpret and understand, not suitable for too many predictive variables [48].

*2.6. Least Absolute Shrinkage and Selection Operator (LASSO).* The least absolute shrinkage and selection operator (LASSO) is a regression analysis method with strong robustness and a strong generalization ability for simultaneous feature selection and regularization. The $L1$ norm is introduced to generate sparse solutions at the feature level, which will shrink the unimportant coefficients in the parameters to be estimated, so as to reduce redundancy and make the model more stable when processing different data, thus improving the accuracy and robustness of regression prediction [25].

*2.7. Ridge Regression.* Ridge differs from LASSO in terms of regularization items, and Ridge introduces the $L2$ norm. Ridge regularization uses the sum of squares of regression coefficients as a penalty function and compresses regression coefficients, making it difficult to compress the coefficients of redundant predictive variables to 0 and easier to over-compress more important regression coefficients [49].

*2.8. Artificial Neural Network (ANN).* The ANN structure usually consists of three main parts: the input layer, the hidden layer, and the output layer. Each layer is composed of many neurons. The input layer is used to load known parameters and directly determine the output results [25], such as performance index and maintenance type in this study. The hidden layer contains all known information and establishes a nonlinear relationship between the input parameters and the output results. The output layer is used to obtain the unknown prediction result $Y$. As shown in Figure 1, this study has set up 2 hidden layers with 128 neurons in each layer. The selection range of the hidden layers was set as [32, 64, 128], and the nonlinear hyperbolic tangent (tanh) activation function was adopted. The detailed neural network structure diagram is as follows:

*2.9. Support Vector Regression (SVR).* The core principle of the support vector machine regression algorithm SVR is to find a regression plane so as to minimize the overall observation error and maximize deviation [50]. The traditional regression methods consider the prediction correct if and only when the regression fitting function is completely equal to $y$. For example, $(f(x)-y)^2$ is commonly used to calculate the loss in linear regression [51]. However, SVR believes that as long as $f(x)$ deviates from $y$ not too much, the prediction can be considered correct. Instead of calculating losses, the threshold a is set to only calculate the loss of the data point $|f(x)-y|>a$. The SVR model is irrelevant of the dimension of the input space and depends on the number of SVs. The goal of SVR is to solve the following basic problems [25]:

$$\min_{\omega,b,\zeta,\zeta^*} \frac{1}{2}\omega^T\omega + C\sum_{i=1}^{n}(\zeta+\zeta^*)$$
$$\text{s.t.}\begin{cases} y_i - \omega^T\phi(x_i) - b \le \varepsilon + \zeta_i \\ \omega^T\phi(x_i) + b - y_i \le \varepsilon + \zeta_i^* \\ \zeta_i \ge 0, \zeta_i^* \ge 0, \quad i = 1,2,\ldots,n, \end{cases} \tag{2}$$

where $\omega$ and $b$ are used to determine the fitting function $f$, $C$ is the regularization constant, $\zeta_i$ and $\zeta_i^*$ are the relaxation variables to define the up and down deviation.

## 3. Methods

*3.1. Digital Twin for Pavement Performance Prediction.* This paper proposes a digital twin for the pavement performance prediction of urban highway tunnels. It is driven by the continuous and circular flow of information and data from the physical world to the digital world and then to the physical world. It adopts a new method by the deep integration of global perception technology and machine learning to establish the digital mapping between the virtual pavement BIM model and physical highway entity. It realizes data sharing, visual analysis, and the intelligent decision support functions of pavement performance trend changes. The digital twin consists of three key parts (Figure 2). (1) Data collection module: the data include pavement performance, maintenance records, tunnel highway structure, traffic flow, and tunnel environment. The pavement performance data come from pavement performance indicators, such as vehicle-mounted laser sensors and high-precision accelerometers. The maintenance records are stored in the operation and maintenance management system. (2) Prediction module: within the stacking integrated learning framework of the MTSS, a pavement performance prediction model based on multiple differentiated models is established to predict the future performance trend change of each segment of the pavement. (3) Parametric analysis module: in the Dynamo environment, which supports visual parameter design, the multisource spatial-temporal data of the BIM model and physical entities are integrated, and the inheritance relationship between the node components is constructed. A Python application is implemented with RevitAPI to realize the visual evolution of the pavement performance.

Figure 3 shows the learning process of digital twins. First, the pavement performance data of the physical environment

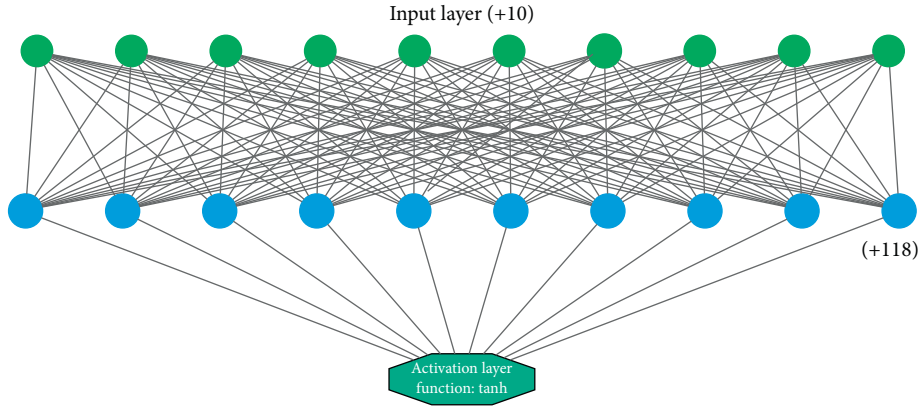


Figure 1: ANN structure diagram.

are collected, and the datasets are divided to build the MTSS prediction model. Then, in the Dynamo environment, the physical pavement entity and the virtual digital BIM model are mapped, the predicted data are synchronized, and the BIM model is assigned. Both the virtual environment and the physical environment contain the bidirectional synchronization process of data acquisition and realization of pavement performance prediction state change [52]. Among them, in the visualization state of pavement performance prediction, the physical pavement entity changes through the digital mapping by using the virtual pavement BIM model. This state change is transferred to the parameter analysis module through the MTSS prediction model. Because the pavement segments may be degraded in the future, the digital twin is used to visualize the decay trend of pavement performance and provide the decision analysis service of the highway tunnel pavement performance prediction and maintenance decision-making by predicting the maintenance timing, analyzing the maintenance cost, and adopting preventive maintenance strategy. The ultimate purpose of all these measures is to extend the life of the highways.

### 3.2. Multiple Time Series Stacking Prediction Model

*3.2.1. Time Series Feature Extraction Based on Multiple Time Series.* Feature extraction is very important for the performance and generalization ability of the model. It is used to trim, transform, and refine the input factors, which can improve the interpretability and prediction accuracy of the prediction model [53]. The feature engineering used in this paper includes temporal feature extraction, feature transformation, feature filtering, and feature standardization and one-hot for feature transformation and model-based method for feature filtering [54]. In the preliminary exploratory data analysis (EDA) of the dataset, it is found that the pavement performance indicators, maintenance information, and environmental information dataset have the basic characteristics of the time series. However, it is difficult to process multiple time series in parallel.

The general feature filtering method filters only by the correlation between a single factor and the dependent variable, while the model-based feature filtering method filters by the comprehensive effect of each factor, which can make full use of the combinative characteristics among factors and retain more useful factors. In view of the rapid increase in the number of features as well as feature extraction of time series information, in order to avoid feature collinearity and decreasing of the prediction accuracy by adding useless information, a model-based feature filtering method was adopted to filter the redundant features according to the 95% cumulative contribution threshold (proportion) of the feature factors. Therefore, this paper proposes a method based on multiple time series feature extraction to construct and enhance features and uses a tree-based model to select potentially important features to improve the accuracy of the model.

The time series feature refers to the information contained in the historical sequence. The traditional regression prediction method uses the feature data of the time section at time $t$ to predict the target value at time $t+1$. This method uses only the data of a single time section. However, although the time series method can make use of the characteristics of historical sequences over a period of time, it applies only to the characteristics of a single series and has a strong restriction on the richness of the features. The multiple time series feature extraction method proposed in this paper combines historical sequence information with multiple factors and simultaneously uses the temporal features of multiple factors as the factor input of the regression model, that is, the factor feature data from time $t-m$ to time $t$ are used to predict the target value at time $t+1$. This feature extraction method can effectively combine the features of multiple heterogeneous factors at the same time. Due to the use of temporal features, the change pattern along the time dimension (such as the curvature) of factors can be fully utilized, which can provide richer and more valuable information for prediction and improve the prediction accuracy.

The temporal feature extraction process is shown in Figure 4, where $T_j$ is the target time series, $T_1 - T_{j-1}$ is the characteristic time series, $Y_t$ is the predicted target scalar value of the corresponding sample at time $t$, and $X_t$ is the factor input of the corresponding sample at time $t$. $X_t$ is a vector composed of $t-k$ to $t-1$ characteristic data extracted from each characteristic time series by $T_1 - T_{j-1}$

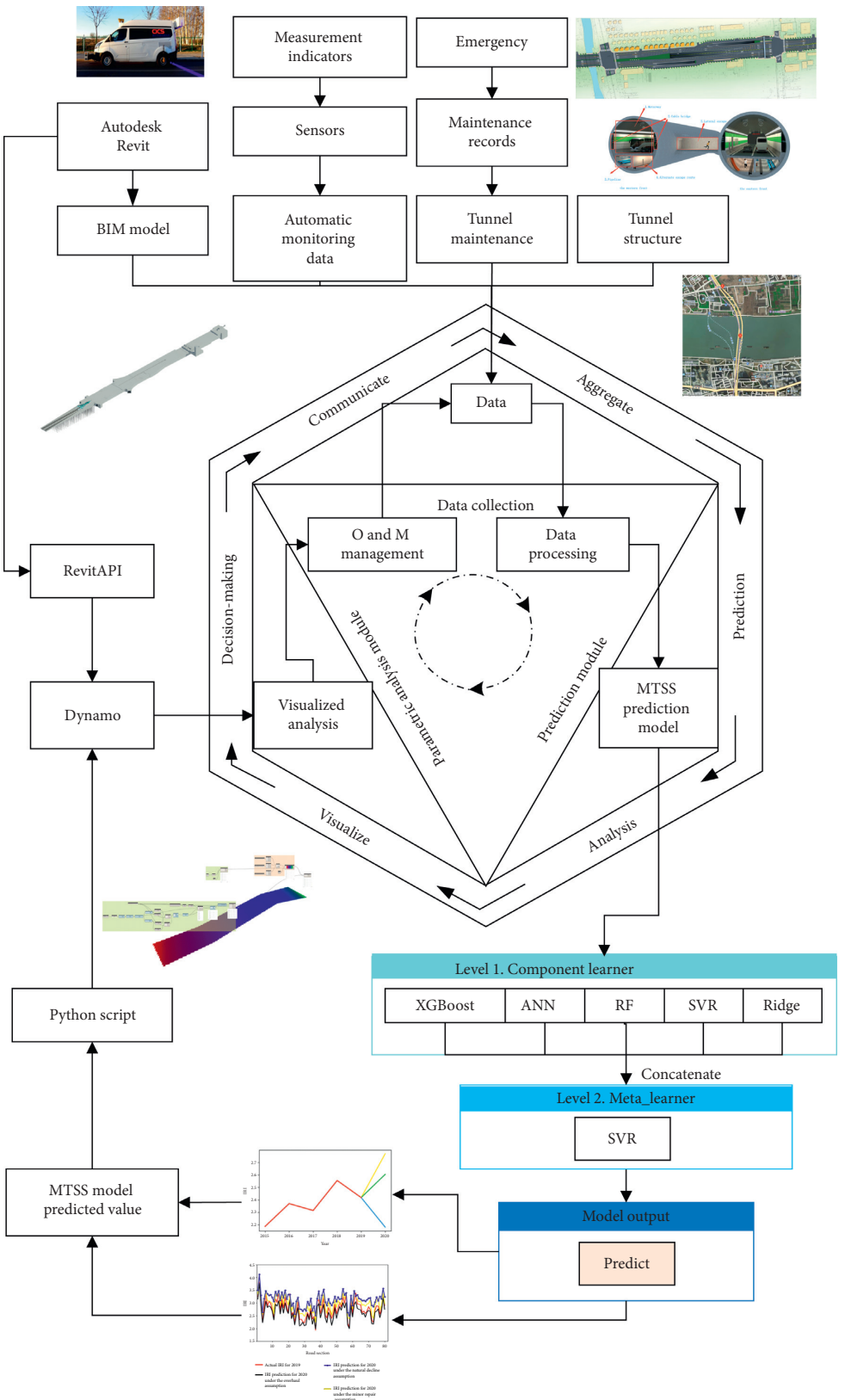


Figure 2: A digital twin for pavement performance prediction.

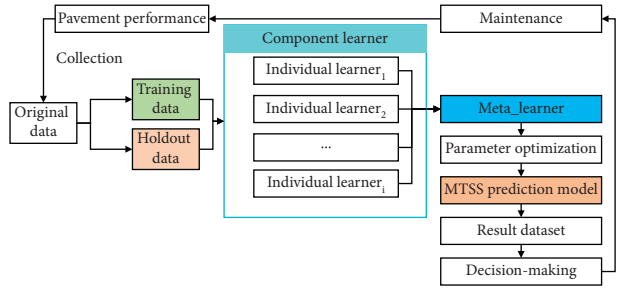


Figure 3: The digital twin learning process.

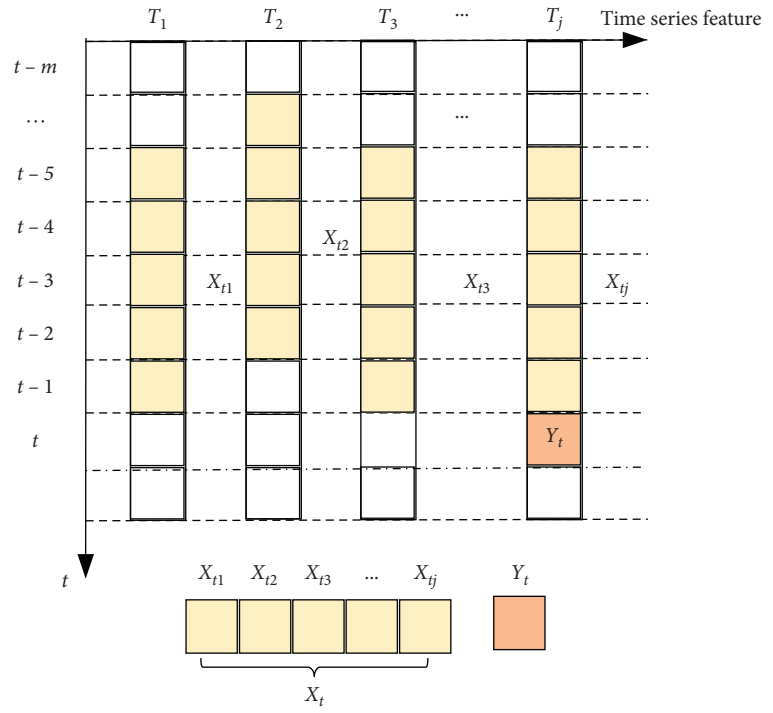


$t$_time, $t = 1, 2, ..., n$

$m$ _the service life of a highway, $m = 1, 2, ..., n$

$T_j$_the $j$ temporal feature, $j = 1, 2, ..., n$

$X_{tj}$_the feature factor of the j temporal feature at $t$

$Y_t$_the predicted value of the pavement performance at $t$

Figure 4: Time series feature extraction.

characteristic time series. The sample $(X_t, Y_t)$ formed by feature extraction constructs the samples of the regression model.

*3.2.2. Filter for Component Learners.* In order to make the stacking learning model achieve the optimal prediction effect and improve the robustness of the model, not only the predictive ability of a single individual learner must be considered but also necessary to consider the combined effects of individual learners. Individual learners with stronger learning ability will help improve the overall predictive effect of the model. In the first level, heterogeneous models with a large degree of difference are selected as the component learners, which can maximize the advantages of various algorithms, and at the same time, each differentiated model can learn from each other's strengths [55]. Therefore, this paper conducted a stacking experiment to optimize the stacking method of the component learners when building the model. A total of 9 individual learners, XGBoost, GBDT, LightGBM, RF, Linear, LASSO, Ridge, ANN, and SVR, are initially selected. The essence of the stacking of different models is to observe data from different data space perspectives and data structure perspectives. Based on this principle, base learners should be different from each other. Therefore, this paper uses the Pearson correlation coefficient

to calculate the differences of each model. By selecting algorithms with large differences, we maximize the advantages of different algorithms and obtain the best prediction effect. Pearson correlation formula is shown as equation (3), where $X$ and $Y$ are two single models' outputs.

$$\rho_{X,Y} = \frac{E(XY) - E(X)E(Y)}{\sqrt{E\left(X^2\right) - (E(X))^2}\sqrt{E\left(Y^2\right) - (E(Y))^2}}. \quad (3)$$

The stronger the learning ability of each individual learner in stacking and the lower the degree of correlation, the better the prediction effect of the stacked model. The threshold value of correlation between component learners is set to be 0.95. Above the threshold, the correlation is stronger, and less than the threshold, the correlation is weak. As shown in Figure 5, XGBoost, ANN, RF, Ridge, and SVR are selected as the first level of component learners, and SVR as the second level of metalearner. XGBoost has a higher correlation with GBDT and LightGBM, which are both trees boosting algorithms. The correlation between XGBoost and RF is relatively low. This is because although RF is also a tree-based integrated class model, it is a bagging type. The correlations between Ridge and LASSO and linear is strong because Ridge and LASSO are both improved versions of linear regression. ANN is quite different from other models, so the correlation is low.

After the filtering of correlation analysis and combination optimization experiment, as shown in Figure 6, this paper selects XGBoost, ANN, RF, Ridge, and SVR as component learners of level 1 and SVR as metalearner of level 2.

*3.2.3. Fusion of the MTSS Prediction Model.* This paper first uses the $k$-fold ($k = 5$) method to train each component learner with the training set and then uses the predicted values from the testset of component learners to train the metalearner. Stacking ensemble learning divides the original dataset $S = \{(X_t, Y_t), t = 1, \ldots, n\}$ into several data subsets, where $X_{tj}$ is the input vector of the sample $t$ with $j_{\text{th}}$ temporal features, $Y_t$ is the corresponding predicted value of the sample $t$, and $N$ is the number of temporal features, that is, each $X_t$ feature vector is $(X_{t1}, X_{t2}, X_{t3}, \ldots, X_{\text{tn}})$. In this paper, the five-fold cross validation method is used. This paper randomly divides the data into five equal size and disjoint subsets $S_1, S_2, S_3, \ldots, S_K$ of the original dataset, where $S_K = S - S_K$ defines $S_K$ and $S_{-K}$ as the $k$-fold training set and testset, respectively. One of them is taken as the testset, and the other four are used as the training set to train the model each time. $\text{MSE}_t$ is calculated based on the testset. Then, the average value is calculated to obtain $\text{CV}_k$:

$$\text{CV}_{(k)} = \frac{1}{k}\sum_{t=1}^{k} \text{MSE}_t. \quad (4)$$

The process of stacking learning is as follows:

Step 1 Divide the original sample data into training data and holdout data and divide the training data into $K$ subsets of basically equal size

Step 2 Uses the $k$-fold cross validation method to train each individual learner on the training data and validate it on the holdout data

Step 3 Repeat step 2 until all the component learners are trained

Step 4 Use the first level output as the input of the second-level metalearner and train the second-level metalearner, namely, the meta-model (SVR)

As shown in Figure 7, the first level prediction algorithm contains $K$ base learners. The training set $S_{-K}$ is trained with the $k_{\text{th}}$ algorithm to obtain the base learner $L_k$. In $k$-fold cross validation, for each sample $X_{tj}$ in the $k$-fold testset $S_K$, the prediction of the base learner $L_k$ is denoted as $Z_{ktj}$. After cross validation, the output data of $K$ base learners form a new data sample $S_{\text{new}} = \{((Z_{1tj}, \ldots, Z_{ktj}), Y_t), t = 1, \ldots, k, j = 1, \ldots, N, k = 1, \ldots, K\}$, which is used as the input data of the second level. Train the metalearner $L_{\text{new}}$ of the second-level prediction model to detect and correct the prediction errors in the first layer learning algorithm. The SVR model in the second level outputs the final prediction results. The stacking learning framework improves the robustness and generalizability of the prediction model by combining the output predictions of multiple models to obtain an improvement in the overall prediction accuracy. In order to prevent overfitting, the training set of the component learner cannot be directly used in the training of the metalearner. It is necessary to divide the original data reasonably.

*3.2.4. Hyperparameter Optimization.* The multilevel stacking learning system involves the setting of many parameters. Nevertheless, the combination of parameters of different values has a greater impact on the prediction accuracy of the model, and unreasonable parameter settings can easily cause underfitting or overfitting of the model. Hyperparameter tuning is an optimization method that can be carried out to preprocess or postprocess any learning algorithm. Grid search can improve the generality of the model. To make the MTSS model perform optimally and prevent underfitting or overfitting, it is necessary to optimize the parameters of each base learner and metalearner. First, the single base learner is predicted and analyzed on the original dataset. The regularization technique is used to avoid overfitting. The $k$-fold cross validation is adopted to divide the dataset into multiple training sets and testsets. The training set is used to construct the model, and the testset is used to evaluate or verify the performance of the model. The structure of the base learner and metalearner algorithm has certain complexity. It is necessary to define many parameters, such as learning_rate, max_depth, and n_estimators. Among the main parameters, learning_rate can control the model weights' updating speed. Max_depth is the maximum depth of a tree. The larger the max_depth is, the more complex the model will be. N_estimators is the number of decision trees. Gamma refers to the complexity penalty term at the level of tree structure. If the value is larger, the number of leaf nodes in the tree will be smaller. Lambda represents the penalty for the output weight of leaf nodes to avoid excessive weight of leaf nodes and

| | ANN | GBDT | LASSO | LightGBM | Linear | RF | Ridge | SVR | XGBoost |
|---|---|---|---|---|---|---|---|---|---|
| ANN | 1.0000 | | | | | | | | |
| GBDT | 0.8703 | 1.0000 | | | | | | | |
| LASSO | 0.9004 | 0.9237 | 1.0000 | | | | | | |
| LightGBM | 0.8804 | 0.9635 | 0.9481 | 1.0000 | | | | | |
| Linear | 0.9011 | 0.9197 | 0.9975 | 0.9443 | 1.0000 | | | | |
| RF | 0.8647 | 0.9439 | 0.9011 | 0.9450 | 0.8972 | 1.0000 | | | |
| Ridge | 0.9070 | 0.9245 | 0.9661 | 0.9353 | 0.9616 | 0.9163 | 1.0000 | | |
| SVR | 0.8623 | 0.8749 | 0.9553 | 0.8908 | 0.9509 | 0.8595 | 0.9337 | 1.0000 | |
| XGBoost | 0.8583 | 0.9515 | 0.9161 | 0.9562 | 0.9126 | 0.9197 | 0.8991 | 0.8576 | 1.0000 |

Figure 5: Correlation analysis.

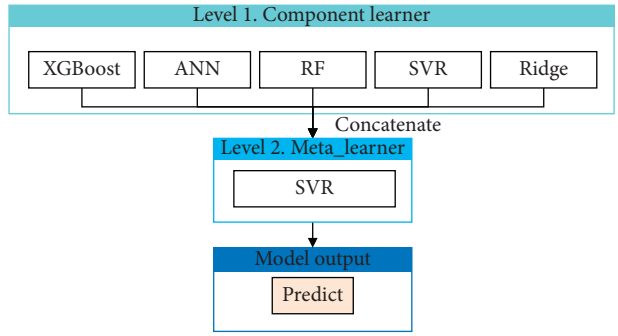


Figure 6: Construction of the integration model.

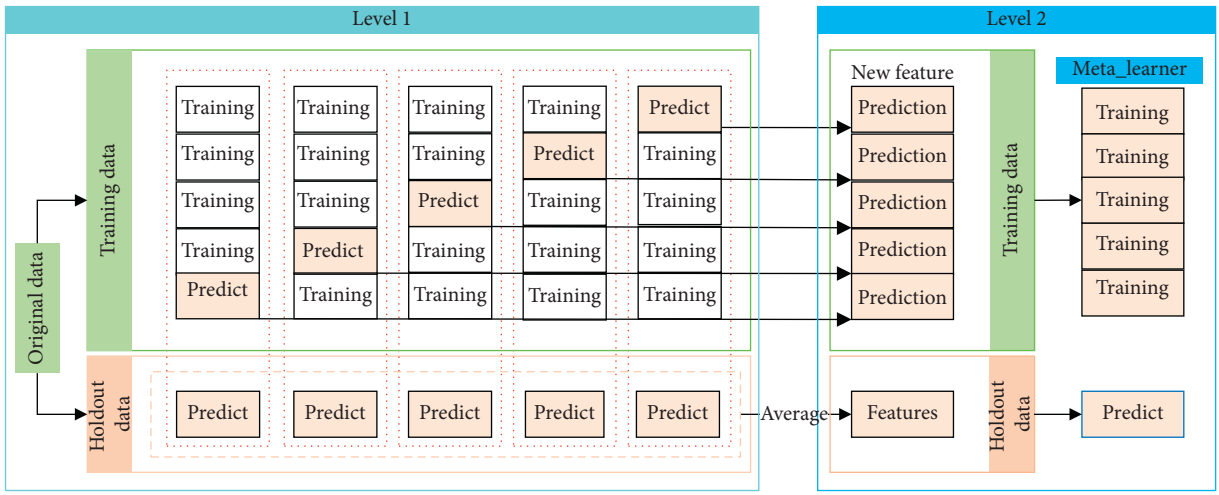


Figure 7: Description of the stacked generalization process.

improve the robustness of the model. The stacking model tuning is different from single model tuning. First, the original sample data are divided into training set and holdout dataset. Second, using the training set, the $k$-fold cross validation is combined with the grid search method to optimize the parameters of each component learner. In this paper, $k$ is set as five, and the training set is divided into five parts, that is, there are five different subtraining sets and subtestsets. For each component learner, five models are generated based on the training of subtraining sets, respectively, and these five models are, respectively, used to predict their corresponding subtestsets. The optimal parameters are selected with the best five models' testset average accuracy. The parameter range of grid search is carried out according to the hyperparameter set of each model in Table 1. Then, based on the training set generated by the first level model, the parameters of the second level model are also optimized by the combination of $k$-fold cross validation and the grid search method. The total stacking model is validated on the validation set generated by the first layer model. Finally, the experimental results show that the parameter tuning method can effectively optimize the parameters of the stacking model, and the prediction effect of the stacking model has been improved. The hyperparameter range of each model algorithm grid search method is shown in Table 1.

*3.3. Parametric Analysis Module.* The parametric analysis module is based on Dynamo's visual programming environment, which associates the physical tunnel entity with the BIM model by constructing the mapping relationship between the components. It realizes the integration of real-time dynamic evolution visualization of pavement performance prediction and data science and provides support for managers' decision-making. The workflow is shown in Figure 8, including six steps: importing the Revit highway BIM model, creating highway segment elements, importing a Python script, importing MTSS highway segment performance prediction results, creating a chromatogram, and visualizing the changing trend of highway segments. First, this paper collects the data information of the 3D BIM model created in Autodesk Revit. Then, we link the MTSS prediction model as a custom node to the Dynamo environment. Finally, the predicted pavement performance trend is displayed in the form of graph visualization to support the decision-making reasoning process.

Step 1 Import the Revit highway BIM model

Dynamo is a lightweight model engine with a series of built-in graphics and bidirectional conversion nodes [56]. In this paper, the four nodes categories, all elements of a category, element geometry, PolyCurve, and ByjoinedCurves, which are wrapped by RevitAPI, are used to realize the component function of importing the highway BIM model into the dynamo engine from Revit.

Step 2 Create highway segment elements

As shown in Figure 8, according to the basic principle of bounding box regression in computer graphics, the bounding box of the highway BIM model in Figure 9(a) is created, and the computational element with the center point of the cube as the minimum (Figure 9(c)) is generated to realize the cut split and create the component function of highway segment elements

Step 3 Import Python script to highway segment elements

The bounding box-generated border range is much larger than the site boundary of the BIM model of the highway surface (Figure 9(b)), and graph screening is more complicated than a numerical screening calculation. Therefore, to improve the efficiency of graphic calculation, this article customizes the Python script and links it to Dynamo by calling the DesignScript library, judging the position of the unit cube according to the projective method and filtering out the unit cubes belonging to the pavement boundary as a highway segment element.

Step 4 Import MTSS highway segment performance prediction results

Through the file. Path node (Figure 8(d)), the dataset of the MTSS model prediction results is imported into Dynamo in the form of an Excel file to provide data support for the visualization of the pavement performance prediction digital twin

Step 5 Create a chromatogram

Create a gradient color chromatogram based on the three primary colors of red, yellow, and blue, map the predicted value to the chromatogram in Figure 10, and display the changes in the performance of the physical image elements of the highway segment through colors to enhance the visualization of the pavement performance

Step 6 Visualize the changing trend of highway segments

Taking each highway segment as a unit, finite element analysis is used to show the future change trend of the current highway segment. The red part indicates that the pavement performance will be reduced, and corresponding maintenance measures need to be taken. The pavement performance trend should be improved. Finally, according to the numerical results of the pavement performance prediction, the future trend of the highway segment is visually displayed in different colors to provide support for maintenance decision-making.

## 4. Case Study

*4.1. Materials.* With a total length of 2500 meters and four lanes in both directions, the Dalian highway tunnel in Shanghai is the first cross-river project in China, which

Table 1: Hyperparameter range of each algorithm.

| Algorithm name | Hyperparameters selected |
|---|---|
| XGBoost | learning_rate = [0.01, 0.1, 0.2]<br>n_estimators = [100, 50]<br>max_depth = [30, 50, 100]<br>Gamma = [0.1, 0.2, 0.5]<br>Subsample = [0.9, 0.5]<br>colsample_btree = [0.9, 0.5] |
| RF | Criterion = [“mse,” “mae”],<br>n_estimators = [10, 100]<br>max_depth = [10, 50, 100]<br>max_features = [0.5, 0.9]<br>min_samples_split = [10]<br>min_samples_leaf = [2, 10] |
| Ridge | Solver = {“auto,” “svd,” “cholesky,” “lsqr,” “sparse_cg,” “sag”} |
| SVR | alpha = [0.1, 1, 10]<br>$C$ = [0.01, 0.1, 1], kernel = [“linear,” “poly,” “rbf,” “sigmoid”] |
| ANN | hindden_cell_num = [32, 64, 128]<br>Activation = [“tanh,” “relu”]<br>Scoring = [ “neg_mean_squared_error” ]<br>Epochs = [300, 100]<br>batch_size = [20, 50] |

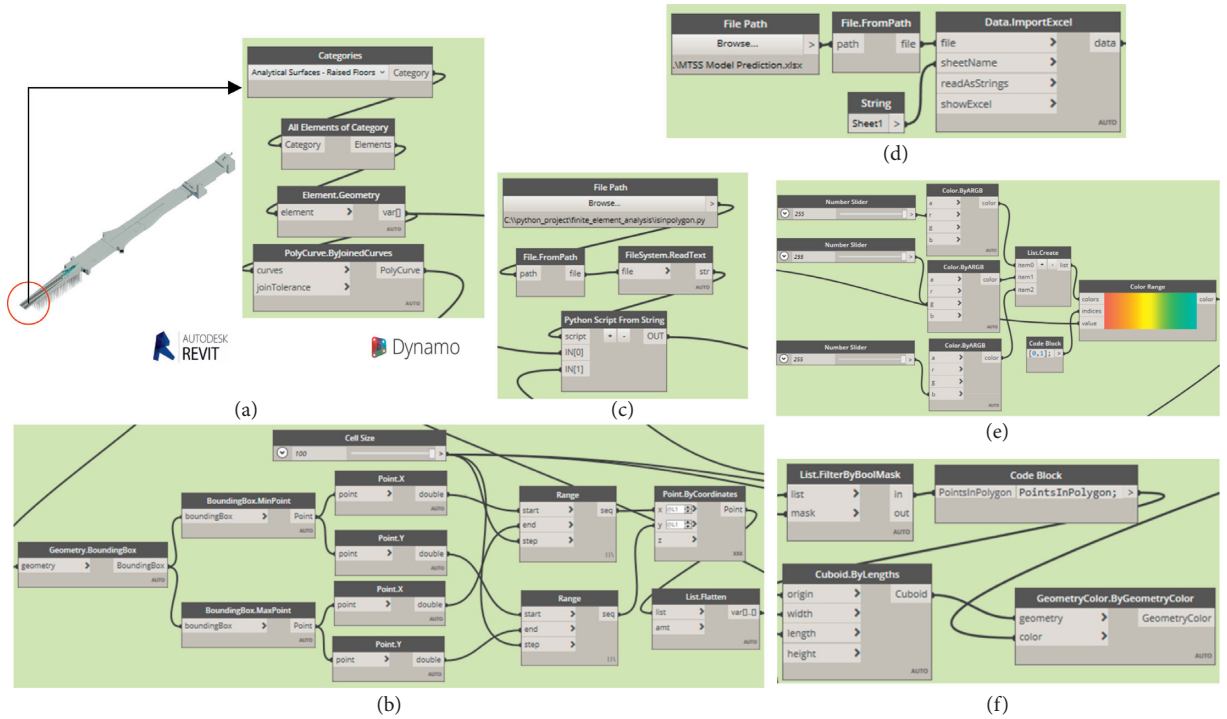


Figure 8: Dynamo’s digital twin workflow. (a) Import the Revit highway BIM model. (b) Create highway segment element. (c) Import Python script. (d) Import MTSS highway segment performance prediction results. (e) Create a chromatogram. (f) Visualize the changing trend of highway segments.

simultaneously adopts two large-scale shields to promote the new technology. This paper uses the historical dataset of the Dalian highway tunnel, including maintenance information and measured IRI data from 2010 to 2019. After data preprocessing, 80% of the dataset is randomly selected as the training set to construct the model, and the other 20% is used as the testset to evaluate and verify the performance of the model. Then, this paper uses the trained model to predict the pavement performance in 2020.

*4.2. Data Processing.* Whereas the maintenance data of the Dalian highway come from the records of special projects and subprojects over the years, the dataset only records

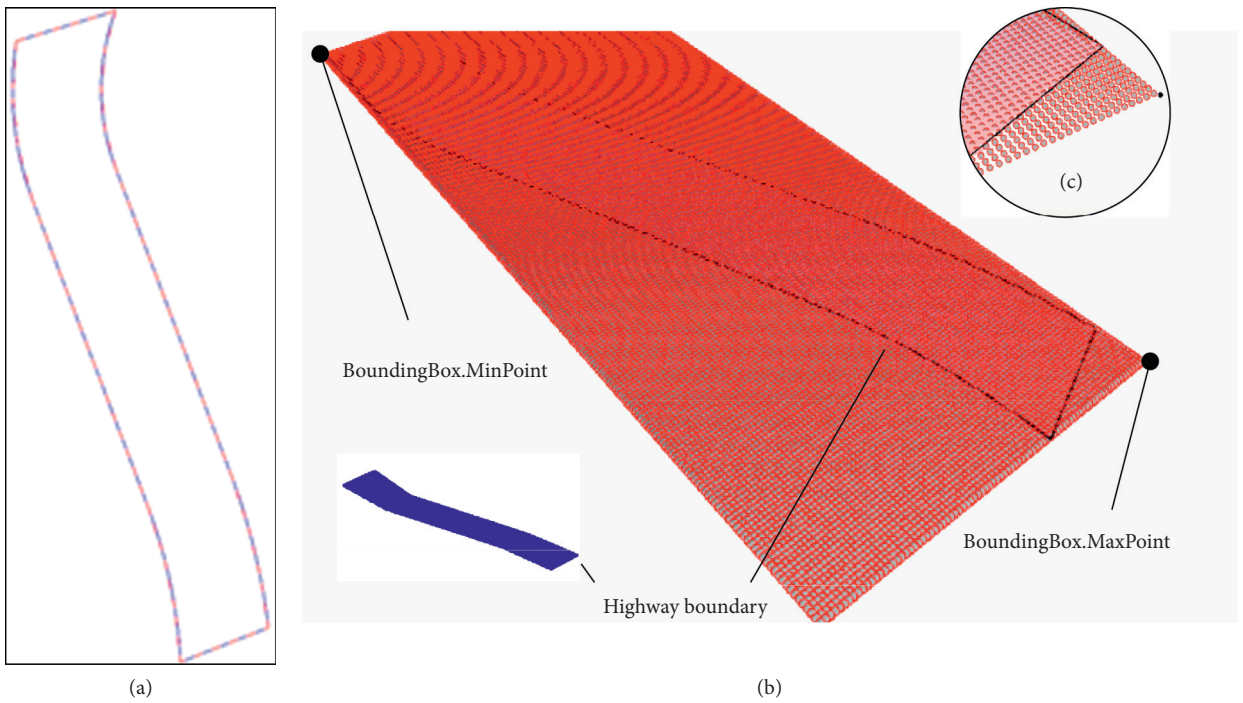


Figure 9: (a) The bounding box of the highway segment element. (b) Instantiate bounding box. (c) Limited cells of highway segments.

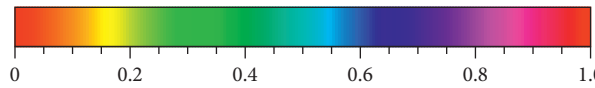


Figure 10: Mapping relationship between pavement performance and chromatography.

information such as east-west lines, fast and slow lanes, and light numbers. There is no direct record of highway segment elements, which does not meet the data requirements of the MTSS prediction model. Therefore, according to the actual tunnel space structure and the light number arrangement rules, this paper maps each maintenance record to the highway segment elements in accordance with the recorded natural decay, minor repair, or overhaul maintenance to solve the problem that the current maintenance record does not satisfy the prediction model to subdivide the highway into segments.

### 4.3. Result of Feature Selection

*4.3.1. Results Based on Temporal Feature Extraction.* The measured data of pavement roughness are affected by factors such as the service life of highways, maintenance level, COVI, traffic volume, and other factors. Among them, the service life of highways, maintenance conditions, and history performance data have the most significant influence on pavement performance prediction. Clearly, the pavement performance prediction is affected by multiple time series, and the measured data have multiple temporal features. The study of Kitaha et al. showed that the performance change was more reliable than the value itself [57]. Therefore, this paper selects IRI $P_{t-m_i}(i = 0, 1, 2, 3, 4, 5)$ of the previous five years as the feature factors describing IRI, defines $M_{t-m_i-q}(i = 1, 5; q =$ natural decay, minor repair, andoverhaul) as the maintenance feature factors, and defines $S_m(m = 0, 1, \ldots, 10)$ as the feature factor of the service life of highways. The extraction process based on the time series features is shown in Figure 11. The results of the extraction are shown in Tables 2-3. The sample is composed of each record $X_t$ and the predicted value $Y_t$ of the pavement performance.

*4.3.2. The Significance of Feature Factors.* To verify the temporal, spatial, and exogenous dependencies between pavement performance data and multiple factors, this paper uses the MTSS model to score $P_{t-m_i}$, $M_{t-m_i-q}$, and $S_m$ multiple feature factors in the year $t$ during the training process. The feature importance score is calculated based on the gain of the number of branches in the tree structure, mainly calculating the sum of the number of occurrences of features in all trees. If the number of occurrences is higher, the characteristic factor is more important. In Figure 12, the feature factors for 2020 are automatically ranked. According to the significance of the feature factors, it is found that the importance of maintenance features in the $t$ year accounts for the largest proportion, that is, the maintenance situation in the predicted year has the greatest impact on pavement performance prediction; $P_{t-1}$, that is, pavement performance changes in the previous year have a greater impact on the

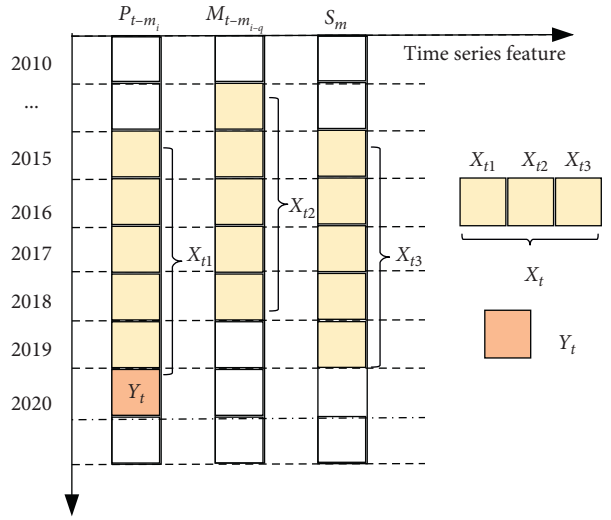


$t$_time, $t$ = 2020, 2019, ... , 2010

$m$_the service life of a highway, $m$ = 1, 2, 3, ... , 10

$T_j$_ the $j$ temporal feature $j$ = 1, 2, ... , $n$

$X_{tj}$–the feature factor of the $j$ temporal feature at $t$

$Y_j$–the predicted value of the pavement performance at $t$

Figure 11: Time series feature extraction of the Dalian highway.

Table 2: Extraction results of time series feature.

| Sample | IRI (m/km) | | | | | Maintenance status | | | | | Year |
|---|---|---|---|---|---|---|---|---|---|---|---|
| | t−5 | t−4 | t−3 | t−2 | t−1 | t−1 | t−2 | t−3 | t−4 | t−5 | |
| 0 | 2.84 | 2.23 | 3.14 | 3.37 | 2.83 | Natural decay | Overhaul | Minor repair | Natural decay | Overhaul | 2015 |
| 1 | 2.23 | 3.14 | 3.37 | 2.83 | 3.56 | Overhaul | Minor repair | Natural decay | Overhaul | Minor repair | 2016 |
| 2 | 3.14 | 3.37 | 2.83 | 3.56 | 3.77 | Minor repair | Natural decay | Overhaul | Minor repair | Natural decay | 2017 |
| 3 | 3.37 | 2.83 | 3.56 | 3.77 | 3.22 | Natural decay | Overhaul | Minor repair | Natural decay | Minor repair | 2018 |
| 4 | 2.83 | 3.56 | 3.77 | 3.22 | 3.20 | Overhaul | Minor repair | Natural decay | Minor repair | Minor repair | 2019 |

Table 3: All $X$ factors after one-hot transformation.

| Factor name | Sample number | | | | |
|---|---|---|---|---|---|
| | 0 | 1 | 2 | 3 | 4 |
| $P_{t-5}$ | 2.84 | 2.23 | 3.14 | 3.37 | 2.83 |
| $P_{t-1}$ | 2.83 | 3.56 | 3.77 | 3.22 | 3.20 |
| $P_{t-3}$ | 3.14 | 3.37 | 2.83 | 3.56 | 3.77 |
| $P_{t-2}$ | 3.37 | 2.83 | 3.56 | 3.77 | 3.22 |
| $P_{t-4}$ | 2.23 | 3.14 | 3.37 | 2.83 | 3.56 |
| $M_{t-1_overhaul}$ | 0 | 1 | 0 | 0 | 1 |
| $M_{t-1_minor\ repair}$ | 0 | 0 | 1 | 0 | 0 |
| $M_{t-1_natural\ decay}$ | 1 | 0 | 0 | 1 | 0 |
| $M_{t-4_overhaul}$ | 0 | 1 | 0 | 0 | 0 |
| $M_{t-4_minor\ repair}$ | 0 | 0 | 1 | 0 | 1 |
| $M_{t-4_natural\ decay}$ | 1 | 0 | 0 | 1 | 0 |
| $M_{t-3_overhaul}$ | 0 | 0 | 1 | 0 | 0 |
| $M_{t-3_minor\ repair}$ | 1 | 0 | 0 | 1 | 0 |
| $M_{t-3_natural\ decay}$ | 0 | 1 | 0 | 0 | 1 |
| $M_{t_overhaul}$ | 1 | 0 | 0 | 0 | 0 |
| $M_{t_minor\ repair}$ | 0 | 1 | 0 | 1 | 1 |
| $M_{t_natural\ decay}$ | 0 | 0 | 1 | 0 | 0 |
| $M_{t-2_overhaul}$ | 1 | 0 | 0 | 1 | 0 |
| $M_{t-2_minor\ repair}$ | 0 | 1 | 0 | 0 | 1 |
| $M_{t-2_natural\ decay}$ | 0 | 0 | 1 | 0 | 0 |

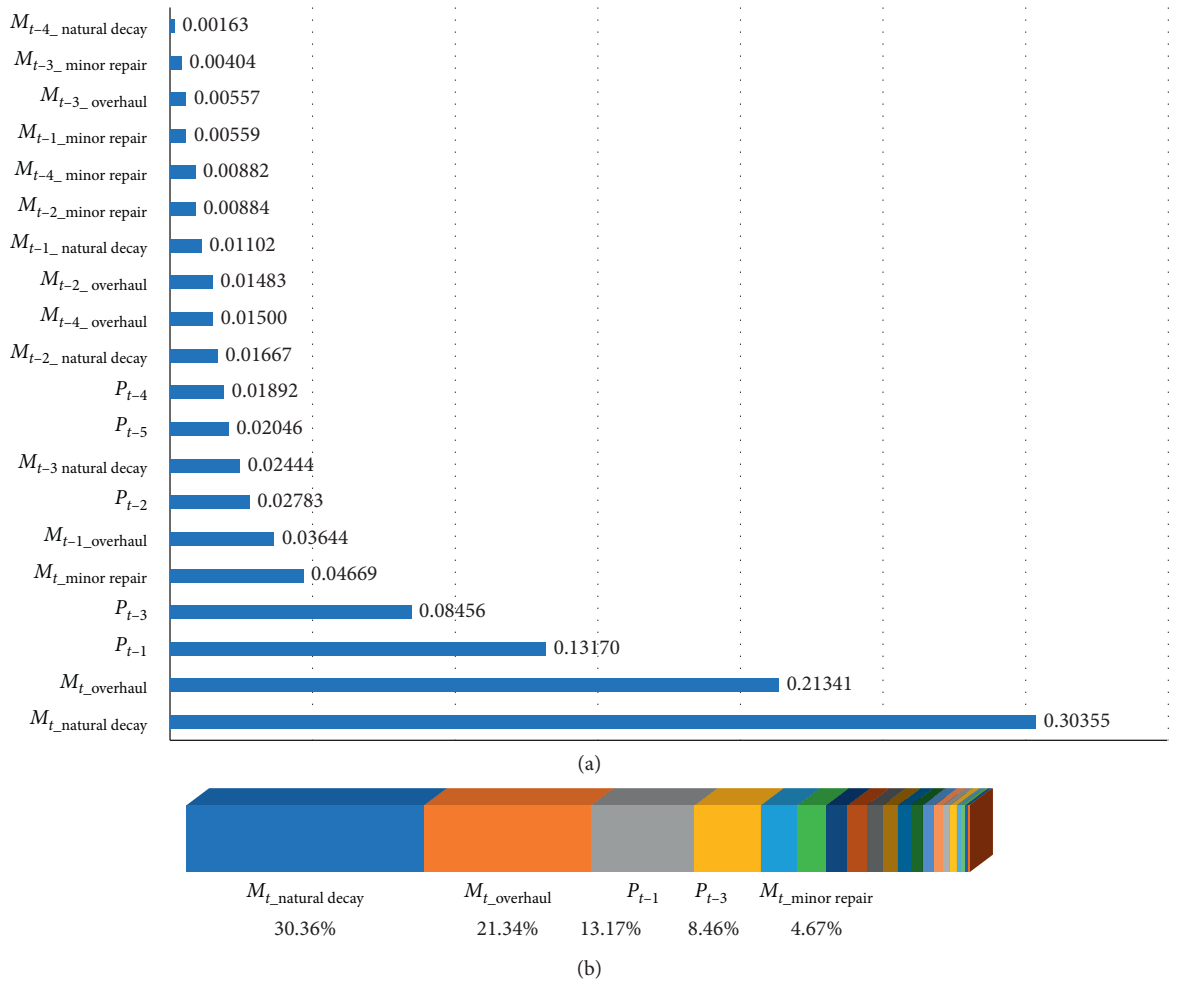


Figure 12: Feature significance.

predicted year; the overhaul has a greater impact on $P_{t-m_i}$ than the minor repair. The closer the $m_i$ value is to zero, the greater the feature importance is of $P_{t-m_i}$. It can be seen that maintenance types have a great impact on pavement performance.

### 4.4. Analysis of MTSS Prediction Model Results

*4.4.1. MTSS Prediction Model Evaluation.* Without the loss of generality, to evaluate the accuracy of the MTSS prediction model, this paper compares the stacking method with a single SVR, Ridge, XGBoost, ANN, and RF machine learning models using the same data to conduct a multicriterion evaluation. MAE and RMSE are standard indicators for model evaluation in machine learning. Their values are often used to directly measure the pros and cons of the prediction model results, and they can also better reflect the degree of deviation of the predicted value from the true value. The lower the value is, the smaller the error and the higher the prediction accuracy. When the outliers have a very large degree of individual deviation, even if the number

Table 4: Prediction error considering time series features.

| Algorithm name | Prediction error | | |
|---|---|---|---|
| | MAE | RMSE | MAPE |
| SVR | 0.1527 | 0.0435 | 5.51% |
| Ridge | 0.1526 | 0.0429 | 5.66% |
| XGBoost | 0.1603 | 0.0491 | 5.75% |
| ANN | 0.1533 | 0.0439 | 5.64% |
| RF | 0.1689 | 0.0514 | 6.52% |
| Stacking | 0.1314 | 0.0386 | 5.10% |

Table 5: Prediction error without considering time series features.

| Algorithm name | Prediction error | | |
|---|---|---|---|
| | MAE | RMSE | MAPE |
| SVR | 0.1815 | 0.0653 | 7.31% |
| Ridge | 0.2033 | 0.0746 | 8.00% |
| XGBoost | 0.1994 | 0.0748 | 7.69% |
| ANN | 0.1937 | 0.0745 | 7.71% |
| RF | 0.1909 | 0.0706 | 7.57% |
| Stacking | 0.1808 | 0.0643 | 7.23% |

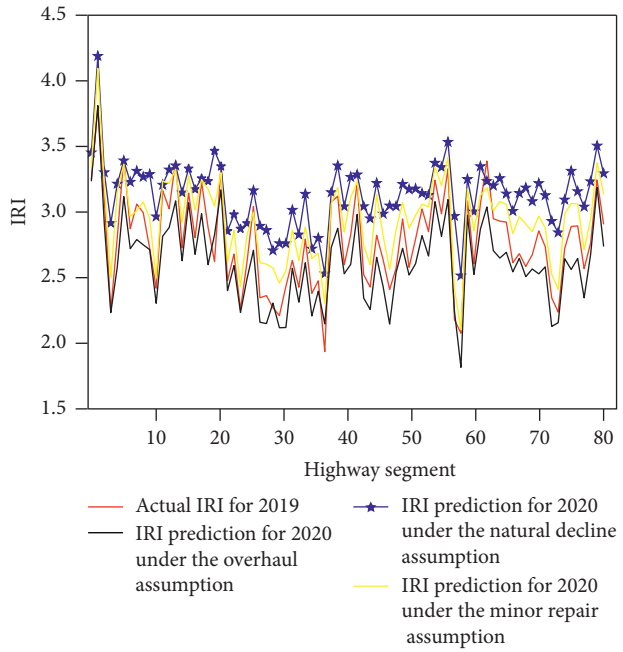


Figure 13: Variation prediction trend of the pavement performance of the Dalian highway in 2020.

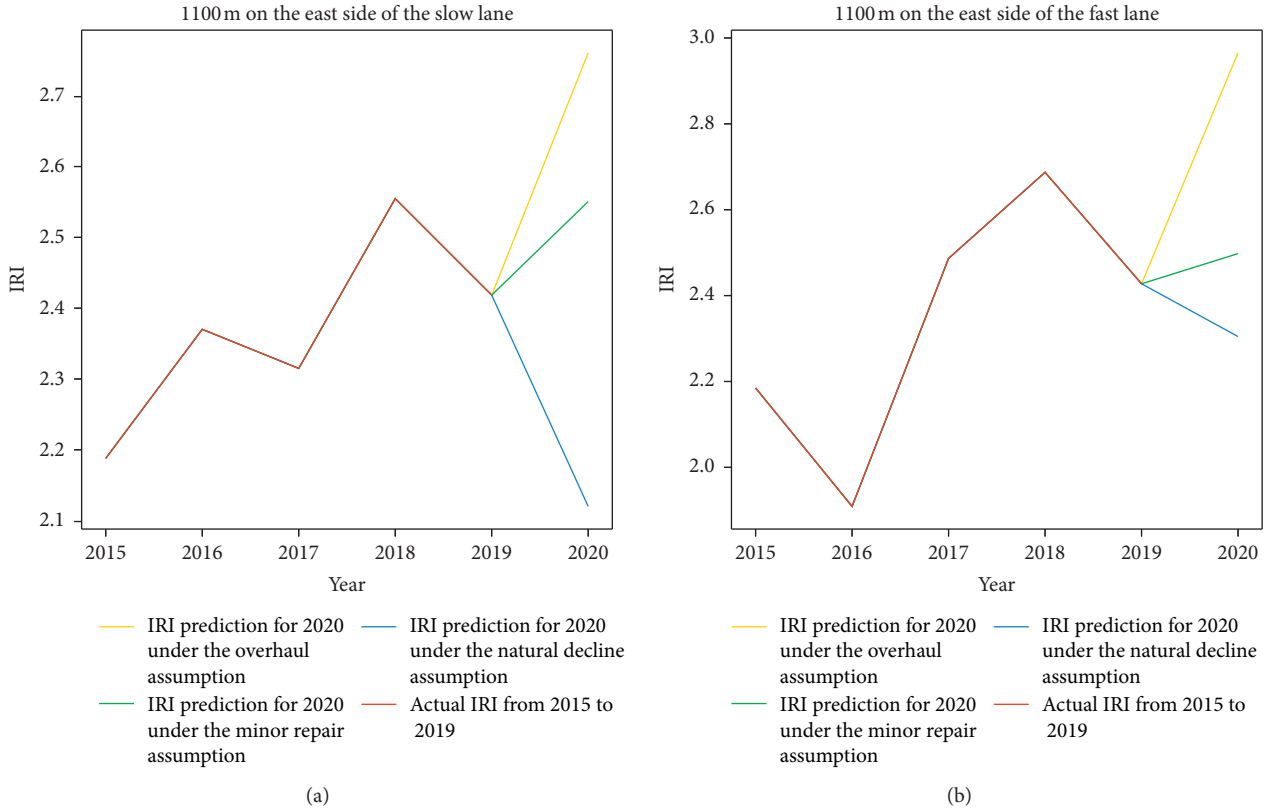


Figure 14: Continued.

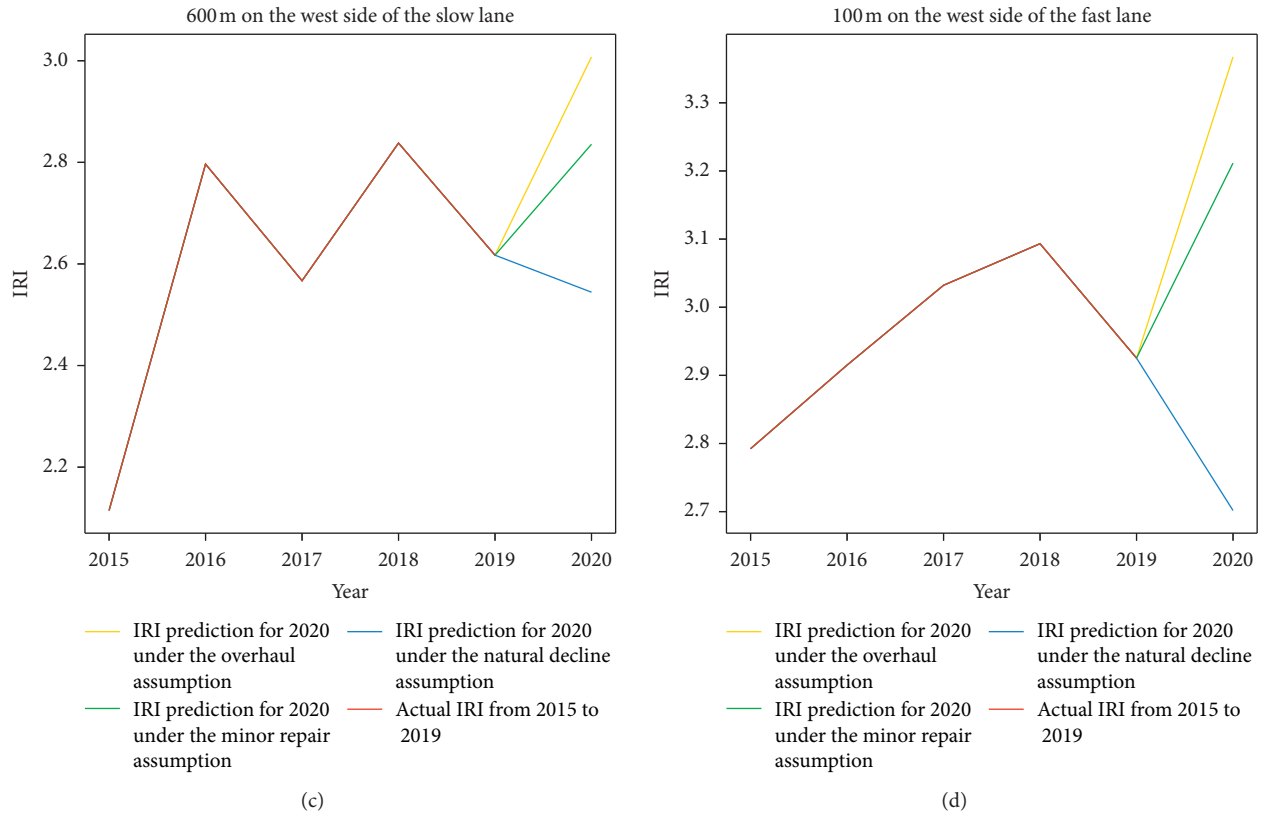


Figure 14: Trend chart of some segments of the pavement performance of the Dalian highway in 2020. (a) 1100 m on the east side of the slow lane. (b) 1100 m on the east side of the fast lane. (c) 600 m on the west side of the slow lane. (d) 600 m on the west side of the fast lane.

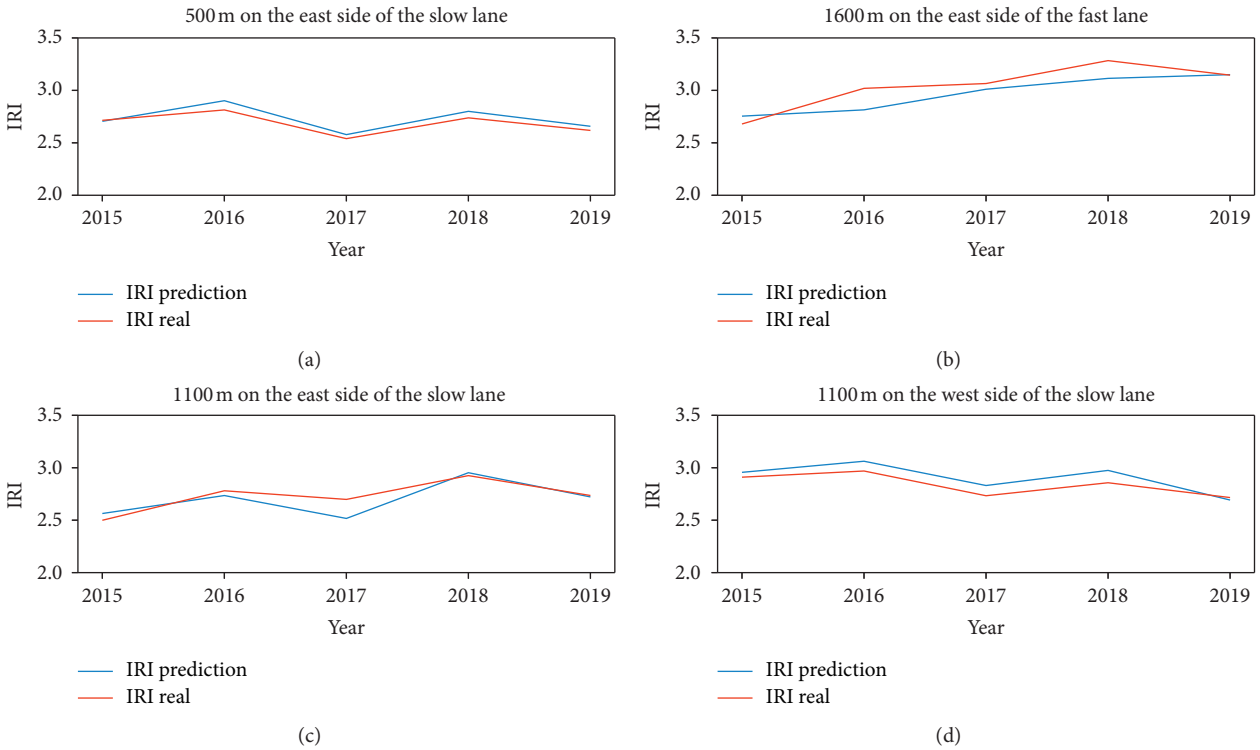


Figure 15: Segment prediction accuracy. (a) 500 m on the east side of the slow lane. (b) 1600 m on the east side of the fast lane. (c) 1100 m on the west side of the slow lane. (d) 1100 m on the west side of the slow lane.

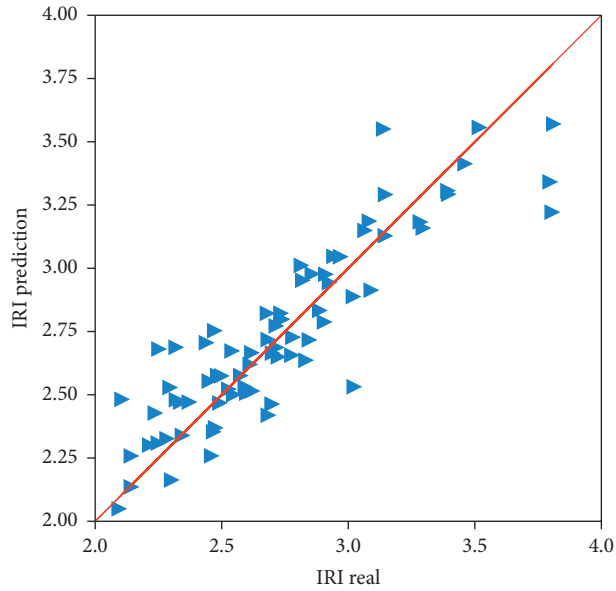


Figure 16: MTSS model prediction and actual error map.

Table 6: Pavement performance evaluation criteria.

| The evaluation indicator | Superior (A) | Good (B) | Qualified (C) | Unqualified (D) |
|---|---|---|---|---|
| Expressway | ≤2.6 | > 2.6, ≤4.1 | > 4.1, ≤7.3 | > 7.3 |
| Primary and secondary arterial highways | ≤4.1 | > 4.1, ≤5.7 | > 5.7, ≤7.8 | > 7.8 |
| Branch pavement | ≤4.6 | > 4.6, ≤6.6 | > 6.6, ≤8.3 | > 8.3 |

of outliers is small, the performance of the standard indicators will deteriorate. Therefore, this paper also adds an MAPE indicator to solve the problem of the robustness of the evaluation indicator by replacing the average with the quantile of the error. Suppose $y_i$ is the true value of sample $i$, $\hat{y}_i$ is the predicted value of sample $i$, and $n$ is the number of samples, the evaluation index is defined as

$$\begin{aligned} \text{MAE} &= \frac{1}{n}\sum_{i=1}^{n}\left|y_i - \hat{y}_i\right|, \\ \text{RMSE} &= \sqrt{\frac{1}{n}\sum_{i=1}^{n}\left(\hat{y}_i - y_i\right)^2}, \\ \text{MAPE} &= \frac{1}{n}\sum_{i=1}^{n}\left|\frac{\hat{y}_i - y_i}{\hat{y}_i}\right| \times 100\%, \end{aligned} \tag{5}$$

where MAE denotes the average absolute error between the predicted value and the actual value, RMSE denotes the root mean square error, and MAPE denotes the average relative error.

In Table 4, the stacking model has the best performance in comparison with the single model. The MAE of the stacking model is only 0.1314, the RMSE is 0.0386, and the MAPE is only 5.10%. The results show that the accuracy of the predicted value obtained by the MTSS model can reach 94.90%, which is higher than that of other single models. In the single prediction model, the SVR prediction error is small and the accuracy is the highest.

Without considering multiple timing features, the MAE of stacking was 0.1808, the RMSE was 0.0643, and the MAPE is 7.23% (Table 5). Considering multiple timing features, the MAE of stacking was 0.1314, the RMSE was 0.0386, and the MAPE is 5.10% (Table 4). Regarding the benchmark performance without considering multiple timing features, the MTSS prediction model shows better results that MAE is decreased by 0.0494, RMSE is decreased by 0.0257, and MAPE is decreased by 2.13%. Without considering the timing characteristics, the accuracy of model prediction is significantly reduced. It can be seen that multitemporal feature extraction is effective for improving the accuracy of the model, and the supplement of historical information can improve the prediction accuracy of the model.

In summary, the stacking model integrates a variety of heterogeneous prediction algorithms and can use the advantages of multiple algorithms in different data spaces and structures to construct better models. Therefore, the MTSS model is better than a single machine learning in terms of pavement performance prediction. The MTSS model shows better performance.

*4.4.2. MTSS Prediction Model Results.* From the analysis of the forecast cycle of the entire pavement of the Dalian highway, Figure 13 shows the comparison trend of the actual IRI value in 2019 and the IRI predicted values under three

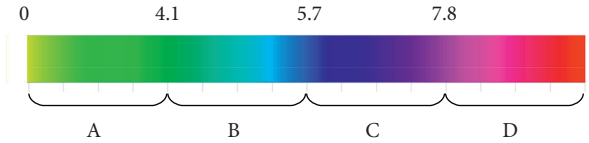


Figure 17: Pavement performance chromatogram of the Dalian highway tunnel.

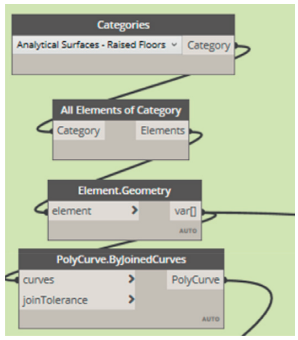


(a)

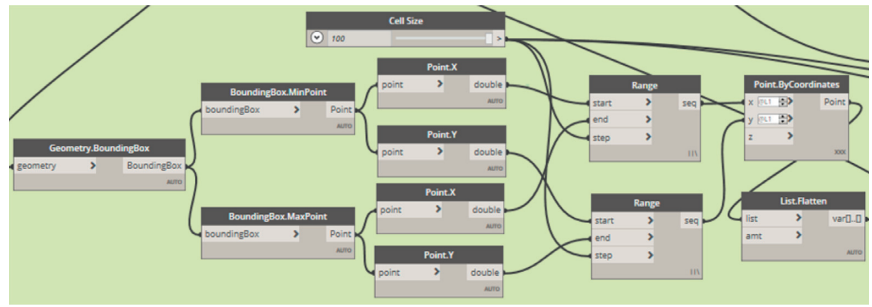


(b)

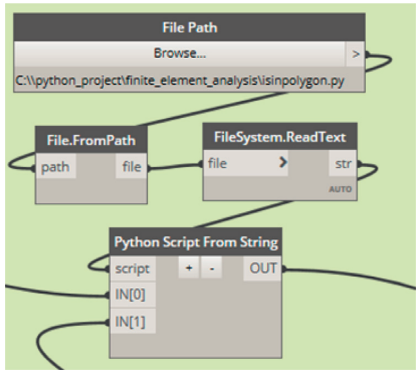


(c)

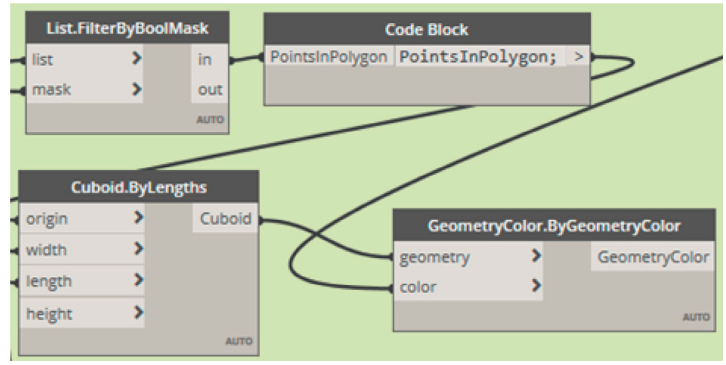


(f)

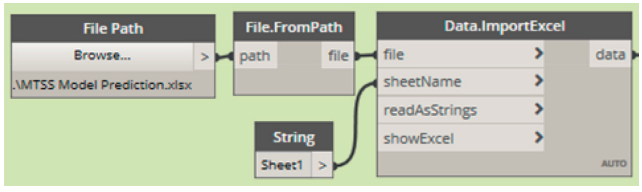


(d)

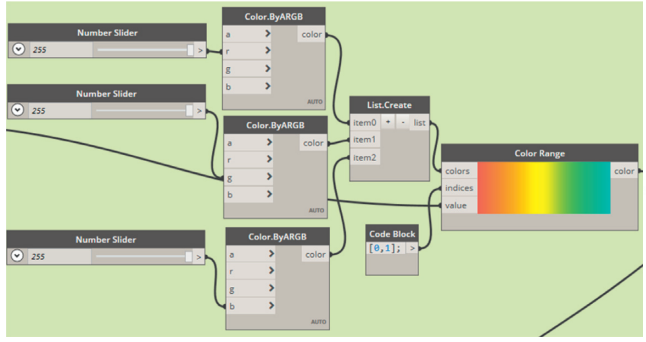


(e)

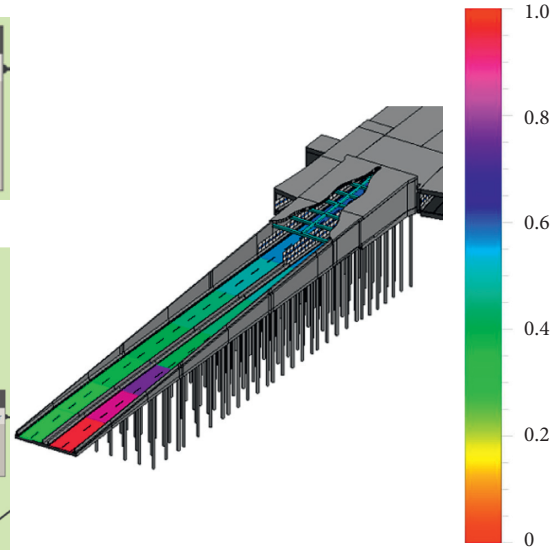


Figure 18: Visual presentation of pavement performance prediction in Dynamo. (a) Import the Revit highway BIM model. (b) Create highway segment element. (c) Import Python script. (d) Import MTSS highway segment performance prediction results. (e) Create a chromatogram. (f) Visualize the changing trend of highway segments.

different maintenance assumptions in 2020. The pavement performance will decline in turn under the assumption of overhaul, minor repair, and natural decay, which is in line with the normal law. In other words, the pavement performance after major repair is obviously higher than that after minor repair, and the pavement performance after minor repair is higher than that after natural decay.

According to the prediction of each segment in Figure 14, the IRI will decrease by 0.2 under the assumption of natural decay for the 1100 km slow lane from Puxi to Pudong (Eastern Route) in 2020. Under the assumption of minor repair, the IRI will be improved by 0.2. Under the assumption of overhaul, the IRI will be improved by 0.4. In 2020, on the 1100 km segment of the Puxi to Pudong (Eastern Route) expressway, the IRI decreases by 0.1 under the assumption of natural decay; under the assumption of minor repair, the IRI is improved by 0.2; under the assumption of overhaul, the IRI is increased by 0.6. The IRI will decrease by 0.05 under the assumption of natural decay for the 600 km slow lane from Pudong to Puxi (West Route) in 2020. Under the assumption of minor repair, the IRI will be improved by 0.3; under the assumption of overhaul, IRI will be improved by 0.6. The IRI will decrease by 0.1 in the 100 km segment of the expressway from Pudong to Puxi (West Route) in 2020 under the assumption of a natural recession. Under the assumption of minor repair, IRI will be improved by 0.2; under the assumption of overhaul, IRI will be improved by 0.6.

Figure 15 shows the comparison between the predicted value and the actual value of some highway segments. In scatter Figure 16, diagonals identify that the line $X$ equals to $Y$, and the $X$-axis and $Y$-axis, respectively, represent the actual value and predicted value of IRI on the verification set. The closer the scatter is to the diagonal line, the better the prediction accuracy is. It is obvious that the model has a good fitting effect, which further indicates that the prediction effect of the MTSS model is feasible.

*4.5. Application of Digital Twins.* According to Shanghai Engineering Construction Code DGJ08-92-2013 "Technical Regulations for Urban Pavement Maintenance," the main highway network connected at both ends of the Dalian highway tunnel belongs to the primary and secondary arterial highways. It needs to be classified according to the ratings in Table 6 to map the pavement performance values and the chromatogram.

Applying the digital twin for pavement performance prediction proposed in Section 3.1, taking each section of the Dalian highway tunnel as an example, as shown in Figure 17, the performance numerical results of the visualized prediction highway segments are used to enhance the visualization by the color mapped in the chromatogram. According to the pavement performance evaluation standard level, the pavement performance trend is predicted by the MTSS prediction model in the Dynamo visualization parametric analysis module (Figure 18), and the change law of the highway segment performance varies under different maintenance assumptions.

## 5. Conclusions

In this paper, a highway tunnel pavement performance prediction approach based on a digital twin + MTSS is proposed. This method adopts digital twin technology and machine learning technology to predict the pavement performance data through the established MTSS model. The multiple time series feature extraction method and the automatic hyperparameter tuning technology of the MTSS model are the key factors improving the accuracy of pavement performance prediction. The stacking integrated learning method can effectively reduce the risk of poor generalization performance of a single model and falling into a local minimum. The relative error between the predicted value and the actual value of the MTSS model is small, which improves the accuracy of the prediction. The visual information service of the digital twin provides a reliable data-driven management method for preventive maintenance, which helps to improve the management efficiency of prediction and decision-making.

## Data Availability

The online access data used to support the findings of this study have not been made available because the data source involves the internal life cycle operation and maintenance management system and is not open to the public.

## Conflicts of Interest

The authors declare that there are no conflicts of interest.

## Acknowledgments

This research was supported by the National Natural Science Foundation of China (71701121), the Chinese Ministry of Education of Humanities and Social Science Project (17YJC630021), and the Key Program of the Shanghai Science and Technology Commission: research on intelligent identification and control strategy optimization of the shield tunneling state.

## References

[1] R. Eghbalpoor, M. Baghani, and H. Shahsavari, "An implicit finite element framework considering damage and healing effects with application to cyclic moving load on asphalt pavement," *Applied Mathematical Modelling*, vol. 70, pp. 139–151, 2019.

[2] D. Zhang, B. Birgisson, X. Luo, and I. Onifade, "A new long-term aging model for asphalt pavements using morphology-kinetics based approach," *Construction and Building Materials*, vol. 229, p. 117032, 2019.

[3] A. C. Collop and D. Cebon, "A model of whole-life flexible pavement performance," *Proceedings of the Institution of Mechanical Engineers, Part C: Journal of Mechanical Engineering Science*, vol. 209, no. 6, pp. 389–407, 1995.

[4] S. Shirzad, M. A. Aguirre, L. Bonilla, M. A. Elseifi, S. Cooper, and L. N. Mohammad, "Mechanistic-empirical pavement performance of asphalt mixtures with recycled asphalt

shingles," *Construction and Building Materials*, vol. 160, pp. 687–697, 2018.

[5] X. Ma, Z. Dong, F. Chen, H. Xiang, C. Cao, and J. Sun, "Airport asphalt pavement health monitoring system for mechanical model updating and distress evaluation under realistic random aircraft loads," *Construction and Building Materials*, vol. 226, pp. 227–237, 2019.

[6] J. Chao and Z. Jinxi, "Prediction model for asphalt pavement temperature in high-temperature season in Beijing," *Advances in Civil Engineering*, vol. 2018, Article ID 1837952, 11 pages, 2018.

[7] X. Chen, Q. Dong, X. Gu, and Q. Mao, "Bayesian analysis of pavement maintenance failure probability with Markov chain Monte Carlo simulation," *Journal of Transportation Engineering, Part B: Pavements*, vol. 145, no. 2, pp. 1–9, 2019.

[8] A. Bianchini and P. Bandini, "Prediction of pavement performance through neuro-fuzzy reasoning," *Computer-Aided Civil and Infrastructure Engineering*, vol. 25, no. 1, pp. 39–54, 2010.

[9] N.-F. Pan, C.-H. Ko, M.-D. Yang, and K.-C. Hsu, "Pavement performance prediction through fuzzy regression," *Expert Systems with Applications*, vol. 38, no. 8, pp. 10010–10017, 2011.

[10] A. Abed, N. Thom, and L. Neves, "Probabilistic prediction of asphalt pavement performance," *Road Materials and Pavement Design*, vol. 20, no. sup1, pp. S247–S264, 2019.

[11] R. Li, Y. Huang, and J. Wang, "Long-term traffic volume prediction based on type-2 fuzzy sets with confidence interval method," *International Journal of Fuzzy Systems*, vol. 21, no. 7, pp. 2120–2131, 2019.

[12] H. Gong, Y. Sun, X. Shu, and B. Huang, "Use of random forests regression for predicting IRI of asphalt pavements," *Construction and Building Materials*, vol. 189, pp. 890–897, 2018.

[13] S. Xiao and M. Nie, "The preventive maintenance of highway based on data mining," *MATEC Web of Conferences*, vol. 139, pp. 1–5, 2017.

[14] J. Bi, H. Yuan, and M. Zhou, "Temporal prediction of multiapplication consolidated workloads in distributed clouds," *IEEE Transactions on Automation Science and Engineering*, vol. 16, no. 4, pp. 1763–1773, 2019.

[15] T. Lintonen and T. Raty, "Self-learning of multivariate time series using perceptually important points," *IEEE/CAA Journal of Automatica Sinica*, vol. 6, no. 6, pp. 1318–1331, 2019.

[16] B. Liu, S. Yan, H. You et al., "Road surface temperature prediction based on gradient extreme learning machine boosting," *Computers in Industry*, vol. 99, pp. 294–302, 2018.

[17] H. Gong, Y. Sun, Z. Mei, and B. Huang, "Improving accuracy of rutting prediction for mechanistic-empirical pavement design guide with deep neural networks," *Construction and Building Materials*, vol. 190, pp. 710–718, 2018.

[18] H. Gong, Y. Sun, W. Hu, and B. Huang, "Neural networks for fatigue cracking prediction using outputs from pavement mechanistic-empirical design," *International Journal of Pavement Engineering*, vol. 145, no. 2, pp. 1–11, 2019.

[19] Q. Hu, "A review of data analytic applications in road traffic safety. Part 2: prescriptive modeling," *Sensors (Switzerland)*, vol. 20, no. 4, 2020.

[20] G. Wang, J. Qiao, J. Bi, W. Li, and M. Zhou, "TL-GDBN: growing deep belief network with transfer learning," *IEEE Transactions on Automation Science and Engineering*, vol. 16, no. 2, pp. 874–885, 2019.

[21] S. Gao, M. Zhou, Y. Wang, J. Cheng, H. Yachi, and J. Wang, "Dendritic neuron model with effective learning algorithms for classification, approximation, and prediction," *IEEE Transactions on Neural Networks and Learning Systems*, vol. 30, no. 2, pp. 601–614, 2019.

[22] J. Wang and T. Kumbasar, "Parameter optimization of interval Type-2 fuzzy neural networks based on PSO and BBBC methods," *IEEE/CAA Journal of Automatica Sinica*, vol. 6, no. 1, pp. 247–257, 2019.

[23] D. H. Wolpert, "Stacked generalization," *Neural Networks*, vol. 5, no. 2, pp. 241–259, 1992.

[24] F. Lin, J. Jiang, J. Fan, and S. Wang, "A stacking model for variation prediction of public bicycle traffic flow," *Intelligent Data Analysis*, vol. 22, no. 4, pp. 911–933, 2018.

[25] B. Zhai and J. Chen, "Development of a stacked ensemble model for forecasting and analyzing daily average PM2.5 concentrations in Beijing, China," *Science of The Total Environment*, vol. 635, pp. 644–658, 2018.

[26] J. Chen, J. Yin, L. Zang, T. Zhang, and M. Zhao, "Stacking machine learning model for estimating hourly PM2.5 in China based on Himawari 8 aerosol optical depth data," *Science of The Total Environment*, vol. 697, p. 134021, 2019.

[27] M. Jiang, J. Liu, L. Zhang, and C. Liu, "An improved Stacking framework for stock index prediction by leveraging tree-based ensemble models and deep learning algorithms," *Physica A: Statistical Mechanics and Its Applications*, vol. 541, no. 258, p. 122272, 2020.

[28] Y. Li, Z. Yang, X. Chen, H. Yuan, and W. Liu, "A stacking model using URL and HTML features for phishing webpage detection," *Future Generation Computer Systems*, vol. 94, pp. 27–39, 2019.

[29] X. Yang, B. Dindoruk, and L. Lu, "A comparative analysis of bubble point pressure prediction using advanced machine learning algorithms and classical correlations," *Journal of Petroleum Science and Engineering*, vol. 185, Article ID 106598, 2020.

[30] L. Feng, Y. Li, Y. Wang, and Q. Du, "Estimating hourly and continuous ground-level PM2.5 concentrations using an ensemble learning algorithm: the ST-stacking model," *Atmospheric Environment*, vol. 223, Article ID 117242, 2020.

[31] D. Systèmes, *Meet Virtual Singapore, the City's 3D Digital Twin Available*, GovInsider, Adelaide, Australia, 2019.

[32] C. Boje, A. Guerriero, S. Kubicki, and Y. Rezgui, "Towards a semantic construction digital twin: directions for future research," *Automation in Construction*, vol. 114, p. 103179, 2020.

[33] Y. Lu, C. Liu, K. I.-K. Wang, H. Huang, and X. Xu, "Digital Twin-driven smart manufacturing: connotation, reference model, applications and research issues," *Robotics and Computer-Integrated Manufacturing*, vol. 61, p. 101837, 2020.

[34] S. Liu, J. Bao, Y. Lu, J. Li, S. Lu, and X. Sun, "Digital twin modeling method based on biomimicry for machining aerospace components," *Journal of Manufacturing Systems*, pp. 1–16. In press, 2020.

[35] Q. Lu, L. Chen, S. Li, and M. Pitt, "Semi-automatic geometric digital twinning for existing buildings based on images and CAD drawings," *Automation in Construction*, vol. 115, p. 103183, 2020.

[36] Z. Ma and Z. Liu, "BIM-based intelligent acquisition of construction information for cost estimation of building projects," *Procedia Engineering*, vol. 85, pp. 358–367, 2014.

[37] Z. Ma, S. Cai, N. Mao, Q. Yang, J. Feng, and P. Wang, "Construction quality management based on a collaborative system using BIM and indoor positioning," *Automation in Construction*, vol. 92, pp. 35–45, 2018.

[38] Z. Wang and E. Rezazadeh Azar, "BIM-based draft schedule generation in reinforced concrete-framed buildings," *Construction Innovation*, vol. 19, no. 2, pp. 280–294, 2019.

[39] M. Sami Ur Rehman, M. J. Thaheem, A. R. Nasir, and K. I. A. Khan, "Project schedule risk management through building information modelling," *International Journal of Construction Management*, pp. 1–11, 2020.
[40] C.-S. Shim, N.-S. Dang, S. Lon, and C.-H. Jeon, "Development of a bridge maintenance system for prestressed concrete bridges using 3D digital twin model," *Structure and Infrastructure Engineering*, vol. 15, no. 10, pp. 1319–1332, 2019.
[41] J. Heaton, A. K. Parlikad, and J. Schooling, "Design and development of BIM models to support operations and maintenance," *Computers in Industry*, vol. 111, pp. 172–186, 2019.
[42] G. Y. N. N. Adi, M. H. Tandio, V. Ong, and D. Suhartono, "Optimization for automatic personality recognition on twitter in Bahasa Indonesia," *Procedia Computer Science*, vol. 135, pp. 473–480, 2018.
[43] T. Chen and T. He, "xgboost: eXtreme Gradient Boosting," pp. 1–4, 2015.
[44] H. Meng, X. Wang, and X. Wang, "Expressway crash prediction based on traffic big data," in *Proceedings of the ACM's International Conference Proceedings Series*, pp. 11–16, New York, NY, USA, July 2018.
[45] G. Ke, "LightGBM: A highly efficient gradient boosting decision tree," *Advances in Neural Information Processing Systems*, vol. 30, pp. 3147–3155, 2017.
[46] S. Zhou, L. Sun, W. Xing et al., "Hyperspectral imaging of beet seed germination prediction," *Infrared Physics & Technology*, vol. 108, no. 74, p. 103363, 2020.
[47] Y. L. Pavlov, "Random forests," *Machine Learning*, vol. 45, pp. 5–32, 2019.
[48] A. Mechelli and S. Vieira, *Machine Learning: Methods and Applications to Brain Disorders*, Academic Press, London, UK, 2019.
[49] R. Kissell, *Lgorithmic Trading Methods: Applications Using Advanced Statistics, Optimization, and Machine Learning Techniques*, Academic Press, Cambridge, MA, USA, 2020.
[50] M. Ali, I. Ullah, W. Noor, A. Sajid, A. Basit, and J. Baber, "Predicting the session of an P2P IPTV user through support vector regression (SVR)," *Engineering, Technology & Applied Science Research*, vol. 10, no. 4, pp. 6021–6026, 2020.
[51] Z. Nie, F. Shen, D. Xu, and Q. Li, "An EMD-SVR model for short-term prediction of ship motion using mirror symmetry and SVR algorithms to eliminate EMD boundary effect," *Ocean Engineering*, vol. 217, Article ID 107927, 2020.
[52] D. Jones, C. Snider, A. Nassehi, J. Yon, and B. Hicks, "Characterising the Digital Twin: a systematic literature review," *CIRP Journal of Manufacturing Science and Technology*, vol. 29, pp. 36–52, 2020.
[53] E. A. G. Isabelle, *An Introduction to Feature Extraction*, Springer, Berlin, Germany, 2006.
[54] S. O. M. Smith and D. Susarla, *Feature Engineering Made Easy*, pp. 211–264, Packt Publishing, Birmingham, UK, 2018.
[55] P. Ruano, *Introduction to Machine Learning*, MIT press, Cambridge, MA, USA, 4th edition, 2016.
[56] N. C. Brown, V. Jusiega, and C. T. Mueller, "Implementing data-driven parametric building design with a flexible toolbox," *Automation in Construction*, vol. 118, Article ID 103252, 2020.
[57] A. Kitaha and K. P. Biligiri, "Prioritization-optimization process algorithm to manage pavement networks during the non-availability of historical data," *Journal of Testing and Evaluation*, vol. 45, no. 2, Article ID 20150287, 2017.

Hindawi
Advances in Civil Engineering
Volume 2020, Article ID 8848965, 15 pages
https://doi.org/10.1155/2020/8848965

*Research Article*

# Factors Influencing BIM Adoption for Construction Enterprises in China

**Ruixue Zhang,[1] Yuyan Tang,[1] Liang Wang ,[2] and Zeyu Wang[3]**

[1]*School of Business Administration, Liaoning Technical University, Fuxin 125105, China*
[2]*School of Maritime Economics and Management, Dalian Maritime University, Dalian 116026, China*
[3]*School of Management, Guangzhou University, Guangzhou 510006, China*

Correspondence should be addressed to Liang Wang; liangwang@dlmu.edu.cn

Received 3 August 2020; Revised 21 October 2020; Accepted 6 November 2020; Published 29 November 2020

Academic Editor: Jiansong Zhang

Copyright © 2020 Ruixue Zhang et al. This is an open access article distributed under the Creative Commons Attribution License, which permits unrestricted use, distribution, and reproduction in any medium, provided the original work is properly cited.

The construction industry is one of the important pillars of the Chinese national economy. BIM, as a new information technology tool, provides an intelligent digital representation of buildings to support diverse activities and brings about a wide range of benefits throughout the life cycle of projects. However, BIM has not been widely adopted in construction enterprises in China. It is necessary to make a comprehensive and systematic analysis of the influencing factors for BIM adoption. This paper sums up 13 influencing factors from four aspects, namely, technology, economy, institution, and environment aspect. The questionnaire survey and statistical analysis were used to collect and process data which is applied to determine the influencing factors. Based on relevant literature, a hypothesis model was established by the structural equation modeling method. SPSS software and AMOS software were used to test the model. Then, the key factors influencing BIM adoption are induced. The results show that the key factors that influence BIM adoption in China include personnel quality, investment in personnel training, BIM standardization, and the influence of senior managers in the organization. Combined with the above conclusion, this paper puts forward some suggestions for promoting BIM adoption and specific measures to realize the wide application of BIM technology in the Chinese construction industry.

## 1. Introduction

Building information modeling (BIM) is a set of information technology that integrates technology and information closely and is widely used by the architecture, engineering, and construction (AEC) industries. BIM has the advantages of high visualization, effective coordination, and robust simulation, which can effectively promote collaboration among participants in the construction projects. BIM plays a synergistic role in the whole life cycle of the project [1] and has a significant effect on the innovation and promotion of construction enterprises [2]. The use of BIM will bring enormous benefits, including improving production efficiency and product quality, achieving sustainability, and providing broader opportunities for burgeoning industries in the construction industry [3–6]. In most developed countries, as its normative BIM standards, sufficient talents, and corresponding legal norms, the advantages of BIM are particularly prominent [7].

Although the potential benefits of BIM are appealing, its adoption rate varies among different countries [8]. Previous research indicated that BIM adoption and usage is increasing in most developed countries [9]. Nevertheless, the extent of BIM adoption is stagnant in developing countries. For most developing countries, BIM has not been applied in the whole construction cycle of construction projects [10]. Especially, in China, although BIM has experienced the stages of concept introduction, theoretical research, preliminary application, rapid development, and deep application in the past ten years, it has not yet penetrated the whole process of the project construction cycle. BIM adoption in small- and medium-sized enterprises in China is just at an elementary stage [11] even though the government has taken actions to promote the use of BIM [12]. There is no substantial change

in the traditional construction industry up to now [13]. The wide BIM adoption is still facing challenges in China.

Recent studies reporting the factors influencing BIM adoption have been proposed in the very recent literature. BIM has led to the breakthrough development of the AEC industry. BIM adoption is facing the development trend from integration, collaboration, and multilevel [13]. It is a tool and a process and assists in building performance while improving the effective management of construction projects. Many challenges and problems have aroused with the rapid development of the construction industry, for example, large and complex construction technology, enormous investment, the determination of construction period, and the relationship between multiagent stakeholders [14]. There are many obstacles in the practical implementation process as well such as the lack of relevant professional talents, difficulties in coordination between the main bodies, and poor software compatibility [15, 16]. Several researchers found out that BIM adoption in enterprises is still low due to limited cooperation, dispersal stakeholder, and existing risk [17]. In the aspect of BIM adoption, it is concluded that whether to use BIM to complete a construction project is not only limited by the user's individual willingness but also depends on whether the senior managers within the organization want to use it for information management in the whole life cycle of the project [18].

Although existing literature on BIM adoption is very extensive, some deficiencies still exist. It is evident from the aforementioned previous studies that they analyzed the BIM adoption issue in a particular aspect. For instance, a model was proposed to predict project owner's BIM adoption behaviors in reference to the particular BIM practices in China [19]. Cao et al. discussed that the motivation of design units and general contractors in BIM adoption is closely related to the project scale and organizational nature [11]. Also, most studies are based on a specific adoption model perspective to study the influencing factors. Ahuja et al. developed a model using the technology-organization-environment framework to investigate factors influencing BIM adoption and reasons for the slow adoption [20]. Qin et al. proposed an integrated TAM (technology acceptance model) and TOE (technology-organization-environment) framework to investigate factors that hinder BIM adoption in the construction industry [21]. The TOE framework identifies technology, organization, and environment as three groups of contextual factors for organization to adopt innovations [22]. Besides, Songer et al. proposed to introduce economic factors into the adoption framework [23]. At present, from the perspective of the Chinese construction enterprises, the research on factors influencing BIM adoption is not deep enough. Furthermore, there is a lack of empirical research. It is therefore expedient to carry out an explicit study that comprises a comprehensive analysis of BIM adoption in all AEC firms in China. This study distinguishes and discusses the key factors influencing BIM adoption from the perspective of all construction enterprises in China. Based on the technology adoption framework, a theoretical model of factors influencing BIM adoption is constructed. The data are analyzed with statistical methods, and the influence degree is sorted and arranged. In addition, based on the research results of BIM adoption model, this paper analyzes and puts forward reasonable suggestions from the four dimensions of adoption strategy, investment planning, government departments, and the internal environment within the organization. It improves the scientific level of decision-making and promotes the BIM adoption in China's construction enterprises.

This paper aims to reveal factors influencing BIM adoption among construction enterprises in China. The study proposes a means for influencing factor analysis method by adopting structural equation modeling. Also, AMOS and SPSS software were used to analyze the data results. The following research questions will be answered in this paper:

(1) What is the current situation of BIM adoption and how to classify the factors influencing BIM adoption in construction enterprises?

(2) What are the key factors influencing BIM adoption and how do they affect adoption efficiency in construction enterprises in China?

(3) How to realize the rapid development of Chinese construction enterprises by improving BIM adoption efficiency?

The remainder of this paper is organized as follows: Section 2 reviews previous research on BIM adoption in construction enterprises. Section 3 elaborates the research methodology and proposes research hypotheses. Data collection and data processing are displayed in Section 4. Section 5 tests the hypothesis model from the perspective of exploratory factor and confirmatory factor. Section 6 discusses the critical influencing factors and corresponding strategies. Section 7 summaries this paper and explores future research on BIM adoption.

## 2. Literature Review

*2.1. BIM Adoption Research.* BIM has become increasingly popular in construction enterprises over the past few years. Many research studies have been performed worldwide to identify factors that influence the adoption of BIM [8, 24–26]. Through the study of BIM adoption in Chinese construction enterprises, it is found that the key factors are attitude, technology, and organization [26]. At the organizational level, BIM adoption has gone through three stages: the first stage is the interdisciplinary object-based modeling process, the second is the synergy based on the established model, and the last is the network-based synergy [27]. This three-stage BIM adoption model has been used in the United States, Australia, and other developed countries. They are aiming to make BIM widely adopted [28, 29]. On the contrary, compared with developed countries, developing countries have not formed such a three-stage process to support BIM adoption. For example, the BIM adoption level is not very high in China [30, 31]. The maturity of BIM adoption is considered to be very low in India [25]. In the construction industry, designers are the first to use BIM to

complete engineering projects [3]. In terms of BIM adoption, construction enterprises have been at the forefront. In general, the design team will give priority to BIM adoption in the course of the project [32]. Hence, BIM adoption is suitable and efficient for improving productivity effects in construction enterprises in order to promote the proceeds throughout the whole life cycle.

So as to determine the factors influencing BIM adoption, many theoretical models have been developed, such as technology acceptance model and technology-organization-environment framework. Previous studies have attempted to study technology adoption through innovation diffusion. Technology Adoption Model is one of the most commonly used framework models from individual and organizational perspectives. However, a few scholars point out that technology adoption model, Theory of Planned Behavior, and Unified Theory of Acceptance and Use of Technology are mostly used to study the adoption problem between individuals [33]. The technology-organization-environment framework model focuses on different stages of adoption and different levels of organizational adoption process.

Based on the theory of reasonable behavior, Davis studies the technology acceptance model. TAM is widely used to explain the information technology adoption or acceptance behavior. It consists of two specific factors that affect user behavior, namely, how and when to use new technologies: perceived usefulness and perceived ease of use [34]. These two parameters are based on the "Self-efficacy theory" research [35]. Although there are a number of empirical studies, people's intention to use determines whether a new technology can be well adopted. TAM is widely used to predict various types of technology acceptance behavior activities, for example, virtual reality [36], smart grid [37], and transportation [38]. However, it needs to be integrated into a broader model, including variables related to human and social factors [39]. Technology-organization-environment framework was first proposed by Tornatzky and Fleischer [40]. It represents a company's model of technological, organizational, and environmental impacts in the process of adopting and implementing technological innovation [41]. In the meantime, it describes three aspects in which an enterprise decides to adopt technology: technology, organization, and environment. Technical background refers to the internal and external technologies currently applied by the organization, as well as technologies that are already on the market but not yet used by the company. Organizational background refers to the size of the company, organizational structure, and human resources. Environmental background includes factors beyond organizational control, such as competition, partners, and industry environment. In addition to the above, Songer et al. proposed to introduce economic factors into the technology adoption framework considering that enterprises may try to use information technology at a lower cost [23]. Because it contains a new factor, environmental factor, the TOE framework structure is considered to be able to better explain the innovation diffusion within enterprises [33, 42].

*2.2. Influencing Factors of BIM Adoption.* At present, BIM is gradually spread all over the world, and the utilization rate of relevant software is also gradually increasing [43]. Compared with most developed countries, BIM adoption has just begun in developing countries. For instance, the development depth and breadth of BIM in China are far less than that in Europe. Therefore, there is still a lot of room for improvement in its application and promotion [44]. Through the research and analysis of the promotion factors of BIM adoption in the Chinese engineering design industry, it can be concluded that the factors influencing BIM adoption include software advantages, laws and regulations, localization degree, standards, BIM application cases, and experience [45]. Technology, legal system, personnel, organization, and economy are also the main factors influencing BIM adoption [46]. It is found that the support of senior managers within the organization, personal subjective will, and technical specifications affect whether designers want to adopt BIM [47]. Meanwhile, high-quality employees, efficient management and leadership, the availability of information, and the complexity of the project itself will also affect the smooth implementation of BIM [48, 49]. From the individual, technical and organizational levels, design units, and construction enterprises pay more attention to the factors influencing BIM cooperation [50].

According to the research on the factors influencing BIM adoption in the European construction industry, it is concluded that the obstacle factors include more time spent in training staff, high investment, and large amounts of labor [51]. In addition, in the practical application of BIM adoption, the lack of relevant laws and regulations, relevant standards and implementation guidelines, and unclear ownership will also hinder the implementation effect [52]. Based on the economic, technical, and legal perspectives, the reasons hindering the application can be summarized, including contract mode and business model [53]. Under the current market background, there are still many problems in the application and in-depth development of BIM, for example, no consensus on BIM adoption, no clear provisions in existing laws and regulations, and lack corresponding industry standards [52]. The research studies the application and future development trend of BIM throughout the whole life cycle of construction projects such as interests, risks, and trends and analyzes the problems and challenges that will be faced in the application process [15]. Through the questionnaire survey, the key factors influencing BIM adoption are identified, including BIM experience, leader support, organizational, technical training, and other 12 influencing factors [54].

Most of the scholars' results are to analyze one aspect of the factors, and the comprehensive research and analysis of each factor is missing. Based on the structural equation model, this paper focuses on the factors influencing BIM adoption in construction enterprises in China, selecting technology, economy, institution, and environment as four potential variables and corresponding thirteen observation variables, analyzing the influence of each factor on BIM adoption, arranging from large to small on the basis of the factor load, and giving policy suggestions to promote BIM adoption.

## 3. Research Methodology

There are many factors influencing BIM adoption. It is difficult to classify the key influencing factors reasonably only through the existing literature research methods. Therefore, combined with the research of existing literature with expert consultation and interview, the influencing factors summarized are designed into a questionnaire, which is issued and recycled through the Internet. This paper selects technology, economic, institution, and environment factors as four external latent variables, corresponding to thirteen observation variables, respectively, and BIM adoption is as internal latent variables.

*3.1. Hypothesis.* BIM technical characteristics normally reflect the applicability, ease of use, compatibility, and interoperability of its applications. Compared with traditional methods, BIM has great superiority. Using BIM requires specialists with relevant industry experience and knowledge. At present, the lack of technical personnel is a prominent problem in China [55, 56]. The development of BIM is still in elementary. BIM brings quantifiable benefits, which can significantly offset the relevant application costs. However, it is difficult to capture the cost and benefit in the process of BIM adoption. Also, BIM adoption has a lot of intangible benefits, which increase the difficulty in calculating the return on investment [47]. Thus, the paper proposes the following hypotheses:

(i) H1: technological factor has an impact on BIM adoption.

(ii) H1a: technical advantage positively affects BIM adoption.

(iii) H1b: production efficiency positively affects BIM adoption.

(iv) H1c: the quality of employees within an organization positively affects BIM adoption.

BIM is widely used as new information technology. Although it will bring huge profits to enterprises and improve production efficiency, the initial cost investment is not small. Young et al. affirmed that the capital required for the procurement of BIM software and hardware equipment was considerable [57]. BIM technologies available for sale are costly for purchase and installation [58]. Memon et al. asserted that the transition from the traditional way to the emerging of BIM has huge cost constraints [59]. Hence, enterprises are not willing to implement the process unless they can link it with the substantial reduction of long-term benefits and training costs of their respective companies. Similarly, identifying the benefits of return on investment can improve the BIM adoption rate [60]. Also, the cost of personnel training and the cost of employing consulting units and experts are the expenses of BIM adoption [61]. Accordingly, this study proposes the following hypotheses:

(i) H2: economic factor has an impact on BIM adoption.

(ii) H2a: the investment in technology research and development positively affects BIM adoption.

(iii) H2b: the investment in the application of software positively affects BIM adoption.

(iv) H2c: train-related talents positively affect BIM adoption.

The maturity and standardization of BIM have a significant impact on the company's cognition of new technology. BIM localization contains not only the localization of software running environment but also the adaptation of local project characteristics [62]. BIM standardization defines the project stages, the deliverable, and the objectives to be achieved. BIM adoption needs the integration of many kinds of software. Only the unified data exchange standard can make the data transfer effectively [63]. National policies have a significant impact on the development of BIM adoption in the construction industry in China [64]. In recent years, the Chinese government has also published relevant policies to encourage BIM adoption. Therefore, we propose the following hypotheses:

(i) H3: institutional factor has an impact on BIM adoption.

(ii) H3a: improving law and system positively affects BIM adoption.

(iii) H3b: government subsidies and incentive policies positively affect BIM adoption.

(iv) H3c: improving BIM standards positively affect BIM adoption.

Organizational support plays an important role in stimulating employee potential, allocating resources, and improving job performance [65–67]. Adequate organizational support will have an incentive effect on employees. They feel that they are trusted by the organization. Therefore, they will focus more on their own work and strive to achieve organizational goals. On the contrary, if the necessary support is lost, the work quality of employees will be greatly reduced or even worse [68, 69]. Lin declared that organizational high-level support could improve employees' perceived usefulness and perceived ease of use of BIM adoption [70]. Based on the above, we propose the following hypotheses:

(i) H4: environmental factor has an impact on BIM adoption.

(ii) H4a: intraorganizational mandatory use positively affects BIM adoption.

(iii) H4b: intraorganizational emphasis positively affects BIM adoption.

(iv) H4c: intraorganizational encouragement positively affects BIM adoption.

(v) H4d: intraorganizational talent structure distribution positively affects BIM adoption.

Based on the above review, a theoretical framework is designed, as shown in Figure 1. The unidirectional arrows of this model shown in Figure 1 start from the independent

variables and end at the dependent variables, implying the independent variables affect the dependent variable.

*3.2. Structural Equation Model.* Traditional analysis methods, such as multiple regression, path analysis, and traditional factors analysis, can deal with variables with observed values. Although the dependent variables are allowed to include measurement errors, it is required to assume that the observation values of independent variables have no errors. In many practical problems, the relationship between multi-index variables is complex. Sometimes, it is not always possible to use a set of independent variables to explain a dependent variable. Although traditional factor analysis can deal with measurement errors, it does not involve how to compare or test different models [71]. In this paper, the latent variables, the factors influencing BIM adoption, cannot be measured directly, and the questionnaire survey presents the difference in quantity. Therefore, the structural equation model is used as the analysis method in this paper.

The structural equation model is a statistical technique that is based on the covariance matrix of variables to analyze the relationship between variables. SEM was formally defined by Pearl [72]. The specific implementation is divided into five steps: model setting, model identification, model estimation, model evaluation, and model modification. It is mainly used to deal with the relationship between multiple causes, results, and problems with latent variables. It can deal with multiple variables at the same time. It also can compare and evaluate different theoretical models. Firstly, the model sets observation variables for potential variables that cannot be measured directly. Then, the relationship between each observation variable is analyzed to reflect each latent variable and its structural relationship. The advantages of the structural equation model are that it can deal with multiple dependent variables. It allows both independent and dependent variables to contain measurement errors. It can also simultaneously estimate the factor structure and factor relationship. It can allow a more elastic measurement model. It can estimate the fitting degree of the whole model [73]. Based on this theory, a conceptual model can be drawn, as shown in Figure 2.

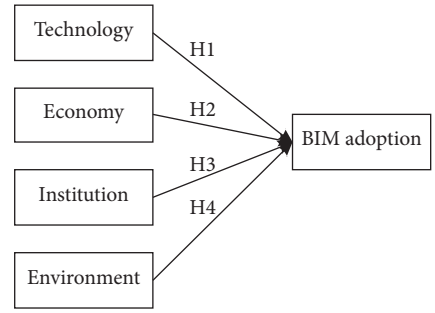


Figure 1: The theoretical model.

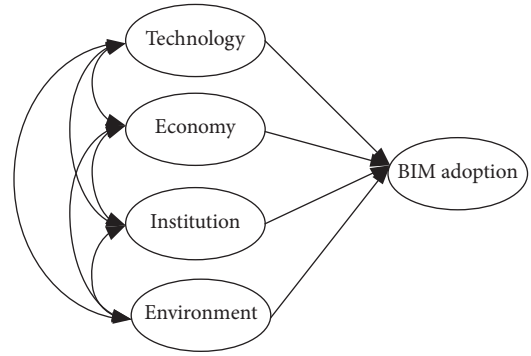


Figure 2: The conceptual model.

## 4. Data Analysis

*4.1. Design of Questionnaire.* For the purpose of ensuring the validity of this questionnaire, it is designed from multiple angles. Through reading the relevant literature and expert interviews, combined with the characteristics of construction enterprises and BIM, a questionnaire has been designed. After the questionnaire is withdrawn, it is necessary to integrate information processing. The design of this questionnaire for this study was structured and multiple-choice type. It was divided into three parts. The first part comprised the basic information of the respondents. It includes personal information (gender, age, working years, and education level), basic information of the enterprise (enterprise-scale and enterprise nature), and understanding of BIM. These questions ensure the validity of the samples and allow the survey results to be classified and cross-analyzed. The second part is the variable measurement. It includes a research hypothesis based on the factors influencing BIM adoption in construction enterprises, which is tested in the form of scale. The third part is the special measurement items. This part of special measurement is mainly to collect some specific factors on the research status of BIM adoption and test the validity of this questionnaire. The aim of the part is to collect respondents' judgments on the degree of influence between variables. For example, the questions on the factors influencing BIM adoption among AEC firms in China were asked on a five-point Likert-type scale, with 1–5 indicating "strongly disagree," "disagree," "generally," "agree," and "strongly agree," respectively. All of these measurement items were adopted from existing studies and combined with practical situations relevant to BIM adoption in the Chinese construction industry.

*4.1.1. Scale Development.* In order to measure the reliability and validity of the factors influencing BIM adoption accurately in construction enterprises and ensure the rationality of the hypothetical model, the observation variable system scale of influencing factors is determined according to relevant literature and expert opinions, as shown in Table 1.

*4.2. Analysis of Basic Characteristics*

*4.2.1. Statistical Analysis of Basic Information.* The research objects of this survey are strictly limited to employees in construction industries, educators engaged in engineering

Table 1: Measurement items.

| Number | Observation variable | Latent variable |
|---|---|---|
| A1 | Visibility advantage | Technical factors |
| A2 | Productivity and returns | |
| A3 | Quality of employees in the organization | |
| B1 | Technology adoption with a lot of money | Economic factors |
| B2 | Investment and application of technology | |
| B3 | Hire and train BIM-related talents | |
| C1 | Establish or improve laws and systems | Institutional factors |
| C2 | Government subsidies or incentives | |
| C3 | Improve standards to adapt localization | |
| D1 | BIM technology is mandatory | Environmental factors |
| D2 | Emphasis on technology adoption within the organization | |
| D3 | Encourage technology adoption within the organization | |
| D4 | Distribution of talent structure within the organization | |

direction, and graduates with relevant internship experience. The method adopted is to send out the questionnaires online and fill in the questionnaires and collect it in a unified way finally. The questionnaire survey lasted as long as three months. A total of 100 questionnaires were distributed, and 85 valid questionnaires were finally selected under the premise of ensuring the quality of the questionnaire. The selected questionnaires data are used as the sample data for empirical analysis. In order to ensure the response rate of the questionnaire, anonymous survey was conducted to reduce the problem setting of personal information. In addition, one extra reward will be offered to the participants. This study screened the returned questionnaires from two perspectives to eliminate the invalid questionnaires: (1) the online electronic questionnaire takes less than one minute to answer. This part of the questionnaire is discarded because the research object did not answer it seriously; (2) if the respondents choose the answers to each index question with significant regularity, the questionnaire is considered to be invalid.

The proportion of men and women in this survey is about 3 : 1. The age of the respondents is mainly 35–45-year-old. They have rich working experience to ensure the authenticity and accuracy of the data. Among them, 67% have a bachelor's degree, 29% have a master's degree, and only 4% have a junior college degree or below. It indicates the higher education that respondents have, the better working environment, and working conditions they own. There are employees and interns of construction enterprises. Most of the working units are construction units. There are also a small number of design units, consulting units, and other units. There is a small part of education workers and experts in related fields who are engaged in engineering. For the working departments of the respondents, they are mainly concentrated in the engineering department. Also, the design department and cost department are in the minority. In terms of BIM proficiency, the majority of staff are familiar with BIM, and only 14.5% can skillfully use BIM. However, even 2% have not heard of BIM at all. The statistical analysis of basic information is shown in Table 2. It mainly focuses on the gender, age, educational background, working years, the nature of the enterprise, and the understanding of BIM of the selected sample population.

*4.2.2. Descriptive Statistical Analysis of Sample Data.* According to the third part of the questionnaire, four potential variables and thirteen corresponding observation variables that affect the BIM adoption in the construction enterprises in China are summarized. The mean value and standard deviation of each variable sample data shown in Table 3 are obtained through the descriptive analysis of the sample data under the selected variables by SPSS software.

The mean value represents the average size of the collected data, namely, the importance of the respondents to the BIM adoption efficiency of the Chinese construction enterprises affected by these factors. The standard deviation represents the dispersion or fluctuation of data points in a set of data sets. It can be concluded from the above that, for each potential variable, the mean and standard deviation of the observed variables are in a relatively stable value. Therefore, the data result is excellent; further research and analysis can be carried out.

## 5. Model Hypothesis Test

To ensure the model fitting degree and the validity of hypothesis test, SPSS software is used to test the reliability and validity of the collected data. In general, reliability and validity were the two most common indicators used to evaluate the measurement model. If the result is significant, then conduct the "violation estimation" test. If the residual estimation value is negative or the standardization coefficient is greater than 0.95, it is illegal. After meeting the above requirements, the model fitness test is carried out to verify whether the hypothesis is tenable according to the results of the interpretation and analysis.

### 5.1. Exploratory Factor Analysis

*5.1.1. Reliability Analysis.* Reliability analysis, also known as the reliability test, is used to test whether the data collected by the questionnaire are consistent. The test method adopted is Cronbach's alpha coefficient. Generally, the coefficient is above 0.7. Previous studies suggested that Cronbach's $\alpha$ greater than 0.7 indicates acceptable reliability [74, 75]. It

Table 2: Basic information statistical analysis.

| Characteristic variables | Type | Frequency | Percentage (%) |
|---|---|---|---|
| Gender | Man | 64 | 75.3 |
| | Woman | 21 | 24.7 |
| Age | Under 25 years | 38 | 44 |
| | 25–35 years | 36 | 43 |
| | 35–45 years | 11 | 13 |
| Education level | Junior college degree or below | 3 | 4 |
| | Bachelor's degree | 57 | 67 |
| | Master's degree and above | 25 | 29 |
| Work unit | Real estate units | 13 | 15.8 |
| | Construction units | 39 | 45 |
| | Design units | 12 | 14.6 |
| | Advisory units | 11 | 13.4 |
| | Others | 10 | 11.2 |
| Work department | Engineering department | 47 | 56.6 |
| | Design department | 16 | 19.3 |
| | Cost department | 9 | 10.8 |
| | Others | 11 | 13.3 |
| Familiarity with BIM | Very familiar | 12 | 14.5 |
| | Familiar | 49 | 59 |
| | Not too clear | 20 | 24.1 |
| | Never know | 2 | 2.4 |

Table 3: Descriptive statistical analysis of sample data.

| Variable name | Number | Subject | Mean | Standard deviation | Variance |
|---|---|---|---|---|---|
| Technical factors | A1 | Visibility advantages | 3.05 | 0.936 | 0.876 |
| | A2 | Productivity and return on investment | 2.81 | 0.876 | 0.767 |
| | A3 | Quality of employees | 3.08 | 0.913 | 0.834 |
| Economic factors | B1 | Invest in technology adoption | 2.69 | 0.854 | 0.730 |
| | B2 | Technology investment and applications | 2.76 | 0.805 | 0.649 |
| | B3 | Hire and train BIM-related talents | 2.80 | 0.838 | 0.701 |
| Institutional factors | C1 | Prepare and improve laws and systems | 3.20 | 0.823 | 0.677 |
| | C2 | Government subsidies or incentives | 3.07 | 0.793 | 0.629 |
| | C3 | Improve standards to adapt localization | 3.20 | 0.793 | 0.628 |
| Environmental factors | D1 | Mandatory use of BIM | 2.72 | 1.051 | 1.105 |
| | D2 | Emphasis on BIM adoption | 2.76 | 0.850 | 0.722 |
| | D3 | Encourage BIM adoption | 2.69 | 0.869 | 0.754 |
| | D4 | Distribution of talent structure | 2.76 | 0.850 | 0.722 |

means that the data of the questionnaire have a good consistency.

According to SPSS, the reliability of the data collected in the questionnaire was tested and is shown in Table 4. The reliability of each dimension is greater than 0.7, indicating that the reliability of each dimension meets the standard of this research, and the data reliability of each dimension is good.

Table 4: Reliability analysis.

| Level | *N* | Cronbach's alpha |
|---|---|---|
| Technology | 3 | 0.853 |
| Economy | 3 | 0.865 |
| Institution | 3 | 0.865 |
| Environment | 4 | 0.885 |

*5.1.2. Validity Analysis.* The validity analysis represents the validity of the data. It judges the consistency between the hypothetical situation and the actual measured data. The higher the validity result value, the closer the relationship between the measurement results and the content to be investigated. Otherwise, the relationship is not close. Generally, the validity is usually divided into content validity and structure validity to analyze the validity of sample data. Content validity refers to whether the selected topic can describe the variables reasonably and accurately. Structural validity refers to whether the selected topic is consistent with the purpose of this research. Structural validity is examined by discriminating validity and convergent validity [26]. Firstly, correlation analysis is conducted; KMO and Bartlett sphere tests are conducted. Bartlett sphere test and KMO sample measure are observed, as shown in Table 5. Only when the correlation is high, factor analysis can be carried

Table 5: KMO and Bartlett sphere test.

| Kaiser–Meyer–Olkin measure of sampling adequacy | | 0.918 |
|---|---|---|
| Bartlett's test of sphericity | Approx. chi-square | 838.267 |
| | df | 78 |
| | Sig. | 0.000 |

out. The KMO value of this scale is 0.918, which is greater than 0.8. It indicates that these data are very suitable for factor analysis. The significance probability of Bartlett's sphere test is 0.000, less than 0.01. It has passed the significance test with a significance level of 1%. And it indicates that the data are relevant; that is, factor analysis can be carried out.

According to the software, the principal component information table can be obtained. If the eigenvalue is approximately greater than or equal to 1, four factors will be approximately selected. And the cumulative contribution rate reaches 81.506%. It shows that the four factors extracted from the 13 topics are ideal for the interpretation of the original data, as shown in Table 6.

According to the rotating component matrix, the factor attribution of each topic can be determined. The maximum variance method is used to rotate the factors to obtain the new factor load of each topic on each factor. The rotation component matrix is shown in Table 7.

*5.2. Establishment of SEM.* According to the data analysis above, it shows that the hypothetical conceptual model is basically reasonable. Technology, economy, institution, and environment can influence the BIM adoption in Chinese construction enterprises. Therefore, AMOS software is used to establish the structural equation model. And the hypothesis model and data are tested for confirmatory analysis and violation estimation. If there is a violation, the model needs to be modified and tested. If each estimation coefficient test is in a reasonable range, the model fitness test can be carried out. After testing and analysis, the estimated coefficients of each potential variable are positive and within a reasonable range. The structural equation model M1 of BIM adoption influencing factors is shown in Figure 3.

*5.3. Confirmatory Factor Analysis.* Based on the results of the exploratory factor analysis, a measurement model is established. Then, the model is verified by AMOS software. There are four latent variables and thirteen observational variables. Firstly, the structure validity is tested to get the whole fitting coefficient table. Chi-square degree of freedom index can avoid the influence of sample size on chi-square statistics. The reasonable index value is greater than 1 and less than 3. In this model, the absolute fitting index CMIN/DF = 1.656 < 3, fitting ideal. The root mean square index of approximation error is less affected by the selected sample review, the reasonable index value is less than 0.08, and the fitness degree of the standard model is acceptable. The absolute fitting index RMSEA = 0.089, approximate to 0.08, is acceptable. The goodness-of-fit index refers to the degree to measure whether the model fitness is good; when the index value is greater than 0.9, it indicates the selected sample data and design. In this model, the absolute fitting index GFI = 0.857 is close to 0.9, acceptable. The relative fitting index CFI = 0.953; when it is greater than 0.9, the result is good. The standard fitting index is to measure whether the set model and the selected data have a good matching degree; when the index value is greater than 0.9, it means good matching. In this model, IFI = 0.954 > 0.9, and the results fit well. TLI = 0.937, greater than 0.9, acceptable. SRMR = 0.049, less than 0.5. Generally, the model fits well and has practical significance, as shown in Table 8.

According to Table 8, the overall standardized test fitting degree of this model is ideal. Therefore, the composition reliability and average variance extraction test of latent variables are further constructed to judge that the model has a good internal quality. The calculation formula of component reliability and mean-variance extraction is as follows:

$$\mathrm{CR} = \frac{\left(\sum \mu_i\right)^2}{\left(\sum \mu_i\right)^2 + \sum \mathrm{Var}\left(\theta_i\right)},$$
$$\mathrm{AVE} = \frac{\sum \mu_i^2}{\sum \mu_i^2 + \sum_i \mathrm{Var}\left(\theta_i\right)}, \quad (1)$$

where CR represents the composition reliability, AVE represents average variance extraction, $\mu i$ represents the standardized factor load of the observed variable, and $\theta i$ represents the standardized residuals of observed variables.

Through the data analysis by SPSS and AMOS, the parameter estimation table of the factor measurement model is obtained in Table 9. The nonstandard estimation parameters can judge that the scale is positive and significant. The standardized factor load of each topic is greater than 0.6. It indicates that each latent variable has high representativeness.

The SMC of each path is greater than 0.36. Most of them are above 0.5, which means the topic has sufficient item reliability. The mean-variance (AVE) of each latent variable is greater than 0.5, which indicates that the convergence validity is acceptable. And the combination reliability (CR) is greater than 0.8, which indicates that there is sufficient internal consistency and the convergence validity is ideal.

Based on the data analysis above and Figure 3, the discriminant validity test is carried out. The correlation analysis of the four dimensions is conducted in turn. According to AMOS and Table 9, the discrimination validity analysis in Table 10 is summarized. There are significant correlations among technology, economy, institution, and environment ($P < 0.01$). The absolute value of the correlation coefficient is less than the square root of the corresponding AVE. It indicates that there is a certain correlation between the latent variables. And there is a certain degree of differentiation between them. Therefore, the discriminant validity of the scale data is ideal.

*5.4. Model Interpretation and Analysis.* The value between potential variables represents the degree of other variables changes caused by one variable. The data results show that

Table 6: Principal component information.

| Principal component number | Original | | | Rotating the sum of squares and loads | | |
|---|---|---|---|---|---|---|
| | Total | % of variance | Cumulation% | Total | % of variance | Cumulation% |
| 1 | 7.810 | 60.080 | 60.080 | 3.723 | 28.639 | 28.639 |
| 2 | 1.311 | 10.087 | 70.167 | 2.807 | 21.595 | 50.234 |
| 3 | 0.924 | 7.106 | 77.273 | 2.566 | 19.740 | 69.974 |
| 4 | 0.550 | 4.233 | 81.506 | 1.499 | 11.533 | 81.506 |
| 5 | 0.469 | 3.607 | 85.113 | | | |
| 6 | 0.401 | 3.086 | 88.200 | | | |
| 7 | 0.325 | 2.499 | 90.699 | | | |
| 8 | 0.255 | 1.963 | 92.661 | | | |
| 9 | 0.251 | 1.934 | 94.596 | | | |
| 10 | 0.209 | 1.611 | 96.207 | | | |
| 11 | 0.193 | 1.484 | 97.691 | | | |
| 12 | 0.170 | 1.304 | 98.995 | | | |
| 13 | 0.131 | 1.005 | 100.000 | | | |

Table 7: Rotating component matrix.

| Items | Factor loading values | | | | Factor |
|---|---|---|---|---|---|
| | 1 | 2 | 3 | 4 | |
| A1 | 0.758 | | | | Technology |
| A2 | 0.850 | | | | |
| A3 | 0.841 | | | | |
| B1 | | 0.821 | | | Economy |
| B2 | | 0.855 | | | |
| B3 | | 0.793 | | | |
| C1 | | | 0.815 | | Institution |
| C2 | | | 0.833 | | |
| C3 | | | 0.833 | | |
| D1 | | | | 0.661 | Environment |
| D2 | | | | 0.880 | |
| D3 | | | | 0.850 | |
| D4 | | | | 0.889 | |

path coefficients are all positive. Technical factors, economic factors, institutional factors, and environmental factors are the main factors influencing BIM adoption in construction enterprises in China. The hypothesis model is basically established. Through the analysis of potential variables and observation variables, the observation variables closely related to the potential variables can be obtained. According to the factor load, the main factors influencing BIM adoption in construction enterprises are further explained, as shown in Figures 4 and 5.

As can be seen from the two figures, they represent standardized parameter estimation and nonstandardized parameter estimation in the hypothesis model used by AMOS. According to the above reliability and validity analysis and confirmatory factor analysis, the structural equation model of factors influencing BIM adoption is tested and revised. It is obvious that the key factors affecting the BIM adoption efficiency can be compared and analyzed by each data representing different meanings. From the correct model, it can be concluded that the key factors influencing BIM adoption in AEC firms in China contain technical factors, economic factors, institutional factors, and environmental factors.

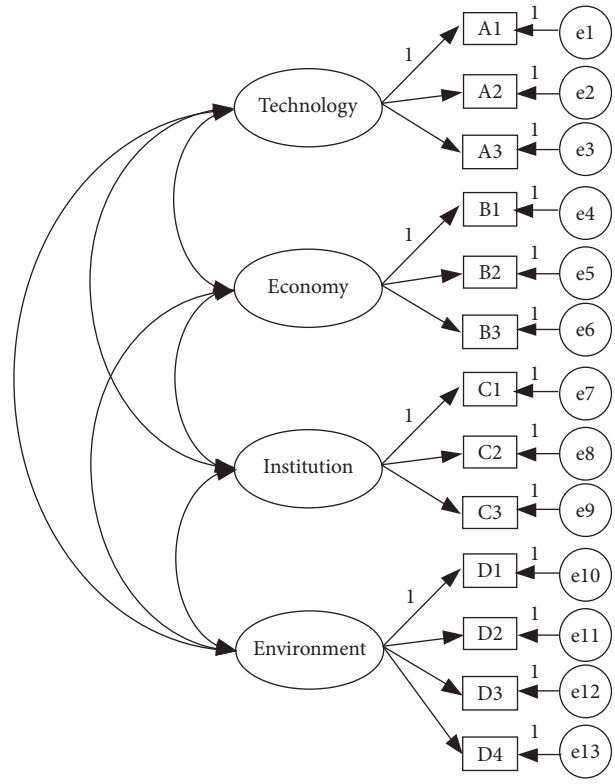


Figure 3: Structural equation model M1.

Technological factor has an impact on BIM adoption; namely, H1 is correct. Technical factors include staff quality, production efficiency, and visibility advantage. The factor load of employee quality is the largest. It shows that the BIM adoption in Chinese construction enterprises has a greater impact on the quality of internal personnel. And the high quality of employees is beneficial to improve the competitiveness of enterprises. Second is production efficiency, and the software of BIM plays a positive role in improving production efficiency and expanding the company's revenue. Compared with other software, BIM has good visibility. It is also one of the factors that affect the BIM adoption.

Table 8: Overall fit index calculation.

| CMIN/DF | RMSEA | GFI | AGFI | CFI | IFI | TLI | SRMR |
|---|---|---|---|---|---|---|---|
| 1.656 | 0.089 | 0.857 | 0.78 | 0.953 | 0.954 | 0.937 | 0.049 |

Table 9: Factor measurement model parameter estimation.

| Title | Path | Factor | Estimation of parameter significance | | | | | | | |
|---|---|---|---|---|---|---|---|---|---|---|
| | | | Unstd. | S.E. | *T*- value | *P* | Std. | SMC | CR | AVE |
| A1 | <--- | Technology | 1.000 | | | | 0.725 | 0.526 | 0.856 | 0.667 |
| A2 | <--- | Technology | 1.107 | 0.160 | 6.923 | *** | 0.857 | 0.734 | | |
| A3 | <--- | Technology | 1.157 | 0.167 | 6.925 | *** | 0.860 | 0.740 | | |
| B1 | <--- | Economy | 1.000 | | | | 0.801 | 0.642 | 0.866 | 0.684 |
| B2 | <--- | Economy | 0.956 | 0.126 | 7.569 | *** | 0.813 | 0.661 | | |
| B3 | <--- | Economy | 1.059 | 0.136 | 7.786 | *** | 0.865 | 0.748 | | |
| C1 | <--- | Institution | 1.000 | | | | 0.767 | 0.588 | 0.867 | 0.685 |
| C2 | <--- | Institution | 1.063 | 0.142 | 7.497 | *** | 0.847 | 0.717 | | |
| C3 | <--- | Institution | 1.086 | 0.144 | 7.544 | *** | 0.865 | 0.748 | | |
| D1 | <--- | Environment | 1.000 | | | | 0.684 | 0.468 | 0.896 | 0.685 |
| D2 | <--- | Environment | 1.048 | 0.147 | 7.117 | *** | 0.887 | 0.787 | | |
| D3 | <--- | Environment | 1.025 | 0.149 | 6.884 | *** | 0.849 | 0.721 | | |
| D4 | <--- | Environment | 1.034 | 0.147 | 7.050 | *** | 0.875 | 0.766 | | |

**The mean *P* value is less than 0.001.

Table 10: Differential validity analysis.

| | Technology | Economy | Institution | Environment |
|---|---|---|---|---|
| Technology | 0.667 | | | |
| Economy | 0.452** | 0.684 | | |
| Institution | 0.439** | 0.315** | 0.685 | |
| Environment | 0.394** | 0.408** | 0.296** | 0.685 |
| Average square root | 0.817 | 0.827 | 0.828 | 0.828 |

**The mean *P* value is less than 0.01, and the diagonal is the extraction amount of variance of AVE evaluation.

Economic factor has an impact on BIM adoption; namely, H2 is correct. Economic factors include training professionals, software application, and investment in R&D. The factor coefficient of training related talents is the largest. It indicates that most companies pay more attention to personnel training. They think that strengthening talent management will have an impact on BIM adoption. Secondly, the wide application level of software and large investment funds show that enterprises pay more attention to capital investment when adopting the technology. Some companies still dare not to take risks, so this is one of the factors that affect the BIM adoption.

Institutional factor has an impact on BIM adoption; namely, H3 is correct. Institutional factors include the completion of BIM standards, the introduction of relevant policies by the government, and the formulation of rules and regulations and laws. Improving BIM standards to adapt to localization and the government's incentive policies is similar. It shows that the government's corresponding behavior and its own standards will have a positive impact on BIM adoption. Therefore, the relevant government and organizations should introduce corresponding incentive policies to encourage users to actively adopt BIM.

Environmental factor has an impact on BIM adoption; namely, H4 is correct. Environmental factors include high-level personnel, making policies within the organization, and changing the organizational structure of personnel. High-level managers attach importance to the technology adoption and change in personnel organizational structure. It shows that, for the internal environment of the organization, the management opinion and management mode of top managers have a great positive impact on BIM adoption. Secondly, the company's internal incentive policies will also promote the application of technology by employees. For the sake of promoting BIM adoption in engineering projects, some rewards should be given to employees who use BIM to complete the project. We can also set up a BIM research group within the company to change the personnel organization structure to better promote the adoption and popularization of BIM.

Based on the above explanation, analysis and research suggestions can be concluded. The four main factors influencing BIM adoption in Chinese construction enterprises are not equally important, and there are also links and influences between them.

## 6. Discussion and Recommendations

*6.1. Discussion.* Combined with the above analysis results, the following conclusions can be proposed: the key factors influencing BIM adoption in Chinese construction enterprises include four main aspects, namely, the technical, economic, institutional, and environmental factors. Based on these results, the priority level of factors can be obtained to help the AEC firms in China in identifying the key factors for BIM adoption efficiency and developing and improving strategies effectively. This is helpful in putting forward the actions of capability improvement in combination with practice project, so as to enhance BIM adoption efficiency and accelerate the pace of information in the Chinese construction enterprises:

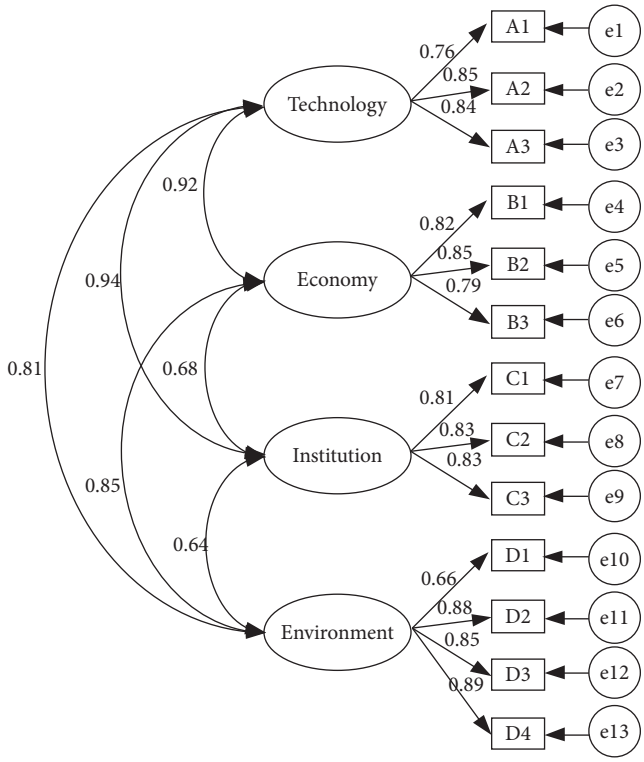


Figure 4: Standardized parameter estimation.

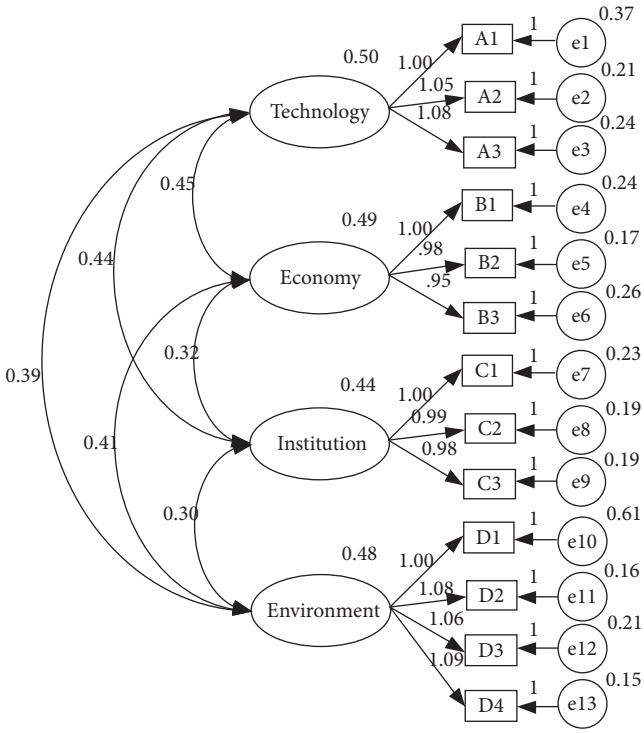


Figure 5: Nonstandardized parameter estimation.

(i) Factor 1: technology. On the basis of the factor loading, the influencing factors are ranked from high to low: production efficiency (A2), quality of employees (A3), and technical advantages (A1). High quality of staff is beneficial to enhance the competitiveness of enterprises. Thus, the awareness of technology adoption will be improved, which will have a positive impact on the BIM adoption. Therefore, construction enterprises pay attention to the cultivation and improvement of employees' skills with the organization. BIM, with its unique advantages, can promote technology adoption. Thereby, it can improve production efficiency and return. Hence, technical factors positively affect BIM adoption in China.

(ii) Factor 2: economy. According to the factor loading, the influencing factors are ranked from high to low: application of software (B2), investment in technology research and development (B1), and train-related talents (B3). To some degree, enterprises pay more attention to capital investment in BIM adoption. The more the investment, the higher the return, the greater the income. Economy is an important point in BIM adoption. However, most of small- and medium-sized Chinese construction enterprises dare not try to invest a lot of money to use BIM. They are afraid of risks in engineering projects, so they will not take action easily. The construction industry is still carried out in the traditional way. Therefore, economic factors are also the key factor affecting the BIM adoption efficiency.

(iii) Factor 3: institution. From the factor loading, the influencing factors are ranked from high to low: government subsidies (C2), improve standards to adapt localization (C3), and improve laws and systems (C1). The finding indicates that government policies also have an impact on BIM adoption. Especially, the external incentives from government will help enterprises' BIM adoption. Improving the corresponding rules and regulations shows that the improvement in laws will also promote the development of BIM. BIM standardization can provide guidance for BIM adoption and promote information delivery and sharing at all stages of the project. In addition, government departments can encourage policy actions to support enterprises to actively adopt BIM. It can also provide official and credible legal and regulatory guidance. More and more organizations would begin to use BIM. Therefore, institution factors will also affect BIM adoption efficiency.

(iv) Factor 4: environment. Based on the factor loading, the influencing factors are ranked from high to low: distribution of talent structure (D4), emphasis on technology adoption (D2), encourage technology adoption (D3), and mandatory use of BIM (D1). It mainly produces external motivation for construction enterprises in BIM adoption by means of compulsory or encouraging. Mandatory use of BIM may promote its implementation in the project and create a better external environment for its

application. When BIM technicians and senior managers pay more attention to the use of BIM, it will positively promote BIM adoption. Thus, environment factors have an impact on BIM adoption.

### 6.2. Recommendations

*6.2.1. Developing a Reasonable Adoption Strategy.* The survey results show that the production efficiency of construction enterprises has a significant impact on BIM adoption. Compared with developed countries, the application depth of BIM is far from enough in China. Therefore, for the promotion and application of BIM, construction enterprises should formulate a clear and reasonable strategic plan to improve the BIM adoption efficiency. For example, employing high-quality employees and preferentially choosing projects requiring BIM is conducive to enhance the company's own competitiveness. It can improve production efficiency and expand industrial income and promote the process of BIM adoption faster and better. It is very important to draw up a reasonable strategic plan for BIM adoption. The performance of construction project will be improved based on the suitable applications associated with multiple BIM technologies. From the technical level, combined with the enterprise's own conditions, the reasonable technology adoption strategy is specified to improve the BIM adoption efficiency. BIM application platform of construction enterprises is the basis of BIM adoption. It is essential to establish a platform suitable for BIM adoption in construction enterprises. The platform can be established by the way of gradual expansion. Firstly, the BIM adoption, data, and other information on the project are integrated. Then, the professional application of BIM is realized. And the data association is completed.

*6.2.2. Optimizing the Direction of Enterprise Investment.* The economic factors that affect the BIM adoption in construction enterprises include the cost of software and hardware, personnel expenses, the cost of restructuring work mode, and the early benefits of using BIM. The survey results show that the cost of training BIM-related talents in technology investment has a significant impact on BIM adoption. A large amount of funds will be an indispensable key condition especially in the secondary development of BIM software and will be put into use. Because it has a certain degree of professionalism and involves many fields, enterprises will have a huge cost investment. The R&D of software should be combined with the characteristics of the Chinese engineering management to speed up BIM's work efficiency. Therefore, the enterprise should make a reasonable resource allocation plan according to its actual situation, for instance, training or hiring BIM professionals in an all-round way, investing a lot of funds in BIM adoption, maximizing the value of BIM, and achieving a direct ratio between investment and return. For this reason, the more the investment, the higher the return, the greater the income. In this way, BIM should make a reasonable investment and investment in technology to the greatest extent.

*6.2.3. Holistic BIM Standard.* BIM was first originated in developed countries and then introduced into China. Most of the research results of BIM and other related contents are developed by external researchers. Therefore, sometimes, in the BIM adoption, due to its technical standards and legal environment that do not meet the relevant requirements of China's construction industry, the adoption efficiency will be reduced. The establishment of BIM standards is the core content of implementation. Only when the BIM adoption experience is refined into the standard of overall application of enterprises, can these experiences be truly transformed into productivity. Thus, the overall BIM adoption efficiency and quality can be improved. First, construction enterprises can refer to the regulations of local government or BIM technical standards formulated by developed countries, forming a set of holistic BIM standards for Chinese construction enterprises to better apply BIM. Second is formulating and improving BIM technical regulations and laws for the long-term development of construction enterprises, so as to adapt to the localization of BIM. Based on this, construction enterprises can protect their rights and interests by specifying their rights and interests in the contract and the delivery standard of the final model. In addition, relevant government departments support BIM adoption and introduce corresponding subsidy policies, which will also promote BIM adoption. Through the above, we can improve the BIM adoption efficiency from the institutional level.

*6.2.4. Changing the Internal Environment of Enterprises.* According to the survey results, top managers within the organization attach importance to the BIM adoption is a major influencing factor. If enterprises want to improve the BIM adoption efficiency, they should encourage senior leaders to accept BIM and enhance their trust in it. Therefore, we can formulate relevant policies and systems to improve the management's recognition of BIM. Construction enterprises can establish a good incentive mechanism to encourage the pilot work of various BIM projects, constantly accumulating experience in the pilot projects, training the team, and improving the BIM standard system. They can also appropriately change the internal talent structure allocation in order to make BIM better applied. For example, special funds are set up to encourage employees who study or apply BIM independently, establish a study group, add corresponding BIM assessment mechanism, hold some related competitions about BIM, and hold a seminar on BIM once a month. Above all, it can fully mobilize the enthusiasm of enterprise employees to adopt BIM and better promote the adoption efficiency of it.

## 7. Conclusions

Compared with developed countries, due to backward technology, lower economy, and incomplete BIM system, the effect of BIM adoption is pessimistic in construction enterprises in developing countries. Although BIM has been invented for years, the depth and breadth of its

popularization are far from enough in developing countries, such as China. Also, there is a lack of comprehensive research on the impact of BIM adoption in Chinese construction enterprises. BIM adoption will encounter great challenges. Therefore, it is necessary to identify and discuss factors influencing BIM adoption in an all-round way. In this way, the key factors are determined. BIM adoption efficiency would be improved by taking appropriate strategies in Chinese construction enterprises.

This paper determines the influencing factors on the basis of previous literature, which is used to form a questionnaire. According to the collected data, the hypothesis model is established. For verifying and modifying the hypothesis model, the structural equation modeling method and AMOS and SPSS software are utilized. These factors were divided into four different levels in a hierarchy in accordance with SEM analysis. The results suggest that the influencing factors are arranged from large to small: technology ($\beta = 0.50$), economy ($\beta = 0.49$), environment ($\beta = 0.48$), and institution ($\beta = 0.44$). According to the factor load, in terms of technical factors, it shows that A2 ($\beta = 0.85$) > A3 ($\beta = 0.84$) > A1 ($\beta = 0.76$). In terms of economic factors, it shows that B2 ($\beta = 0.85$) > B1 ($\beta = 0.82$) > B3 ($\beta = 0.79$). In terms of institutional factors, it shows that C2 ($\beta = 0.83$) = C3 ($\beta = 0.83$) > C1 ($\beta = 0.81$). In terms of environmental factors, it shows that D4 ($\beta = 0.89$) > D2 ($\beta = 0.88$) > D3 ($\beta = 0.85$) >D1 ($\beta = 0.66$). Based on the weight, combined with the practical situation, BIM adoption strategies of construction industries are proposed. The theoretical contributions of this research are as follows: (1) key factors influencing BIM adoption from the perspective of all construction enterprises in China are distinguished and discussed; (2) the analysis system of BIM adoption influencing factors is established by the SEM method. The influencing factors are summarized and sorted from primary to secondary to determine the key factors. The findings of this study are expected to provide a better understanding of the essential elements affecting BIM adoption in the construction industries and guide industry practitioners in developing proper strategies to achieve more effective BIM adoption. Thus, for improving the efficiency faster, the construction enterprises with low efficiency in BIM adoption should focus on solving the main factors. On the contrary, various influencing factors could be balanced to define suitable policies and strategies for construction enterprises with relatively good BIM adoption efficiency. From the perspective of the world, China can be taken as an empirical case. For other developing countries, combined with their own characteristics, it more effectively improves the BIM adoption efficiency and improves the production efficiency of construction enterprises, furthermore developing the economy to a greater extent.

Besides, there are still some limitations on this study. This paper studies the key factors of BIM adoption from the perspective of all construction enterprises in China. When the questionnaire was issued to all types of Chinese construction enterprises, there was no classification study and discussion on different types of AEC firms in China. Owing to the influence of different factors on each type of construction enterprises is different, and the obtained results are also diverse. Therefore, based on large enough sample data and research literature, future research would provide a reasonable classification of Chinese construction enterprises. Then, the key influencing factors of BIM adoption will be studied for different types of construction enterprises from diverse perspectives.

## Data Availability

The data used to support the findings of this study are available from the corresponding author upon request.

## Conflicts of Interest

There are no conflicts of interest regarding the publication of this paper.

## Acknowledgments

This research was funded by the National Natural Science Foundation of China (NSFC) (no. 71801119). The work described in this paper was also supported by the Social Science Planning Foundation of Liaoning Province (nos. L20BGL031 and L20BGL056), the Economic and Social Development Research Foundation of Liaoning Province (nos. 20211slqnkt-014 and 20211slqnkt-019) and the Fundamental Research Funds for the Central Universities (no. 3132020224).

## References

[1] Y. Liu, S. van Nederveen, and M. Hertogh, "Understanding effects of BIM on collaborative design and construction: an empirical study in China," *International Journal of Project Management*, vol. 35, no. 4, pp. 686–698, 2017.

[2] M. Yalcinkaya and V. Singh, "Patterns and trends in building information modeling (BIM) research: a latent semantic analysis," *Automation in Construction*, vol. 59, pp. 68–80, 2015.

[3] McGraw Hill Construction, *The Business Value of BIM for Owners*, McGraw Hill, New York, NY, USA, 2014.

[4] Y. Arayici, P. Coates, L. Koskela et al., "Technology adoption in the BIM implementation for lean architectural practice," *Automation in Construction*, vol. 20, no. 2, pp. 189–195, 2011.

[5] D. Navendren, P. Manu, M. Shelbourn, and A. Mahamadu, "Challenges to building information modelling implementation in UK: designers' perspectives," in *Proceedings of the 30th Annual ARCOM Conference*, pp. 733–742, Association of Researchers in Construction Management, Portsmouth, UK, September 2014.

[6] R. Ramilo and M. R. B. Embi, "Critical analysis of key determinants and barriers to digital innovation adoption among architectural organizations," *Frontiers of Architectural Research*, vol. 3, no. 4, pp. 431–451, 2014.

[7] J. Feng, *Research on Project Management Maturity Model Based on BIM Technology*, Kunming University of Science and Technology, Kunming, China, 2014.

[8] N. Gu and K. London, "Understanding and facilitating BIM adoption in the AEC industry," *Automation in Construction*, vol. 19, no. 8, pp. 988–999, 2010.

[9] S. Ibrahim and I. Birshir, "Review of using building information modeling in Nigerian construction industry," *Journal*

*of Environmental Sciences and Policy Evaluation*, vol. 2, no. 2, pp. 52–62, 2012.

[10] J. Park, H. Lee, and P. Kwak, "Case study on the application of BIM in Korea's civil engineering and improvement of interoperability of BIM models," *International Journal of Software Engineering and Its Applications*, vol. 9, no. 10, pp. 29–38, 2015.

[11] D. Cao, H. Li, G. Wang, and T. Huang, "Identifying and contextualising the motivations for BIM implementation in construction projects: an empirical study in China," *International Journal of Project Management*, vol. 35, no. 4, pp. 658–669, 2017.

[12] J. Zhang, Y. Long, S. Lv, and Y. Xiang, "BIM-enabled modular and industrialized construction in China," *Procedia Engineering*, vol. 145, pp. 1456–1461, 2016.

[13] MOHURD, *China Construction Industry Information Development Report: BIM's Deep Application and Development*, Ministry of Housing and Urban-Rural Development, Beijing, China, 2015.

[14] Y. Li, Z. Liao, and H. Yuan, "Investigating the Impacts of BIM on project parties and its application," *Construction Technology*, vol. 43, no. 6, pp. 522-523, 2014, in Chinese.

[15] S. Azhar, "Building information modeling (BIM): trends, benefits, risks, and challenges for the AEC industry," *Leadership and Management in Engineering*, vol. 11, no. 3, pp. 241–252, 2011.

[16] S. Zheng, H. Si, and L. Zhang, "The empirical research of BIM technology adoption intention based on UTAUT," *Science and Technology Management Research*, vol. 19, pp. 230–235, 2016, in Chinese.

[17] P. Goodridge, J. Haskel, and G. Wallis, *UK Innovation Index: Productivity and Growth in UK Industries*, Imperial College, London, UK, 2012.

[18] S. Lee, J. Yu, and D. Jeong, "BIM acceptance model in construction organizations," *Journal of Management in Engineering*, vol. 31, no. 3, 2015.

[19] H. Yuan, Y. Yang, and X. Xue, "Promoting owners' BIM adoption behaviors to achieve sustainable project management," *Sustainability*, vol. 11, no. 14, p. 3905, 2019.

[20] R. Ahuja, M. Jain, A. Sawhney, and M. Arif, "Adoption of BIM by architectural firms in India: technology-organization-environment perspective," *Architectural Engineering and Design Management*, vol. 12, no. 4, pp. 311–330, 2016.

[21] X. Qin, Y. Shi, K. Lyu, and Y. Mo, "Using a Tam-toe model to explore factors of building information modelling (Bim) adoption in the construction industry," *Journal of Civil Engineering and Management*, vol. 26, no. 3, pp. 259–277, 2020.

[22] C. Carnaghan and K. Klassen, ""Exploring the determinants of web-based E- business evolution in Canada," in americas conference on information systems (AMCIS)," p. 225, 2007.

[23] A. Songer, R. Young, and K. Davis, "Social architecture for sustainable IT implementation in AEC/EPC," in *Proceedings of IT in Construction of Africa*, Mpumalunga, South Africa, 2001.

[24] H. C. J. Linderoth, "Understanding adoption and use of BIM as the creation of actor networks," *Automation in Construction*, vol. 19, no. 1, pp. 66–72, 2010.

[25] A. Sawhney, *State of BIM Adoption and Outlook in India*, RICS School of Built Environment, Amity University, Noida, India, 2014.

[26] H. Xu, J. Feng, and S. Li, "Users-orientated evaluation of building information model in the Chinese construction industry," *Automation in Construction*, vol. 39, pp. 32–46, 2014.

[27] B. Succar, "Building information modelling maturity matrix," *Concepts and Technologies*, pp. 65–103, IGI Global, Hershey, PA, USA, 2010.

[28] A. Chew and M. Riley, "What is going on with BIM? On the way to 6D," *International Construction of Law Review*, vol. 30, pp. 253–265, 2013.

[29] NATSPEC, *National BIM Guide v1.0*, NATSPEC, Sydney, Australia, 2011.

[30] Y. X. Gong, "Analysis on the application status and development obstacles of BIM in China," *Electronic Commerce*, vol. 46, pp. 204-205, 2012.

[31] NBS International BIM Report, *Newcastle upon Tyne*, NBS International BIM Report, London, UK, 2016.

[32] A. Elmualim and J. Gilder, "BIM: innovation in design management, influence and challenges of implementation," *Architectural Engineering and Design Management*, vol. 10, no. 3-4, pp. 183–199, 2014.

[33] T. Oliveira and M. F. Martins, "Literature review of information technology adoption models at firm level," *The Electronic Journal Information Systems Evaluation*, vol. 14, no. 1, pp. 110–121, 2011.

[34] F. D. Davis, R. P. Bagozzi, and P. R. Warshaw, "User acceptance of computer technology: a comparison of two theoretical models," *Management Science*, vol. 35, no. 8, pp. 982–1003, 1989.

[35] A. Bandura and D. Cervone, "Differential engagement of self-reactive influences in cognitive motivation," *Organizational Behavior and Human Decision Processes*, vol. 38, no. 1, pp. 92–113, 1986.

[36] K. T. Manis and D. Choi, "The virtual reality hardware acceptance model (VR-ham): extending and individuating the technology acceptance model (TAM) for virtual reality hardware," *Journal of Business Research*, vol. 100, pp. 503–513, 2019.

[37] T. M. Broman, G. Schuitema, and J. Thogersen, "Responsible technology acceptance: model development and application to consumer acceptance of smart grid technology," *Applied Energy*, vol. 134, pp. 392–400, 2014.

[38] G. Prati, V. Marín Puchades, M. De Angelis et al., "Evaluation of user behavior and acceptance of an on-bike system," *Transportation Research Part F: Traffic Psychology and Behaviour*, vol. 58, pp. 145–155, 2018.

[39] P. Legris, J. Ingham, and P. Collerette, "Why do people use information technology? A critical review of the technology acceptance model," *Information & Management*, vol. 40, no. 3, pp. 191–204, 2003.

[40] L. G. Tornatzky and M. Fleischer, *The Processes of Technological Innovation*, Lexington Books, Lanham, MD, USA, 1990.

[41] R. Drazin, "The processes of technological innovation," *The Journal of Technology Transfer*, vol. 16, no. 1, pp. 45-46, 1991.

[42] P.-F. Hsu, K. L. Kraemer, and D. Dunkle, "Determinants of E-business use in U.S. Firms," *International Journal of Electronic Commerce*, vol. 10, no. 4, pp. 9–45, 2006.

[43] J. X. Zhang, "Research on application obstacles of building information model in engineering design industry in China," *Journal of Engineering Management*, vol. 4, pp. 387–392, 2010.

[44] Q. H. He, L. L. Qian, Y. F. Duan, and Y. K. Li, "Application status and obstacles of BIM at home and abroad," *Journal of Engineering Management*, vol. 26, no. 1, pp. 12–16, 2012.

[45] Y. Li, *Research on Influencing Factors of BIM Application in Construction Enterprises*, Wuhan Technology University, Wuhan, China, 2015, in Chinese.

[46] L. Y. Zhang, Y. W. Li, and Y. Gao, "Application obstacles and countermeasures of BIM technology," *Journal of Civil Engineering and Management*, vol. 3, pp. 65–154, 2013.

[47] D. Cao, G. Wang, H. Li, M. Skitmore, T. Huang, and W. Zhang, "Practices and effectiveness of building information modelling in construction projects in China," *Automation in Construction*, vol. 49, pp. 113–122, 2015.

[48] B. Ozorhon and U. Karahan, "Critical Success factors of building information modeling implementation," *Journal of Management Engineering*, vol. 33, no. 3, 2017.

[49] J. Won, G. Lee, C. Dossick, and J. Messner, "Where to focus for successful adoption of building information modeling within organization," *Journal of Construction Engineering and Management*, vol. 139, no. 11, 2013.

[50] Y. Liu, S. V. Nederveen, and M. Hertogh, "Understanding effects of BIM on collaborative design and construction: an empirical study in China," *International Journal of Project Management*, vol. 35, no. 4, pp. 686–698, 2016.

[51] Y. Han and P. Damian, "Benefits and barriers of building information modeling," in *Proceedings of the 12th. International Conference on Computing in Civil and Building Engineering*, Beijing, China, October 2008.

[52] A. Salman, H. Michael, and S. Blake, "Building information modeling (BIM): benefits risks and challenges," in *Proceedings of the 44th ASC Annual Conference on CDROM*, Auburn, Alabama, April 2008.

[53] U. Lsikdag, "Design patterns for BIM-based service-oriented architectures," *Automation in Construction*, vol. 25, pp. 59–71, 2012.

[54] A. Mutai, *Factors Influencing the Use of Building Information Modeling (BIM) within Leading Construction Firms in the United States of America*, Indiana State University, Terre Haute, IN, USA, 2009.

[55] Shanghai Construction Industry Association and Shanghai Luban Consulting Company, *Annual Research Report on BIM Technology Application Status in Construction Enterprises*, Shanghai Construction Industry Association and Shanghai Luban Consulting Company, Shanghai, China, 2014.

[56] X. Qin, M. Mancini, and A. Travaglini, "A comparative study on barriers between China and Italy in BIM adoption from the construction market perspective," *Chinese Journal of Management*, vol. 13, no. 11, pp. 1718–1721, 2016.

[57] N. W. Young, S. A. Jones, and H. M. Bernstein, *Building Information Modeling Transforming Design and Construction to Achieve Greater Industry Productivity*, McGraw-Hill Construction, New York, NY, USA, 2008.

[58] M. E. Obiegbu and F. O. Ezeokoli, "Building information modeling, a panacea for timely project delivery," in *Proceedings of the River State Quantity Surveyor's Week Holding at the Arena Event Centre*, Port Harcourt, Nigeria, 2014.

[59] A. H. Memon, I. A. Rahman, I. Memon, and N. A. Azman, "BIM in Malaysian construction industry: status, advantages, barriers and strategies to enhance the implementation level," *Research Journal of Applied Sciences, Engineering and Technology*, vol. 8, no. 5, pp. 606–614, 2014.

[60] R. Balocco, R. Mogre, and G. Toletti, "Mobile internet and SMEs: a focus on the adoption," *Industrial Management & Data Systems*, vol. 109, no. 2, pp. 245–261, 2009.

[61] J. Li, *Hinder Research of BIM Technology Diffusion*, Harbin Institute of Technology, Harbin, China, 2014, in Chinese.

[62] Y. Li, *BIM Application in the Building Construction Enterprise*, Wuhan University of Science and Technology, Wuhan, China, 2015, in Chinese.

[63] M. R. Hosseini, E. Azari, L. Tivendale, and N. Chileshe, "Barriers to adoption of building information modeling (BIM) in Iran: preliminary results," in *Proceedings of the 6th International Conference on Engineering, Project, & Production Management (EPPM2015)*, Griffith University, Logan City, Australia, 2015.

[64] Y. Wang, *BIM Technology Adoption Model and Implication Research*, Harbin Institute of Technology, Harbin, China, 2013, in Chinese.

[65] R. Eisenberger, P. Fasolo, and V. Davis-LaMastro, "Perceived organizational support and employee diligence, commitment, and innovation," *Journal of Applied Psychology*, vol. 75, no. 1, pp. 51–59, 1990.

[66] L. M. Shore and S. J. Wayne, "Commitment and employee behavior: comparison of affective commitment and continuance commitment with perceived organizational support," *Journal of Applied Psychology*, vol. 78, no. 5, pp. 774–780, 1993.

[67] C. L. Pearce and P. A. Herbik, "Citizenship behavior at the team level of analysis: the effects of team leadership, team commitment, perceived team support, and team size," *The Journal of Social Psychology*, vol. 144, no. 3, pp. 293–310, 2004.

[68] R. Eisenberger, R. Huntington, S. Hutchison, and D. Sowa, "Perceived organizational support," *Journal of Applied Psychology*, vol. 71, no. 3, pp. 500–507, 1986.

[69] R. Mcmillan, *Customer Satisfaction and Organizational Support for Service Providers*, University of Florida, Gainesville, FL, USA, 1997.

[70] H.-F. Lin, "An investigation into the effects of is quality and top management support on ERP system usage," *Total Quality Management & Business Excellence*, vol. 21, no. 3, pp. 335–349, 2010.

[71] S.-Y. Lee and X.-Y. Song, "Model comparison of nonlinear structural equation models with fixed covariates," *Psychometrika*, vol. 68, no. 1, pp. 27–47, 2003.

[72] J. Pearl, *Causality: Models, Reasoning, and Inference*, Cambridge University Press, Cambridge, UK, 2000.

[73] R. P. Bagozzi and Y. Yi, "On the evaluation of structural equation models," *Journal of the Academy of Marketing Science*, vol. 16, no. 1, pp. 74–94, 1988.

[74] J. C. Nunnally, *Psychometric Theory*, McGraw-Hill, New York, NY, USA, 2nd edition, 1978.

[75] J. F. Hair, R. E. Anderson, R. L. Atham, and W. C. Black, *Multivariate Data Analysis with Readings*, Prentice-Hall, Upper Saddle River, NJ, USA, 1998.

Hindawi
Advances in Civil Engineering
Volume 2020, Article ID 8842113, 18 pages
https://doi.org/10.1155/2020/8842113

*Review Article*

# Special Issue "Digital Twin Technology in the AEC Industry"

**Jisong Zhang**,[1] **Lihua Zhao**,[1] **Guoqian Ren**,[2] **Haijiang Li**,[2] **and Xiaofei Li**[3]

[1]*School of Civil Engineering, Dalian Jiaotong University, Dalian 116028, China*
[2]*Cardiff School of Engineering, Cardiff University, Cardiff CF24 3AA, UK*
[3]*Institute of Road and Bridge Engineering, Dalian Maritime University, Dalian 116026, China*

Correspondence should be addressed to Guoqian Ren; reng@cardiff.ac.uk

Received 30 July 2020; Revised 20 October 2020; Accepted 11 November 2020; Published 27 November 2020

Academic Editor: Qian Wang

Copyright © 2020 Jisong Zhang et al. This is an open access article distributed under the Creative Commons Attribution License, which permits unrestricted use, distribution, and reproduction in any medium, provided the original work is properly cited.

Sustainable building design has become a hot topic over the past decades. Many standards, databases, and tools have been developed for achieving a sustainable building. Not until recently have the importance of structural engineering and its contribution to sustainable building design been full recognised. However, due to the highly fragmented and diversity of knowledge across building and infrastructure domains, there is a lack of approach that can address all the sustainable issues within the structural design. This paper reviews the sustainable design from the perspective of structural engineering: (1) reviewing the current situation; (2) identifying the gaps and difficulties; and (3) making recommendations for future improvements. The strategies and indicators, as well as BIM-enabled methodology, for sustainable structural design (SSD) are also discussed in a holistic way. The results of this investigation show that most of the methods are not doing well in terms of delivering a successful sustainable structural design. It is expected that the future BIM could probably provide such a platform to address these issues.

## 1. Introduction

What is a "sustainable building?" Written works define it as being designed to adhere to several objectives: (1) to preserve energy and materials and ensure that resources are recycled and that the release of toxic substances is limited throughout the building's process, encompassing the design, building, functioning, preservation, and destruction; (2) to suitably comply with the local environment, values, and societal structure; and (3) to maintain and enhance the standard of people's living whilst preserving the ecosystem's aptitude domestically and globally [1]. This definition brought together what is now known as the three pillars of sustainability [2–4]: environmental, economical, and social well-being. In general, design methods for achieving a sustainable building are called "sustainable design."

There are many standards, databases, and tools dedicated to sustainable design in the building sector. The standards including ISO/TC 59/SC 17, ISO/TC 207/SC 5, and CEN/TC 350 lay the foundations for assessing the sustainability of a building during the life cycle. These standards measure the influence and elements of buildings in terms of their environmental, social, and financial impact via quantitative and qualitative signs [5–7]. In most cases, these series of standards are merely served as guidelines and need to be used in conjunction with a specific database or rating score system since they provide little information on benchmarks, levels of performance, and detailed information [8]. Several databases currently exist for the measurement of embodied energy or embodied carbon: Inventory of Carbon and Energy (ICE), U.S. Life Cycle Inventory (LCI), GaBi, European Reference Life Cycle Database (ELCD), and Ecoinvent [9, 10]. In order to automate the sustainability assessment of a building, many companies and international organisations have initiated rating systems and tools to facilitate the assessment process. The rating systems such as BREEAM and LEED group the environmental impacts into several sections, produce an overall score for the building depending on points gained in each section, and deliver a certificated assessment [11–13]. However, these assessments are normally conducted after the design phase and serve primarily as a verification document rather than a decision-aid tool, providing little guidance for the designer during the design process [14, 15]. Despite the emerging life cycle assessment

(LCA) tools (i.e., Athena and Tally) provide more opportunity to assist sustainable design on a building scale, the procedure is similar to the rating systems (i.e., sustainable assessment after the design stage). It seems difficult to integrate sustainability idea/knowledge into the early design stage. This forces us to rethink of the nature of the building design process.

A building is better expressed as a process than a product. The design process of a building normally requires effective and close cooperation among different disciplines (i.e., structural engineers, architects, and MEP engineers). Architects can start drafting architectural designs once they know the needs of the consumer, the tone and idea of the design, and the core mechanical requirements. The models devised outline the relevant geometrical aspects and appearance of the building. At times, this is accompanied by a range of recommendations regarding the structure; this is compiled into either a model or a drawing of the building's design. Emphasis will then be given to the structural and MEP consideration. The structural engineer is required to make the designs more straightforward so that the model can be structurally analysed and optimised to improve the structural performance. This iterative mechanism ceases when the aims of the design are fulfilled [16]. Ultimately, the structural models, architectural models, and MEP information need to be assembled together for the purpose of sustainability assessment. The above describes the current sustainable design process, a "bottom-up" process, while a more reasonable procedure should be a "top-down" process where sustainability is considered at an early design stage for each engineer [17]. This poses a challenge to planning and handling the process properly.

On the contrary, the type of structural system is a significant aspect because it sets the foundation for the design and building work that is undertaken; the nature of the structure layout significantly impacts the use of land, resources, and energy, the release of greenhouse gas, preservation, recycling, the cost of the process, and the management of risks [18, 19]. Moreover, the structural material accounts for a large proportion of a building's mass, thus providing over 50% of the embodied energy and carbon of a building [20–22]. However, despite this growing awareness, there is scant evidence that the importance of a structural engineer has been sufficiently recognised. Structural engineers do, however, have less influence over a building's sustainability in comparison to architects and clients. This can be due to the fact that the knowledge of sustainability for structural engineers is highly fragmented, and there are no clear guidance and effective tools to assist structural engineers for performing sustainable design [23, 24]. Some studies focus on methodologies, strategies, and parameters for sustainable structural design. For instance, Anderson and Silman [25] investigated the differential impact of material selection, recycling, adaptability, and thermal mass effects on greenhouse gas reduction. They identified that the thermal mass effects contribute a lot to reducing carbon dioxide emissions, and material selection is the most positive design strategy before the operational stage of a building. Danatzko and Sezen [26] discussed five positive and negative sustainable attributes of sustainable structural design methodologies. They suggested that no single methodology can address the complex issues of sustainable structural design, and a combination of the methodology is recommended. More details are discussed in Section 3.2.

Several researchers pay attention to compare the case study by calculating embodied energy or carbon of a structure. For example, Sinha et al. [27] performed a comparative study for calculating the energy footprint and carbon footprint between the wooden building and concrete building. The results indicated that the energy footprint of the wooden building is 43% lower than that of the concrete building, and the carbon footprint of the wooden building is 75% lower than that of the concrete building. Guggemos and Horvath [28] compared the environmental effects between concrete and steel-framed structures (much of the same layout) over the life cycle. During the construction phase, compared to the steel structure, the concrete structure consumed more energy, $CO_2$, CO, $NO_2$, and $SO_2$ due to the large formwork, longer equipment uses, and more materials to be transported; thus, minimizing the amount of temporary material use is an effective way to reduce the impact. However, when expanding the construction phase to a wider range (i.e., entire life cycle including design, construction, use, and end of life), the differences gradually disappear due to the fact that the use phase accounts for over 80% energy use and $CO_2$ emissions over the life cycle, whatever material is used in the frame structure. Catherine et al. [29] analysed 200 building structures from the industry to benchmark their environmental impact. The normalised material weights for all the structures were 200–1800 kg/m$^2$, and normalised embodied $CO_2$ ranged between 150 and 600 kg $CO_{2e}$/m$^2$.

In theory, these methodologies and strategies can be used for sustainable structural design (SSD) [30, 31], while in reality, they have not been utilised effectively in a holistic way. This can be attributed to several reasons. Firstly, unlike the sustainable design approach for architects, there are no exclusive standard, database, and tools specifically designed for structural engineers to achieve a sustainable structure. Secondly, the structural engineer's tools, such as structural analysis software, sustainability assessment software, and BIM software, exist as separate entities. Despite there exists the interoperability that is based on interoperable languages (i.e., IFC and gbXML), the process for converting the format is a time-consuming task and may lead to data loss at times. Lastly, there is a lack of effective collaboration between architects and structural engineers. Generally, most of the tasks related to sustainability belong to architects who represent the whole design team to communicate with the sustainability consultant. It should be recognised that not only architects but also structural engineers have great potential to reduce the environmental impact over the design process [32–37]. The ultimate goals of sustainable design can be achieved by efficient information exchange and effective collaboration between structural engineers and architects. A central repository, namely, common data environment, would contribute to the high level of

cooperation. In this case, there is a need to have a unified platform that can integrate sustainability considerations within a common environment between designers.

Building information modelling (BIM) involves a standardised process that ensures relevant data and expertise are reused across various fields in the life cycle process. BIM has the trend for constantly growing to utilise the wide array of information that comprises a conventional building project. This information, referenced as being *n*-dimensional (nD), incorporates elements including time, expense, sustainability, and potential risks. As with several other nD building elements, incorporating the issue of sustainability into BIM is yet to be fully developed [38–40]. Currently, there are many methods that can integrate sustainability issues into BIM or conduct sustainable assessment based on the BIM models [41–44]. For example, Ilhan and Yaman [45] extracted the IFC data from BIM models and proposed a green building assessment method for assisting designers in the generation of documentation for obtaining green building certification based on the BREEAM category. The method can automatically calculate the green rating and provide feedbacks to inform the design. Shadram et al. [46] identified the lack of interoperability between BIM and LCA tools and proposed a framework to integrate extract, transform, load (ETL) into BIM to enhance BIM-LCA interoperability and thus enable a semiautomated assessment process. Although structural engineers can use these methods for making a rough sustainable assessment of their design, these methods are specifically tailored for architects or clients. From the structural engineering perspective, several attempts have been made to combine BIM, structural analysis, and LCA or develop API to accomplish structural sustainability appraisal in BIM [47–49]. Yet there exist many papers on green BIM or structural optimization, most of them have several steps for conversion among different formats, the commonly accepted (standardised) procedure is lacking. Currently, BIM software is still a long way from being fully integrated with various databases for the sustainable design project. Better and more seamless integration between BIM and sustainable design may come in the future, but currently, the integration requires considerable effort and time such that the evaluation of sustainable data ends up being performed after the design stage in most cases.

As a result, this paper attempts to fill the gap by reviewing sustainable design with emphases on the structure. The specific objectives are (1) to investigate the current situation of sustainable design, especially sustainable structural design; (2) to identify the challenges and problems associated with integrating the sustainability issue into structural design; and (3) to discuss solutions and potential development for achieving a holistic design. The review consists of mainly two parts: in the first part, a comprehensive investigation of the standards, databases, tools, and software regarding sustainability in the sustainable building design domain is identified through a wide range of sources. The emphasis is put on the aspects that are directly related to the structural design. In the second part, the current statuses of sustainable structural design (SSD) are investigated with emphases on the strategies and indicators. Furthermore, the BIM-enabled methodology for achieving a sustainable structural design is also summarized. The challenge that sustainability-BIM integration faces is discussed, and the solutions to this incorporation are proposed for future improvements.

## 2. Sustainable Design for Buildings

*2.1. Standards.* Over the past decades, a significant number of sustainable design approaches for buildings have been developed by diverse organisations throughout the world. The term "sustainable design approaches" in this paper refers to all the standards, databases, and tools regarding sustainability in the building design domain. The history of sustainability towards standardization can be traced back to 1993 when a standardised approach called the "code of practice" was developed by the Society of Environmental Toxicology and Chemistry (SETAC) [50]. The approach divided the sustainable assessment into a three-step process, including the definition of the goal and scope of the LCA, the Life Cycle Inventory analysis (LCI) phase, the life cycle impact assessment (LCIA) phase. The International Organisation for Standardisation (ISO) attempts to provide an additional definition of this in the mid of 1990s. A series of LCA criteria was then defined or updated by the ISO including Subcommittee 5 (SC 5), Technical Committee 207 (TC 207), and Life Cycle Analysis and Environmental Management. In 1997, based on the three-phase process proposed by the SETAC, ISO 14040 was released by incorporating the "life cycle interpretation" phase into the criteria. Since ISO 14040 provides only the principle and framework without describing and specifying any detailed LCA methodologies and techniques, ISO 14041, ISO 14042, and ISO 14043 were produced with the aim of providing strategies of the methodological basis during 1998 and 2000 [51, 52].

Yet, this criterion is only aimed to provide a universal approach for LCA practice and hence does not correspond with the extensive judgements needed in relation to modelling when conducting an LCA. As a result, the standards proposed by ISO/TC 207/SC 5, ISO identified that the broad array of possible implementations for LCA needed field-specific Technical Committees to provide an additional definition of LCA that incorporated the expert opinion of those working in the area. As a result, Subcommittee 17 (sustainability in building and civil engineering works, SC17) was developed under TC 59 (buildings and civil engineering works) to produce numerous criterions that provide additional definitions of the LCA framework. Therefore, various criteria and guidelines (ISO 21929, ISO 21930, and ISO 21931) were produced under the direct command of ISO/TC 59/SC 17.

The ISO standards outlined above are regarded as the standard international outlook regarding LCA conduct. However, the necessity for a consensus has resulted in the ISO failing to consider certain modelling aspects that are needed for standardised LCA practice. For that reason, the European Committee for Standardisation (CEN) Technical Committee 350 (TC 350) was introduced in 2005, aiming at

ensuring LCA standards being developed for building works. EN 15643, EN 15804, and EN 15978 were established under CEN/TC 350 by considering more factors in regard to the preservation of the environment. In a similar way to ISO/TC 59/SC 17, CEN/TC 350 started by placing its emphasis on guidelines for buildings rather than civil engineering, although TC 360 has of late implemented Working Group 6 (WG 6) that is intended to advance guidelines for the future that are relevant to civil engineering. All the aforementioned standards are summarized in Table 1 with more detail.

The biggest challenge for the standard is that there is a lack of reliable, comparable benchmarks and transparency in the methodologies. The results of building assessment are not comparable to one another. Furthermore, the above series of standards are used as frameworks or guidelines for sustainable design since they do not provide benchmarks, levels of performance, and detailed information, which need to be used in conjunction with a specific database or score system. Whilst LCA is an important mechanism for contemplating the influence of judgements in terms of the system, it is the only one mechanism that should be utilised for considering sustainability from a wider perspective. The limitation of LCA concerns its generic Life Cycle Inventory (LCI) datasets that overlook the viability of special and temporal matters. For instance, "land use" is seldom incorporated into LCA as there are no means of recording it within an inventory that is widely recognised. Studies into LCA have delivered significant process in introducing acknowledged ways of measuring land, water, waste, and flows that happen over a range of locations and times.

*2.2. Databases.* During the LCA process, the inventory analysis is an important step since the LCI database gives the basic data for life cycle assessment. In recent years, there has been an increasing amount of databases worldwide that can be used to carry out an life cycle assessment. These databases can be divided into two types: general database and specific database. The difference between the general database and specific database lies in the data coverage. General database refers to the data that may cover many fields (e.g., transportation, agriculture, manufacturing, building, chemicals, and waste management), whereas the specific database in this paper means that they are targeted for only one field (i.e., building or construction). General databases contain the European Life Cycle Database (ELCD), U.S. LCI, Swiss Ecoinvent, and German GaBi [53–55]. Specific databases include the Inventory of Carbon and Energy (ICE) from UK, Canadian Athena, Australian building products LCI, and New Zealand building material embodied energy database [56, 57]. The specific databases are normally designed for the life cycle assessment of a building. Table 2 gives a nonexhaustive summary of the LCI database around the world.

The biggest challenge for the database is inconsistencies in the data source, which means that the use of different databases leads to a comparison issue. For much the same as the layout of a building, the results from SimaPro, GaBi, and ICE show significant difference due to the lack of reliable and transparent data. There is a demand for a reliable database to be provided by the manufacturing and construction industry. Furthermore, there is still a need for updated values for different countries and regions. As a result, it is likely that, in the future, LCI records will provide the necessary data for the analysis of life cycle impact within LCA research. Moreover, the LCIA stage needs to be spatially and temporally broad to collage the flows happening within the life cycle. There is a need for updated values per country as most of the databases have not been updated with progression of time. As far as the structural aspect is concerned, there are no standards and databases specifically designed for structural engineers. However, this is not a barrier to deliver a successful sustainable structural design since the environmental impact of a structural material can be obtained from these databases.

*2.3. Tools.* The term "tools" in this paper refers to the rating systems and software related to sustainability in the building design domain. Generally, tools to perform environmental impact assessment can be divided into three levels [58–60]: (1) level 1: product or component level tools, such as SimaPro, BEES, Gabi, Umberto, and TEAM; (2) level 2: building level tools assisting design decision-making, such as Tally, Athena, eTool, and Bionova; and (3) level 3: rating system or building, infrastructure, and community assessment tools, such as BREEAM, LEED, Green Star, CASBEE, and SBTool.

Specifically, level 1 considers the resources and elements individually, which are then compiled to devise a life cycle consideration for the building as a whole. Level 2 contemplates the whole building as its initial basis. This could, for instance, be the building's shape, before consideration is steadily given to the selection of resources in walls and frames and suchlike. A whole building's environmental impact can be assessed through the level 1 or level 2 approach. The output indicators of these assessments normally include global warming (kg $CO_2$eq), sometimes containing primary energy (MJ), acidification (kg $SO_2$eq), eutrophication (kg NEQ), ozone depletion (CFC-11eq), smog formation ($O_3$eq), nonrenewable energy (MJ), and renewable energy (MJ). Among these indicators, the global warming, namely, "embodied carbon," expressed in carbon dioxide equivalents (kg $CO_2$eq), is regarded as the most important factor. The other greenhouse gases can be converted into $CO_2$eq using conversion factors in order to obtain a common unit for the environmental impact.

It should be noted that the incorporation of BIM and LCA mechanisms within the initial design process is a growing tendency for automating the judgement process based on the outcome. BIM is utilised to uncover the information relating to the building (material measurements) which are subsequently processed within external LCA software or else incorporated "plug-ins" in which LCA can be calculated within the BIM process. The advantages of BIM in the LCA applications include preventing data from being resubmitted manually, enabling analysis to be conducted in real time, improving the assessment of the building overall, and utilising an assessment interface that is accessible to the

Table 1: Summary of sustainable standards and specifications for building design.

| | Standards and specifications | Level | Environmental | Economic | Social | Release year |
|---|---|---|---|---|---|---|
| ISO/TC59/SC17 | ISO 21929 framework for the development of indicators for buildings | Framework | ✓ | ✓ | ✓ | First version 2006, revised 2011 |
| | ISO/TS 12720 sustainability in buildings and civil engineering works | Framework | ✓ | | | 2014 |
| | ISO/TR 21932 sustainability in buildings and civil engineering works—a review of terminology | Framework | ✓ | | | 2013 |
| | ISO 21931 framework for the methods of assessment of the environmental performance of construction work | Building | ✓ | | | First version 2006, revised 2010, will be replaced by ISO/CD 21931-1 |
| | ISO 21930 environmental declaration of building product | Product | ✓ | | | First version 2007, revised 2017 |
| | ISO 21929-1 sustainability in building construction—sustainability indicators—part 1: framework for the development of indicators and a core set of indicators for buildings | Framework | ✓ | | | First version 2006, revised 2011 |
| | ISO 16745 environmental performance of buildings—carbon metric of a building—use stage | Building | ✓ | | | First version 2015, revised 2017 |
| | ISO 15392 sustainability in building construction—general principles | Framework | ✓ | ✓ | ✓ | First version 2008, revised 2019 |
| CEN/TC 350 | EN 15643-1 general framework | Framework | ✓ | ✓ | ✓ | 2010 |
| | EN 15643-2 framework for the assessment of environmental performance | Framework | ✓ | | | 2013 |
| | EN 15643-3 framework for the assessment of social performance | Framework | | | ✓ | 2012 |
| | EN 15643-4 framework for the assessment of economic performance | Framework | | ✓ | | 2012 |
| | EN 15978 assessment of environmental performance of buildings-calculation method | Building | ✓ | | | 2011 |
| | EN 16309 assessment of social performance of buildings-calculation method | Building | | | ✓ | 2014 |
| | EN16672 assessment of economic performance of buildings-calculation method | Building | | ✓ | | 2015 |
| | EN 15804 environmental product declarations-core rules for the product category of construction products | Product | ✓ | | | 2012 |
| | EN 15942 environmental product declarations-communication format-business to business | Product | ✓ | | | 2011 |
| | CEN/TR 15941 environmental product declarations-methodology for selection and use of generic data | Product | ✓ | | | 2010 |

Table 1: Continued.

| | Standards and specifications | Level | Environmental | Economic | Social | Release year |
|---|---|---|---|---|---|---|
| ISO/TC207/SC 5 | ISO 14040 life cycle assessment-principles and framework | Product | ✓ | | | First version 1997, revised 2006 |
| | ISO 14044 environmental management—life cycle assessment—requirements and guidelines | Product | ✓ | | | First version 2006, revised 2017 |
| | ISO 14045 environmental management—eco-efficiency assessment of product systems—principles, requirements and guidelines | Product | ✓ | | | 2012 |
| | ISO 14046 environmental management—water footprint—principles, requirements, and guidelines | Product | ✓ | | | 2014 |
| | ISO/TR 14047 environmental management—life cycle assessment—illustrative examples on how to apply ISO 14044 to impact assessment situations | Product | ✓ | | | First version 2003, revised 2012 |
| | ISO/TR 14049 environmental management—life cycle assessment—illustrative examples on how to apply ISO 14044 for the goal and scope definition and inventory analysis | Product | ✓ | | | First version 2000, revised 2012 |
| | ISO/TS 14048 environmental management—life cycle assessment—data documentation format | Product | ✓ | | | 2002 |
| | ISO/TS 14071 environmental management—life cycle assessment—critical review processes and reviewer competencies: additional requirements and guidelines to ISO 14044 | Product | ✓ | | | 2014 |
| | ISO/TS 14072 environmental management—life cycle assessment—requirements and guidelines for organizational life cycle assessment | Product | ✓ | | | 2014 |

Table 2: Summary of sustainable databases.

| Database | General purpose database | Construction-specific database | LCA | ECC | EEC | Region |
|---|---|---|---|---|---|---|
| Inventory of Carbon and Energy (ICE) | | ✓ | | ✓ | ✓ | UK |
| European Life Cycle Database (ELCD) | ✓ | | ✓ | ✓ | | Europe |
| U.S. Life Cycle Inventory (U.S. LCI) | ✓ | | ✓ | ✓ | | US |
| Ecoinvent | ✓ | | ✓ | ✓ | | Switzerland |
| Oekobaudat.de (German) | | | ✓ | ✓ | | Germany |
| Milieudatabase.nl (Dutch) | | | ✓ | ✓ | | Netherlands |
| French national database | | | ✓ | ✓ | | French |
| Australia LCI | | | ✓ | ✓ | | Australia |
| SimaPro database | | | ✓ | ✓ | | Netherlands |
| Gabi database | ✓ | | ✓ | ✓ | | Germany |
| CPM LCA | | | ✓ | ✓ | | Sweden |
| EPD database BBRI (Belgian) | | | ✓ | ✓ | | Belgium |
| ProBas | | | ✓ | ✓ | | Germany |
| Japan Sustainable Building Database | | | | | | Japan |
| BEDEC | | | ✓ | ✓ | | Spain |
| Athena database | | ✓ | | | | Canada |
| New Zealand building materials embodied energy database | | ✓ | | | | New Zealand |
| Building Products Life Cycle Inventory | | ✓ | | | | Australia |

LCA: life cycle assessment, EEC: embodied energy coefficients, and ECC: embodied carbon coefficients.

user. On the contrary, the drawback may lead to data loss and format conversion from different software. Although the industry foundation class (IFC) has been used to enhance interoperability between different software for many years, a more automatic and integrated BIM-enabled LCA method is still lacking.

Level 3 is generally a scoring system that provides comparisons throughout the building industry. It is used to analyse the results for the building overall in terms of the sustainability across the built environment life cycle, from new construction to in-use and refurbishment. This process is to advocate the spread of design processes and to advocate to designers the notion of exceeding the building guidelines

in place. They contemplate the product overall to a degree but additionally scrutinise design of the building from the perspective of health elements and the sustainability of the society. It has been suggested that the scoring tool is basically a way of standardising various buildings from the perspective of environmental outcomes. Whilst the rating system might differ according to the specific system followed, there is large consistency in how the system functions. For example, the BREEAM (Building Research Establishment Environmental Assessment Method) was first launched in 1990 by the Building Research Establishment (BRE) in UK. Other rating system such as LEED, Green Star, CASBEE, DGNB, and HQE were developed based on the idea of the BREEAM [61–65]. Among these systems, the DGNB (Germany) is deemed as the latest system that is based on the experience from all the former rating systems, which is called "A Second-Generation Certification System." Its main features include (1) early design stage precertificate, goal definition, and integrated planning; (2) risk management with real transparency; and (3) goal-oriented system. Figure 1 shows all the aforementioned standards, databases, and tools to facilitate understanding.

Yet, assessing these systems critically is beyond the viability of this paper, which instead places its emphasis on how it relates to sustainable structural design. Despite the fact that some of the structural design work is not directly related to the rating system, even reduced use of water in concrete can contribute to the water protection and natural environment by integrating the water collection systems and structural systems. The impact that the design of the structure has on the rating tool incorporates various factors including the use of resources, the structural system that is chosen, the disassembly design, and the dematerialisation. Eight rating systems have been considered within this work to analyse the current contribution of SSD to the rating process and to outline enhancements to them. The analysis considers embodied energy and other potential signs of sustainability for the design structure. The work chooses them for being original, transparent, and extensive. The influence of SSD on rating credits, or in other words, the structural points in the rating system, can be divided into three parts: direct, indirect, and supporting. Taking BREEAM as an example, the full credit is 100 points which contains ten sections: management, health and well-being, energy, transport, water, materials, waste, land use and ecology, pollution, and innovation. Four out of these 10 sections are related to structural design. They are energy (direct), materials (direct), waste (indirect), and land use and ecology (supporting). Thus, the total credits of these four parts are 44 points. Other rating systems can be done in the same manner.

Table 3 outlines the credits connected to structural trades within the process of measuring sustainability, indicating that the average figure of SSD-associated credits was greater than expected at approximately 46% [24, 33, 38]. This can be explained by the fact that the influence that structural design exerts on the rating system credits can be divided into two categories based on the involvement of structural engineers: direct influence and indirect influence. The direct influence

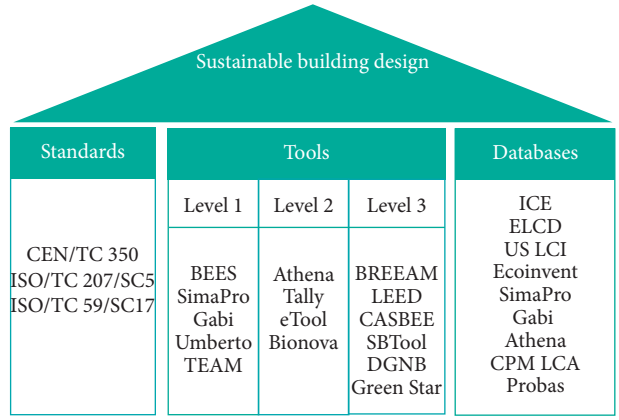


Figure 1: Methods for achieving sustainable buildings.

deals with the material and component level (i.e., material use or cost of a beam and column), while the indirect influence is related to the whole building level, such as shortening the construction schedule, increasing the net height and net area, reducing equipment and labour, and improving the lifespan of a building, which need to be considered accordingly. From authors' point of view, these previous studies have underestimated the contribution of structural design to the rating system credits since they consider only the direct influence. Moreover, there are various rating tools enabling a significantly greater proportion of credits to be ascertained, suggesting that these rating tools provide a greater array of SSD openings to acquire the certification.

Whilst the majority of the research referenced emphasised the limitations of the rating tools in measuring the influence of the design of the structure, the consideration here has identified that the rating methods are fairly progressive in analysing SSD processes, taking into account the majority of issues in this regard. Furthermore, they frequently utilise quantitative measures where they can. These processes give varying significance to various SSD issues based on the area in which they were introduced. For instance, in China, the elements connected to off-site environment are given emphasis, perhaps because the construction process within China is presently especially extensive.

Based on the review of sustainable design approaches for buildings, it can be inferred that the biggest challenge for the standards and databases is the lack of reliable, comparable benchmarks and inconsistencies in databases. Furthermore, the current sustainable design tools typically assess the sustainable performance of a building at a later design stage, thus being a verification or show-off document rather than a decision-aided tool, providing little guidance for designers over the design process. Despite efforts which have been made towards integrating the sustainability issue into the early design stage, no single solution can be reached to come up with a holistic and comprehensive sustainable design. This can be attributed to the fact that there is a lack of efficient approach and tools that can support systematic and effective information exchange between different

Table 3: Summary of the sustainable rating systems for building design (%).

| Section | BREEAM (UK) | LEED (US) | Green Star (Australia) | SBTool | DGNB (Germany) | Green Globe (Canada) | HQE (France) | GBAS (China) |
|---|---|---|---|---|---|---|---|---|
| Management | 11 | 10.1 | 9 | | | 5 | 12.5 | |
| Off-site environment | | | | | 22.5 | | | 21 |
| Economical quality | | | | 1.3 | 22.5 | | | |
| Sociocultural and functional | | | | 0.3 | 22.5 | | | |
| Technical quality | | | | | 22.5 | | | |
| Process quality | | | | | 10 | | | |
| Site selection | | | | 6.4 | | 11.5 | | |
| Indoor environment quality | | 18.8 | 17 | 2 | | 16 | 12.5 | 18 |
| Operation and maintenance | | | | 26.9 | | | 12.5 | |
| Service quality | | | | 4 | | | | |
| Health and well-being | 14 | | | | | | | |
| Energy | 17 | 18.8 | 24 | 19 | | 39 | 12.5 | 24 |
| Transport | 7 | | 9 | 13.7 | | | | |
| Water | 5 | 7.3 | 11 | | | 11 | 12.5 | 20 |
| Materials (resource) | 11 | 21.7 | 16 | 8 | | 12.5 | 12.5 | 17 |
| Waste | 7 | | | | | | | |
| Land use and ecology | 9 | | 5 | | | | | |
| Pollution | 9 | | | | | | | |
| Emission | | | 9 | 18.3 | | 5 | 12.5 | |
| Implantation quality | | 20.3 | | | | | 12.5 | |
| Innovation | 10 | 3 | | | | | | |
| Total | 100 | 100 | 100 | 100 | 100 | 100 | 100 | 100 |
| Relevance to structural design | 44 | 47.8 | 51 | 27 | 45 | 62.5 | 37.5 | 61 |

participants. Furthermore, although structural design plays an important role in sustainable design (score in the rating system), there is scant evidence that the importance of a structural engineer has been sufficiently recognised. The higher percentage of credits offers a great opportunity for structural design acquiring the accreditation of sustainable design. In the next section, the current situations in the sustainable structural design in terms of strategies and indicators will be investigated. The challenges and difficulties associated with integrating the sustainability issue into structural design are also identified and discussed.

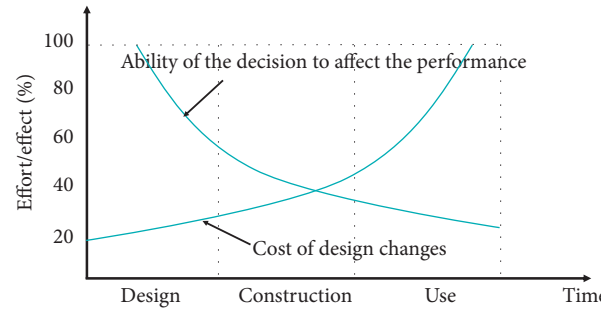


Figure 2: Life cycle stage and its influence on sustainability.

## 3. Sustainable Structural Design

*3.1. General Processes of Structural Design.* A building process can be divided into four major periods: design, construction, in-use, and demolition. The design work not only highly influences the overall cost but also greatly affects the environmental impact. The possibility of changing the sustainable performance is high over the design stage and gradually declines as a project progresses (Figure 2). Generally, a structural case—the design of a building, for example—commences with theoretical foundations relating to aspects connected to the structure and the architecture. From contemplation of the needs of the consumers' design, its thematic base and its core mechanical values can enable architects to start drafting resolutions for an initial judgement. This judgement will incorporate self-regulation for preserving cohesion in the design concept, viability tests, and

suchlike. When the concepts have been judged to be viable, the extensive stage of architectural moulding will commence. The results of this process outline the relevant aspects relating to arithmetical aspects or its look. These are presented in either model or drawing form. The emphasis will then turn to a structural consideration.

In implementing the model or drawing for the subsequent stage of evaluating the structural design, it is necessary to make the work produced more simplistic so that only the mechanical sentiment is preserved. This might include, for instance, a beam-truss structure within a case made out of a steel frame. This simplified outline can thus be judged for its consistency during this process, and the outcome can be additionally enhanced by altering the structure to maximise the procedure. It is normally expert structural engineers who possess considerable experience and who decide whether a different option is better or if modifications should be made. The state-of-the-art optimization values state that this is a reoccurring stage that concludes once the aims of the design have been fulfilled. Subsequently, additional models or drawings might be suggested for improving the acquisition and manufacturing process. Ordinarily, judging the maintenance of the models proposed also occurs at the subsequent design stage.

Once the acquisition and manufacturing stage has occurred, further alterations can still be necessary due to problems with resources or the construction process. Required alterations to the architectural and structural aspects can be proposed, and the present formation of the design is reviewed. Within the construction stage itself, people asking for alterations is frequent. This can be instigated by a variety of aspects, including the identification of the collision or conflict, and problems with establishing or maintaining the building. This indicates that being adaptable is crucial within the whole design and building process and ought to be given appropriate scrutiny.

*3.2. Sustainable Structural Design Strategies and Indicators.* It is not the intention of this paper to provide an extensive and deeper discussion on the process of structural design. The focus will be put on the area that is related to sustainability. From authors' point of view, the following aspects should be well understood before the commencement of SSD:

(1) What phase will be considered? (i.e., embodied phase, operational phase, end-of-life phase, or the whole life cycle).

(2) What scope will be considered? (i.e., component level, structure level, or the whole building).

(3) How to quantify the SSD? What are the strategies and indicators? When to perform the SSD? (i.e., early, middle, or late design stage). What tools can be used?

The life cycle phase for SSD can reference the classification of sustainable design, which can be divided into three phases, namely, embodied phase, operational phase, and end-of-life phase (Figure 3). The structural system

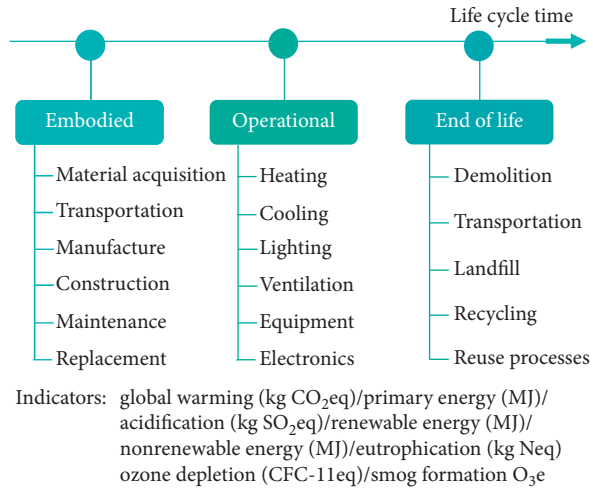


Figure 3: Life cycles and indictors of sustainable design.

contributes a lot to the embodied and end-of-life impacts, not much affects operational impacts. The detail analysis is showed as follows:

(1) Embodied impacts: the structural type ordinarily comprises a significant proportion of a building's mass. Thus, it is a significant factor of the influence on the environment at the beginning stage. Office building LCA research that monitors this indicates that the structure of a building can be responsible for a figure ranging from 30 to 70% of the embodied energy over the construction process. Embodied energy refers to the overall amount of energy used to remove, create, implement, and eradicate a part or system. The vast array is because of various aspects, such as contrasts in the form and scale of a building, the construction sort, and the way in which the structure is defined (impacting upon whether features such as curtain walls are included or excluded).

(2) Operational impacts: from a structural perspective, the influence of structure thermal mass and thermal aspects are the prominent aspects that impact upon the energy results within the functioning stage.

(3) End-of-life impacts: getting rid of structural resources can have a notable influence because of the restricted landfill space and the possible pollution of disposal locations.

It is obvious that the scope of SSD should focus on the component and structure level. The influence of structural design over the sustainability can be seen from two different angles: direct influence and indirect influence. The direct influence deals with the material and component level (i.e., material use), while the indirect influence is related to the whole building level, such as shortening the construction schedule, increasing the net height and net area, reducing equipment and labour, and improving the lifespan of a building, which need to be considered accordingly. On the contrary, these strategies focus only on the material or component level performance, which may result in making

the overall building system less sustainable by not considering the relationship and interactions with other parts, or in other words, not in a holistic way (multiperspectives). As such, an all-encompassing strategy that optimises a building's mechanical, financial, ecological, and energy functioning is yet to be fully expanded. For instance, when structural engineers are optimising a beam's height, they are required to judge the impact on the sustainability not only at the component level but also at a building level. The optimum sustainable solution for the slab might not be the optimum solution for the whole building if the optimum solution minimises embodied carbon of the slab and, at the same time, increases the depth of the slab. The indirect influence of optimising a structural component or material on a macroscopic level needs to be considered in a holistic way. Furthermore, some approaches or objectives might contradict other aims relating to sustainability. For instance, restrictions on a structure's carbon and energy might result in the structure's expense being elevated. Any construction projects need to achieve a balance between a lower cost and a higher reliability [66]. This notion can also be applied to the formation of a structural design, meaning that an appropriate arrangement between theories focusing on health and the environment can be reached.

To indicate the correlation between design theories and their influence on sustainability, various approaches have been conducted to categorise them in a natural manner. Danatzko and Sezen [26] suggested that SSD approaches be categorised as indicated in the following: (1) least material condition; (2) minimizing embodied energy; (3) reducing material production energy; (4) performing life cycle assessment; and (5) reuse of the structural system. Yet, the aforementioned categorisations can instigate uncertainty for a variety of aspects. Limiting the utilisation of resources, the production of energy and the embodiment of energy incorporate similarities and can be categorised more specifically. The life cycle assessment is a mechanism used for making a judgement as opposed to being a theoretical approach. Optimising the replication of structural systems incorporates restoration as opposed to a fresh, original assignment.

A further categorisation was indicated by Anderson and Silman [25] which emphasised theories intending to limit the carbon footprint of buildings. They were (1) design for adaptability; (2) design for efficiency; (3) design for energy; (4) design for recycling; and (5) design for materials. This partly linked with the categorisation proposed by Danatzko and Sezen. For example, design for materials corresponds with resources being selected to represent products being used again. This relates in part to the notion of minimizing material production energy. The concept of design for energy partly compares to Danatzko and Sezen's minimizing embodied energy concept, comprising techniques intended to limit the operational energy of the building. Design for adaptability is connected to reusing structures already in ready and devising fresh ones that can be reused subsequently, which is similar to the reuse of the structural system. Webster [36] suggested that the structural engineer can contribute to the environmental impact by using the following methods: (1) use of salvaged materials or the content of the material can be highly recycled; (2) improve the durability of the concrete structure since it would last at least 50 years; (3) improve the adaptability of the structure that can be adjusted over its entire life; (4) efficient use of structural materials towards minimizing the environmental impact; and (5) use of structural materials that can be reused or recycled, and the structural system can be easily disassembled. SEI Sustainability Committee incorporated durability, adaptability, and human health into the SSD method. They reported that durability and adaptability are broad perspectives and are difficult to quantify. The human health much corresponds to the internal finishes rather than the structural design aspect.

Having recognised the impact that the building structure has on the sustainability, researchers and practitioners have investigated the structure performance on the environment from a practical perspective. Several researchers have studied the embodied $CO_2$ emissions and cost from a structural element level (i.e., beam, slab, and column). For example, Hájek et al. [68] applied the life-cycle assessment methodology to assess the performance of the concrete slab. Three structural floor alternatives ranging from NSC to HPC were chosen for the environmental assessment. They suggested that when evaluating the environmental impacts of concrete structures, a detailed and uniform LCA is greatly demanded. Yeo and Gabbai [69] performed a study for optimising a simple reinforced concrete beam with the fixed moment and shear strengths in terms of sustainable design. The results indicated that in order to reduce 10% of the embodied energy of a beam, the cost will increase 5% accordingly. A further study by Yeo and Potra [70] presented an optimization approach for a structural engineer to evaluate the sustainability and economic objectives. A reinforced concrete frame was used as a case to illustrate the proposed approach. The results indicate the developed approach can reduce carbon emission by 5% to 15%. Foraboschi et al. [71] studied the embodied energy of tall building structures in the range of 20 to 70 stories. The results indicated that the lowest weight of a structure does not necessarily mean it has the lowest embodied energy. The embodied energy largely depends on what type of slab is used in a structure. They also concluded that the steel structure consumes more embodied energy compared to that of a reinforced concrete structure. Gan et al. [72] developed an optimization approach for cost-optimal and low-carbon design of the high-rise reinforced concrete structure by using parametric modelling and genetic algorithm to define the relationship between structural members and the behavior of the entire building structure. The proposed approach can reduce the carbon emissions and material cost by 18–24% after performing the optimization. Weerasuriya et al. [73] proposed a framework to estimate accurately the potential of natural ventilation of a high-rise residential building considering indoor and outdoor air flows, heat gain, and occupant thermal comfort by combining the computational fluid dynamics (CFD) simulation, multizone airflow modelling, and building energy simulation (BES). The results showed that the electricity consumption can be reduced up to 25% by employing wind-

driven natural ventilation and up to 45% by facilitating the buoyancy-driven natural ventilation.

The most recent analysis of the sustainable structure design was undertaken by Pongiglione and Calderini [24]. They observed the significant elements and stages for undertaking the design of a sustainable structure, which incorporates the desired influence, approaches, and boundaries. Additionally, Bakhoum and Brown [34] suggested a sustainable scoring mechanism to measure structural materials. The tool incorporated reference to various sustainable aspects that impact upon the structural resources that are chosen. Cole and Kernan [67] examined the overall energy utilised in an orthodox 4620 $m^2$ three-storey, generic office building in terms of varying wood, steel, and concrete provisions. They deduced that the structure can constitute of a sizable element of the energy used within the early stages of a business establishment. Their conclusions verify the findings of other research studies that the structure can be the biggest individual aspect of energy at the embodied stage (Figure 4). For an overview of some of these efforts, refer to the Ph.D. thesis of Hou [74].

Based on the above question and previously reviewed strategies, the classification for methodologies of SSD can be divided into the following parts: minimize material use; minimize global warming; minimize energy; minimize nonrenewable energy; minimize total cost; minimize total weight; maximize material or system reuse; maximize material recycling; and maximize human health. Table 4 shows a summary of strategies and classification method to deliver a sustainable structural design.

On the basis of the sustainable structural design strategies and indicators, a holistic decision supporting the approach that integrates structural design and sustainability issue to assist structural engineer decision-making is needed. In the following section, various methods of incorporating the sustainability issue into structural design through BIM are identified and discussed with the aim of providing insight into the current situation.

*3.3. Current Practice of BIM-Enabled SSD.* In order to automate the process of SSD, some vendors have developed tools to assess the environmental impact of a structure. The trend is to integrate the sustainability into BIM software. As a prerequisite, the structural analysis needs to be conducted in advance before generating a model in BIM software for the sustainable assessment. Currently, there are several methods that can integrate sustainability issues into BIM or conduct sustainable assessment based on the BIM models [29, 76–80], as follows:

(1) Export the BIM model to external software, normally LCA software, to conduct sustainable assessment, such as IES VE, EnergyPlus, Ecotect, Green Building Studio™ (GBS), SimaPro, Athena EcoCalculator, DesignBuilder, Bentley Hevacomp, and TAS. This process often requires the BIM model to be saved as another format, such as IFC, gbXML, DXF, and Excel. The advantage of this method is that it is easy to use, and the disadvantage of this method includes time consumption and the process is complicated, like a verification document rather than a decision-making tool.

(2) Use of the "Quantity Takeoff or Material Takeoff" function in BIM: the new parameters such as sustainability indicators can be added as project parameters by creating a formula. The indicators such as embodied $CO_2$ can be calculated by multiplying the mass of the material and embodied $CO_2$ per kg. The mass of the material can be obtained from "Materail Takeoff," and embodied $CO_2$ is taken from an Excel format database, such as Bath ICE database. The disadvantage of this method is that some of the parameters need to be extracted from the database manually and input into the Material Takeoff spreadsheet because they sometime mismatch.

(3) Preinstall LCA software within the BIM environment, and connect with a structural analysis tool—this kind of software is like a "plug-in" or "add-in," such as Tally and Environmental Analysis Tool™ (EA Tool™). Compared with methods (1) and (2), this method is more "advanced." The positive attribute of this method is that it allows users to calculate the environmental impacts of the building material directly within the BIM environment right after the completion of the model.

(4) Use of API to accomplish BIM extension [46, 81]: developers depend on a range of techniques to coordinate with the BIM model. For instance, numerous software packages depend on an open file format, including STEP, IFC, and CIS/2. These applications are used to transfer data across various applications. Alternative integrations are found on an impartial database driver such as ODBC, which functions as a converter between different applications. There are many types of programmers that can be used in the Revit platform API, such as C#, VB, SQL, and JAVA. It should be recognised that xBIM is a .NET open-source software advancement BIM toolkit that permits.NET developers the opportunity to access, devise, and monitor BIM models within the IFC format. There is comprehensive assistance for geometric, topological operations and visualisation. Furthermore, xBIM encourages bidirectional translation across COBie and IFC format. Essential libraries for influencing data are all outlined in C#. The prominent element of the geometry engine is produced in C++.

(5) Use of ontology to connect BIM and LCA database [23, 49]: firstly, a LCA database ontology is developed. Secondly, a BIM model is constructed in Revit and exported to an IFC format and then to an OWL format—BIM ontology. Eventually, by combining the two ontologies, a new BIM ontology is constructed and transferred to IFC and then to a BIM model. Overall embodied carbon of the building is calculated through a BIM schedule. The disadvantage of this method is that the ontology for the integration

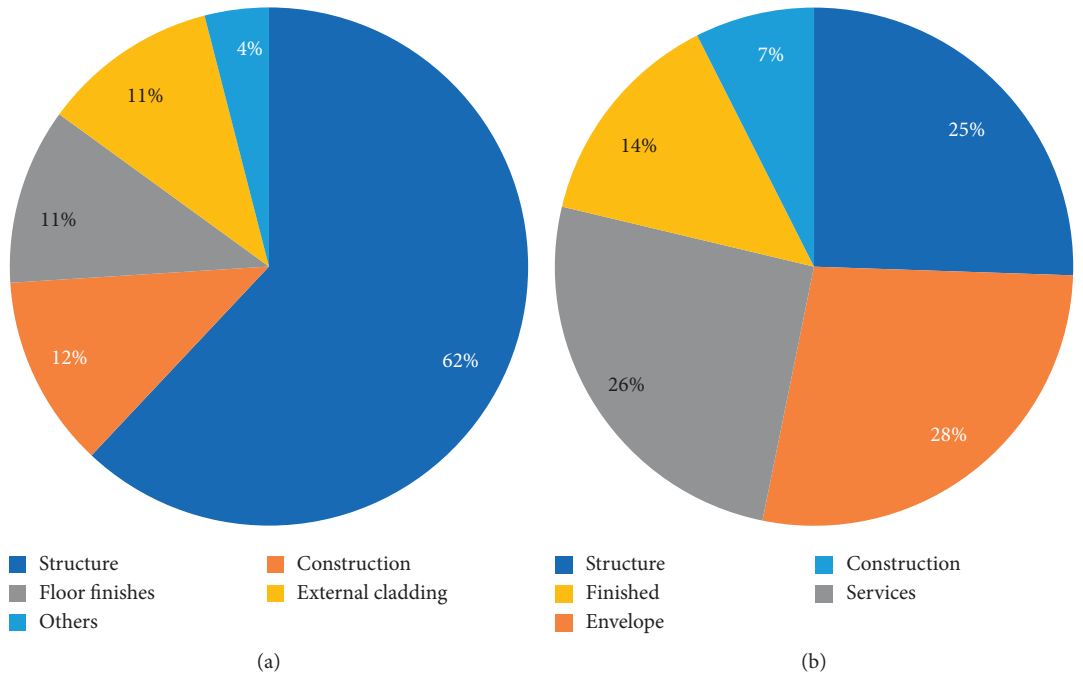


Figure 4: (a) Average embodied carbon in office buildings [22]. (b) Average embodied energy in office buildings [67].

Table 4: Summary of SSD strategies and classifications.

| Strategy | Indicator | Scope/level | Embodied phase | Life cycle operational phase | End-of-life phase |
|---|---|---|---|---|---|
| Minimize material use [26] | Volume ($m^3$)/weight (kg) | Material/ structure/building | ✓ | | |
| Minimize global warming [37] | Equivalent carbon (kg $CO_2$eq) | Material/structure | ✓ | | |
| Minimize energy [25] | MJ | Material/ structure/building | ✓ | ✓ | ✓ |
| Minimize nonrenewable energy [24] | MJ | Material/ structure/ | ✓ | | |
| Minimize total cost [75] | USD/GBP/EUR | Structure/building | ✓ | | ✓ |
| Minimize total weight [75] | Weight (kg/ton) | Structure/building | ✓ | | |
| Maximize material or system reuse [36] | Volume ($m^3$)/weight (kg) | Material/structure | | | ✓ |
| Maximize material recycling [36] | Volume ($m^3$)/weight | Material/structure | | | ✓ |
| Maximize human health [35] | VOC (volatile organic compound) | Structure/building | ✓ | ✓ | |

of the LCA database and BIM is still not fully automated, and importing IFC back into BIM can result in some loss of data. Figure 5 graphically shows the above methods with more detail.

## 4. Discussion

From the methods mentioned, a number of elements should be recognised. To achieve a sustainable structure, a joint effort is needed to come up with a holistic design both within and outside structural engineers. The challenges that structural engineers face include the following:

(1) A sustainable structural design, allowing consideration of varying aims—including safety, environmental impact, cost, functionality and aesthetics—necessitates an extensive review of the orthodox sequential structural process. Centralisation of different domain information (i.e., structural analysis, sustainability assessment, and detailing software) in a common data environment is a trend. As mentioned earlier in this paper, the interoperability among different software often leads to data loss and difficulties in conversion and change. Additionally, BIM mechanisms presently give restricted assistance in regulating alterations over a

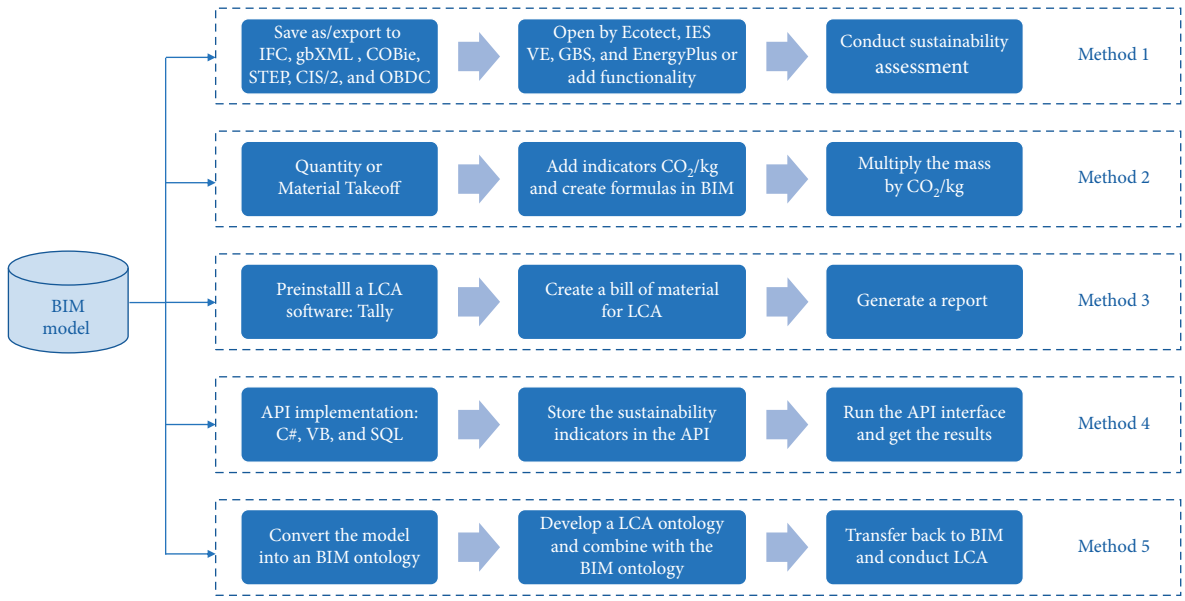


Figure 5: Summary of SSD methods with the integration of BIM.

range of models relevant to a certain discipline. Ontology-based method can be used to reflect, organise, and monitor alterations to design in BIM's context of cooperation over various disciplines. A greater extent of BIM collaboration across varying software is required. The core issue is about multi-objective decision-making in a common environment. It is also believed that semantic web technology and open BIM could probably provide such a platform to address these issues.

(2) Consideration of not only structural material's impact but also impact from structural components and structural form: from the literature review, most of the SSD use the strategies of structural material quantities for minimizing the environmental impact. This, however, is not the only important parameter. For example, from a whole structure perspective, the layout of columns, beams, and slabs also has a significant impact on the overall sustainable performance of a structure. Furthermore, the structural analysis focuses on the material or component level for optimising the environmental impact, which may result in making the overall structure or building less sustainable by not considering the relationship and interactions with other parts. The optimal components are not necessarily optimal for the structure as a whole. A higher degree of impact assessment among different building levels is needed. How to take these factors into full consideration is indeed a challenge.

(3) Strengthened, efficient, and systematic information exchange between architects and structural engineers: a greater engineering response is needed at the initial stage of the design process. However, currently, the architectural model from the architect that aims to deliver to the structural engineer cannot be used directly for the structural analysis. The structural engineer needs to reconstruct the same model from structural analysis software. Although some of the software provided are compatible with BIM tools (i.e., Autodesk Revit), a more streamlined and integrative process is highly needed.

(4) Presently, the majority of structures is devised to limit the embodied influence, as opposed to the overall influence. Minimal advancement in expenses at the initial stage could drastically diminish the influence of the life cycle by reducing the maintenance and permitting salvage or disposal at the process's conclusion. Furthermore, designers ought to try and optimise the adaptability of the design of any structure to permit further alterations in the building's function.

(5) Consideration of the potential influence of the structural material and structural system (form) on the construction and building sustainability, such as lifespan, construction schedule, labour and equipment, and material availability: small changes in initial design could dramatically change the way of construction, which in turn influences the overall sustainability of a building.

It is argued that structural design is not directly relevant to the operational energy use or $CO_2$ emissions during the use phase, but it has potential influence on the operational phase from the following three aspects. Firstly, the operational $CO_2$ emissions or energy use can be reduced with the emerging technology over time, but the embodied energy and carbon dioxide cannot be reversed. The structure accounts for the greatest weight in buildings and therefore

contributes, on average, to more than half of the total carbon dioxide emissions due to materials. In terms of infrastructure, such as bridges, roads, or stadia, the energy consumption and $CO_2$ emissions during the operational phase seem rather low, while the structural part (i.e., material production, transport, construction, and demolition) accounts for most of the energy consumption and $CO_2$ emissions over the life cycle. Secondly, with the effective reductions in operational carbon dioxide of the building in future decades, embodied carbon dioxide will become a more significant percentage of GHG emissions. Some buildings have a short life, resulting in a high percentage of embodied carbon dioxide over the total environmental impact of the life cycle. Thirdly, the structural material selection and the processing and manufacture of structural materials cause enormous off-site impacts prior to the construction or use phase.

The development of a holistic and integrated system becomes an important prerequisite for effective and efficient information sharing and exchange. The fundamental idea of system integration is enabling two or more systems to communicate, share, and exchange information and to interoperate to achieve a common objective. Interoperability, the ability that data generated by one party can be interpreted by all other parties, is the first and most important step towards system integration. Data interoperability focuses on developing common data models, while framework interoperability is achieved by common communication language and protocols. IFC is the most comprehensive international standard for BIM interoperability. Developed and managed by building SMARTIFC, IFC specifies a conceptual data schema and an exchange file format for BIM data, providing a comprehensive description of project structure, physical components, spatial components, analysis items, processes, resources, controls, actors, and context definition. Currently, it has been recognised as the mainstream standard for open BIM and supported by more than 20 vendors. Although the richness of information offered by IFC has been constantly improved since the release of IFC4, the identified barriers to interoperability and applicability include (1) limited expression range; (2) lack of logical formalism that enables rigorous semantics; (3) difficulties in partitioning the information; and (4) multiple descriptions of the same information. The barriers seem to be mainly caused by the nature of the EXPRESS language behind the IFC.

The emergence of semantic web technologies can connect all kinds of information into one semantic web and provide a semantically rich methodology for improving the interoperability by enriching the EXPRESS data. The great advantage of using semantic web technologies is that the schema, the instances, and the rules can all be described using one and the same language. Beetz et al. [82] and Krima et al. [83, 84] discussed that the logic-based language such as OWL can bring modelling advantages in knowledge representation, reuse of existing information, semantic data sharing, and interoperability with semantic web. The initial effort to convert EXPRESS into OWL was made by Schevers and Drogemuller [85]. The developed prototype and mapping create the opportunity to use semantic web-related technologies for building information models. This initial effort was extended by Beetz [86] and Knublauch et al. [87] with proposing a semiautomatic method and system for the conversion from EXPRESS to OWL. Pauwels and Terkaj [88] proposed a semiautomatic method for converting EXPRESS schemas into OWL ontologies and showed how Semantic Web Rule Language (SWRL) rules can be exploited to enrich an OWL version of IFC and create a semantic checking environment. To enable the encoding of semantics with the data, technologies such as Web Ontology Language are used to formally represent metadata. Ontology can describe concepts, relationships between entities, and knowledge representation [89]. These embedded semantics offer significant advantages such as reasoning over data and operating with heterogeneous data sources. Compared with the IFC used for BIM data models, ontology-based approach has a number of advantages:(1) ontology enables linking other domain data (such as sustainability) into the building information model; (2) ontology provides a formal and consistent taxonomy and classification structure to map concepts between domains; and (3) ontology can provide reasoning function for automated information processing and decision support by adopting semantic rules [90].

Currently, several studies have attempted to combine BIM and ontology for performing analyses, such as facility management [86], plan verification [91], precast components [92], construction cost estimation [93, 94], and sustainable design [95, 96]. As a result, it is expected that the use of ontology for integration of sustainability with BIM models will extend the interoperability of BIM and thus facilitate the sustainable structural design in the future.

Apart from the semantic web technologies, artificial intelligence (AI) has attracted great interest due to the capability of learning how to perform a specific task from known data. Many of the AI branches, such as machine learning, pattern recognition, neural networks, fuzzy logic, evolutionary computation, deep learning, expert systems, probability theory, discriminant analysis, swarm optimization, metaheuristic optimization, and decision trees, have been used in structural engineering. Among the different AI techniques, machine learning (ML), pattern recognition (PR), and deep learning (DL) have acquired considerable attention and are establishing themselves as a new class of intelligent methods for use in structural engineering [97]. AI techniques can be effectively used to check the general validity of laboratory and help minimize time-consuming laboratory or field tests. However, the application of AI techniques in the sustainable design remains to be developed. Recently, effort has been made [98] to combine BIM, data mining (knowledge discovery), and semantic technique to enable BIM-based information retrieval in support of evidence-based sustainable design in the early design phase. The proposed approach was based on the data and knowledge discovered in previous projects to enhance decision-making with the case-based design. The knowledge and data repository consists of 531 building models, while data mining was performed over the sensor data using motif discovery and association rule mining. It is a pioneer work

that decision-making is based on knowledge discovery in previous projects and embedded in digital data by combining data mining and semantic modelling for case-based sustainable design. This approach highlights the potential benefits of using AI technology on the sustainable structural design in the future. A recent study conducted by Hao et al. [99] applied 3D graphic statics within a neural network model to facilitate the structural geometric form selection, which provides a more flexible method for the mutiobjective assessment of the solution space and thus enables designers to obtain different recommended solutions. In the future, it is evident that there is a tendency for designers to combine more advanced technology such as AI and semantic web to facilitate the repetitive and creative work and thus provide more solutions to advise designers in support of sustainable structural design.

The challenges that outside structural engineers face include that there is a need for architects to have effective corporation with structural engineers. The ultimate goals of sustainable design can be achieved by efficient information exchange and effective collaboration between structural engineers and architects. A central repository, namely, common data environment, would contribute to the high level of cooperation. In this case, there is a need to have a unified platform that can integrate sustainability considerations within a common environment between designers. The emerging technology, such as semantic web, knowledge graph, and even artificial intelligence, offers the greatest opportunities to achieve sustainable structural design. The fast-growing ontology technology can represent domain knowledge, entities, and their relationships in a variety of ways. Ontology not only enables cross-database search and database interoperability but also provides the means to represent any data formats, including unstructured, semi-structured, or structured data, enabling automated reasoning about data. Furthermore, in terms of the participant of a project, the clients should realize the importance of a structural engineer for a sustainable building and should have effective communication with structural engineers. The future legislation and organization also need to offer incentives to motivate structural engineers to consider the environmental performance of structural design.

## 5. Conclusions

Amidst the extensive scrutiny worldwide, environmental structural engineers have recently started to contemplate the influence of their outlines in terms of searching for efficient methods of reviewing energy and mechanisms for casting judgements which could compensate for the environmental downsides of their design resolutions. This significantly alters the outlook of the design industry in establishing building structures as the difficulty with measuring the impact of environmental energy is not simple, particularly when considering the sustainability factors impacting on the building.

This paper presents a state-of-the-art review of sustainable design from all the standards, databases, and tools regarding sustainability in the building design domain for the current practice of sustainable structural design. An extensive modern insight into sustainable structural design, including strategies and indicators, as well as BIM-enabled methodology, is also presented. The contribution from structural engineers in striving for resolute and sustainable objectives is now known, particularly in terms of the advancement of processes to fulfil these aims. Furthermore, the notion of sustainability in connection to structural design has gradually obtained a more comprehensive sentiment, incorporating environmental, social, and financial factors over the process. Regardless of a great deal of efforts made towards streamlining the LCA process, the highly fragmented knowledge and the way of working within the building domain increase the difficulty of the multiobjective structural design (i.e., safety, cost, and environmental impact). There is always a priority or tradeoff among these factors. How to balance these parameters remains a challenge. A systematic approach (multiobjective) beginning with the standardised calculation procedure for SSD is essential for practitioners to achieve a sustainable structure and building.

The challenge for achieving a sustainable structure is multiple: from centralisation of different domain knowledge in a common environment to an explicit process that enables efficient and systematic information exchange between designers. The authors anticipate the forthcoming AI and semantic technology together with open BIM as a chance for achieving a holistic sustainable design in the future.

## Conflicts of Interest

The authors declare that they have no conflicts of interest.

## Acknowledgments

The authors would like to acknowledge the financial support provided by the Educational Department of Liaoning Province (Grant nos. JDL2019036 and JDL 2019018) and the Department of Science and Technology of Liaoning Province (Grant no. 2019-BS-041).

## References

[1] AIJ and IBEC, Architecture for a Sustainable Future, *All about the Holistic Approach in Japan*, Institute for Building Environment and Energy Conservation, Tokyo, Japan, 2005.

[2] United Nations Environment Program Sustainalbe Buildings and Climate Initiative, *Buildings and Climate Change. Summary for Decision-Makers*, United Nations Environment Program Sustainalbe Buildings and Climate Initiative, Paris, France, 2009.

[3] J. McLennan, *The Philosophy of Sustainable Design: The Future of Architecture*, Ecotone Publishing, Topeka, KS, USA, 2004.

[4] K. Tsimplokoukou, M. Lamperti, and P. Negro, *Building Design for Safety and Sustainability*, Joint Research Centre, European Union, Brussels, Belgium, 2014.

[5] ISO/TC207/SC5, *Life Cycle Assessment*, International Organization for Standardizaion, Geneva, Switzerland, 1993.

[6] ISO/TC59/SC17, *Sustainability in Buildings and Civil Engineering Works*, International organization for Standardization, Geneva, Switzerland, 2002.

[7] CEN/TC350, *Sustainability of Construction Works*, European Committee for Standardization, Brussels, Belgium, 2004.

[8] Coldstream Consulting, *LCA Protocol for Clean Environment Commission Keeyask Proceedings*, Coldstream Consulting Ltd., Vancouver, Canada, 2013.

[9] G. Hammond and C. Jones, *Inventory of Carbon and Energy (ICE)*, University of Bath, Bath, UK, 2010.

[10] C. D. Wolf, F. Pomponi, and A. Moncaster, "Measuring embodied carbon dioxide equivanlent of buildings: a review and critique of current industry practice," *Energy and Buildings*, vol. 140, pp. 68–80, 2017.

[11] C. Say and A. Wood, "Sustainable rating systems around the world," *CTBUH*, vol. 2, pp. 18–29, 2008.

[12] S. G. Al-Ghamdi and M. M. Biles, "Green building rating systems and whole-building life cycle assessment: comparative study of the existing assessment tools," *Journal of Architectural Engineering*, vol. 23, no. 1, pp. 1–9, 2017.

[13] F. Jalaei and A. Jrade, "Integrating building information modelling (BIM) and energy analysis tools with green building certification system to conceptually design sustainable buildings," *Journal of Information Technology in Construction*, vol. 19, pp. 494–519, 2014.

[14] J. Basbagill, F. Flager, M. Lepech, and M. Fischer, "Application of life-cycle assessment to early stage building design for reduced embodied environmental impacts," *Building and Environment*, vol. 60, pp. 81–92, 2013.

[15] A. Oti and J. Tah, *Disitizing the Assessment of Embodied Energy and Carbon Footprint of Buildings Using Emerging Building Information*, CRC Press, Taylor & Francis Group, Boca Raton, FL, USA, 2015.

[16] H.-L. Chi, X. Wang, and Y. Jiao, "BIM-enabled structural design: impacts and future developments in structural modelling, analysis and optimisation," *Archives of Computational Methods in Engineering*, vol. 22, no. 1, pp. 135–151, 2015.

[17] M. A. Zanni, R. Soetanto, and K. Ruikar, "Towards a BIM-enabled sustainable building design process: roles, responsibilities, and requirements," *Architectural Engineering and Design Management*, vol. 13, no. 2, pp. 101–129, 2017.

[18] N. Wang and H. Adeli, "Sustainable building design," *Journal of Civil Engineering and Management*, vol. 20, no. 1, pp. 1–10, 2014.

[19] D. Miller, J.-H. Doh, K. Panuwatwanich, and N. van Oers, "The contribution of structural design to green building rating systems: an industry perspective and cpmparison of life cycle energy considerations," *Sustainable Cities and Society*, vol. 16, pp. 39–48, 2015.

[20] S. Kaethner and J. Burrideg, "Embodied $CO_2$ of structural frames," *The Structural Engineer*, vol. 90, no. 5, pp. 33–40, 2012.

[21] M. D. Webster, "Relevance of structural engineers to sustainable design of buildings," *Structural Engineering International*, vol. 14, no. 3, pp. 181–185, 2004.

[22] D. Wood, "The structural engineer and sustainable design," 2015, http://www.douglaswood.biz/greenbulletin.pdf.

[23] S. Hou, H. Li, and Y. Rezgui, "Ontology-based approach for structural design considering low embodied energy and carbon," *Energy and Buildings*, vol. 102, pp. 75–90, 2015.

[24] M. Pongiglione and C. Calderini, "Sustainable structural design: comprehensive literature review," *Journal of Structure Engineering*, vol. 142, pp. 1–15, 2016.

[25] J. E. Anderson and R. Silman, "A life cycle inventory of structural engineering design strategies for greenhouse gas reduction," *Structural Engineering International*, vol. 19, no. 3, pp. 283–288, 2009.

[26] J. M. Danatzko and H. Sezen, "Sustainable structural design methodologies," *Practice Periodical on Structural Design and Construction*, vol. 16, no. 4, pp. 186–190, 2011.

[27] R. Sinha, M. Lennartsson, and B. Frostell, "Environmental footprint assessment of building structure: a comparitive study," *Building and Environment*, vol. 104, pp. 162–171, 2016.

[28] A. A. Guggemos and A. Horvath, "Comparison of environmental effects of steel- and concrete-framed buildings," *Journal of Infrastructure Systems*, vol. 11, no. 2, pp. 93–101, 2005.

[29] D. W. Catherine, F. Yang, C. Duncan, and A. Charlson, "Material quantities and embodied carbon dioxide in structures," *Engineering Sustainability*, vol. 169, no. 4, pp. 150–161, 2015.

[30] Y.-B. Jung and K.-H. Yang, "Low $CO_2$ design approach of reinforced concrete structures for the targeted $CO_2$ reduction," *Journal of Structural Integrity and Maintenance*, vol. 1, no. 2, pp. 81–87, 2016.

[31] D. Miller and J. H. Doh, "Incorporating sustainable development principles into building design: a review from a structural perspective including case study," *Struct. Design Tall Spec. Build*, vol. 24, no. 6, pp. 412–439, 2015.

[32] M. Borchers, "Importance of structural engineering in sustainable and low carbon design," *The Structural Engineer*, vol. 88, no. 9, pp. 14–16, 2010.

[33] M. Chaudhary and A. Piracha, "Examining the role of structural engineers in green building ratings and sustainable development," *Australian Journal of Structural Engineering*, vol. 14, no. 3, pp. 217–227, 2013.

[34] E. S. Bakhoum and D. C. Brown, "Developed sustainable scoring system for structural materials evaluation," *Journal of Construction Engineering and Management*, vol. 138, no. 1, pp. 110–119, 2012.

[35] D. M. Kestner, *Sustainability Guidelines for the Structural Enginner*, ASCE, Reston, VA, USA, 2010.

[36] M. D. Webster, *"The Relevance of Structural Engineers to Green Building Design," in Structures Congress*, ASCE, Reston, VA, USA, 2005.

[37] C. D. Wolf, O. Iuorio, and J. Ochsendorf, "Structural material quantities and embodied carbon coefficients: challenges and opportunities," in *Proceedings of the Sustainable Structures Symposium*, Portland State University, Portland, OR, USA, April 2014.

[38] A. H. Oti, W. Tizani, F. H. Abanda, A. Jaly-Zada, and J. H. M. Tah, "Structural sustainability appraisal in BIM," *Automation in Construction*, vol. 69, pp. 44–58, 2016.

[39] G. Aouad, A. Lee, and S. Wu, *Constructing the Future: ND Modelling*, Taylor & Francis Group, Milton, UK, 2006.

[40] C. Eastman, P. Teicholz, R. Sacks, and K. Liston, *BIM Handbook: A Guide to Building Information Modeling for Owners, Managers, Designers, Engineers and Contractors*, John Wiley & Sons, Hoboken, NJ, USA, 2nd edition, 2011.

[41] H.-Y. Chong and X. Wang, "The outlook of building information modeling for sustainable development," *Clean Technologies and Environmental Policy*, vol. 18, no. 6, pp. 1877–1887, 2016.

[42] N. O. Nawari and M. Sgambelluri, "The role of national BIM standard in structural design," in *Proceedings of the 2010 Structures Congress*, ASCE, Orlando, FL, USA, May 2010.

[43] F. H. Abanda, C. Vidalakis, A. H. Oti, and J. H. M. Tah, "A critical analysis of building information modelling systems used in construction projects," *Advances in Engineering Software*, vol. 90, pp. 183–201, 2015.

[44] S. Eleftheriadis, D. Mumovic, and P. Greening, "Life cycle energy efficiency in building structures: a review of current developments and future outlooks based on BIM capabilities," *Renewable and Sustainable Energy Reviews*, vol. 67, pp. 811–825, 2017.

[45] B. Ilhan and H. Yaman, "Green building assement tool (GBAT) for integrated BIM-based design decisions," *Automation in Construction*, vol. 70, pp. 26–37, 2016.

[46] F. Shadram, T. D. Johansson, W. Lu, J. Schade, and T. Olofsson, "An integrated BIM-based framework for minimizing embodied energy during building design," *Energy and Buildings*, vol. 128, pp. 592–604, 2016.

[47] A. Stadel, J. Eboli, A. Ryberg, J. Mitchell, and S. Spatari, "Intelligent sustainable design: integration of carbon accounting and building information modeling," *Journal of Professional Issues in Engineering Education and Practice*, vol. 137, no. 2, pp. 51–54, 2011.

[48] H.-Y. Chong, C.-Y. Lee, and X. Wang, "A mixed review of the adoption of building information modelling (BIM) for sustainability," *Journal of Cleaner Production*, vol. 142, pp. 4114–4126, 2017.

[49] Y. Schwartz, S. Eleftheriadis, R. Raslan, and D. Mumovis, "Semantically enriched BIM life cycle assessment to enhance buildings' environmental performance," in *Proceedings of the CIBSE Technical Symposium*, Edinburgh, UK, 2016.

[50] F. Consoli, *Guidelines for Life-Cycle Assessment: A Code of Practice*, Society of Environmental Toxicology and Chemistry, Sesimbra, Portugal, 1993.

[51] J. B. Guinée, R. Heijungs, G. Huppes, and A. Zamagni, "Life cycle assessment: past, present, and future," *Environmental Science & Technology*, vol. 45, no. 1, pp. 90–96, 2011.

[52] M. C. McManus and C. M. Taylo, ""The changing nature of life cycle assessment," biomass and [62] ELCD, European reference life cycle database," 2016, http://eplca.jrc.ec.europa.eu/ELCD3/.

[53] US LCI Database, "National renewerbale energy laboratory," 2017, http://www.nrel.gov/lci/.

[54] Ecoinvent, 2017, http://www.ecoinvent.org/.

[55] "GaBi database," *Bioenergy*, vol. 82, pp. 13–26, 2015, http://www.gabi-software.com/international/databases/gabi-databases/.

[56] Athena, Athena Sustainable Material Institute, 2017, http://www.athenasmi.org/our-software-data/lca-databases/.

[57] A. M. Moncaster and J.-Y. Song, "A comparative review of existing data and methodologies for calculating embodied energy and carbon of buildings," *International Journal of Sustainable Building Technology and Urban Development*, vol. 3, no. 1, pp. 26–36, 2012.

[58] A. Haapio and P. Viitaniemi, "A critical review of building environmental assessment tools," *Environmental Impact Assessment Review*, vol. 28, no. 7, pp. 469–482, 2008.

[59] O. Ortiz, F. Castells, and G. Sonnemann, "Sustainability in the construction industry: a review of recent developments based on LCA," *Construction and Building Materials*, vol. 23, no. 1, pp. 28–39, 2009.

[60] M. Erlandsson and M. Borg, "Generic LCA-methodology applicable for buildings, constructions and operation services—today practice and development needs," *Building and Environment*, vol. 38, no. 7, pp. 919–938, 2003.

[61] BREEAM, Building Research Establishment (BRE) Group, 2017, http://www.breeam.com/.

[62] LEED, US Green Building Council, 2017, http://www.usgbc.org/leed.

[63] Green Star rating system, Green Building Council Australia, 2017, http://gbca.org.au/green-star/rating-system/.

[64] CASBEE, *Comprehensive Assessment System for Built Environment Efficiency (CASBEE)*, Japan Sustainable Building Consortium (JSBC) and Institute for Building Environment and Energy Conservation (IBEC), Baton Rouge, LA, USA, 2017, http://www.ibec.or.jp/CASBEE/english/.

[65] DGNB, German Sustainable Building Council, 2017, http://www.dgnb.de/en/.

[66] D. M. Frangopol, K.-Y. Lin, and A. C. Estes, "Life-cycle cost design of deteriorating structures," *Journal of Structural Engineering*, vol. 123, no. 10, pp. 1390–1401, 1997.

[67] R. J. Cole and P. C. Kernan, "Life-cycle energy use in office buildings," *Building and Environment*, vol. 31, no. 4, pp. 307–317, 1996.

[68] P. Hájek, C. Fiala, and M. Kynclova, "Life cycle assessments of concrete structures—a step towards environmental savings," *Structural Concrete*, vol. 12, no. 1, pp. 13–22, 2011.

[69] D. Yeo and R. D. Gabbai, "Sustainable design of reinforced concrete structures through embodied energy optimization," *Energy and Buildings*, vol. 43, no. 8, pp. 2028–2033, 2011.

[70] D. Yeo and F. A. Potra, "Sustainable design of reinforced concrete structures through $CO_2$ emission optimization," *Journal of Structural Engineering*, vol. 141, no. 3, 2015.

[71] P. Foraboschi, M. Mercanzin, and D. Trabucco, "Sustainable structural design of tall buildings based on embodied energy," *Energy and Buildings*, vol. 68, pp. 254–269, 2014.

[72] V. J. L. Gan, C. L. Wong, K. T. Tse, and J. C. P. Cheng, "Parametric modelling and evolutionary optimization for cost-optimal and low-carbon design of high-rise reinforced concrete buildings," *Advanced Engineering Informatics*, vol. 42, pp. 100962.1–100962.16, 2019.

[73] A. U. Weerasuriya, X. Zhang, V. J. L. Gan, and Y. Tan, "A holistic framework to utilize natural ventilation to optimize energy performance of residential high-rise buildings," *Building and Environment*, vol. 153, pp. 218–232, 2019.

[74] S. Hou, *An ontology-based holistic approach for multi-objective sustainable structural design*, Ph.D. thesis, Cardiff University, Cardiff, UK, 2015.

[75] K. S. Moon, "Sustainable structural engineering strategies for tall buildings," *The Structural Design of Tall and Special Buildings*, vol. 17, no. 5, pp. 895–914, 2008.

[76] S. Eleftheriadis, D. Mumovic, P. Greening, and A. Chronis, "BIM enabled optimisation framework for environmentally responsible and structurally efficient design systems," in *Proceedings of the 32nd International Symposium on Automation and Robotics in Construction and Mining*, Oulu, Finland, 2015.

[77] F. Abanda, A. Oti, and J. Tah, "Digitizing the assessment of embodied energy and carbon footprint of buildings using emerging building information modeling," in *The Carbon Footprint Handbook*, pp. 303–330, CRC Press, Boca Raton, FL, USA, 2015.

[78] S. Liu, X. Meng, and C. Tam, "Building information modeling based building design optimization for sustainability," *Energy and Buildings*, vol. 105, pp. 139–153, 2015.

[79] D. M. Kestner, J. Goupil, and E. Lorenz, *Sustainability Guidelines for the Structural Engineer*, ASCE, Reston, VA, USA, 2010.

[80] R. Brahme, A. Mahdavi, K. P. Lam, and S. Gupta, ""Complex building performance analysis in the early stages of design," in

*Proceedings of the Seventh International IBPSA Conference*, pp. 661–668, IBPSA, Rio de Janeiro, Brazil, August 2001.

[81] A. H. Oti and W. Tizani, "BIM extension for the sustainability appraisal of conceptual steel design," *Advanced Engineering Informatics*, vol. 29, no. 1, pp. 28–46, 2015.

[82] J. Beetz, J. Van Leeuwen, and B. De Vries, "IfcOWL: a case of transforming express schemas into ontologies," *Artificial Intelligence for Engineering Design, Analysis and Manufacturing*, vol. 23, no. 1, pp. 89–101, 2009.

[83] S. Krima, R. Barbau, X. Fiorentine, R. Sudarsan, and R. Sriram, *OntoSTEP: OWL-DL Ontology for STEP*, National Institute of Standards and Technology, NISTIR, Gaithersburg, MA, USA, 2009.

[84] R. Barabu, S. Krima, S. Rachuri, and A. Narayanan, "OntoSTEP: enriching product model data using ontologies," *Computer-Aided Design*, vol. 44, no. 6, pp. 575–590, 2012.

[85] H. Schevers and R. Drogemuller, "Converting the industry foundation classes to the web ontology language," in *Proceedings of the First International Conference on, Semantics, Knowledge and Grid, SKG 05*, IEEE, Beijing, China, November 2005, http://www.ieeeplore.ieee.org/xpl/articleDetails.jsp?arnumber=4125861.

[86] C. Mignard and C. Nicolle, "Merging BIM and GIS using ontologies application to urban facility management in ACTIVe3D," *Computers in Industry*, vol. 65, no. 9, pp. 1276–1290, 2014.

[87] H. Knublauch, R. W. Fergerson, N. F. Noy, and M. A. Musen, "The Protégé OWL plugin: an open development environment for semantic web applications," in *The Senmantic Web-ISWC 2004*Springer, Berlin, Germany, 2004.

[88] P. Pauwels and W. Terkaj, "EXPRESS to OWL for construction industry: towards a recommendable and usable ifcOWL ontology," *Automation in Construction*, vol. 63, pp. 100–133, 2016.

[89] H. M. T. Joseph and F. A. Henry, "Sustainable building technology knowledge representation: using Semantic Web techniques," *Advanced Engineering Informatics*, vol. 25, pp. 547–558, 2011.

[90] E. P. Karan and J. Irizarry, "Extending BIM interoperability to preconstruction operations using geospatial analyses and semantic web services," *Automation in Construction*, vol. 53, pp. 1–12, 2015.

[91] B. T. Zhong, L. Y. Ding, P. E. D. Love, and H. B. Luo, "An ontological approach for technical plan definition and verification in construction," *Automation in Construction*, vol. 55, pp. 47–57, 2015.

[92] G. Costa and L. Madrazo, "Connecting building component catalogues with BIM models using semantic technologies: an application for precast concrete components," *Automation in Construction*, vol. 57, pp. 239–248, 2015.

[93] S.-K. Lee, K.-R. Kim, and J.-H. Yu, "BIM and ontology-based approach for building cost estimation," *Automation in Construction*, vol. 41, pp. 96–105, 2014.

[94] Z. Ma and Z. Liu, "Ontology-and freeware-based platform for rapid development of BIM applications with reasoning support," *Automation in Construction*, vol. 90, pp. 1–8, 2018.

[95] M. Niknam and S. Karshenas, "Sustainable design of building using semantic BIM and semantic web services," *Procedia Engineering*, vol. 118, pp. 909–917, 2015.

[96] J. Zhang, H. Li, Y. Zhao, and G. Ren, "An ontology-based approach supporting holistic structural design with the consideration of safety, environmental impact and cost," *Advances in Engineering Software*, vol. 115, pp. 26–39, 2018.

[97] H. Salehi and R. Burgueño, "Emerging artificial intelligence methods in structural engineering," *Engineering Structures*, vol. 171, pp. 170–189, 2018.

[98] E. Petrova, P. Pauwels, K. Svidt, and R. L. Jensen, "From patterns to evidence: enhancing sustainable building design with pattern recognition and information retrieval approaches," in *Proceedings of the 12th European Conference on Product and Process Modelling*, ECPPM, Copenhagen, Denmark, September 2018.

[99] Z. Hao, V. Moosavi, and M. Akbarzadeh, "Machine learning assisted evaluations in structural design and construction," *Automation in Construction*, vol. 119, pp. 1033–1046, 2020.

Hindawi
Advances in Civil Engineering
Volume 2020, Article ID 8846667, 13 pages
https://doi.org/10.1155/2020/8846667

*Research Article*

# Digital Twin Hospital Buildings: An Exemplary Case Study through Continuous Lifecycle Integration

**Yang Peng, Ming Zhang, Fangqiang Yu, Jinglin Xu, and Shang Gao**

*Shanghai Construction No. 4 (Group) Limited Company, Shanghai 201103, China*

Correspondence should be addressed to Fangqiang Yu; fqyu007@163.com

Received 7 August 2020; Revised 29 October 2020; Accepted 3 November 2020; Published 19 November 2020

Academic Editor: Hugo Rodrigues

Copyright © 2020 Yang Peng et al. This is an open access article distributed under the Creative Commons Attribution License, which permits unrestricted use, distribution, and reproduction in any medium, provided the original work is properly cited.

Hospital buildings usually contain sophisticated facility systems and special medical equipment, strict security requirements, and business systems. Traditional methods such as BIM are becoming less capable of real-time updates of building status and big data volume. By proposing innovations both in technique and management—a "continuous lifecycle integration" method based on the concept of Digital Twin (DT) and "early movement" of the general contractor, this paper reported a successful project case in a large hospital in China. The case realized continuous, scheduled integration of static data and dynamic data of more than 20 management systems from the design, construction, pre-O&M phase up to the O&M phase. Then, a DT software system with real-time visual management and artificial intelligent diagnosis modules was developed and deployed in a newly built DT control center. Managers have the ability to grasp the detailed status of the whole hospital by visual management and receive timely facility diagnosis and operation suggestions that are automatically sent back from the digital building to reality. The case has been steadily running for more than a year in the hospital and achieved desired performance by reducing energy consumption, avoiding facility faults, reducing the number of requested repairs, and enhancing the quality of daily maintenance work.

## 1. Introduction

As the increasing volume or complexity of newly constructed building projects, daily management efficiency, and operational safety issues are becoming more important than ever. Difficulties arise from both static and dynamic factors: there are often hundreds of rooms in large public buildings, each with distinct use requirements. How to manage in a precise manner is a challenging puzzle. Besides, numerous mechanical and electrical systems are embedded, such as cold/heat sources, water supply and drainage, power transformation and distribution, lighting, weak current, ventilation/air conditioning, and elevator systems. Even for professional workers, to maintain and repair these systems is not far from tedious. Another challenge is managing people in the house—the most unpredictable factor of all, such as visitor behaviors or staff collaboration for different tasks.

Hospital buildings have not only common difficulties as public buildings but also have unique characteristics of the medical industry [1]. There are special systems in hospitals such as the medical gas system, pneumatic logistics system, medical sewage system, etc. According to the national standards of China, hospital space is strictly divided into public, medicine, clinical, surgery areas, and other special technical regions. These areas all have high-standard requirements for O&M quality—temperature, humidity, sewage, exhaust, and air exchange. In daily activities, all patients, family members, doctors, and administrative personnel may cause dense and complex intersections. Thus security requirement appears much more crucial than ordinary buildings. Another feature is, many operation tasks in Chinese hospitals are entrusted to the outsourcing team, which brings additional quality uncertainties and management problems.

Among all solutions towards management issues of large hospital buildings, BIM (Building Information Modeling) is one of the most promising and mature theories [2]. BIM provides a graphic platform with 3D building entities for facility managers to retrieve, analyze, and process various data in a unified software interface [3]. Some successful cases were reported about BIM-based facility management [4, 5], energy management [6], and safety management [7]. BIM

platforms also coordinate well with the Computer Maintenance Manage System (CMMS), which addressed basic activity recording of routine maintenance.

Despite BIM's achievements, three main concerns in building operation management, especially on large hospital buildings, remain unsolved:

(1) Existing software platforms lack a constantly updated display of real-world buildings [8]. For example, sudden people flow at the entrance of hospitals is dangerous and should be immediately reported. Most building data on existing platforms are preimported then remain unchanged. Managers cannot inspect the truly up-to-date status as they wish.

(2) There are still difficulties when gathering digital data from various sources. In a hospital, about 20 systems are potential dynamic data sources. Each system has unique hardware devices, interfaces, and data formats. Besides, sensor data can accumulate extremely fast. Data transformation strategies and storage work of such big data volume also need improvements [9].

(3) Typical in-use management software like BIM platforms mainly focus on browsing or checking business data with a 3D model, but not mass analysis. If using a separate offline database analysis to fill this gap, it would be poor in timely feedback mechanisms. Therefore, advanced data analysis effort is required in the form of timely decision-making suggestions.

To address these problems, a relatively new concept—Digital Twin (DT)—has been borrowed from the manufacturing industry. Although manufacturing DT has been developing for about ten years, it was far less popular in the building industry, with only a few use cases related to AEC and O&M phases [10, 11].

When a DT is established, it aims to describe the real-time information mapping between virtual models and real products. Consider a certain hospital building as an example below. The real-world part of digital twin refers to a touchable building block that every day embraces all doctors, patients, pharmacists, and medical equipment. A "digital shadow" of this hospital building is the virtual part of the digital twin [12], automatically receiving data flow from the real hospital [13]. With the help of visual management functions and diagnosis algorithms linked to the digit shadow, hospital managers are capable of monitoring current operation status and make optimization decisions back to the real-world hospital. The above-mentioned feature of DT naturally addresses the first concern by providing a methodology of linkage from a virtual model to real building entities.

A survey shows more than half of declared DT research papers about manufacture only reached the digital shadow level of integration [13]. The situation was even more gloomy in the building industry. It is clear that similar studies usually took advantage of the same shortcut, which directly upgraded existing functional modules of a BIM system to a digital twin system [14–17]. Although this shortcut has brought significant convenience for the building industry to quickly accept the digital twin concept, BIM seems closer to a single digital shadow, thus only partially realizes a digital twin. In fact, DT can be much more powerful, enabling the whole lifecycle mirroring, supporting decision-making by timely optimization suggestions based on this mirror of current status [18]. DT improves common functions during the lifecycle service of buildings, such as real-time monitoring, energy consumption forecast, failure prediction, operation guide, etc. [19]. In this paper, the real-world part of DT is emphasized more than existing BIM systems.

Smart device integration is always a crucial but difficult step when establishing DT [15]. Modern smart sensors will produce valuable insights by generating extremely huge data. One of the main contributions of this paper is the continuous integration and manipulation method of device data through the whole lifecycle, which has addressed the second concern. Further, to analyze these data and feedback useful information back to reality, diagnosis functions should be tightly integrated into DT management systems. Artificial intelligence (AI) is naturally introduced in DT's framework to make further analysis after data integration, including event identification, fault diagnosis, and automated decision-making. Analysis usually involves powerful machine learning models or deep neural networks. For example, some papers reported spatial models and a guiding system for movement/evacuation path management in large buildings [17, 20]. Natural Language Process (NLP) and clustering algorithms were employed to find fault patterns from routine repairs [21–23]. Based on collected up-to-date information flow, analysis results will be highly usable due to guaranteed synchronization [24]. In this paper, an intelligent diagnosis engine is embedded into the heart of the DT software system, which successfully addresses the third concern in Section 4.

For the exemplary case in this paper, a DT hospital building constructed by the concept of "continuous lifecycle integration" is proposed. In Section 2, the continuous lifecycle integration method is introduced. In Section 3, a concrete DT management system is developed. Section 4 presents detailed on-site applications of the DT hospital building. Discussions and conclusions are given in the end.

## 2. Case Background and Methodology

*2.1. Case Background before Introducing DT.* Shanghai East Hospital affiliated to Tongji University (generally known as East Hospital) is an A-grade general hospital located at Lujiazui business zone of Shanghai, East China. The case building was the new clinical center integrating medical treatment, teaching, scientific research, first aid, prevention, and health care. Compared to old clinical buildings, this new building mainly focused on major public medical security and high-level medical care services. The building consisted of 24 floors above ground and 2 floors underground with 500 beds, with a total construction area of about 83000 square meters.

Before constructing the new clinical building, East Hospital's mechanical and electrical equipment involves separately working complex systems, including professional medical systems such as gas systems, sewage treatment systems, and the medical equipment system. The BA, maintenance, and space management system currently in use are independent of each other and cannot naturally integrate a unified system according to the medical service demand. It is not convenient for middle and high-level managers of East Hospital to make timely decisions, leading to low operation and maintenance efficiency. Also, the hospital building needs continuous running for 24 hours every day; therefore, O&M Management Department will be under great pressure. Traditional manual, book-keeping management strategies were obsolete and unintuitive because it was nearly impossible to monitor and analyze large data sets from numerous sources.

*2.2. Innovation.* The main technical innovation employed in this case study was called "continuous lifecycle integration method," which refers to a detailed schedule guiding the integration of proper content gradually and punctually over the full lifecycle. The timeline of building projects usually involves AEC (Architecture, Engineering, and Construction) and O&M (Operation and Maintenance) activities. Accordingly, the full lifecycle can be divided into several phases, typically, the design phase, construction phase, O&M phase, etc. Among them, the O&M phase is of special importance as it occupies the majority of the building's lifetime and budget cost. However, O&M cannot be isolated from AEC. Main static information like geometry, facility attached information, space division, electric system logic, and so on are determined in the design phase. Intelligent hardware devices that are utilized to collect dynamic operation data are equipped or preserved in the construction phase.

"Early movement" of general contractors was another innovation about management practice, which ensured data consistency of DT. The consistency from the digital model to the real-world conditions at any time, which is the exact meaning of the "twin" word, is a delicate feature of DT employed in this case. The fact of consistency is significant throughout the full lifecycle of buildings, especially in the O&M phase. For example, consistency in facility management refers to both static information and dynamic status. If digital models failed to update according to construction changes, workers would fail to locate an alarming air conditioner unit. If monitoring signals were inconsistent with the actual situation, workers might incorrectly operate an electric device, causing unexpected consequences. Traditionally, general contractors are only able to take control of the construction phase. In this paper, the general contractor's DT consultant team involved early in the planning & design phase, directly submitting requests about data interfaces to owners and designers. They also collected important design metadata, such as serial codes of facilities and sensor position. Then in construction, the general contractor took the lead in coordinating contracts of various system suppliers, constructing networks of smart devices, tracking changes of point information, etc. By integrated project delivery (early movement), the general contractor guarantees that all DT information was consistent in the full building lifecycle, not limited to the construction phase.

*2.3. Steps of Continuous Lifecycle Integration.* Figure 1 shows the main steps to establish a DT for the hospital building, starting from a real-world hospital and end with a complete DT. The first step was to digitize the hospital through geometry modeling. Geometry modeling was mainly conducted with CAD drawings from the design phase, while the 3D point cloud method by laser scanning or photogrammetry [8] was tested upon complex mechanical rooms. After that, the modeling process of BIM was one of the main integration steps. Generally, splitting static ontology data and dynamically generated information is necessary to ensure system-inherent data security [25] and also to suit proper storage strategies. Therefore, a basic BIM was first built, integrating static models and ontology information. By monitoring processes through business systems and sensor devices, a dynamic BIM or digital shadow emerged. Analysis engines with predefined knowledge and AI model should be added right after monitor data coming. Finally, the object mapping process by the on-site investigation was important to link to the real-world hospital. All functional modules and diagnosis suggestions should be sent back to a real-world hospital building based on correct object mapping.

*2.4. Detailed Contents of Integration.* Doing the right things at the right time was the core idea when planning the DT schema. Beginning from the design phase, all contents (refer to static data, dynamic information, and possible diagnosis models from corresponding stakeholders in charge) should be integrated on schedule at different stages of the lifecycle. Table 1 gives some examples of integration contents. From a consistent point of view, critical information from one phase must have received from previous phases, not arbitrarily recollected and overwritten (some examples are marked triangles in Table 1). This would make sure only one copy of basic data at any time while saving lots of unnecessary modeling costs.

## 3. DT System Development

A unified DT system across desktop client, smartphone app, and tablet app was developed based on the continuous integration method. Figure 2 shows visual management-centered major components of the system and their operating logic. First, raw data from a real hospital and digital shadow were processed, some through Apache Kafka engine as high-density stream data (Step 1 and 2). Then, two kinds of big data methods, the Apache Flink engine and scheduled Extract-Transform-Load (ETL), both continuously transformed analysis data of building status into a predefined data warehouse—a tidy format suitable for AI training (Step 3). The data warehouse first provided proper training data to AI models. After proper training, these AI models formed a

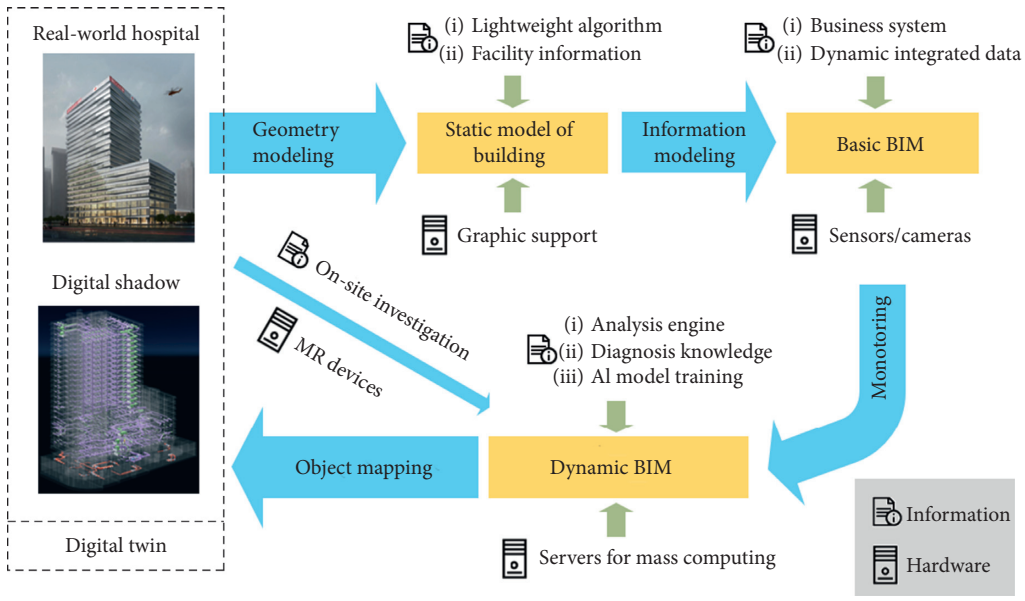


Figure 1: Main steps from real-world hospital to DT.

Table 1: A nonexhaustive list of integration contents during lifecycle phases.

| | Static data | Dynamic information | Diagnosis model |
|---|---|---|---|
| Design phase | Geometry of building elements<br>▲Space division | — | Consistency check from drawings to BIM |
| Construction phase | Material information<br>▲Factory information of important machinery<br>Position points of sensor devices and cameras | Continuous changes to the original designs | — |
| Pre-O&M phase | ▲Control logic of HVAC systems | — | Range of influence analysis |
| O&M phase | Repair knowledge<br>Maintenance requirements | BA monitoring data<br>Energy consumption<br>Repair business system<br>Systems for medical use<br>Real-time weather | Abnormal electric usage detection<br>Air-handling unit fault prediction<br>Frequent repair pattern recognition |

"▲" denotes data that ensure consistency in subsequent phases or final DT.

diagnosis engine and frequently received diagnosis data from the data warehouse (Step 4). Once a problem was detected by the engine, it should be immediately prompt back to visual management interfaces (Step 5). Finally, some targeted commands or suggestions were given towards the digital twin hospital building (Step 6). If any diagnosis suggestion was confirmed as incorrect, it was sent back to the engine as negative training sets. The AI algorithms should make corresponding adjustments (Step 7). Key aspects of system development are introduced in the following sections.

*3.1. Data Processing during Design and Construction Integration.* Data integration of DT lasted for about three years. Although most dynamic data were collected in the O&M phase, the design and construction phase had taken the most time. To make sure data from design and construction keep consistent for so many years and still fit the interface of the DT platform, the consultant group published a considerably thick booklet of interior data standards. Workers in the project department could collect various data in standard formats, and modeling workers produced easy-to-integrate digital models in a unified style.

During static modeling, geometry data were getting larger along with continuously integrated model files, especially HVAC elements. At the end of the construction phase, primary geometry data reached 15 GB, which was obviously too heavy for GPUs. A series of proposed original lightweight algorithms were executed, including merging linked pipe segments, eliminating minor details, and mesh

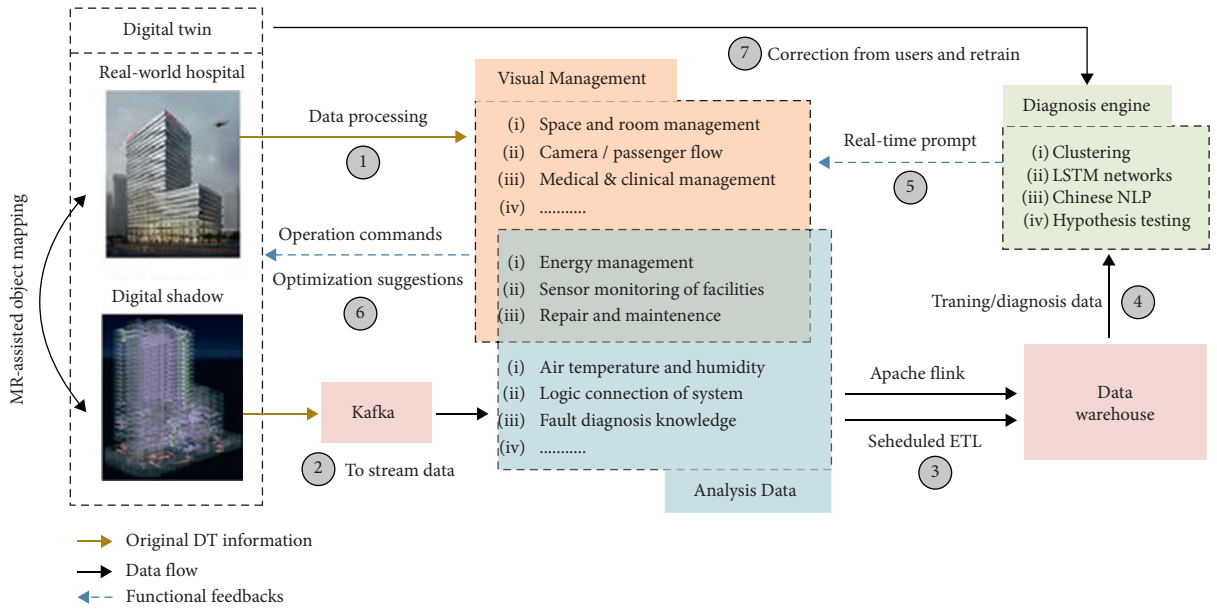


Figure 2: The operating logic of major components of the DT system.

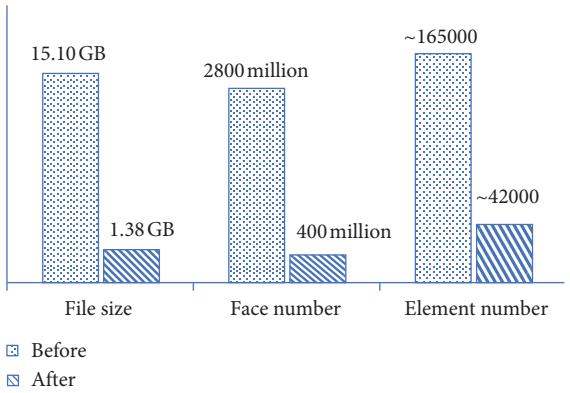


Figure 3: Model volume comparison before and after geometry simplification.

grid simplification. They reduced file size, triangle face number, and element number to less than 20% (as shown in Figure 3).

*3.2. Dynamic Operation System Integration.* In the DT platform, six aspects of dynamic systems were integrated as data sources. Table 2 lists corresponding protocols used when connecting and data processing frameworks. Due to the budget limit, big data services were powered by free, open-source engines. Big data frameworks like Kafka and Flink were capable of transforming quick and dense stream data that were continuously sent from numerous sensors. Both frameworks have been widely adopted in the product industry for several years and are believed stable enough. As for repair business systems or armarium systems, far fewer records were sent. Therefore, some Python ETL scripts with Pandas managed by a schedule dispatcher APScheduler would do the work more concisely.

In East Hospital, the hardware networks of BA consisted of more than 1900 intelligent sensors from 13 subsystems including the elevator system, meanwhile about 230 digital meters from two energy monitoring systems (electricity and water supply), and 100 sensors from three medical gas systems. Because positions and serial codes of all sensors were already ensured consistent by early involvement of the general contractor, dynamic data could be integrated automatically into DT ruled by correct correspondence. These devices generated about 2 million records per day and more than 10 TB of record data in total. Despite the huge volume, the data format was relatively simple. The continuous integration worked smoothly with the help of steady networks. The only issue was database backup every three months. In contrast, records extracted from repair systems, armarium systems, or outpatient information systems contained quite complex properties, thus were far more difficult to develop flexible ETL scripts.

Safety issues about secret data, such as security monitoring videos and visiting records of patients, were also considered. According to the software development contracts, DT systems should only visit private cloud HTTP APIs inside hospital firewalls. This had caused enormous puzzles during the developing phase. Therefore, the security monitoring system and outpatient information were more or less the last coming data integrated. Finally, a private cloud was deployed in the DT control center and Oriental Hospital's information department, which stored secret business data.

*3.3. Mixed Reality (MR) Assisted Object Mapping: From Digital Shadow to DT.* During the data period of system development, correct object mapping from the real hospital to digital shadow was of significant importance. If building elements' position, size, properties, or relationships in the

Table 2: Dynamic data connection and processing method.

| Data source (amount) | Connection protocol | Processing framework |
|---|---|---|
| BA systems (13) | OPC/Modbus/BAC.net | Apache Kafka and Flink |
| Energy monitoring system (2) | Modbus/BAC.net | Apache Kafka and Flink |
| Repair and maintenance systems (2) | CMMS restful API | Scheduled ETL and MYSQL |
| Security monitoring system (1) | Http API ruled by devices | Private cloud storage |
| Medical gas pipeline systems (3) | Modbus/BAC.net | Apache Kafka and Flink |
| Armarium system (1) | Http API from hospital | Scheduled ETL and MYSQL |
| Outpatient information system (1) | Http API from hospital | Scheduled ETL and MYSQL |

digital part were not consistent with the real-world part, workers would feel confused and corresponding diagnosis based on the wrong data would be consider useless. On-site investigations were carried out across the lifecycle but more frequently in the pre-O&M phase. In order to help to check object mapping, an MR app was developed on an iPad tablet. MR technology can seamlessly overlap virtual scenarios upon real entities and display in special optical equipment. As shown in Figure 4, through precise position matching, digital model shapes of critical rooms were displayed together with real scenes inside helmet glasses. Any differences in position were quite obvious from the MR point of view. Instant measurement was supported as well. Input property data such as material, type, or factory information could be called through apps and then compared with machine tags. Those necessary geometry and property data were automatically extracted from the digital shadow part. The MR app helped correctly modeling a DT.

*3.4. Diagnosis Engine and Big Data Backend.* Core algorithms of diagnosis were developed via Python language. AI models were implemented by popular frameworks like TensorFlow wrapping by Keras and Pytorch deep learning. Detailed applications of diagnosis engines are introduced in Section 4.

Big data services performed well upon stream data from sensor devices. In detail, first, a Java daemon process worked at background gathering different data sources to Kafka producer "topics." Kafka then managed and sent raw data as streams. On the other hand, Flink constantly consumed each stream, transforming into standard formats according to the data warehouse. Big data services in the DT system managed to hide low-level manipulations such as keeping consistency, avoiding duplicate calculations, data-saving & backups. This simplified system development APIs.

## 4. On-Site Application

The management platform of DT hospital buildings was successfully developed right before construction delivery. Then it was deployed inside East Hospital. The operation department of the hospital had regrouped its personnel and arranged about ten members switching from traditional positions to DT management jobs. In addition, a consultant group from the DT product team took charge of training on-site workers and software users. By now, all DT applications have been steadily running for about 15 months.

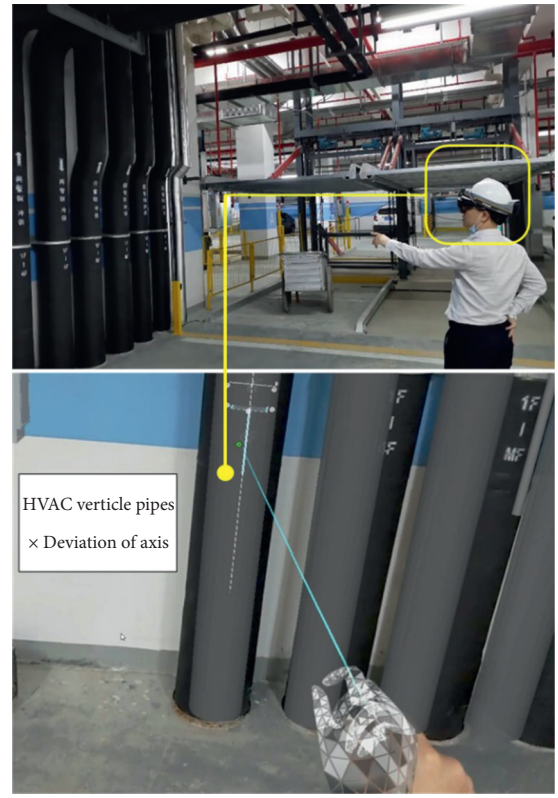


Figure 4: On-site object checking by MR app.

*4.1. DT Large Screen and Control Center.* In the design phase, executive leaders of East Hospital had foreseen to reserve a 200 $m^2$ region in the new clinical building for more advanced BA use. Then, a DT control center was built at the core region of B1 floor right next to HVAC and electric machine rooms, shown in Figure 5. The control center was equipped with perfect working conditions to ensure robust running, including server room, inner network, UPS (Uninterrupted Power Supply), individual office area, facial recognition access, communication lines, and environmental controls. With higher authority and full data access, the DT control center was not only a branch of building management offices but also had become a centralized brain that was able to harmonize daily activities over the hospital.

The main display device for the DT system was a large integral screen (height and width: 2.6 m ∗ 4.7 m) in front of the command deck. For staff use, three graphic stations supported the DT software platform, one BA monitoring

Figure 5: The main hall of the DT control center.

screen, two server terminal computers, and several regular office computers.

### 4.2. Hospital Visual Management

*4.2.1. Hospital Overview Screen.* When stepping into the control center every day, the default screen showed a large frontpage of a hospital overview. The left part was a full discipline 3D model, supporting visual transformation, free roam, element selection, and switching among facility systems. The right part listed the most critical information that should be checked by on-site managers, such as alarming sensors, predicted machine fault risks, unhandled repair requests, the trend of passenger flow, and monitoring video at the clinical areas, etc.

*4.2.2. Space Management.* Based on the hospital's request, the spatial information of rooms and halls was established, which supports room allocation, statistical analysis, and other functions in the 3D view and list view. All spatial information was maintained here (Figure 6) as background knowledge for energy diagnosis in the next section. QR code or Bluetooth beacon for each space was generated as an indoor positioning tag, and support automatically positioning for repair workers. Some statistical analysis of space use was given as well. The space occupation and utilization rate of each medical department were calculated, and the space use efficiency was analyzed considering the operation of the hospital. This helped the planning of rooms and optimization of space.

*4.2.3. Energy Management.* This function constantly monitored the energy consumption of the hospital building, including water and electricity consumption. Water usage was divided into kitchens, toilets, medical water. Electricity usage was divided into standard categories like lighting & switches, power system, air conditioning, and special electric consumption. The absolute amount of energy consumption was shown by line charts, while the linked relative ratio was listed by categories. In the graphic platform of DT, red biased colors emphasized relatively dense energy usage (Figure 7).

*4.2.4. Facility Management.* Major facility information, logical structure, and physical structure of each system were displayed. Through seamless docking with BA, the operation status and alarm status of each device are displayed in the 3D model view. According to integration contents in Section 2, dynamic facility data streams covered HVAC, water supply and drainage, power distribution, and other systems.

The system displays the historical monitoring data of each monitoring point in the form of a list and trend chart to facilitate the backstage management personnel to directly grasp the operation of all key machines and evaluate its performance as well. Take the air conditioning system as an example. A high-level detailed monitoring model has been established for the air conditioning unit (Figure 8). The detailed model displayed 12 monitoring points such as filter status, air supply temperature and humidity, and $CO_2$/CO concentration. After setting the threshold value of the temperature and humidity of the incoming air, $CO_2$, and CO concentration monitoring value, if the real-time data is detected to exceed the threshold value, warnings or alarms were prompted in different colors (left part of Figure 8). Corresponding repair workers would receive a work assignment on their smartphone at the same time when workers needed to know the effect of upstream or downstream devices (In facility systems, an upstream/downstream device means where air or water flows to/from the current device. For instance, if water flows through $A \longrightarrow B \longrightarrow C$, we say A is the upstream device of B, and C is the downstream device of B), they acquired connection information from the DT control center. Information on pipe flow logic and controlling areas was already integrated into the pre-O&M phase. This additional knowledge greatly helped reasonable and timely reactions to facility failures. For example, the influence regions of an alarming air-handling unit (AHU) were displayed with moving arrows and sent to an on-site repair team (right part of Figure 8). Some workers took the responsibility of finding potential

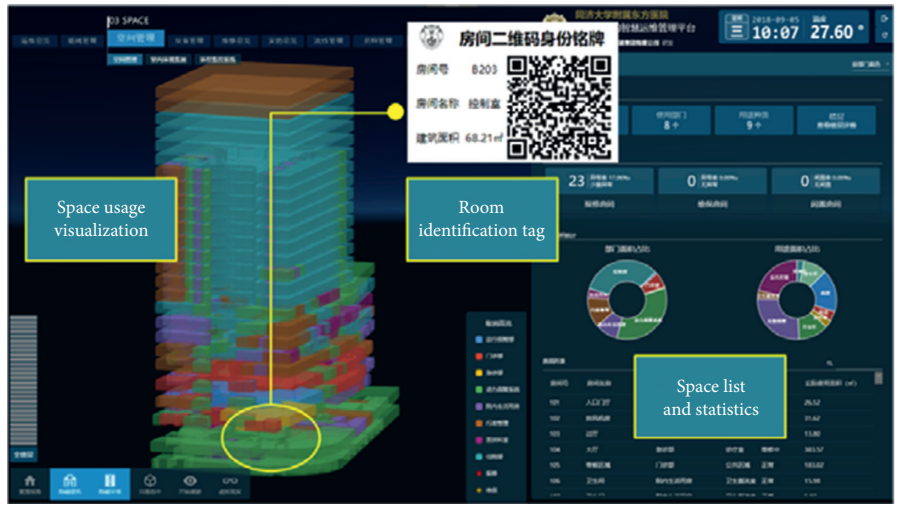


Figure 6: Core functions of space management.

Figure 7: Core functions of visual energy management.

abnormal behaviors along air pipes. Other workers went to open windows of influenced rooms, enabling better air exchange while AHU was under repair.

Another highlight was the elevator system monitoring. The position signals of all 18 elevators were sent back every five seconds. In this way, the graphic system displayed a real-time animation for managers. When a busy elevator was observed, the DT control center would connect to nearby speakers and guide waiting for passengers to another available elevator.

*4.2.5. Repair and Maintenance Subsystem.* This subsystem was the service window of the DT system, which facilitates users at any level to initiate and handle repair requests or maintenance plans conveniently. Here included the emergency repair initiation, reception, task assignment, work order generation, maintenance processing, and maintenance calendar. Maintenance plans supported the customization of different emergency maintenance, daily maintenance, and on-demand maintenance processes according to different clinical departments or different machinery requirements, to support the adjustment of the task process according to actual situations. A regular user in the building could initiate a repair request via the mobile app, submitting multimedia descriptions and text messages of a question. App supported text, photos, voice recording, and videos. The system also collected requests from automatic fault diagnosis modules. Both manual and automatically generated tasks were assigned to the nearest worker in the hospital building. The DT model was employed to help locate the spatial position of faults, analyze, and then judge the influence range or key points of faults. This improved the efficiency of equipment maintenance and emergency repair.

Figure 8: Facility management and connection logics.

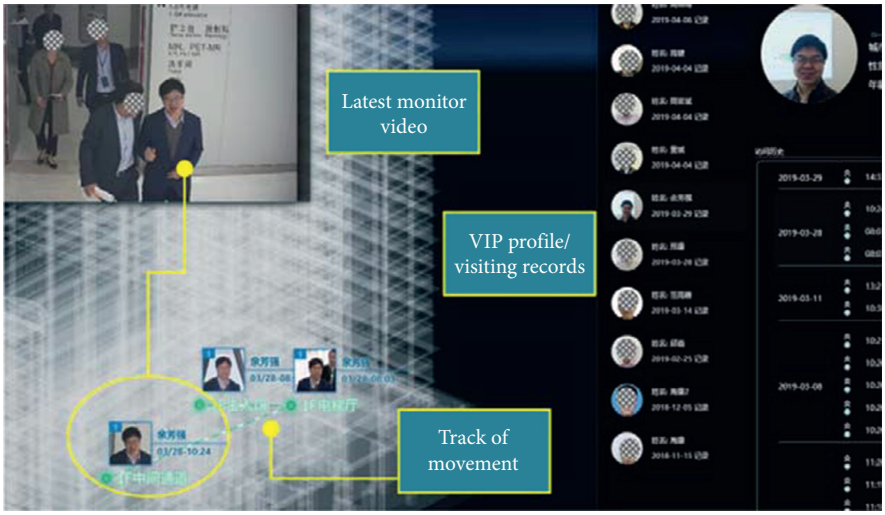


Figure 9: Security system integration (the face images of security camera snapshots have been authorized by corresponding people).

*4.2.6. Security Subsystem.* The platform integrated all security cameras by docking with the video monitoring platform of the hospital. As shown in Figure 9, the system includes real-time monitoring, trajectory monitoring, and key area monitoring. By clicking the camera icons on the 3D building model, real-time videos were directly called, achieving seamless target tracking around 360 degrees. The advanced tracking function was running for important guests and dangerous persons as well. The problems of "medical dispute profiteer" seriously threatened medical order. With the help of the security subsystem, facial recognition warnings would be triggered as soon as medical dispute personnel invaded the range of any security cameras, based on their photo profiles. The DT control center would directly inform security guards on corresponding floors.

*4.2.7. Guest Flow Management.* Through facial recognition cameras at all entrances on each floor, real-time guest flow management was realized. The sum of flow was calculated every five minutes by ETL. As soon as average flow strength (defined as the percentage of incoming/outcoming flow to the current entrance's maximum volume) exceeded a threshold of 0.25, a warning would be sent to the control center. Managers of security guards would receive a prompt on mobile apps as well. Vehicle license plate recognition was embedded into the main entrance cameras. Car number, entering time, leaving time, and parking lane of every visited car was recorded. Managers could check photos and accumulated numbers of car flow.

### *4.3. Intelligent Diagnosis for Hospital Optimization*

*4.3.1. Abnormal Electric Usage Detection.* Various electrical circuits in the hospital show different laws of usage. For example, the lighting of the outpatient waiting area consumed less electricity in the daytime, more in the evening, and almost zero at night, while the consumption of the

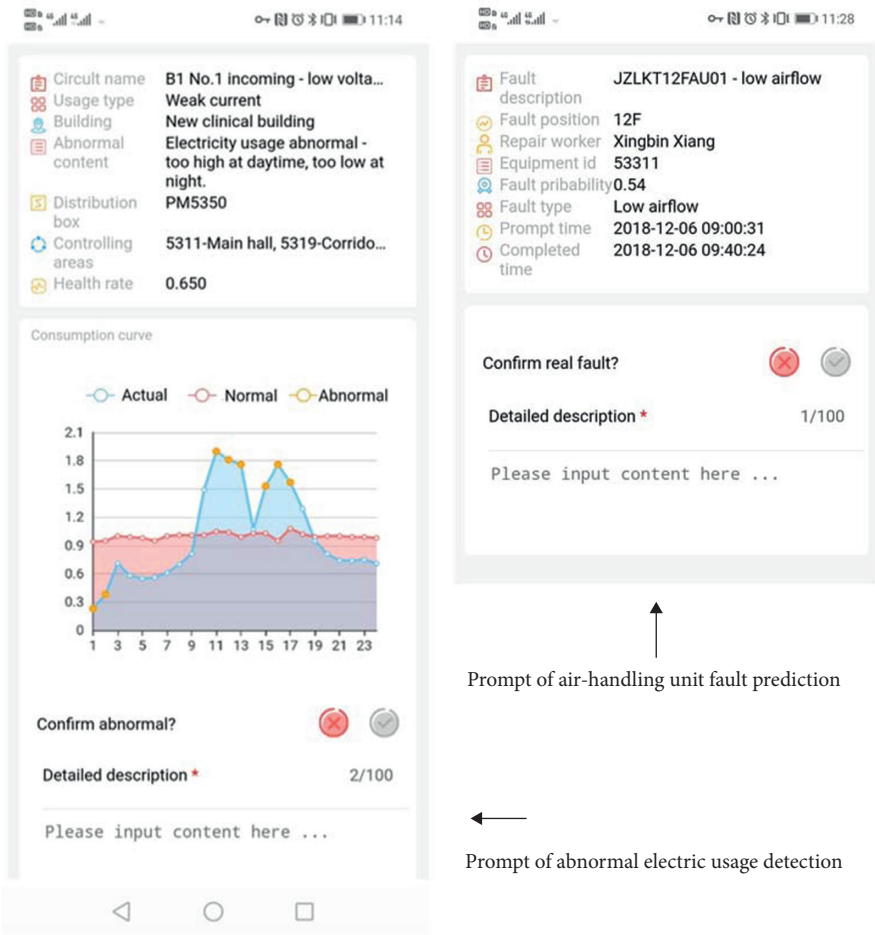


Figure 10: Intelligent diagnosis prompts on mobile apps.

power system is higher in the morning and remains relatively low after that. The monitoring data of 230 smart meters were automatically classified by the k-means cluster algorithm. This method is unsupervised and fully automated, thus very suitable to find unknown patterns. Seven kinds of normal electricity consumption behaviors and corresponding groups of meters were obtained. The DT system continuously monitored the electricity usage and identified any abnormal meter that exceeds or falls below the 20% threshold from corresponding normal behavior. Abnormal circuits were displayed on a large screen, and check tasks were prompted via mobile app (left part of Figure 10). For confirmed abnormally high consumption hours, workers must locate related facilities and stop unnecessary energy consumption. As for confirmed abnormally low consumption, they should check if any machine stops working.

*4.3.2. Air-Handling Unit Fault Prediction.* The raw data comes from the combination of BA monitoring data and repair records. To be specific, after an AHU confirmed a real fault alarm, take out the monitoring data of the last 24 hours and take out the specific type of fault as a pair of training sets. To learn prediction rules from such time-series data, Long Term and Short Term Memory (LSTM) networks were employed. This kind of network has a flexible memory, tracking the abnormal data changes over time. The LSTM prediction model covered 10 types of faults in total, such as overheat and undercooling, low airflow, clogged filters, etc. On the other hand, the data warehouse continuously inputs the latest 24-hour monitoring data of all AHUs. If the predicted failure probability was greater than 0.6, an early warning would be issued in the system and mobile app (right part of Figure 10). As the number of real failures increases, the prediction model continued to receive new training data, which in turn increased its accuracy.

*4.3.3. Frequent Repair Pattern Recognition.* The maintenance requests of the repair service system were recorded in Chinese natural language. There were about 400 records per month, often in one or two short sentences describing the repair location and reasons, so the hidden laws behind these sentences could not be analyzed directly. Unlike English, word segmentation is a crucial preprocessing in Chinese language analysis. Therefore, an open-source Chinese NLP algorithm was adopted. Information including repair floor, department, room, and type of damage was extracted. The

Table 3: A pattern of frequent repairs.

| Chinese description & word segment | English translation* | Request time | Extracted position & connected ID in DT | Extracted repair type |
|---|---|---|---|---|
| 四楼/ICU/水龙头/坏 | The faucet was broken in ICU on the fourth floor. | 2018-12-05 14:12 | 4F ICU-4003 | Basin/faucets |
| 五楼/ICU/台盆/漏水 | The basin was leaking in ICU on the fifth floor. | 2018-12-07 8:42 | 5F ICU-5005 | Basin/faucets |
| 五楼/ICU/水龙头/损坏 | The faucet was broken in ICU on the fifth floor. | 2018-12-19 10:20 | 5F ICU-5005 | Basin/faucets |
| 4F/ICU/水龙头/不/出水 | The faucet did not work in ICU on 4F. | 2018-12-22 8:13 | 4F ICU-4003 | Basin/faucets |

*English translations of repair descriptions are only for the reader's reference. They were not listed in the original DT system.

Table 4: Two examples of low-quality maintenance checking.

| | 3 weeks before | 2 weeks before | 1 week before | 1 week after | 2 week after | 3 week after | $p$ value |
|---|---|---|---|---|---|---|---|
| Elevator faults | 12 | 6 | 9 | 11 | 5 | 7 | **0.62** |
| AHU faults | 11 | 9 | 10 | 22 | 17 | 14 | **0.074** |

system automatically puts similar repairs in the same group as a repair pattern. These patterns were attached to the monthly report. When managers found interesting patterns, they would make some optimization decisions. For example, the washbasin faucets in two Intensive Care Unit (ICU) rooms had been damaged 4 times in December (detailed listed in Table 3). After inspection, it was found that they all belonged to the same brand, so they were all replaced. Despite additional cost, it ensured normal medical activities, and tens of hours of maintenance time were saved.

*4.3.4. Low-Quality Maintenance Checking.* Some outsourcing companies contracted the maintenance work of some main facility units of the hospital. In the past, there were only simple qualitative evaluation methods to judge the business quality of these outsourcing companies. After using the DT system to manage the maintenance work, the maintenance records of each equipment and its fault repair records could be automatically analyzed. Using the $t$-test of the hypothesis test method, if the mean value of the repair amount sequence after maintenance was greater than that before maintenance and statistically significant, the quality was considered low. Table 4 lists the fault numbers of two kinds of maintenance. A $t$-test was executed in three week's range. The AHU maintenance team was believed of low quality because the $p$ value of the hypothesis test was less than 0.1, indicating significantly more faults happening even after maintenance. While maintenance work of elevators was considered normal as usual.

## 5. Discussion and Conclusion

The exemplary DT project in East Hospital has been running for more than a year and considered reaching desired performance: (1) A survey showed a 10 percent increment in management satisfaction compared to the old clinical building. (2) The overall energy consumption was estimated to save about 1% every year. (3) More than 10% of facility faults and requested repairs were avoided by DT diagnosis. Although the exemplary case was conducted in Shanghai, China, the "continuous lifecycle integration" concept is not limited to countries or regions. Because of common management requirements and similar electric systems, this case will provide some problem-solving references to other modern hospitals around the world.

In summary, according to the proposed concept of continuous lifecycle integration and early movement of the general contractor, a full functional DT was successfully established. This case mainly highlighted in (1) continuous integration of huge data throughout the lifecycle. From design, construction, pre-O&M phase all the way up to the O&M phase, terabytes of static information and dynamic data were managed to integrate as a unified DT system, including building geometry model, attached property information, common BA systems, repair and maintenance systems, security management system, and hospital's special business systems. The continuous integration process over the full lifecycle and early movement of general contractors have both been proved valid in this paper. This method can be directly employed by similar hospital projects and partially imitated by other complex public buildings. (2) Real-time visual management—managers can grasp the detailed status of the whole hospital by visual management, which is far more efficient than manual work. Big data services were developed as a backend to consistently display high-density data streams. Now, the real-time status of the hospital building is displayed in a modern control center as operation brain guiding everyday management activities. With this real-time mechanism, DT has shown much more potential than traditional BIM technology, which will help professionals upgrade from BIM to DT. (3) Intelligent DT diagnosis functions—professional AI models were assembled as a diagnosis engine, and it works seamlessly with visual management functions. Huge amounts of dynamic integrated data supported timely facility diagnosis and operation suggestions that are automatically sent back to reality. This

exemplary case showed the potential strength of AI and modern data analysis skills in DT applications. It is proved that an intelligent diagnosis module values the most, thus should be carefully developed.

During the implementation of the exemplary case, the consultant group found that DT is still not totally adapted to the need of building projects. At least, three aspects of shortages or puzzles required further research:

(1) BA systems or medical systems were too professional for the DT platform to directly control. Therefore, the existing DT has not realized the automatic control of the faulty equipment. Now only the real-time alarm was sent back to the control center, and the management personnel will assign the task to the maintenance workers to manually solve the equipment failure. For example, this case did not try to link an automated energy-saving mechanism. All abnormal behaviors were directly processed by on-site works. If the control function was implemented, additional system debugging would be required, which would lead to an unaffordable expense. However, if DT can truly achieve the reliable automatic adjustment of critical machines and autonomously eliminate the fault state, say, reduce energy consumption, it will greatly enhance the practical value of DT.

(2) Financial risks are still considerable when using DT widely among building projects. Establishing a DT involves large-scale construction of networks for intelligent sensors, cameras, wireless communicators, etc. Without careful planning at the beginning of the design phase, it will be very difficult or even impossible to add such hardware devices to an as-built building project. Control centers for the management system are also expensive. Therefore, proprietors must have strong motivation and clear foresight. One project should employ DT technologies with no hesitation if proved financially beneficial.

(3) Although the early movement of general contractors was proved valid in data processing, system development afterward still involved tedious bargaining with proprietors of the building. There are always sensitive data integrated. If secret data, such as personal data of patients for facial recognition, was open to developers, the borders of safety responsibilities would not be so clear. If not open, the visual management functions of the DT system will be incomplete. Proprietors should find the balance between system function and information safety. Both technical and management innovations are required.

In future research, these puzzles are expected to be addressed by more advanced DT application cases. The practice is believed to be more convincing than pure theory in the DT field because major obstacles often emerge on management and budget issues but not technical issues. Along with accumulating cases, developers can even publish their successful software components as trendy "micro-service" modules that can be distributed and downloaded individually. Building industry associations should also make data standards for diagnosis models. According to these public standards, other DT developers just need to process dynamic data from DT into standardized input and then choose a suitable as-built diagnosis model. Advanced AI coders can contribute model repositories like open-source communities, while nonprofessionals do not need to put extra effort into developing existing functions. Ideally, the ecosystem of DT applications will gradually emerge and benefit both users and software developers from the building industry.

## Data Availability

The data used to support the case study are available from the corresponding author upon request or download from open data on the product website: https://www.ibuildingsh.com.

## Conflicts of Interest

The authors declare no conflicts of interest.

## Acknowledgments

This work was financially supported by the Shanghai Industry Internet Development Foundation (2019-GYHLW-01002), Shanghai Rising-Star Program (18QB1402300), and Shanghai Sailing Program (18YF1410400 and 19YF1421100). The authors would like to thank Shanghai East Hospital Affiliated to Tongji University for the authorization to report this case project.

## References

[1] P. Yu, W. Wen, D. Ji, C. Zhai, and L. Xie, "A framework to assess the seismic resilience of urban hospitals," *Advances in Civil Engineering*, vol. 2019, Article ID 7654683, 11 pages, 2019.

[2] Z.-Z. Hu, P.-L. Tian, S.-W. Li, and J.-P. Zhang, "BIM-based integrated delivery technologies for intelligent MEP management in the operation and maintenance phase," *Advances in Engineering Software*, vol. 115, pp. 1–16, 2018.

[3] X. Gao and P. Pishdad-Bozorgi, "BIM-enabled facilities operation and maintenance: a review," *Advanced Engineering Informatics*, vol. 39, pp. 227–247, 2019.

[4] P. Pishdad-Bozorgi, X. Gao, C. Eastman, and A. P. Self, "Planning and developing facility management-enabled building information model (FM-enabled BIM)," *Automation in Construction*, vol. 87, pp. 22–38, 2018.

[5] C. Moreno, S. Olbina, and R. R. Issa, "BIM use by architecture, engineering, and construction (AEC) industry in educational facility projects," *Advances in Civil Engineering*, vol. 2019, Article ID 1392684, 19 pages, 2019.

[6] T. Gerrish, K. Ruikar, M. Cook, M. Johnson, M. Phillip, and C. Lowry, "BIM application to building energy performance visualisation and management: challenges and potential," *Energy and Buildings*, vol. 144, pp. 218–228, 2017.

[7] L. Deng, M. Zhong, L. Liao, L. Peng, and S. Lai, "Research on safety management application of dangerous sources in engineering construction based on BIM technology," *Advances in Civil Engineering*, vol. 2019, Article ID 7450426, 10 pages, 2019.

[8] V. Stojanovic, M. Trapp, R. Richter, B. Hagedorn, J. Döllner, and M. Alamaniotis, "Towards the generation of digital twins for facility management based on 3D point clouds," in *Proceedings of the 34th Annual ARCOM Conference*, Belfast, UK, 2018.

[9] Q. Lu, X. Xie, A. K. Parlikad, J. M. Schooling, and E. Konstantinou, "Moving from building information models to digital twins for operation and maintenance," *Proceedings of the Institution of Civil Engineers—Smart Infrastructure and Construction*, pp. 1–9, 2020.

[10] V. Q. Lu, A. K. Parlikad, and P. Woodall, "Developing a dynamic digital twin at a building level: using Cambridge campus as case study," in *Proceedings of the 2019 International Conference on Smart Infrastructure and Construction 2019 (ICSIC) Driving Data-Informed Decision-Making*, Cambridge, UK, 2019.

[11] R. Alonso, M. Borras, R. H. E. M. Koppelaar, A. Lodigiani, E. Loscos, and E. Yöntem, "SPHERE: BIM digital twin platform," *Proceedings*, vol. 20, no. 1, p. 9, 2019.

[12] D. Wohlfeld, V. Weiss, and B. Becker, *Digital Shadow–From Production to Product*, Springer, Berlin, Germany, 2017.

[13] W. Kritzinger, M. Karner, G. Traar, J. Henjes, and W. Sihn, "Digital twin in manufacturing: a categorical literature review and classification," *IFAC-PapersOnLine*, vol. 51, no. 11, pp. 1016–1022, 2018.

[14] S. Kaewunruen and N. Xu, "Digital twin for sustainability evaluation of railway station buildings," *Frontiers in Built Environment*, vol. 4, 2018.

[15] Q. Lu, X. Xie, J. Heaton, A. K. Parlikad, J. Schooling, and M. Alamaniotis, "From BIM towards digital twin: strategy and future development for smart asset management," in *Proceedings of the 2019 International Workshop on Service Orientation in Holonic and Multi-Agent Manufacturing*, Valencia, Spain, 2019.

[16] S. Kaewunruen, P. Rungskunroch, and J. Welsh, "A digital-twin evaluation of net zero energy building for existing buildings," *Sustainability*, vol. 11, p. 159, 2019.

[17] T. Delbrügger, L. T. Lenz, D. Losch, and J. Roßmann, "A navigation framework for digital twins of factories based on building information modeling," in *Proceedings of the 2017 22nd IEEE International Conference on Emerging Technologies and Factory Automation (ETFA)*, Limassol, Cyprus, 2017.

[18] M. Macchi, I. Roda, E. Negri, and L. Fumagalli, "Exploring the role of digital twin for asset lifecycle management," *IFAC-PapersOnLine*, vol. 51, no. 11, pp. 790–795, 2018.

[19] F. Tao, J. Cheng, Q. Qi, M. Zhang, H. Zhang, and F. Sui, "Digital twin-driven product design, manufacturing and service with big data," *The International Journal of Advanced Manufacturing Technology*, vol. 94, no. 9–12, pp. 3563–3576, 2018.

[20] Y. Peng, S.-W. Li, and Z.-Z. Hu, "A self-learning dynamic path planning method for evacuation in large public buildings based on neural networks," *Neurocomputing*, vol. 365, pp. 71–85, 2019.

[21] H. B. Gunay, W. Shen, and C. Yang, "Text-mining building maintenance work orders for component fault frequency," *Building Research & Information*, vol. 47, no. 5, pp. 518–533, 2019.

[22] Y. Peng, J.-R. Lin, J.-P. Zhang, and Z.-Z. Hu, "A hybrid data mining approach on BIM-based building operation and maintenance," *Building and Environment*, vol. 126, pp. 483–495, 2017.

[23] R. Bortolini and N. Forcada, "Analysis of building maintenance requests using a text mining approach: building services evaluation," *Building Research & Information*, vol. 48, no. 2, pp. 207–217, 2020.

[24] M. Austin, P. Delgoshaei, M. Coelho, and M. Heidarinejad, "Architecting smart city digital twins: combined semantic model and machine learning approach," *Journal of Management in Engineering*, vol. 36, Article ID 04020026, 2020.

[25] T. H.-J. Uhlemann, C. Lehmann, and R. Steinhilper, "The digital twin: realizing the cyber-physical production system for industry 4.0," *Procedia CIRP*, vol. 61, pp. 335–340, 2017.

Hindawi
Advances in Civil Engineering
Volume 2020, Article ID 8812928, 14 pages
https://doi.org/10.1155/2020/8812928

*Research Article*

# A Deep Learning-Based Approach to Enable Action Recognition for Construction Equipment

**Jinyue Zhang,[1] Lijun Zi,[2] Yuexian Hou,[3] Mingen Wang,[3] Wenting Jiang,[2] and Da Deng[3]**

[1]*College of Management and Economics, Tianjin University, Tianjin, China*
[2]*Guangzhou Metro Design and Research Institute Co., Ltd., Guangzhou, China*
[3]*College of Intelligence and Computing, Tianjin University, Tianjin, China*

Correspondence should be addressed to Yuexian Hou; yxhou@tju.edu.cn

Received 10 June 2020; Revised 21 October 2020; Accepted 22 October 2020; Published 5 November 2020

Academic Editor: Jia-Rui Lin

Copyright © 2020 Jinyue Zhang et al. This is an open access article distributed under the Creative Commons Attribution License, which permits unrestricted use, distribution, and reproduction in any medium, provided the original work is properly cited.

In order to support smart construction, digital twin has been a well-recognized concept for virtually representing the physical facility. It is equally important to recognize human actions and the movement of construction equipment in virtual construction scenes. Compared to the extensive research on human action recognition (HAR) that can be applied to identify construction workers, research in the field of construction equipment action recognition (CEAR) is very limited, mainly due to the lack of available datasets with videos showing the actions of construction equipment. The contributions of this research are as follows: (1) the development of a comprehensive video dataset of 2,064 clips with five action types for excavators and dump trucks; (2) a new deep learning-based CEAR approach (known as a simplified temporal convolutional network or STCN) that combines a convolutional neural network (CNN) with long short-term memory (LSTM, an artificial recurrent neural network), where CNN is used to extract image features and LSTM is used to extract temporal features from video frame sequences; and (3) the comparison between this proposed new approach and a similar CEAR method and two of the best-performing HAR approaches, namely, three-dimensional (3D) convolutional networks (ConvNets) and two-stream ConvNets, to evaluate the performance of STCN and investigate the possibility of directly transferring HAR approaches to the field of CEAR.

## 1. Introduction

Human action recognition (HAR) is one of the most popular research areas in computer vision (CV), and the outcomes have been extensively applied in video surveillance and human-machine interaction for a variety of application scenarios such as safety monitoring and control [1]. A basic methodology for recognizing human actions is to detect a human in a video/photograph, segmenting and mapping the body attributes followed by the result [2]. A number of methods for achieving HAR have been developed in the past few decades. Poppe [3] and Purohit and Chauhan [4] reviewed and classified different recognition algorithms for human actions. The deep learning (DL) method has attracted more attention in the area of CV following the success of AlexNet [5] in using convolutional neural networks (CNN) for image classification, gradually replacing the traditional HAR approaches based on the spatial and temporal structure of body movements. With advances in action recognition and the popularization of high-end hardware such high-resolution surveillance cameras, HAR is increasingly applied at work (e.g., in video surveillance at airports for security purposes) and at home (e.g., in health monitoring for elderly people).

In the construction industry, digital twin has been a well-recognized concept for smart construction. Beside the analysis and optimization supported by a digital representation of the facility itself, there is also a need to enhance the performance of workers and equipment, which is facilitated by automated perception and analysis of on-site activities. This requires the computer to not only identify workers and equipment but also recognize their locations and actions [6]. Many potential benefits could be realized if HAR could be applied for the monitoring and control of construction

equipment. With a detailed analysis of equipment actions and a continuous optimization of equipment operation, a construction project can be better managed: for example, equipment productivity would be improved by reducing the idle time, the environment would be protected by lowering carbon emissions, and accidents would be avoided by coordinating the movement of workers and equipment [7]. Currently, the analysis of construction machinery activity is mainly performed by human workers, a process that can be time-consuming, costly, and prone to errors. A low-cost, reliable construction equipment action recognition (CEAR) method can enable automated analysis of many scenarios at construction sites and can support smart construction applications.

Researchers have long studied the recognition of construction equipment actions and shown promising results. The CEAR methods can be roughly divided into sensor-based methods and visual-based methods. In the works that use sensors for recognizing the activity of construction equipment, of note are real-time location systems (RTLS) [8, 9], audio signals [10, 11], inertial measurement units (IMU) [12, 13], and so forth. In the works using visual-based methodology, many studies have adopted image processing-based approaches. Zou and Kim [14] used image color space (hue, saturation, and value) as the basis for image segmentation and tracing algorithms to identify the changing centroid coordinates of an excavator in successive images taken at fixed time intervals to achieve recognition of equipment movement. Gong et al. [15] proposed a visual learning approach to classify actions of construction workers and equipment using the Harris 3D interest point detector as the feature detector, local histograms as the feature representation, a bag-of-words model as the feature model, and Bayesian network models as the learning mechanism. Using a similar method, Golparvar-Fard et al. [7] studied single actions of construction equipment used for earthmoving. In this method, a video is initially represented as a collection of spatiotemporal visual features by extracting space-time interest points and describing each feature with a histogram of oriented gradients (HOG). The algorithm automatically learns the distributions of the spatiotemporal features and action categories using a multiclass support vector machine (SVM) classifier.

Many existing CEAR approaches rely on hand-crafted features, which is necessary to manually segment the time-series data to extract statistical features. This feature extraction process will be limited by human knowledge and can only extract shallow features specified by humans. Thus, they will only work well for simple actions that can be easily distinguished. The results will no longer be reliable once the viewpoint has changed, more background noise is present, and the views become blocked [3], which will be inevitable due to the dynamic nature of a construction site. Furthermore, these traditional methods require manual intervention at multiple points to adjust parameters, which limits the application of these methods in cases where end-to-end output is desired. Moreover, nearly all current methods for action recognition are data driven; that is, they require a large amount of data in order to train the recognition model to achieve a better recognition rate. As such, a large-scale dataset is of considerable significance. Golparvar-Fard et al. [7] developed the first comprehensive video dataset for action recognition of excavators and dump trucks. However, it is rare to find similar datasets for other types of construction equipment.

As a part of this research, a video dataset for excavators and dump trucks is first established to expand the size of the existing datasets on construction equipment, along with a corresponding optical flow dataset that can be used for related algorithm studies. Second, a deep learning-based CEAR model was proposed by taking advantage of deep learning, which has good generalization performance, is capable of end-to-end training, and requires no feature engineering [16]. Lastly, the deep learning-based method is compared with existing similar methods and some of the best HAR methods to determine whether the proposed method is advanced and whether advanced HAR algorithms could be directly transferred to CEAR. Related research works in HAR and CEAR are discussed in the next section, along with their limitations. Following that, the dataset development is illustrated in terms of camera arrangement, data acquisition method, and data processing method, and a detailed presentation of proposed deep learning-based CEAR model is provided. The experimental results and a comparison of the results of the proposed model to those of two HAR algorithms are discussed. The final section presents the conclusions that can be made based on the results of this research study.

## 2. Materials and Methods

*2.1. Related Works.* In recent years, numerous research efforts have been made to apply action recognition technologies in the construction industry. Some of these studies used construction workers as their research subjects and focused on worker health and safety, while other studies used construction equipment as the research subject and aimed to improve productivity and reduce costs for the construction project. According to different data sources, the approaches used in these studies can be divided into methods based on visual data and methods based on sensors data. In the current construction industry, cameras are generally installed for surveillance and other purposes. This makes the acquisition of visual data more convenient and cost-effective. Moreover, visual data can usually provide richer information. As such, this research focuses on determining the activities of construction equipment from visual data. Previous works that use vision-based methods, known as computer vision (CV), are discussed in this section. Seo et al. [17] reviewed previous attempts to apply CV for construction safety and health monitoring from both a technical perspective and a practical perspective. They categorized previous studies into three groups—object detection, object tracking, and action recognition—based on the type of information required to evaluate unsafe conditions and actions. However, in the current status of CV application in construction sites, even the most advanced theories are faced with challenges such

as a lack of high-quality datasets and the slow development of algorithms. At the same time, the development of deep learning technology, the increased image processing power provided by a graphics processing unit (GPU), and the decrease in price of specialized cameras bring about new opportunities for adopting CV-based applications in the construction industry.

*2.1.1. Human Action Recognition.* Many research studies have investigated CV-based human action recognition (HAR) systems, including both traditional hand-crafted and learning-based action representation approaches. The difference between these two approaches lies mainly in the method used to extract features from images. A traditional hand-crafted representation-based approach relies on the expert-designed feature detectors and descriptors such as Hessian3D, scale-invariant feature transform (SIFT), HOG, enhanced speeded-up robust features (ESURF), and local binary pattern (LBP). On the contrary, a learning-based representation approach uses a trainable feature extractor that automatically learns features from the raw data, eliminating the need for manual assignment and enabling end-to-end learning.

The traditional hand-crafted action representation approach has been popular in the HAR community and has achieved remarkable results when using various well-known public datasets [18]. This approach includes four techniques: the space/time-based method [19], the appearance-based method [20, 21], the LBP-based method [22], and the fuzzy logic-based method [23]. Using these methods, the important features from a sequence of image frames are extracted to build the feature vector prior to classification by a trained classifier. For example, dense trajectory (DT) uses trajectories to capture the local motion information of the video, and a dense representation guarantees good coverage for capturing foreground motions as well as the surrounding context [24]. Wang and Shmid [25] proposed an improved DT (iDT) approach to improve the performance of video representation by making corrections that take camera motion into account. Currently, researchers are aiming to increase the quantity and quality of the dataset for human action recognition. However, most successful hand-crafted representation methods are based on local densely sampled descriptors, which will result in a higher computational cost.

The appropriate and efficient representation of data is the key to HAR. Unlike the above-mentioned approaches, where an action is represented by hand-crafted feature detectors and descriptors, learning-based representation approaches have the ability to learn a feature automatically from the raw data, thus introducing the concept of end-to-end learning, which refers to transformation from the pixel level to an action classification and is not limited by human knowledge [18]. Some learning-based approaches are based on genetic programming [26] and dictionary learning [27], while others employ deep learning-based models for action representation.

Deep learning is an important area of machine learning which aims to achieve learning at multiple levels of representation and abstraction in order to make sense of data such as speech, images, and text. The research of Karpathy et al. [28] showed the potential of CNN for large-scale video classification tasks. Simonyan and Zisserman [29] proposed a two-stream convolutional networks (two-stream ConvNets) architecture that incorporates spatial and temporal networks and demonstrated that a ConvNet trained on multiframe dense optical flow is able to achieve very good performance despite the limited amount of available training data. Tran et al. [30] argued that deep three-dimensional (3D) ConvNets trained on a large-scale supervised video dataset are effective for spatiotemporal feature learning. The 3D ConvNets build on two-dimensional (2D) ConvNets but include a time dimension; thus, they solve the issue of the inability of CNNs to extract temporal features. Carreira and Zisserman [31] introduced a new two-stream inflated 3D (I3D) ConvNet, where filters and pooling kernels of very deep image classification ConvNets are expanded into 3D, making it possible to learn seamless spatiotemporal feature extractors from video while leveraging successful ImageNet architecture designs and even their parameters. Varol et al. [32] made identifications from video representations using neural networks with long-term temporal convolutions (LTC) and demonstrated that LTC-CNN models with increased temporal extents improve the accuracy of action recognition. Ng et al. [33] employed a recurrent neural network that uses long short-term memory (LSTM) cells that are connected to the output of the underlying CNN. This LSTM-CNN approach exhibits significant performance improvement over previously published results on the Sports 1 million dataset and the UCF101 dataset [34]. Donahue et al. [35] developed a novel recurrent convolutional architecture suitable for large-scale visual learning, which is end-to-end trainable, and they demonstrated the value of these models for benchmark video recognition tasks. Sevilla-Lara et al. [36] investigated the impact of different flow algorithms and input transformations to better understand how these would affect a state-of-the-art action recognition method, and they recommended a better way of using optical flow in the future.

Recently, the research community has paid a great deal of attention to deep learning-based approaches, mainly due to their excellent performance as compared to hand-crafted action representation approaches. However, some of the best learning-based methods still rely on hand-crafted features. The main reason is the lack of huge datasets for action recognition which are required to train the feature extractors. As no huge dataset such as ImageNet in the field of object recognition exists, the HAR community is working on the development of useful datasets. HMDB [37] is an action video database with 51 action categories, which in total contain around 7,000 manually annotated clips. UCF101 [34] consists of 101 action classes in a total of 13,320 clips of video data. More recently, the development of a large-scale dataset called ActivityNet [38] provides samples from 203 activity categories with an average of 137 untrimmed videos per class and 1.41 activity instances per video, for a total of 849 hours of video. YouTube-8M is the largest multilabel video classification dataset [39] and it includes about 8

million videos (approximately 500,000 hours of video), annotated with a vocabulary of 4,800 visual entities.

*2.1.2. Construction Equipment Action Recognition.* Although many research studies have investigated the use of HAR in the construction industry for health/safety monitoring and for the control of construction workers, the study of construction equipment action recognition (CEAR) is still premature. The first work that can be found in CEAR was conducted by Gong and Caldas [40], who developed an intelligent video computing method to interpret videos of cyclic construction operations and translate the images automatically into productivity information through the recognition of actions of a concrete bucket in the concrete pour process. Akhavian and Behzadan [41] used built-in smartphone sensors as ubiquitous multimodal data collection and transmission nodes in order to detect detailed construction equipment activities, which can ultimately contribute to the process of simulation input modeling. In a case study of front-end loader activity recognition, certain key features are extracted and are used to train supervised machine learning classifiers. Cao et al. [42] proposed a classification algorithm based on acoustics processing for four types of excavation equipment. They developed new acoustic statistical features (short frame energy ratio, concentration of spectrum amplitude ratio, truncated energy range, and pulse interval) to characterize acoustic signals; then, based on the probability density distributions of these acoustic features, a novel classifier was proposed. This approach has a great potential to be generalized. Han and Golparvar-Fard [43] investigated current strategies for leveraging emerging big visual data in construction performance monitoring from the standpoints of reliability, relevance, and speed, and they structured a road map for research in visual sensing and analytics for construction. Roberts and Golparvar-Fard [44] presented a new benchmark dataset consisting of ten videos that can be used to detect, track, and analyze construction work activities of excavators and dump trucks. They also gave an action recognition framework composed of detection module, tracking module, and recognition module. This method can automatically identify excavators and dump trucks from per-frame of the video sequence and track their activities and finally identify their construction actions. Rashid and Louis [45] proposed a data-augmentation framework for generating synthetic time-series training data for RNN-based deep learning networks. Their research results show that deep learning framework outperformed the shallow network regarding model accuracy and generalization, and the data-augmentation methodology has the ability to correctly simulate real-world dataset. Kim and Chi [46] proposed a vision-based action recognition framework that considers the sequential working patterns of earthmoving excavators. The framework includes three main processes: excavator detection, excavator tracking, and excavator action recognition. Among them, the action recognition process used CNN-DLSTM model. The framework demonstrates good generalization performance and proves the important positive impact of sequential pattern modeling on recognition performance. Rashid and Louis [13] researched the use of activity-specific equipment motions instead of vibration for action recognition. The study showed that using inertial measurement unit (IMU) data of different articulated elements can significantly improve the activity recognition results.

Previous CV-based research in the construction industry mainly focused on either identifying/tracking workers and equipment or recognizing workers' actions. Although deep learning-based action recognition algorithms have dominated the field of HAR, they are not widely investigated for CEAR. The challenges in doing so are threefold.

The most significant challenge is the lack of comprehensive datasets for CEAR. Deep learning-based approaches largely rely on large numbers of high-quality raw video clips to train the feature extractor for a better performance in the later classification task. Although the number of available datasets for HAR is increasing, as mentioned earlier, this is not the case in the field of CEAR. A comprehensive dataset for CEAR needs to include video clips from a variety of working environments, from different viewing angles, and with various amounts of background clutter.

Currently, there is a shortage of algorithms that can be applied at real construction sites. Most existing researches of CEAR in the construction industry use pattern recognition methods and those algorithms rely on hand-crafted features and will be limited by human knowledge. When they are applied to actual cases, their recognition performance will be greatly affected by human factors.

At the present time, there is no clear benchmark for CEAR. The number of studies in CEAR is fewer than that for HAR and, due to the shortage of standard video datasets for construction equipment, it is hard to compare different approaches that are based on the same dataset.

Focusing on these three aspects, in this study, a new dataset for excavators and dump trucks was initially developed. This dataset was used to expand the existing dataset for the same types of equipment [7] and to train/verify the feature extractor using the deep learning-based method proposed in this research. The action recognition method is based on deep learning theory, which can automatically extract high-level features from raw data without feature engineering. The possible problems of manual operation features can be avoided. Comparison with existing similar CEAR method [46] proves that it has comparable performance. By comparing the results after applying two advanced deep learning-based HAR approaches to the same dataset, this research study investigates the possibility of transferring some of the best HAR algorithms to CEAR and broadens the path of researching CEAR methods.

### 2.2. Dataset Development

*2.2.1. Dataset Collection.* The construction equipment considered in the new dataset includes an excavator and a dump truck. For these two pieces of equipment, there are five activities in all, as listed in Table 1 and shown in Figure 1.

Table 1: Construction equipment activities.

| Equipment | Activities |
|---|---|
| Excavator | Digging, swinging, dumping |
| Dump truck | Moving forward, moving backward |

To take advantage of the recent improvements to cameras in smartphones, this research used smartphones with a 12-megapixel rear camera to collect raw data. Video footage was collected at a resolution of 720 progressive scan (720p) and at 25 frames per second (fps). The selection of camera placement needs to be taken into account to prevent possible obstructions and to ensure a good proportion of construction equipment in the picture. Based on the site survey, it was found that the front views and the side views of construction equipment can provide more effective information about their actions than other views. The front view refers to the projection view from the direction that the driver faces when driving the device normally moving forward. Therefore, in order to capture the various views of the construction equipment and their actions from different perspectives, four cameras were used to collect videos within a 180-degree range around the construction equipment, as shown in Figure 2. Cameras 1, 2, and 3 were used to capture the front view, the side view, and the rear view, and Camera 4 was placed at a position in between Camera 1 (front view) and Camera 2 (side view), as can be seen in Figure 2, in order to provide supplemental information. This camera configuration guarantees a sufficient number of action views while using a minimum amount of video capturing resources. Finally, an annotation document was created based on the five action types for construction equipment. Table 2 shows the annotations for the action types, the total number of video clips of each type, and the numbers of video clips for various subsets of data.

*2.2.2. Data Processing.* DivX, a video codec developed by DivX, LLC, was used to transcode the original videos to MPEG-4 format with a resolution of 480 pixels by 360 pixels. The transcoded videos were classified according to the four recording angels as shown in Figure 2; then videos were cut into shorter clips to ensure that each video clip, which had a duration ranging from 3 to 20 seconds, would contain only one complete action of a single piece of equipment. The format for the file-naming convention for the shorter video clips is "v_equipment_action_ID#" (e.g., v_evacuator_swing_001.MPEG). Finally, in the category of each recording angle, video clips were classified according to the five action types, and stratified sampling was performed according to a ratio of 6 : 2:2 to form a training set, a test set, and a verification set.

For the processed data, corresponding optical flow dataset was developed by the method of Lucas-Kanade algorithm [46]. This dataset will be used to verify the performance of the HAR algorithm used for CEAR and can be used as a complement to the development of CEAR datasets. The examples of the optical flow dataset are shown in Figure 3. The video dataset developed in this research was of open source. Everybody can obtain the dataset from https://github.com/hnpyn/CEAR_dataset. The authors will update and maintain this project regularly.

*2.3. Development of a Simplified Temporal Convolutional Network (STCN).* Ng et al. [33] proposed a method for modeling video frames into ordered frame sequences by using a recurrent neural network (RNN), which connects the LSTM units to the output of the CNN. The CNN structure is based on GoogLeNet [47], while the RNN adopts a deep LSTM structure [48] with five LSTM layers. This model performed very well in action recognition as compared to the best approaches available at the time. Similarly, Donahue et al. [35] also employed a method of directly connecting the RNN to the CNN structure and found that when nonlinearity is incorporated into the network status updates, learning of long-term dependencies is possible. As such, temporal dynamics and convolutional perceptual representations can be learned by jointly training the RNN and the CNN. It has been proved that the joint architecture of the RNN and the CNN is effective and feasible. Inspired by these studies, the authors have proposed a CEAR process (described in Figure 4) that can automatically extract video data features and perform end-to-end training for action recognition. The core of this process is the neural network shown in the dashed frame, which combines a CNN for extracting features from video clips and a LSTM for extracting the temporal dynamics. A fully connected layer is employed to connect the CNN and the LSTM, and a softmax layer is used to determine the classification of the equipment action.

*2.3.1. Deep Learning.* As an emerging research direction in the field of machine learning [49], deep learning was first proposed by Hinton et al. [50]. The merit of deep learning lies in the additional levels of nonlinear operation that it encompasses [51], and deep learning is able to form more abstract high-level representations or features by combining low-level features, thereby displaying the hierarchical feature representation of the data. Therefore, deep learning is able to automatically learn to obtain the hierarchical feature representations [16] that are more conducive to classification tasks. Traditional machine learning and pattern recognition methods require the manual extraction of features. The model itself only classifies or predicts according to the features, and the hand-crafted features, to a large extent, will determine the quality of the method. It requires both professional knowledge and enough time to allow for manual extraction of features. Thus, it will be limited by human knowledge, and most of the models can only obtain shallow features. This is the intrinsic driving force of this research to develop action recognition algorithm based on deep learning.

*2.3.2. Convolutional Neural Network.* A convolutional neural network (CNN) refers to a class of feedforward neural networks (FNNs) having a convolutional structure, and this

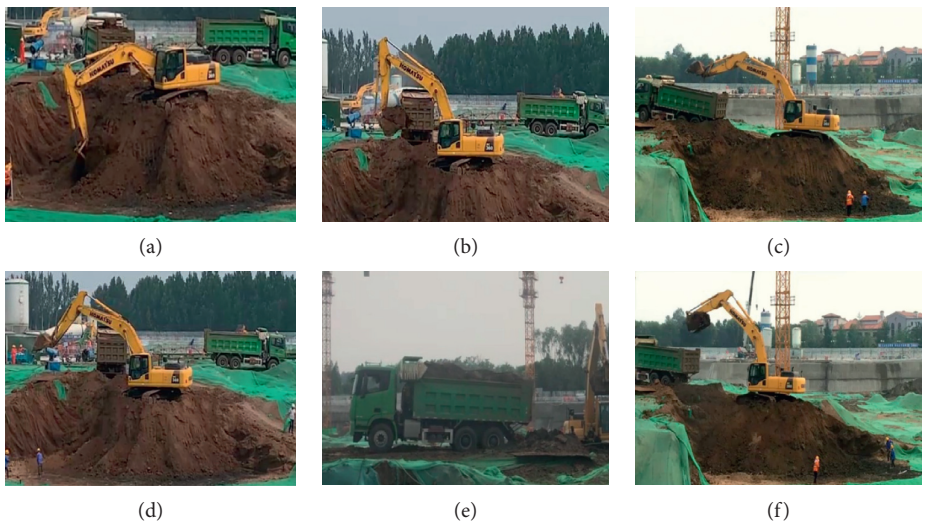

(a) (b) (c)

(d) (e) (f)

Figure 1: Examples of the activities of an excavator and a dump truck: (a) excavator digging, (b) excavator swinging, (c) excavator dumping, (d) excavator swinging, (e) dump truck moving forward, and (f) dump truck moving backward.

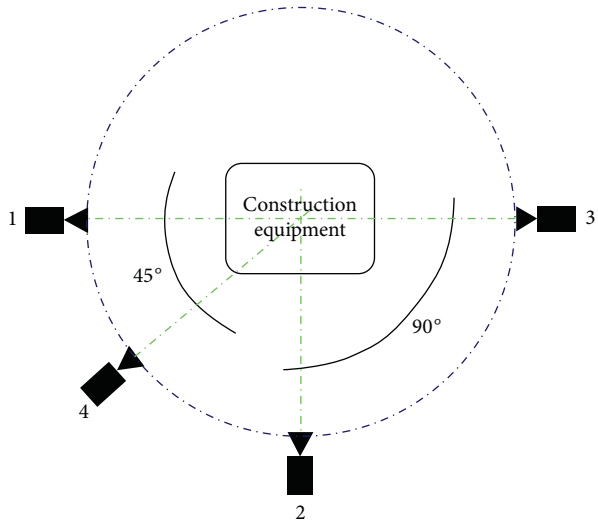


Figure 2: Camera setup used for recording the movement of construction equipment.

Table 2: Dataset composition and action annotations.

| Equipment | Action type | Type annotation | Videos of this type | Videos in training set | Videos in test set | Videos in validation set |
|---|---|---|---|---|---|---|
| Excavator | Digging | 0 | 498 | 298 | 100 | 100 |
| | Dumping | 1 | 513 | 307 | 103 | 103 |
| | Swinging | 2 | 940 | 565 | 187 | 188 |
| Dump truck | Moving backward | 3 | 54 | 32 | 11 | 11 |
| | Moving forward | 4 | 59 | 34 | 13 | 12 |

type of network is one of the representative algorithms in deep learning. The CNN uses the idea of sparse connection and weight sharing to solve the parameter explosion in ordinary FNNs, and it adopts convolution and pooling operations to obtain local features and reduce the dimension of feature space. The CNN generally completes the final classification through softmax by connecting to a fully connected layer.

CNN can use the original data as the input characteristics, which avoids the complex feature extraction process in a traditional machine learning algorithm, and it reduces the number of weights in the weight-sharing structure, thus

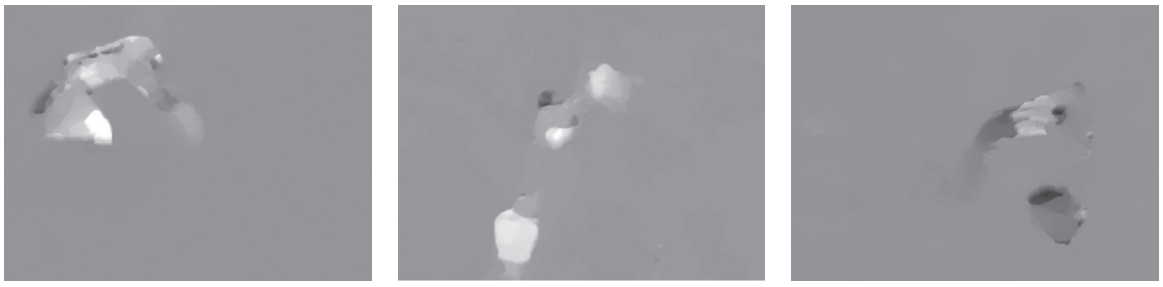

(a) (b) (c)

Figure 3: Examples of the optical flow dataset.

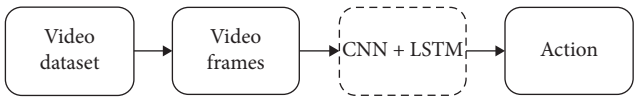


Figure 4: Flow chart for the process of construction equipment action recognition.

decreasing the complexity of the model. At the same time, the feature map is subsampled by using the principle of local correlation in images at the subsampling stage, which effectively reduces the amount of data processing required while retaining useful structural information [49]; because of this, CNNs have been widely used in CV-related tasks in recent years.

LeNet-5 [52] was a milestone in early CNN development, and it has been used to determine the basic structure of a CNN—which contains convolutional layers, pooling layers, and fully connected layers. Later CNNs have basically followed this same structure, with less or more optimization and improvement. AlexNet [5] adopted a structure consisting of five convolutional layers and three fully connected layers, which helped it to succeed in the ImageNet competition. The success of AlexNet indicates that deep learning is a reliable method, and it lays the foundation for using deep learning in image classification and object recognition tasks.

*2.3.3. Long Short-Term Memory.* Long short-term memory (LSTM) [53] is a variant of RNN, which is a feedback neural network that not only inherits most features of the RNN model but also solves the issue of vanishing gradients in regular RNNs [54]. As a nonlinear model, it can be used to build larger and more complex deep neural networks. A common LSTM architecture is composed of a cell (the memory part of the LSTM unit) and three "gates" of the flow of information inside the LSTM unit: an input gate, an output gate, and a forget gate, as shown in Figure 5. These gates are used to either remove or add information to the cell. Cells are circularly connected to each other, replacing the hidden unit in the regular recurrent network. The state unit has a linear self-loop structure whose weight is controlled by the forget gate.

LSTM has two states, the cell state and the hidden state. The cell state changes slowly with time, while the hidden state can vary widely at different times. The gate mechanism

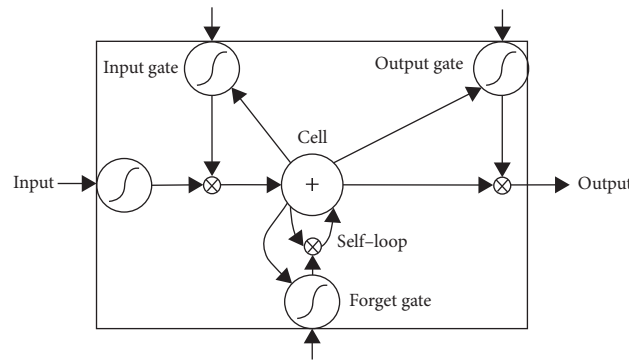


Figure 5: Cell structure in long short-term memory (LSTM).

can adjust the focus of memory according to the training target and then recode to control the trade-off between the input at one time and the input at a subsequent time. Therefore, LSTM can remember the information that needs to be remembered for a long time, while forgetting any relatively unimportant information. With LSTM, it is easier to learn long-term dependency than in the simple RNN architecture, and it is useful for dealing with problems that are highly related to time series, such as the video sequences used for CEAR.

*2.3.4. Simplified Temporal Convolutional Network for CEAR.* Considering that video sequences contain dynamic images that include information on both space and time, that it is difficult to extract temporal features using a simple CNN, and that a regular RNN is not able to extract image features well, a combination of CNN and LSTM is proposed in this research for CEAR [54], where the CNN is used to extract the image features of the video frame sequences and LSTM is used to extract the temporal features. In this process, the probabilities for all frames generated by the softmax layer are averaged, and the label with the highest probability is selected as the final classification result. This proposed method is called a simplified temporal convolutional network (STCN), and the structure of the STCN is shown in Figure 6.

Theoretically, a model with more parameters will have a higher complexity, and when the amount of training data is insufficient, a complex model is easy to be subjected to overfitting [55]. At present, considering the small amount of data in the field of CEAR, a less complex CNN model

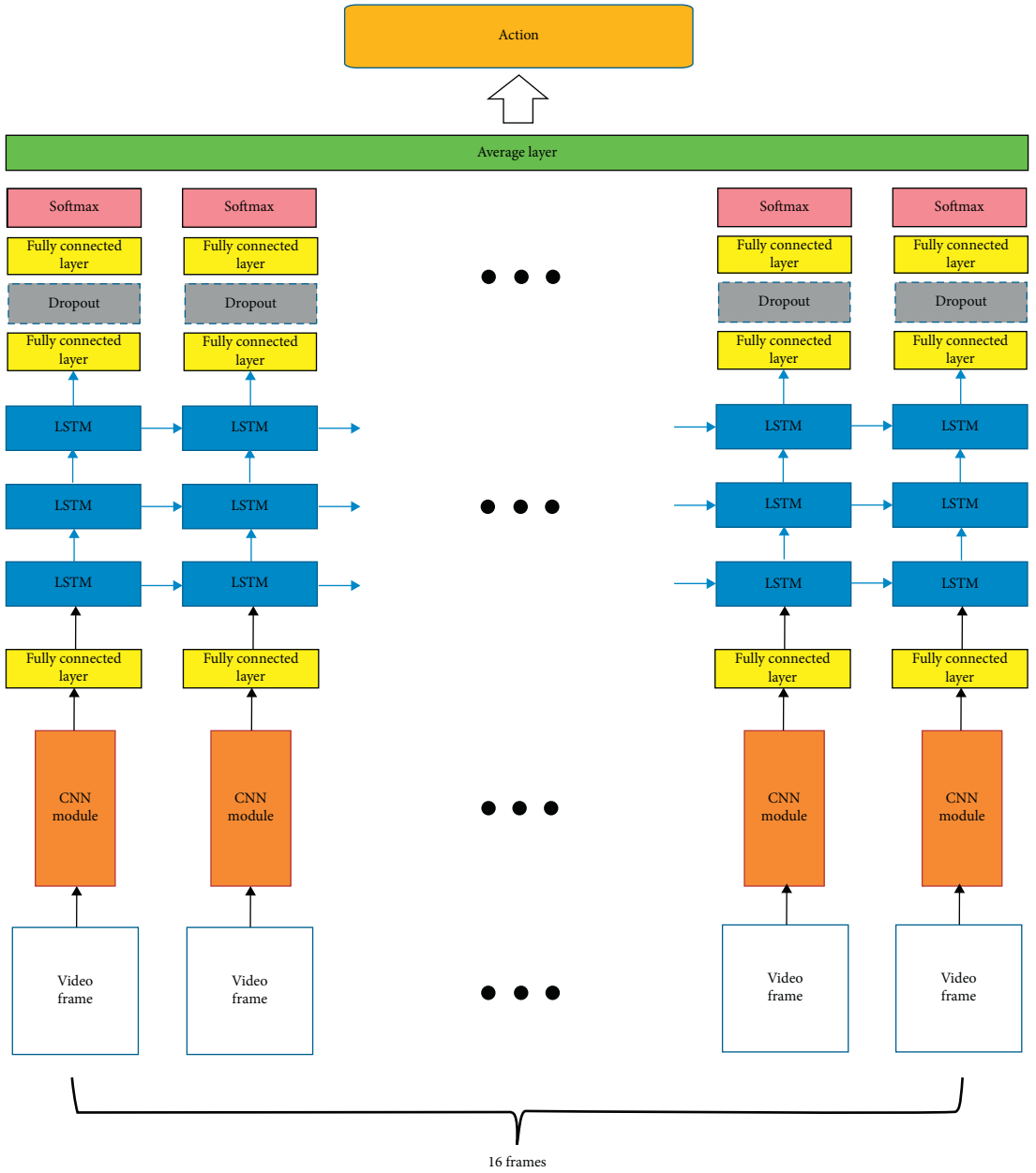


Figure 6: Structure of the simplified temporal convolutional network (STCN).

consisting of five convolutional layers is employed in this research, as shown in Figure 7. In order to obtain a sufficient number of effective receptive fields [56], the CNN model uses $7 \times 7$ and $5 \times 5$ convolution kernels in the Conv1 and Conv2 layers, respectively, and $3 \times 3$ convolution kernels for the other convolutional layers. In order to ensure the stability of data distribution in each layer to improve the training efficiency, batch normalization is used in all convolutional layers [57]. Because the maximum pooling operation can reduce the estimated mean shift caused by parameter errors in the convolutional layers while maintaining translation invariance, thereby minimizing the number of parameters and reducing model complexity [58], a max pooling layer is added at the end of each convolutional layer, and $2 \times 2$ convolution kernels are used in all pooling layers.

There is no pretraining in STCN because, based on the research result of Glorot et al. [59], the performance of a rectified linear unit (ReLu) network is far better than those of other activation function networks even without pretraining. Sparsity can be introduced to the ReLu activation function to allow each neuron to fully play its screening effect—those values matching the median value of a certain feature will be amplified, while the outlying values will be abandoned. Since the ReLu activation function only needs to perform the calculation for the maximum value, it is also superior in terms of calculation speed. As a result, ReLu is chosen as the activation function in the proposed model.

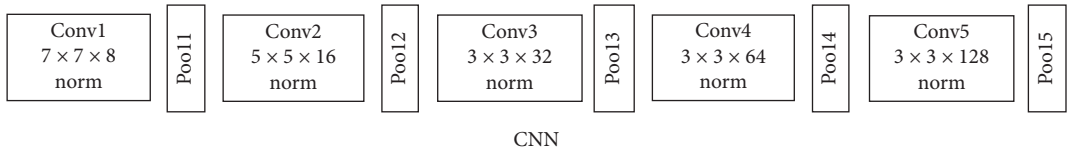


Figure 7: Structure of the convolutional neural network (CNN) used in this study.

A fully connected layer is used to transmit the output of the CNN model to the three subsequent layers of the LSTM network. LSTM units for all continuous image subsequences were connected to each other. The probability of each action category is then generated using the fully connected layers and the softmax function. In order to generate the action prediction label of a given video clip, an average layer is employed to take the average probability of all image frames in the video clip, and the category label with the maximum probability is used as the result for action recognition.

## 3. Results and Discussion

*3.1. Results.* Using the dataset introduced in Section 2.2, the authors extracted 16 image frames from each video clip to train the algorithm discussed in Section 2.3. For video clips that are less than 4 seconds, between 5 and 10 seconds, and longer than 10 seconds, image frames were extracted at an interval of 5 frames, 10 frames, and 15 frames. If there were less than 16 frames that can be extracted based on this rule for a very short video clip, the last frame was repeated to complement 16 frames. After that, all images were adjusted to a resolution of 320 pixels by 240 pixels, and a random cropping with a size of 224 pixels by 224 pixels was used as data augmentation. Finally, all these frames were sent into the STCN model in a chronological order.

All the work was carried out by PyTorch on a workstation with a 6-core 3.8 GHz Intel processor, 16 GB memory, a GTX1060 graphics card with 6 GB memory, and Windows 10 operating system. In order to quantify the performance of the action recognition algorithm, three common performance metrics are employed, that is, precision, recall, and $F$-1 score. Calculating the precision and recall rate of the model can assess the costs associated with misclassification. The $F$-1 score is the harmonic mean of accuracy and recall, which takes into account both precision and recall. Their mathematical equations are shown as follows:

$$\begin{aligned}\text{Precision} &= \frac{\text{True Positive}}{\text{True Positive} + \text{False Positive}} \times 100\%,\\ \text{Recall} &= \frac{\text{True Positive}}{\text{True Positive} + \text{False Negative}} \times 100\%,\\ F1\ \text{score} &= 2 \times \frac{\text{Precision} \times \text{Recall}}{\text{Precision} + \text{Recall}}.\end{aligned} \quad (1)$$

As mentioned above, STCN model is mainly composed of two parts, that is, CNN module and LSTM module. The inputs to the model are the video clip frames. Experiments were conducted on the parameter configuration of the STCN model. In the experiment for weight initialization, this study performed Xavier initialization [60] on the CNN module. The results showed that the model with weights initialization has a better $F$-1 score (2.31% higher) than a scenario where no parameter initialization was performed. Then there was an experiment on the parameter settings of the CNN module. This experiment mainly studies the influence of the size of the convolution kernels on the recognition performance. The experimental results are shown in Table 3. Four sets of convolution kernels configurations were used for control experiments. The results indicated that this model has the best performance, when Conv1 and Conv2 used $7 \times 7$ and $5 \times 5$ convolution kernels and the other convolution layers used $3 \times 3$ convolution kernels.

Next, the experimental research on LSTM parameter settings showed that the number of LSTM layers has a greater impact on recognition performance of the dataset developed in this research. In this study, the LSTM model architecture used is shown in Figure 5. Experiment shows that the three-layer LSTM model has the highest $F$-1 score, which is at least 2% higher than the $F$-1 score of other LSTM layer settings. The result is shown in Figure 8. In contrast, it was found that the number of hidden units in the LSTM had little effect on the $F$-1 score. The authors tested the STCN model with 64, 128, and 256 hidden units in the LSTM module, and the difference in $F$-1 score was within 1%, as shown in Table 4. Therefore, in order to reduce the complexity of the model to save computational cost and reduce overfitting, this model employs 64 hidden units.

In the experiment of this research, all models use Adam optimization algorithm [61] as the optimizer, the learning rate is set at 0.001, and the other parameter settings are $\beta 1 = 0.9$, $\beta 2 = 0.999$, and $\varepsilon = 10e - 8$. Under the above settings, the STCN model achieves a precision of 77.55%, a recall rate of 75.00%, and an $F$-1 score of 76.25%, as shown in Table 5.

In addition, this research also studied the recognition effect of the STCN model for each action category. The experimental results are shown in Table 6. In this experiment, accuracy was used as the main evaluation metric, that is, the ratio of the number of examples that are correctly predicted to the number of all examples that are predicted to be that category for each action category. The results indicate that in general this model can recognize the action of excavators better than dump truck.

*3.2. Discussion.* In order to compare the performance of the STCN method and investigate the possibility of transferring some of the best HAR methods for use in CEAR, the dataset developed in this research was used to examine the

Table 3: *F*-1 scores of STCN models under different size convolution kernels configurations.

| Conv1 | Conv2 | Conv3 | Conv4 | Conv5 | *F*-1 score (%) |
|---|---|---|---|---|---|
| 3 × 3 | 3 × 3 | 3 × 3 | 3 × 3 | 3 × 3 | 75.26 |
| 5 × 5 | 5 × 5 | 3 × 3 | 3 × 3 | 3 × 3 | 74.88 |
| 7 × 7 | 5 × 5 | 3 × 3 | 3 × 3 | 3 × 3 | **76.25** |
| 7 × 7 | 7 × 7 | 3 × 3 | 3 × 3 | 3 × 3 | 74.33 |

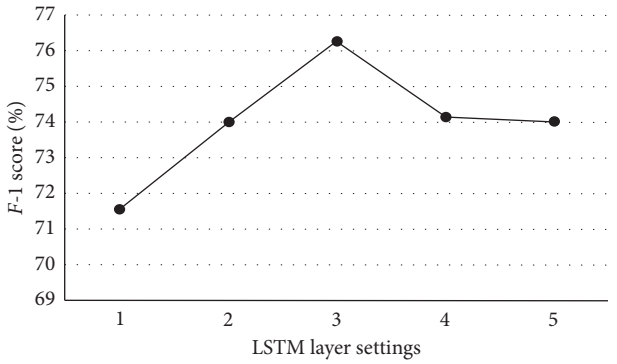


Figure 8: The *F*-1 score of different LSTM layer settings in STCN.

Table 4: *F*-1 scores of STCN models with different LSTM hidden units.

| The number of hidden units | *F*-1 score (%) |
|---|---|
| 64 | **76.25** |
| 126 | 76.09 |
| 256 | 76.28 |

Table 5: Performance measures of different action recognition methods.

| Method | Precision (%) | Recall (%) | *F*-1 score (%) |
|---|---|---|---|
| CNN | 71.26 | 68.01 | 69.60 |
| LSTM | 44.48 | 44.43 | 44.46 |
| CNN-DLSTM | 76.40 | 74.14 | 75.25 |
| STCN | 77.55 | 75.00 | 76.25 |
| 3D ConvNets | 75.45 | 71.74 | 73.55 |
| Two-stream ConvNets | 77.80 | 74.79 | 76.26 |
| I3D | 78.13 | 75.02 | 76.54 |

performance of the CNN-DLSTM model used by Kim and Chi [46] for CEAR, 3D ConvNets proposed by Tran et al. [30], two-stream ConvNets proposed by Simonyan and Zisserman [29], and I3D ConvNets proposed by Carreira and Zisserman [31]. The results, which are summarized in Table 5, indicate that the STCN method has a performance comparable to those of the method proposed by Kim and Chi, the 3D ConvNets method, and the two-stream ConvNets in precision, recall, and *F*-1 score.

The results of using CNN module and LSTM module for CEAR, respectively, are also presented in Table 3. Their performance when working alone is not very satisfactory, and it is also verified that extracting key visual features and extracting context features have a significant positive impact on CEAR performance. The CNN-DLSTM model refers to the method used by Kim and Chi [46] in the action recognition process. Its CNN consists of 10 convolutional layers and 5 pooling layers, and the sequential patterns learning module consists of two LSTM models.

The 3D ConvNets model was reproduced as shown in Figure 9. The convolutional and pooling operations of the 3D ConvNets model were performed in the temporal dimension. All 3D convolution filters are $3 \times 3 \times 3$ in size with a stride of $1 \times 1 \times 1$. The first 3D pooling layer is $1 \times 2 \times 2$ with a stride of $1 \times 2 \times 2$, and the remaining 3D pooling layers are $2 \times 2 \times 2$ with a stride of $2 \times 2 \times 2$. This design preserves the temporal information in the early stages. The model can simulate both appearance information and action information simultaneously, and it produces excellent results in HAR tasks. Using the same dataset, the 3D ConvNet model achieved *F*-1 score of 73.55%.

Two-stream ConvNets were also examined using the same dataset. As shown in Figure 10, the two-stream ConvNet consists of two convolutional network structures: a spatial stream and a temporal stream. The spatial stream convolution network is essentially an image classification network that acquires static appearance features using the input of a single frame image. The temporal stream network uses multiframe optical flow images as input, as shown in Figure 11. In order to employ the two-stream ConvNets, a corresponding optical flow dataset was created to extract temporal features. An action classification result was obtained by taking the average of the classification scores. The two-stream ConvNets model is in a leading position in HAR tasks in terms of its performance, and it achieved an *F*-1 score of 76.26% in CEAR in this research.

By comparing the results for the STCN method, the CNN-DLSTM method, the 3D ConvNets method, the two-stream ConvNets method, and the I3D ConvNets method, it is found that the STCN method proposed in this study exhibits a performance in CEAR tasks which is comparable to those of other deep learning-based methods that have proven to have good results. Figure 12 shows the time consumption of training these methods. It can be seen that, in the case of close performance, STCN requires the shortest training time, so it has a certain speed advantage. As what has been mentioned before that the two-stream ConvNets model achieved a slightly better *F*-1 score than STCN (76.26% versus 76.25%) but the two-stream ConvNets model and I3D ConvNets model consumed much more computing time (9 h 28 m and 17 h 22 m versus 7 h 43 m), the STCN model is still better in general. In addition, the study demonstrates the feasibility of directly transferring some HAR methods to the CEAR field, as the 3D ConvNets model and the two-stream ConvNets model both achieved an acceptable rate of accuracy when using the same dataset as input.

Table 6: Construction equipment action recognition results per activity.

| Equipment | Activity | Precision (%) | Recall (%) | $F$-1 score (%) |
|---|---|---|---|---|
| Excavator | Digging | 76.38 | 74.06 | 75.20 |
| | Dumping | 83.78 | 80.57 | 82.14 |
| | Swinging | 78.58 | 76.10 | 77.32 |
| Dump truck | Moving backward | 56.27 | 55.13 | 55.69 |
| | Moving forward | 54.48 | 53.72 | 54.10 |

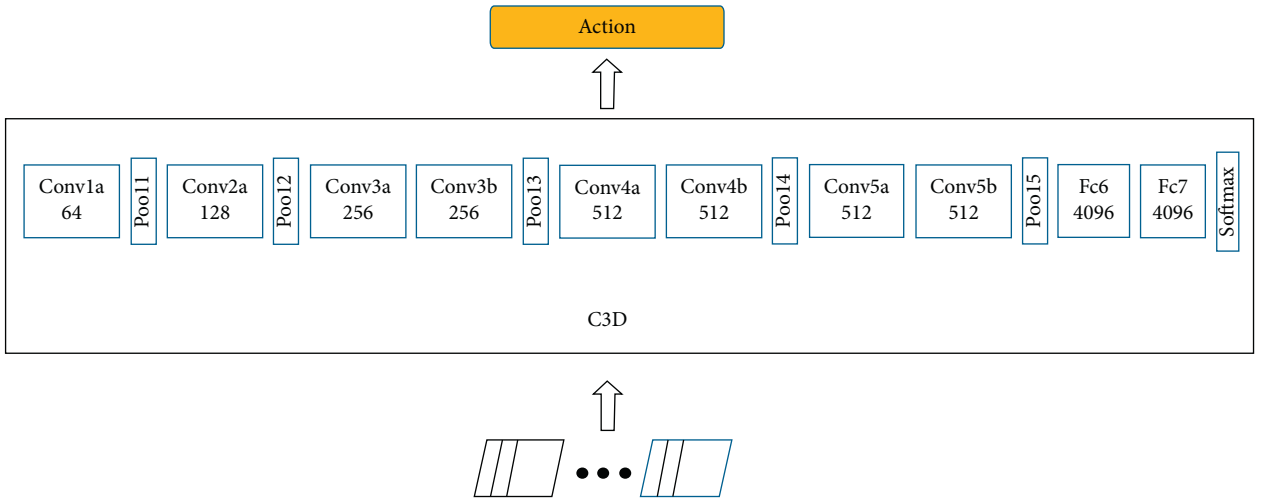


Figure 9: Structure of the 3D ConvNets model.

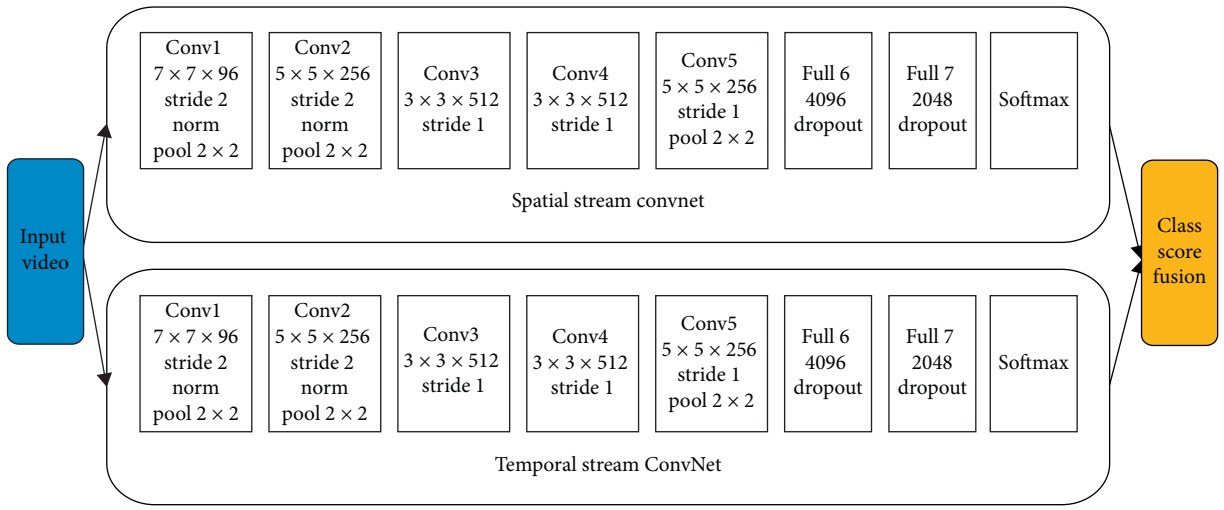


Figure 10: Two-stream architecture for action recognition.

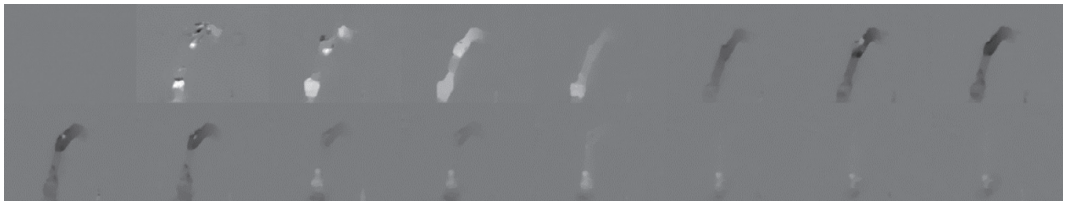

Figure 11: An example of optical flow images for the input of the two-stream ConvNets.

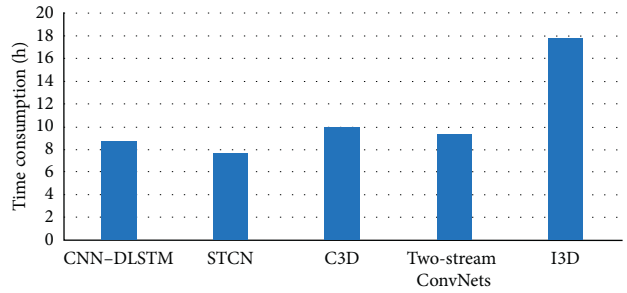


Figure 12: Time consumption of different action recognition methods.

## 4. Conclusions

Digital twin is not only for the facility to be built but also for the workers and construction equipment on a construction site. Research in CEAR is no less significant than that of HAR in terms of smart construction, because the perception of a construction activity needs to understand the what (object identification), where (object tracking), and how (action recognition) for both construction workers and equipment. Much of the research in the field of HAR can be applied in the construction industry. However, the research in the field of CEAR is very limited to date, due to a lack of high-quality datasets, the complexity of the application environment at construction sites, and the difficulty to benchmark the performance in CEAR.

In this research, the authors developed an open-source video dataset of 2,064 video clips with five action types for excavators and dump trucks, including a corresponding optical flow dataset. This dataset supplements the existing datasets for CEAR research and could potentially be used by other researchers in later studies. One major reason that hinders the research in the area of CEAR is the lack of high-quality datasets, and the authors encourage other researchers to share their datasets. Another contribution of this research in the field of CEAR is a new deep learning-based approach, STCN, which combines CNN and LSTM—where CNN is used to extract the image features from the video frame sequences and LSTM is used to extract the temporal features. The STCN proposed in this research achieved an $F$-1 score of 76.25% for the dataset developed earlier. In order to evaluate the performance of the STCN, a similar CEAR method and three of the best-performing deep learning-based approaches in the field of HAR, namely, the 3D ConvNets method, the two-stream ConvNets method, and I3D ConvNets method, were examined using the same dataset as input, and they achieved the $F$-1 scores of 75.25%, 73.55%, 76.26%, and 76.54, respectively. Those four methods either underperformed in comparison to STCN method or had a similar performance but needed significantly higher computing time. The time consumption of training the STCN is the shortest. This comparison indicates not only the advantage of the STCN but also the possibility of directly transferring some HAR methods to the field of CEAR.

There are some limitations in this research. First, the dataset developed in this study is still relatively insufficient compared to datasets available in other application areas using deep learning-based solutions. It is expected that a better accuracy rate would be achieved once a much larger dataset is developed. With a limited dataset, one possible solution is to pretrain the recognition algorithm using datasets for HAR. Second, this research only studied the recognition of actions for two types of construction equipment (excavators and dump trucks) and did not investigate whether different types of equipment (e.g., equipment with apparent joints such as excavators and equipment with no joints such as dump trucks) require different recognition algorithms in order to achieve better action recognition.

There is much important work to be done in the future. There exist hundreds of types of construction equipment in the construction industry, and each type of equipment has multiple actions. It is important to develop more comprehensive video datasets for various types of equipment under different conditions, for example, camera motion or disruptive weather (e.g., heavy winds or rain). In addition, it is important to study the perception of activities where multiple types of construction equipment are moving at the same time. In many cases, a surveillance camera will capture a scene of a construction site containing several pieces of equipment; this becomes a challenge when different types of equipment in the same frame require different action recognition algorithms to achieve better recognition performance.

## Data Availability

The dataset used to support the findings of this study may be released upon application to Tianjin University, which can be contacted at jinyuezhang@tju.edu.cn.

## Conflicts of Interest

The authors declare that there are no conflicts of interest regarding the publication of this paper.

## Authors' Contributions

Jinyue Zhang, Lijun Zi, and Yuexian Hou contributed equally to this paper.

## Acknowledgments

This work was supported in part by the National Key R&D Program of China (2018YFC0406900 and 2017YFE0111900), the National Natural Science Foundation of China (61876129), and the European Union's Horizon 2020 Research and Innovation Programme under the Marie Skłodowska-Curie (721321).

## References

[1] R. Zhang, Q. S. Li, and J. Chu, "Human action recognition algorithm based on 3D convolution neural network," *Computer Engineering*, vol. 45, no. 1, pp. 259–263, 2019.

[2] Y. Zhu, J. K. Zhao, N. Yi, and B. B. Zheng, "A review of human action recognition based on deep learning," *Acta Automatica Sinica*, vol. 42, no. 6, pp. 848–857, 2016.

[3] R. Poppe, "A survey on vision-based human action recognition," *Image and Vision Computing*, vol. 28, no. 6, pp. 976–990, 2010.

[4] A. Purohit and S. S. Chauhan, "A survey on human action recognition," *IOSR Journal of Computer Engineering*, vol. 19, pp. 43–50, 2017.

[5] A. Krizhevsky, I. Sutskever, and G. Hinton, "ImageNet classification with deep convolutional neural networks," in *Proceedings of the 26th Neural Information Processing Systems*, Lake Tahoe, CA, USA, December 2012.

[6] C. T. Haas, P. M. Goodrum, and C. C. Caldas, "Leveraging technology to improve construction productivity," *Technology Field Trials*, CII, vol. 3, p. 106, Austin, TX, USA, 2010.

[7] M. Golparvar-Fard, A. Heydarian, and J. C. Niebles, "Vision-based action recognition of earthmoving equipment using spatio-temporal features and support vector machine classifiers," *Advanced Engineering Informatics*, vol. 27, no. 4, pp. 652–663, 2013.

[8] L. Song and N. N. Eldin, "Adaptive real-time tracking and simulation of heavy construction operations for look-ahead scheduling," *Automation in Construction*, vol. 27, pp. 32–39, 2012.

[9] F. Vahdatikhaki, A. Hammad, and H. Siddiqui, "Optimization-based excavator pose estimation using real-time location systems," *Automation in Construction*, vol. 56, pp. 76–92, 2015.

[10] C.-F. Cheng, A. Rashidi, M. A. Davenport, and D. V. Anderson, "Activity analysis of construction equipment using audio signals and support vector machines," *Automation in Construction*, vol. 81, pp. 240–253, 2017.

[11] C. A. Sabillon, A. Rashidi, B. Samanta, C.-F. Cheng, M. A. Davenport, and D. V. Anderson, "A productivity forecasting system for construction cyclic operations using audio signals and a Bayesian approach," in *Proceedings of the Construction Research Congress*, pp. 295–304, New Orleans, LA, USA, April 2018.

[12] N. Mathur, S. S. Aria, T. Adams, C. R. Ahn, and S. Lee, "Automated cycle time measurement and analysis of excavator's loading operation using smart phone-embedded IMU sensors," in *Proceedings of the International Workshop on Computing in Civil Engineering*, pp. 215–222, Austin, TX, USA, June 2015.

[13] K. M. Rashid and J. Louis, "Automated activity identification for construction equipment using motion data from articulated members," *Frontiers in Built Environment*, vol. 5, p. 144, 2020.

[14] J. Zou and H. Kim, "Using hue, saturation, and value color space for hydraulic excavator idle time analysis," *Journal of Computing in Civil Engineering*, vol. 21, no. 4, pp. 238–246, 2007.

[15] J. Gong, C. H. Caldas, and C. Gordon, "Learning and classifying actions of construction workers and equipment using bag-of-video-feature-words and bayesian network models," *Advanced Engineering Informatics*, vol. 25, no. 4, pp. 771–782, 2011.

[16] Y. Lecun, Y. Bengio, and G. Hinton, "Deep learning," *Nature*, vol. 521, no. 7553, p. 436, 2015.

[17] J. Seo, S. Han, S. Lee, and H. Kim, "Computer vision techniques for construction safety and health monitoring," *Advanced Engineering Informatics*, vol. 29, no. 2, pp. 239–251, 2015.

[18] A. Sargano, P. Angelov, and Z. Habib, "A comprehensive review on handcrafted and learning-based action representation approaches for human activity recognition," *Applied Sciences*, vol. 7, no. 1, 2017.

[19] D. Dawn and S. H. Shaikh, "A comprehensive survey of human action recognition with spatio-temporal interest point (stip) detector," *The Visual Computer*, vol. 32, no. 3, pp. 289–306, 2015.

[20] H. Li and M. Greenspan, "Multi-scale gesture recognition from time-varying contours," in *Proceedings of the Tenth IEEE International Conference on Computer Vision*, IEEE, Beijing, China, October 2005.

[21] D. Weinland, R. Ronfard, and E. Boyer, "Free viewpoint action recognition using motion history volumes," *Computer Vision and Image Understanding*, vol. 104, no. 2-3, pp. 249–257, 2006.

[22] T. Ojala, M. Pietikainen, and D. Harwood, "Performance evaluation of texture measures with classification based on Kullback discrimination of distributions," in *Proceedings of the 12th IAPR International Conference on Pattern Recognition*, Jerusalem, Israel, October 1994.

[23] S. Sadek, A. Al-Hamadi, B. Michaelis, and U. Sayed, "An action recognition scheme using fuzzy log-polar histogram and temporal self-similarity," *EURASIP Journal on Advances in Signal Processing*, vol. 2011, no. 1, 2011.

[24] H. Wang, A. Kläser, C. Schmid, and C.-L. Liu, "Dense trajectories and motion boundary descriptors for action recognition," *International Journal of Computer Vision*, vol. 103, no. 1, pp. 60–79, 2013.

[25] H. Wang and C. Schmid, "Action recognition with improved trajectories," in *Proceedings of the Third IEEE International Conference on Computer Vision*, pp. 3551–3558, Sydney, Australia, June 2013.

[26] L. Liu, L. Shao, X. Li, and K. Lu, "Learning spatio-temporal representations for action recognition: a genetic programming approach," *IEEE Transactions on Cybernetics*, vol. 1, no. 46, pp. 158–170, 2016.

[27] F. Zhu, L. Shao, J. Xie, and Y. Fang, "From handcrafted to learned representations for human action recognition: a survey," *Image and Vision Computing*, vol. 55, pp. 42–52, 2016.

[28] A. Karpathy, G. Toderici, S. Shetty, T. Leung, R. Sukthankar, and F. F. Li, "Large-scale video classification with convolutional neural networks," in *Proceedings of the 27th IEEE Conference on Computer Vision and Pattern Recognition*, pp. 1725–1732, Columbus, OH, USA, June 2014.

[29] K. Simonyan and A. Zisserman, "Two-stream convolutional networks for action recognition in videos," in *Proceedings of the 28th Neural Information Processing Systems*, pp. 568–576, Montreal, Canada, December 2014.

[30] D. Tran, L. Bourdev, R. Fergus, L. Torresani, and M. Paluri, "Learning spatiotemporal features with 3D convolutional networks," in *Proceedings of the 15th IEEE International Conference on Computer Vision*, pp. 4489–4497, Santiago, Chile, December 2015.

[31] J. Carreira and A. Zisserman, "Quo vadis, action recognition? a new model and the kinetics dataset," in *Proceedings of the IEEE Conference on Computer Vision and Pattern Recognition*, Honolulu, HI, USA, July 2017.

[32] G. Varol, I. Laptev, and C. Schmid, "Long-term temporal convolutions for action recognition," *IEEE Transactions on Pattern Analysis and Machine Intelligence*, vol. 40, no. 6, pp. 1510–1517, 2017.

[33] Y. H. Ng, M. Hausknecht, S. Vijayanarasimhan et al., "Beyond short snippets: deep networks for video classification," in *Proceedings of the 28th IEEE Conference on Computer Vision and Pattern Recognition*, pp. 4694–4702, IEEE, Boston, MA, USA, June 2015.

[34] K. Soomro, A. R. Zamir, and M. Shah, "UCF101: a dataset of 101 human actions classes from videos in the wild," 2012, http://www.crcv.ucf.edu/data/UCF101.php.

[35] J. Donahue, L. A. Hendricks, M. Rohrbach et al., "Long-term recurrent convolutional networks for visual recognition and description," *IEEE Transactions on Pattern Analysis and Machine Intelligence*, vol. 39, no. 4, pp. 677–691, 2016.

[36] L. Sevilla-Lara, Y. Y. Liao, F. Güney et al., "On the integration of optical flow and action recognition," in *Proceedings of the 5th Global Conference on Psychology Researches*, pp. 281–297, Istanbul, Turkey, February 2018.

[37] H. Kuehne, H. Jhuang, E. Garrote, T. A. Poggio, and T. Serre, "HMDB: a large video database for human motion recognition," in *Proceedings of the IEEE International Conference on Computer Vision*, pp. 2556–2563, IEEE, Barcelona, Spain, November 2011.

[38] F. C. Heilbron, V. Escorcia, B. Ghanem, and J. C. Niebles, "ActivityNet: a large-scale video benchmark for human activity understanding," in *Proceedings of the 28th IEEE Conference on Computer Vision and Pattern Recognition*, pp. 961–970, IEEE, Boston, MA, USA, June 2015.

[39] S. Abu-El-Haija, N. Kothari, J. Lee et al., "YouTube-8M: a large-scale video classification benchmark," 2016, http://arxiv.org/abs/1609.08675v1.

[40] J. Gong and C. H. Caldas, "An intelligent video computing method for automated productivity analysis of cyclic construction operations," in *Proceedings of the 2009 ASCE International Workshop on Computing in Civil Engineering*, pp. 64–73, Austin, TX, MSA, June 2009.

[41] R. Akhavian and A. H. Behzadan, "Construction equipment activity recognition for simulation input modeling using mobile sensors and machine learning classifiers," *Advanced Engineering Informatics*, vol. 29, no. 4, pp. 867–877, 2015.

[42] J. Cao, W. Wang, J. Wang, and R. Wang, "Excavation equipment recognition based on novel acoustic statistical features," *IEEE Transactions on Cybernetics*, vol. 42, no. 99, pp. 1–13, 2016.

[43] K. K. Han and M. Golparvar-Fard, "Potential of big visual data and building information modeling for construction performance analytics: an exploratory study," *Automation in Construction*, vol. 73, pp. 184–198, 2016.

[44] D. Roberts and M. Golparvar-Fard, "End-to-end vision-based detection, tracking and activity analysis of earthmoving equipment filmed at ground level," *Automation in Construction*, vol. 105, 2019.

[45] K. M. Rashid and J. Louis, "Times-series data augmentation and deep learning for construction equipment activity recognition," *Advanced Engineering Informatics*, vol. 42, Article ID 100944, 2019.

[46] J. Kim and S. Chi, "Action recognition of earthmoving excavators based on sequential pattern analysis of visual features and operation cycles," *Automation in Construction*, vol. 104, pp. 255–264, 2019.

[47] C. Szegedy, W. Liu, Y. Jia et al., "Going deeper with convolutions," in *Proceedings of the 28th IEEE Conference on Computer Vision and Pattern Recognition*, pp. 1–9, Boston, MA, USA, June 2015.

[48] A. Graves, A. R. Mohamed, and G. E. Hinton, "Speech recognition with deep recurrent neural networks," in *Proceedings of the 38th International Conference on Acoustics, Speech, and Signal Processing*, pp. 6645–6649, Vancouver, Canada, May 2013.

[49] B. C. Yin and L. C. Wang, "Review of deep learning," *Journal of Beijing University of Technology*, vol. 41, no. 1, pp. 48–59, 2015.

[50] G. E. Hinton, S. Osindero, and Y.-W. Teh, "A fast learning algorithm for deep belief nets," *Neural Computation*, vol. 18, no. 7, pp. 1527–1554, 2006.

[51] Y. Bengio, "Learning deep architectures for AI," *Foundations and Trends in Machine Learning*, vol. 2, no. 1, pp. 1–127, 2009.

[52] Y. Lecun, L. Bottou, Y. Bengio, and P. Haffner, "Gradient-based learning applied to document recognition," *Proceedings of the IEEE*, vol. 86, no. 11, pp. 2278–2324, 1998.

[53] S. Hochreiter and J. Schmidhuber, "Long short-term memory," *Neural Computation*, vol. 9, no. 8, pp. 1735–1780, 1997.

[54] Y. Bengio, P. Simard, and P. Frasconi, "Learning long-term dependencies with gradient descent is difficult," *IEEE Transactions on Neural Networks*, vol. 5, no. 2, pp. 157–166, 1994.

[55] Z. H. Zhou, *Machine Learning*, Tsinghua University Press, Beijing, China, 2016.

[56] W. J. Luo, Y. J. Li, R. Urtasun, and R. S. Zemel, "Understanding the effective receptive field in deep convolutional neural networks," in *Proceedings of the 30th Neural Information Processing Systems*, pp. 4898–4906, ACM, Barcelona, Spain, December 2016.

[57] S. Ioffe and C. Szegedy, "Batch normalization: accelerating deep network training by reducing internal covariate shift," in *Proceedings of the 32nd International Conference on Machine Learning*, pp. 448–456, Lille, France, July 2015.

[58] Y. L. Boureau, F. Bach, Y. Lecun, and J. Ponce, "Learning mid-level features for recognition," in *Proceedings of the 23rd IEEE Computer Society Conference on Computer Vision and Pattern Recognition*, pp. 2559–2566, IEEE, San Francisco, CA, USA, June 2010.

[59] X. Glorot, A. Bordes, and Y. Bengio, "Deep sparse rectifier neural networks," in *Proceedings of the 14th International Conference on Artificial Intelligence and Statistics*, pp. 315–323, Lauderdale, FL, USA, April 2011.

[60] D. P. Kingma and J. Ba, "Adam: a method for stochastic optimization," in *Proceedings of the 2nd International Conference on Learning Representations*, San Diego, CA, USA, May 2015.

[61] X. Glorot and Y. Bengio, "Understanding the difficulty of training deep feedforward neural networks," *Journal of Machine Learning Research*, vol. 9, pp. 249–256, 2010.